UNIVERSITY OF SOUTHAMPTON

FACULTY OF ENGINEERING, SCIENCE AND MATHEMATICS

School of Chemistry

THE DESIGN OF SYNTHETIC TRANSMEMBRANE CARRIERS FOR ANIONS

by

Cally Jo Elizabeth Haynes

Thesis for the degree of Doctor of Philosophy

August 2011
UNIVERSITY OF SOUTHAMPTON

ABSTRACT

FACULTY OF ENGINEERING, SCIENCE AND MATHEMATICS

SCHOOL OF CHEMISTRY

Doctor of Philosophy

THE DESIGN OF SYNTHETIC TRANSMEMBRANE CARRIERS FOR ANIONS

By Cally Jo Elizabeth Haynes

This thesis reports a number of novel receptors found to facilitate the transmembrane transport of anions in synthetic vesicle systems.

A series of structurally simple thioureas were found to function as efficient Cl^-/NO_3^- and Cl^-/HCO_3^- antiporters while the corresponding ureas were inactive. Of these receptors, a simple indolylthiourea was found to be an extremely potent transporter which could function at concentrations as low as 1:25 000 (molar ratio with respect to lipid).

Subsequently, a series of bipodal bis-alkyl-indolylureas were found to mediate Cl^-/NO_3^- antiport, with the observed anion transport found to be highly dependent on the length of the central alkyl chain bridging the two indolylurea moieties. The mechanism of transport and the structure-activity relationships were extensively investigated using a wide range of vesicle-based techniques. The solution phase anion binding properties of these receptors was found to be complex as a result of the flexibility of the receptors and the distance between the binding sites. The binding of dihydrogen phosphate and oxalate by receptors in this series was also demonstrated in the solid state.

A series of bipodal bis-phenylthioureas were also found to mediate Cl^-/NO_3^- and Cl^-/HCO_3^- antiport which was again found to be dependent on the alkyl chain length. The effect of substituent variation on transport activity was also examined, while the solution phase binding properties were found to be similarly complex to the bis-indolylurea receptors.

The anion transport activity of a series of strapped calix[4]pyrroles provided by J. L. Sessler and C.-H. Lee was investigated. It was found that the straps were able to encourage transport mechanisms not exhibited by the parent macrocycle, while a series of control compounds were inactive.

Contents

DECLARATION OF AUTHORSHIP

I, **Cally Jo Elizabeth Haynes**, declare that the thesis entitled

The design of synthetic transmembrane carriers for anions

and the work presented in the thesis are both my own, and have been generated by me as the result of my own original research. I confirm that:

- this work was done wholly or mainly while in candidature for a research degree at this University;
- where any part of this thesis has previously been submitted for a degree or any other qualification at this University or any other institution, this has been clearly stated;
- where I have consulted the published work of others, this is always clearly attributed;
- where I have quoted from the work of others, the source is always given. With the exception of such quotations, this thesis is entirely my own work;
- I have acknowledged all main sources of help;
- where the thesis is based on work done by myself jointly with others, I have made clear exactly what was done by others and what I have contributed myself;
- parts of this work have been published as:

"Structurally simple lipid bilayer transport agents for chloride and bicarbonate" N. J. Andrews, C. J. E. Haynes, M. E. Light, S. J. Moore, C. C. Tong, J. T. Davis, W. A. Harrell and P. A. Gale, *Chem. Sci.*, 2011, **2**, 256-260.

Signed: ……

Date:……

Acknowledgements

I'd like to thank my supervisor, Prof. Philip A. Gale for his help, support and guidance during the course of my PhD. I'd also like to thank all members of the Gale group, both past (Matt, Pete, Christine, Agnieszka and Masafumi) and present (Steve, Sam, Jenny, Marco, Nathalie, Issy) for their continuing help and support, for proof reading this thesis, and for the many enlightening discussions about chemistry and the wider world of zoological science. I'd also like to thank my project student, Jenny, for her hard work and her contributions to this project.

Thanks also go to Dr Mark E Light for X-ray crystallography, and to the NMR and MS and stores departments at the University of Southampton.

I'm grateful to Dr George Attard and Dr Marcus Dymond for their kind advice and assistance on the subject of vesicles.

I'm also grateful to Prof Jonathon L. Sessler and Prof Chang-Hee Lee for the collaborative work on the strapped calix[4]pyrrole systems.

I'd like to thank the EPSRC for funding this project.

Honourable mentions go to Dave, Steph and Michael Bodnarchuk for their contributions to this thesis.

Finally, I'd like to thank my family and Dave for their support and encouragement, without which I would surely have entirely descended into madness long ago.

Abbreviations

Å	Angstrom
AE	Anion exchange protein
ATP	Adenosine triphosphate
bpy	2,2'-Bipyridine
br.	Broad resonance (NMR)
Bu	Butyl
°C	Degrees Centigrade
cAMP	Cyclic adenosine monophosphate
CDI	1,1'-Carbonyldiimidazole
CF	Cystic fibrosis
CFTR	Cystic fibrosis transmembrane regulatory protein
ClC	Chloride channel proteins
clogP	Calculated logP (Octanol:water partition coefficient)
d	Doublet
DCM	Dichloromethane
DMF	Dimethylformamide
DMSO	Dimethylsulphoxide
DNA	Deoxyribonucleic acid
DOPC	1,2-dioleoyl-*sn*-glycero-3-phosphocholine
DPPC	1,2-dipalmitoyl-*sn*-glycero-3-phosphocholine
EDTA	Ethylenediaminetetraacetic acid
Eq.	Equivalents
Et_2O	Diethyl ether
EYPC	Egg yolk phosphocholine
FCCP	Carbonyl cyanide-p-trifluoromethoxyphenylhydrazone
FTIR	Fourier transform infra-red spectroscopy
g	Grams
GABA	γ-Aminobutyric acid
h	Hour(s)
HPTS	8-Hydroxypyrene-1.3.6-trisulfonic acid trisodium salts
HRMS	High resolution mass spectrometry
Hz	Hertz

ISE	Ion selective electrode
ITC	Isothermal titration calorimetry
J	Coupling constant (NMR)
K	Kelvin
K_a	Association constant
KCC	K-Cl co-transporter
LRMS	Low resolution mass spectrometry
m	Multiplet (NMR)
M	Molarity
Me	Methyl
MeCN	Acetonitrile
MDCK	Madin Darby canine kidney
MeOH	Methanol
min	Minutes
mol	Mole(s)
mmol	Millimole(s)
M_p	Melting point
MS	Electrospray (mass spectrometry)
m/z	Mass to charge ratio
NCC	Na-Cl co-transporter
NKCC	Na-K-Cl co-transporter
NDI	Naphthalenediimide
NMR	Nuclear magnetic resonance spectroscopy
PC	Phosphocholine
Pd/C	Palladium on carbon catalyst
PDI	Phenylenediimide
Ph	Phenyl
POPC	1-palmitoyl-2-oleoyl-*sn*-glycero-3-phosphocholine
ppm	Parts per million
Sat.	Saturated
SLC	Sodium lithium co-transporter protein
SPQ	6-Methoxy-N-(3-sulfopropyl)quinolinium
TBA	Tetrabutylammonium
TEA	Tetraethylammonium

Tren	Tris(2-aminoethyl)amine
UV-vis	Ultraviolet-visible spectroscopy
w.r.t.	With respect to

Contributions from other researchers

All of the work presented in this thesis was completed by the author (CJEH) unless otherwise stated. On these occasions, the work is attributed to the contributing researcher by the initials as abbreviated below:

SJM Stephen J. Moore
NA Nathalie Andrews
CCT Dr. Christine C. Tong

The work described in **Chapter 4** was contributed to by Jennifer L. Sutton, an undergraduate project student working under my supervision.

Chapter 1
Introduction

The development of synthetic transmembrane anion transporters is a relatively new and rapidly expanding area of supramolecular chemistry.[1-3] The transport of anions such as chloride and bicarbonate is an important research target due to the critical biological roles that these anions play and the diseases that result from the misregulation of their transport in the cellular environment. Over recent years a wide variety of synthetic anion transporters have been reported, from membrane spanning channels to simple amphiphilic anion receptors which function as anion carriers through the lipid bilayer.

1.1 Biological regulation of ion transport

The hydrophobic interior of the eukaryotic cell membrane enables its function as a barrier between intra- and extra-cellular media.[4] Cell organelles such as mitochondria and the Golgi apparatus are also membrane bound. The membrane is permeable to small, neutral molecules such as water and to gases such as oxygen and carbon dioxide. However, ionic species are unable to cross this barrier unassisted.

The transport of ions across cell membranes is important in many cellular processes. Ion gradients created by ion pumps ("active" membrane transporters which utilize ATP hydrolysis as an energy source) provide the electrochemical gradient to drive the action of passive ion channels and other transport proteins. These processes are used to regulate cell volume, transport nutrients into cells, to produce electrical signals, and to regulate secretions across epithelial layers.[5, 6]

The transport of ions in biological systems is enabled by membrane spanning proteins, which provide a pathway for ions to cross the bilayer. The movement of an ion into the hydrophobic interior of the membrane is highly unfavourable- the energy penalty

can be considered as equivalent to the desolvation energy of the ion. The transporter provides favourable interactions with the ion to compensate for this penalty during the translocation process, thus reducing the energy barrier. Fyles states that an ion transporter may be viewed as "a catalyst of translocation".[7] The most biologically prevalent anions are chloride, bicarbonate and phosphate, of which chloride is the least hydrophilic; thus, anion transporters are likely to be inherently selective for chloride.

Membrane transport may be *via* one of three mechanisms: uniport, in which a single species is transported; antiport, in which two species are transported in opposite directions, or symport, in which two species are transported in the same direction. These processes are represented in **Figure 1.1.** If considered as an isolated process, for the passive transport of an ion to occur, to maintain charge neutrality the ion may be transported by a symport mechanism, with an oppositely charged ion, or transported by an antiport mechanism, in the opposite direction to a similarly charged ion. However, natural transport proteins can passively uniport ions providing the necessary electrochemical gradient has been established by the action of other proteins.

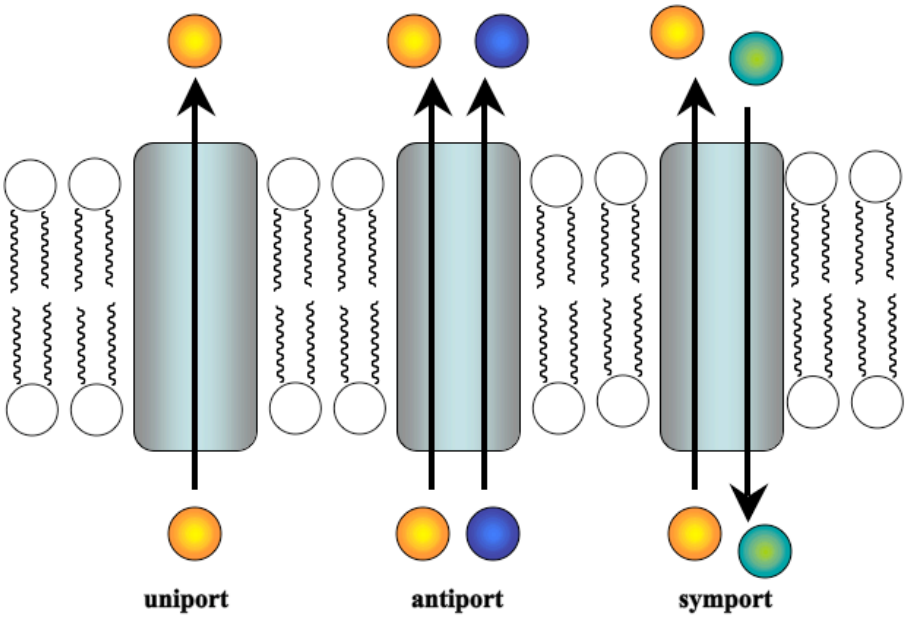

Figure 1.1 Transmembrane transport by uniport, antiport and symport processes.

In the cellular environment, the transmembrane transport of anions is crucial in the maintenance of vital concentration gradients used for signalling and cellular regulation. Of particular biological relevance is the transmembrane transport of chloride.

Biologically, chloride can be transported by a number of different membrane proteins.[1] CFTR (cystic fibrosis transmembrane conductance regulator), is a chloride uniport channel found in epithelial cells. It belongs to the family of cAMP activated channels. The open-close behaviour of this family of channels is regulated by ATP hydrolysis; however, once open they allow the transmembrane flow of anions down an electrochemical gradient.[8] The largest family of Cl^- channels are the ClC proteins. Some ClC proteins function as voltage-gated channels; others facilitate H^+/Cl^- co-transport. Ca^{2+} activated Cl^- channels are also known, which are regulated by an intracellular increase in free Ca^{2+} concentration. Other classes of Cl^- channels are regulated by cell volume, and are vital for the control of osmotic regulation, and by the interaction selectively with neurotransmitters such as glycine and γ-aminobutyric acid (GABA).

Additionally, there are anion transport proteins that do not form channels but instead bind the ions and facilitate their movement across the membrane by a conformational change. The co-transporter SLC12 proteins are responsible for the symport of chloride. Within this family, the NKCC (Na-K-Cl co-transporter) proteins facilitate the symport of 2 Cl^- anions with 1 Na^+ and 1 K^+ cation, while the NCC (Na-Cl co-transporter) proteins are responsible for Na^+/Cl^- symport and the KCC (K-Cl co-transporter) proteins facilitate K^+/Cl^- symport. These proteins are found in a range of tissues and are responsible for renal reabsorption of these ions. Cl^-/HCO_3^- anion exchangers (AEs) are proteins that facilitate the antiport of chloride and bicarbonate. The transport of bicarbonate is important for regulation of cellular pH as it forms a buffer in aqueous equilibrium with CO_2. In this way it is also crucial for cellular respiration, as the majority of CO_2 is transported to the lungs from respiring tissue in aqueous solution in the blood as HCO_3^-.

Biological misregulation of anion transport is associated with a number of diseases (channelopathies).[6, 9] Malfunction of Cl^- channels has ben linked with Bartter's syndrom, Dent's disease, Best disease, nephrolithiasis (kidney stones), osteopetrosis, and most notably, cystic fibrosis (CF). Misregulation of HCO_3^- transport is also associated with CF, along with diseases affecting the brain, heart and lungs.

1.2 Cystic fibrosis and anion transport

Cystic fibrosis (CF) is a genetic disorder associated with mutation of the gene responsible for CFTR production.[10] CF affects the epithelial cells of secretory organs including the lungs, pancreas, intestinal tract and sweat glands, causing the production of thick, sticky mucus. This mucus obstructs ducts and airways. The most common cause of mortality in CF patients is airway disease. In 2009 the median survival age for patients with CF was 35.9, although this is improving.[11] Children born with CF in the UK in the 2000s are now predicted to have a median survival into their 50s.[12]

When the gene responsible for CF was first identified, it was expected that it would code for a chloride channel because CF epithelia had been previously shown to be impermeable to chloride.[13] There are references in medieval folklore which state that infants who tasted "salty" were hexed as they were expected to die at an early age.[14, 15] Today, a common diagnostic test for CF is the measurement of chloride levels in sweat, with abnormally high chloride levels being indicative of CF.[16] These observations indicate the important role that homeostatic regulation of chloride levels plays in the disease.

Mutation of the gene which encodes for CFTR results in the production of CFTR which is defective, inhibiting transmembrane chloride transport *via* this pathway.[10] Individual cellular transport processes are often closely linked, with one transport process providing an electrochemical gradient to drive another. An example of this, in the epithelial cells of the pancreatic duct, is represented in **Scheme 1.1**.[6]

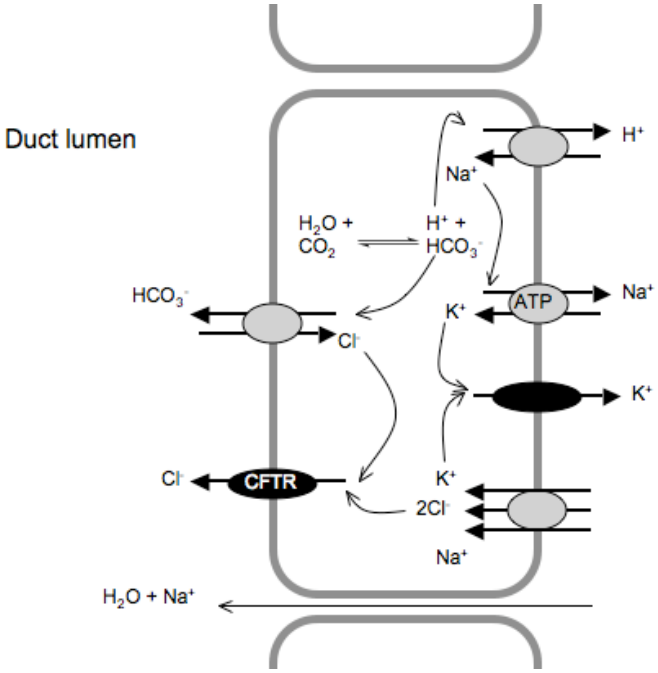

Scheme 1.1 A representation of the ion transport processes in the epithelial cells of the pancreatic duct.

CFTR mediates the excretion of Cl^- from the cell, which in turn drives the action of the Cl^-/HCO_3^- AE protein, causing HCO_3^- efflux. The consequences of this process then drive a variety of other ion transport processes. The net result of this combination of processes is the secretion of water due to the osmotic imbalance that is established; in CF sufferers, the defective nature of CFTR partially inhibits this transport cycle. The interlinked nature of these processes reveals that the disturbance of a single transport event (the transport of Cl^- by CFTR) can cause large disruptions in the regulation of a number of other electrochemical gradients. It is commonly thought that these disruptions lead to the secretion of less water and causes thicker, stickier mucus to be produced.[17] However, Quinton has hypothesized that the abnormal nature of the mucus is also due to reduced HCO_3^- levels affecting the structure of gel forming mucins which make up the mucus.[18] Both of these hypotheses indicate that the development of synthetic transporters for Cl^- and HCO_3^- is of interest due to their potential therapeutic application for CF sufferers; to replace the action of abnormal CFTR and to repair the damaged anion gradients.

1.3 Naturally occurring anion transporters

There are multiple example of natural products which have been found to mediate the transmembrane transport of cations, of which valinomycin (**Figure 1.2**) and gramicidin A are widely known.[19]

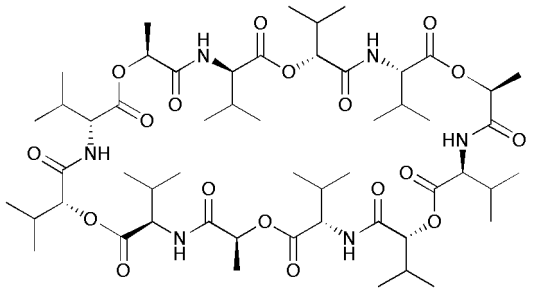

Figure 1.2 Valinomycin, a naturally occurring potassium ionophore and carrier.

However, there are comparatively few examples of naturally occurring, non-protein based anion transporters. The most intensively studied of these is the prodiginine family of natural products, of which the prodigiosins such as **1** (**Figure 1.3**) are members.

Prodigiosins are are a family of tripyrrolic red pigments isolated from microorganisms such as *Streptomyces* and *Serratia*.[20] These molecules have been found to induce a range of biological effects including antibiotic, antitumor and immunosuppresive activity.[21, 22] They have also been shown to bind H^+Cl^- by a combination of electrostatic interactions and hydrogen bonding as shown in **Figure 1.3**. Parr *et al*. have reported the crystal structure of the H^+Cl^- salt of a structurally similar synthetic prodigiosin shown in **Figure 1.3**.[23] This crystal structure shows the Cl^- anion coordinated by three hydrogen-bonding interactions from the protonated tripyrrolic scaffold. Prodigiosin **1** has also been shown to mediate efflux of chloride from phospholipid vesicles in the presence of a pH gradient.[24, 25]

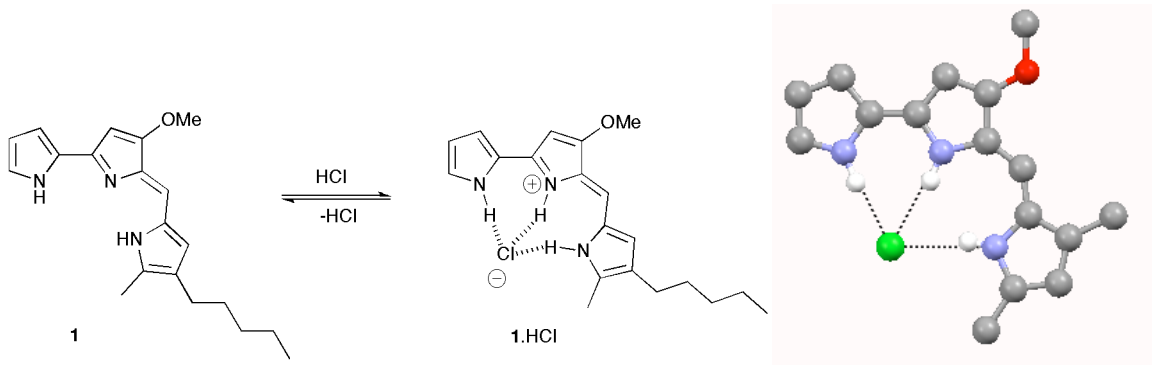

Figure 1.3 The complexation of H^+/Cl^- by prodigiosin **1** and the crystal structure of the H^+Cl^- salt of a structurally similar synthetic prodigiosin.

There are conflicting theories as to how prodigiosins cause the observed biological effects. In particular, it has been proposed that the observed anticancer activity is due to prodigiosin inducing copper mediated cleavage of double stranded DNA.[26-29] However, there is also evidence to suggest that the anticancer activity is related to anion transport capabilities. In particular, there is mechanistic evidence that anticancer treatments which have been found to enhance the drug sensitivity of multidrug resistant cancer cells and to cause their apoptosis function by causing the deacidification of cell organelles by H^+/Cl^- co-transport. [30]

Work by Sessler *et al*. investigated the H^+Cl^- binding and transport ability of a series of synthetic prodigiosin analogues (compounds **2**-**6**), by comparison to their *in vitro* anticancer activity.

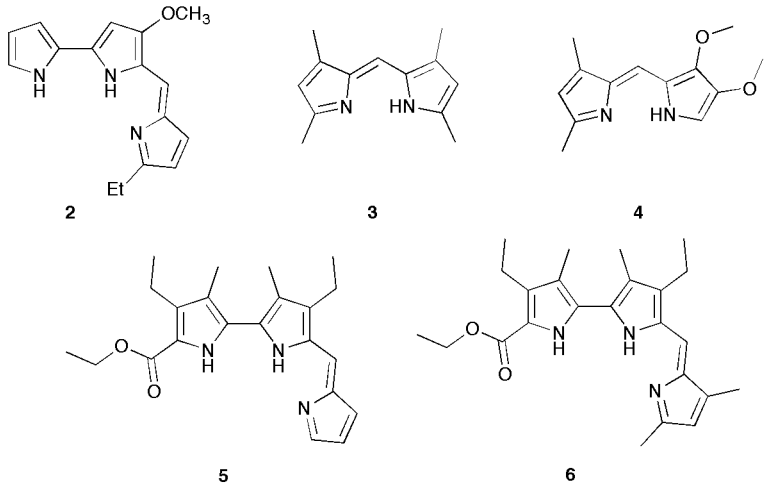

Binding studies performed by isothermal titration calorimetry (ITC) in MeCN indicated that chloride (added as the tetrabutylammonium salt) was bound only to a detectable

degree if the pyrrolic skeleton was protonated. X-ray crystal structure analysis of the HCl salts of these receptors indicated that Cl^- was bound in a 1:1 manner in the solid state by a combination of electrostatics and hydrogen bonding, as shown in **Figure 1.4**. The ability of **2**-**6** to mediate H^+Cl^- efflux from vesicles was investigated, and compound **2**, the most structurally similar to naturally occurring prodigiosins, was found to be the most effective carrier. The structurally simpler dipyrromethanes **3** and **4** were also found to be highly effective carriers. The *in vitro* anticancer activity of these receptors was assessed using a cell proliferation assay with human lung and prostate cancer cell lines. The order of anticancer activity was found to correlate with the observed relative H^+Cl^- transport activities. This significant finding supports the proposed mechanism of anticancer activity and indicates that anion transporters may have a future application as new anticancer therapies.

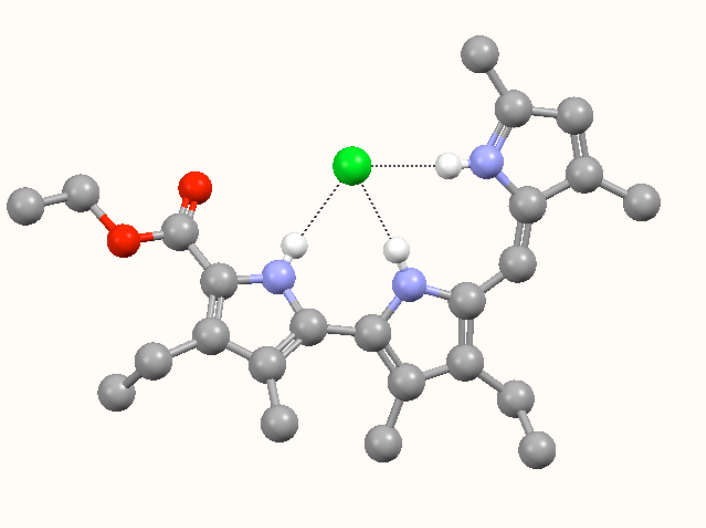

Figure 1.4 The crystal structure of **6**.H^+Cl^-.

J. T. Davis and co-workers have also demonstrated that prodigiosin **1** functions as an efficient Cl^-/NO_3^- antiporter in liposomal systems using a combination of fluorescence based vesicle studies with either HPTS to monitor the intra-vesicular pH or lucigenin to monitor the intra-vesicular chloride concentration. In each case the external anion was chloride. It was found that if the internal anion was sulfate, a small amount of chloride influx occurred accompanied by a decrease in internal pH, consistent with the influx of H^+Cl^-. However, if the internal anion was NO_3^- a larger amount of chloride influx was

observed and the internal pH remained constant, indicating a preference for Cl^-/NO_3^- antiport. Following on from this work, collaborative research from J. T. Davis and Gale found that prodigiosin **1** functions as a potent Cl^-/HCO_3^- antiporter. This high HCO_3^- transport activity was postulated to be a result of the proposed binding mode shown in **Figure 1.5**, utilizing the hydrogen bond donors and acceptors provided by the tripyrrolic skeleton.

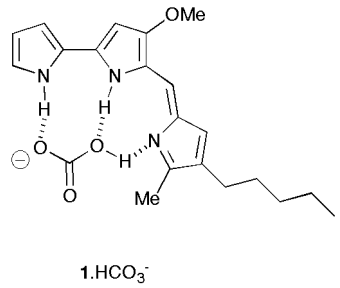

1.HCO_3^-

Figure 1.5 The proposed mode of prodigiosin **1** binding to HCO_3^-.

Structurally related to the prodigiosins is the tambjamine alkaloid family of natural products, which include compounds **7-10**. Recent work from Quesada and co-workers describes the chloride binding and transport properties of these molecules and synthetic analogues **11** and **12**.[31] ^{1}H NMR titration of the hyperchlorate salts of **7-12** with TBACl in DMSO-d_6 resulted in significant shifts of the resonances associated with the NH protons involved in the binding event up to the addition of 1 equivalent of anion. This indicated strong, 1:1 binding of chloride by these receptors in their protonated state. Compounds **7-12** were also found to function as efficient Cl^-/NO_3^- and Cl^-/HCO_3^- antiporters. The highest anion antiport activity was mediated by synthetic analogue **12**.

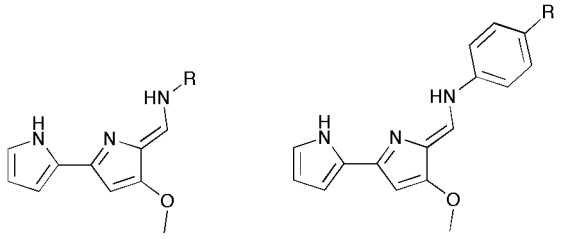

7 R = $CH_2CH(CH_3)_2$
8 R = Et
9 R = CH_2CH_2Ph
10 R = $C_{12}H_{25}$

11 R = H
12 R = ^{t}Bu

J. T. Davis and co-workers have investigated the anion transport activity of the sphingolipid C2-ceramide **13** (**Figure 1.6**).[32] This ceramide is known to form membrane

spanning pore assemblies when added to a lipid bilayer at concentrations above 10 mol% (with respect to lipid).[33] Davis *et al.* demonstrated that at concentrations lower than this, **13** can still facilitate anion transport. Compound **13** was found to mediate Cl^-/NO_3^- and Cl^-/HCO_3^- antiport in EYPC vesicle systems at a concentration of 1 mol%, well below the concentration required for pore formation. Additionally, this concentration of **13** was found not to facilitate the release of carboxyfluorescein from vesicles. Carboxyfluorescein is an anionic fluorescent dye that can be transported across lipid bilayers through large, membrane spanning pores. However, higher concentrations of **13** were found to mediate carboxyfluorescein transport. This indicates that at lower concentrations, **13** does not form pores and must therefore function as a mobile carrier. The 1,3-diol unit of ceramide **13** was found to be essential for its transport activity, as an analogous ceramide in which these OH groups were protected was found to be inactive. Evidence obtained from the ^1H NMR titration of **13** with TBACl in CD_2Cl_2 indicated that these OH groups were involved in hydrogen bond formation to Cl^- anions, in addition to the amide NH. This work highlights that predicting the mode of action of anion transporters within the bilayer is not always straightforward.

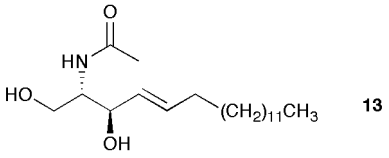

13

Figure 1.6 Ceramide **13**.

1.4 The design of synthetic anion transporters

While ceramide **13** is capable of transporting anions as both a pore and a mobile carrier, in general only one of these two possible transmembrane transport routes are utilized in transporter design. There are many examples of synthetic species that span the bilayer and form anion channels, thus mimicking the action of naturally occurring membrane proteins such as CFTR or gramicidin. Alternatively, smaller molecules have been found to function as mobile carriers. Carrier molecules are designed to bind the ion

and allow its passage across the bilayer by diffusion of the less lipophobic receptor-ion complex. Prodigiosins and tambjamines are naturally occurring examples of mobile carriers, while valinomycin is a well-known example of a potassium carrier. Ion channels may be formed by small molecules which can self assemble within the bilayer; thus, initial prediction of channel formation *vs* carrier activity is not always straightforward. However, there are design principles that are distinct to the development of each class of transporter.

The mode of action of mobile carriers requires that they are able to form a complex with the anion of interest. It is therefore unsurprising that many anion carriers draw inspiration from the well-established field of anion complexation chemistry.

1.5 Anion receptor chemistry

The design of selective hosts for anions is a vast and ever expanding area of supramolecular chemistry.[34-42] The most common means of complexing an anion through non-covalent interactions is by hydrogen bonding. Convergent hydrogen bond donor motifs can be used to selectively bind anions of interest. The most commonly utilized hydrogen bond donors for this purpose are NHs, including amides, ureas, pyrroles, indoles and carbazoles, and combinations of these functionalities. Anion binding by CH hydrogen bond donors is also known; in particular, the CH bond in the 5-position of 1,2,3-triazoles have been reported to form hydrogen bonds of similar strength to amides.[43] Other principles of host-guest supramolecular chemistry can also be applied, including binding site preorganization, chelate and macrocyclic effects. There is now a vast library of literature anion receptors based on hydrogen bond donor motifs which may be of use in the design of new anion carriers. The synthetic prodigiosin and tambjamine analogues described above utilize pyrrole and amide hydrogen bond donors, which are supplemented at acidic pH by an additional hydrogen bond donor resulting from protonation of a basic pyrrolic nitrogen and the corresponding electrostatic attraction to the now cationic receptor.

1.6 From anion receptors to anion carriers

The challenge of designing anion carriers relies not just on complexation of the anion, but also on the lipid-solubilization of the resulting host-guest complex. In addition to a convergent array of hydrogen bond donors for binding the anion, it is desirable for potential anion carriers to possess a certain degree of lipophilicity in order to aid the partitioning of the receptor and the receptor-anion complex within the lipid bilayer. Hydrogen bond donors make the anion binding site polar and hydrophilic- thus, successful carriers have been developed by choosing a scaffold for this site lipophilic enough to counter the strong interactions between the binding site with the aqueous phase, or by effectively screening the binding site, and by extension, the anion from the bilayer.

Some of the first and amongst the most effective anion carriers reported to date are the series of cholapods developed by A. P. Davis and co-workers. These cholic acid derivatives, of the general form shown in **Figure 1.7**, combine a lipophilic steroid skeleton with pendant urea or thiourea arms for anion complexation.

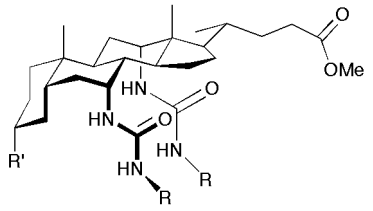

Figure 1.7 The general structure of the cholapods reported by A. P. Davis *et al.*

Earlier work from the same authors had shown carbamoyl-functionalized analogues to form extremely strong complexes with Cl^- and Br^- in chloroform solution.[44, 45] Bis(phenyl)urea derivatives had also been shown to interact strongly with phospholipids and to facilitate flippase activity - the translocation of phospholipid molecules between leaflets of a lipid bilayer - due to strong interaction of the phosphate head groups of the phospholipid molecule.[46, 47] The intrinsic lipophilicity of the cholapod skeleton prompted the authors to assess the possibility that this group of receptors could "shuttle" anions across phospholipid bilayers. Initial investigations found that cholapod **14** (shown in

Figure 1.8) facilitated Cl^-/NO_3^- exchange across vesicle bilayers, while **15-18** were less effective.[48] This correlated with the strength of anion binding by these receptors in wet chloroform (measured by Cram's extraction technique[49, 50] using TBA^+ salts), where compound **14** showed the strongest binding of Cl^- and NO_3^-. The chloride efflux mediated by these receptors was almost entirely inhibited if the external NO_3^- was replaced with SO_4^{2-}, providing evidence for an anion antiport mechanism. A fluorescence transport assay using the potential sensitive dye Safranin-O indicated that addition of receptor **19** to a suspension of Cl^- containing vesicles in which the external anion was SO_4^{2-} induced a transmembrane electric potential due to a small amount of chloride efflux with no corresponding influx of an alternative anion. Cl^- transport was also demonstrated using ^{35}Cl NMR techniques. A mobile carrier mechanism was supported by the observation that chloride efflux in vesicles composed of DPPC was inhibited below the gel/liquid phase transition temperature. Finally, receptor **14** was found to mediate Cl^- transport in Madin Darby canine kidney (MDCK) epithelia using the Ussing chamber technique, in which a layer of cells is grown on a support and the transepithelial current due to ion transport is monitored. The observed current was, as expected, highly anion dependent.

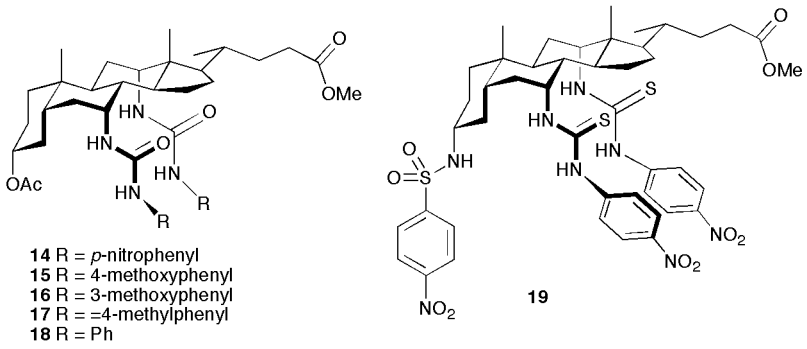

Figure 1.8 The structures of some early cholapod anion carriers.

Further investigation revealed that the anion transport properties of this design could be enhanced by further improving the anion binding strength. Thioureas have been found to bind anions more strongly than analogous ureas due to the greater acidity of the hydrogen bond donors.[51, 52] Compound **19** was found to have a chloride affinity 200 times greater than **15** under the same conditions, and was also found to mediate Cl^-/NO_3^- exchange more effectively.[53] However, the high lipophilicity of this compound prevented

the investigation of its anion transport unless it was preincorporated into the vesicle membranes, as addition of a THF solution of **19** to an aqueous suspension of vesicles resulted in its precipitation.

Building on this work, A. P. Davis *et al.* went on to study in detail a larger series of 12 new cholapods in order to further investigate the effect of small structural changes on the cholapod transport efficiency.[54] The most efficient carrier investigated in this work was compound **20** which, when preincorporated into the lipid bilayer, was remarkably potent, displaying activity at loadings as low as 1:250 000 (carrier:lipid). In general, increasing the anion affinity of the carrier resulted in higher carrier efficiency. For example, examining the effect of modifying the urea groups in positions 7 and 12 from phenyl urea (compound **16**) to *p*-nitrophenyl urea (compound **14**) to *p*-nitrophenyl thiourea (compound **20**) resulted in an observed increase in transport efficiency as expected from the increased anion affinities. However, modifying the substituent in the 3-position resulted in variation of transport efficiency which did not correlate with anion binding strength. Cationic cholapods such as compound **21** were found to be largely inactive. This observation was attributed to the formation of strong, electroneutral chloride complexes that only slowly release anions back into the aqueous phases. Experiments with eicosyl esters such as **22** did not show enhanced transport efficiency from their methyl ester analogues, thus implying that variation of carrier lipophilicity was not a contributing factor to the observed transport trends. Due to the intrinsically high lipophilicity of these carriers, it is likely that all of these receptors are fully contained within the vesicle bilayer.

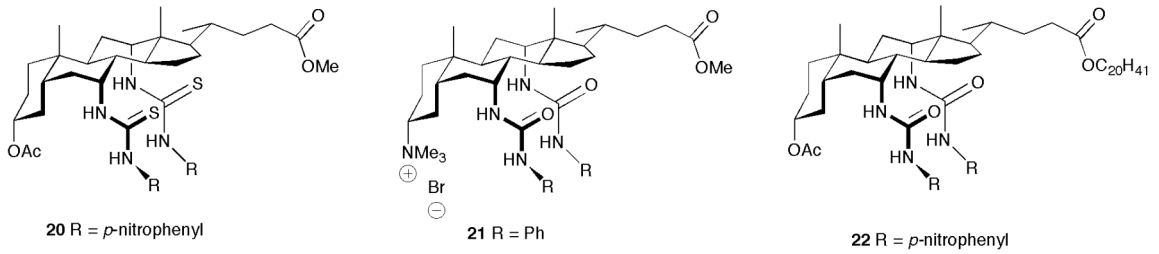

20 R = *p*-nitrophenyl **21** R = Ph **22** R = *p*-nitrophenyl

Figure 1.9 Structural variations on the cholapod scaffold.

More recently, work from the same authors has described the cyclization of the cholapod scaffold into so-called "cholaphanes" such as **23**.[55] These molecules were found to exhibit higher transport efficiencies than their acyclic analogues. This was attributed to greater binding site encapsulation to better shield the anion from the apolar interior of the vesicle membrane. The cholaphanes were found to bind chloride slightly more strongly than acyclic analogues, but nitrate was bound more weakly; this is most likely a result of size selectivity. Simplification of the cholic acid skeleton to a *trans*-decalin scaffold (compounds **24**) has also resulted in highly potent carriers capable of transporting chloride at a 1:25 000 (carrier:lipid) ratio.[56]

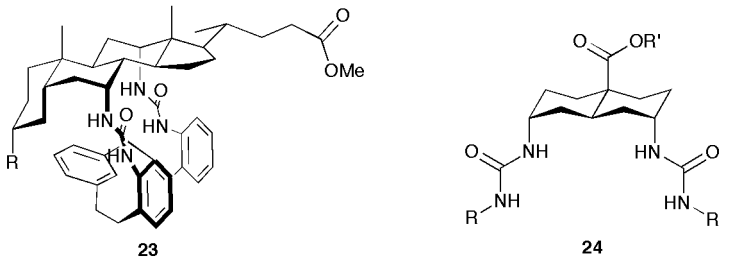

Figure 1.10 The recently published cholaphane and *trans*-decalin, inspired by the cholapod design.

The rigidity of the cholapod framework results in a well preorganised binding site for anions. It is a well established concept within host-guest chemistry that preorganisation of the binding site leads to more favourable guest binding.[57] The benefits of binding site preorganization in anion carriers has also been explored by J. T. Davis, Gale, Quesada and co-workers. They reported that simple hydroxyisophthalamide **25** functioned as a highly efficient Cl^-/NO_3^- antiporters in vesicle systems.[58] The binding site of these receptors is preorganised by intramolecular hydrogen bonding interactions, as shown in **Figure 1.11**, as evidenced by the X-ray crystal structure of the free receptor. Conversely, receptors **26** and **27** are not preorganised in this way. The crystal structure of **27** indicates that intramolecular hydrogen bonding interactions cause the free receptor to adopt a conformation which disfavours anion binding. Consequently, **23** was found to interact more strongly with TBACl in CD_3CN (demonstrated by ^1H NMR titration). **26** and **27** also exhibited no anion transport activity. Building on this work, **26** was reported by the same authors as an effective Cl^-/HCO_3^- antiporter.[59]

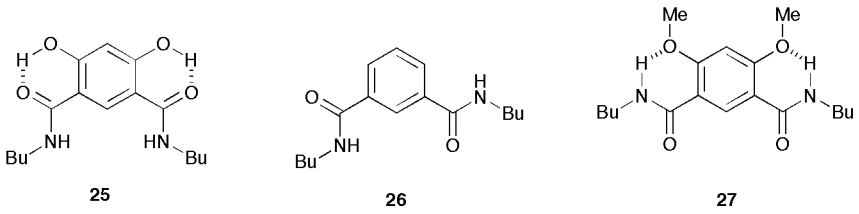

Figure 1.11 Isophthalamide based receptors **25**-**27** adopt conformations according to intramolecular hydrogen bonding.

Meso-octamethylcalix[4]pyrrole **28** was first synthesized by Baeyer in 1886 by the acid catalyzed condensation of acetone and pyrrole.[60] In 1996, J. L. Sessler and co-workers first described the use of **28** and analogue **32** as receptors for F^- and Cl^-. [61]The interaction of these anions with the calix[4]pyrroles was investigated by ^1H NMR titration with the anion tetrabutylammonium salts in CD_2Cl_2, and by X-ray crystallography of the complexes formed on addition of the TBA^+ salts. They found that in the solid state, free calix[4]pyrrole **28** adopts a 1,3-alternate conformation, but on binding Cl^- the ligand adopts a cone-like conformation with all of the pyrrole NHs converging to complex the anion.

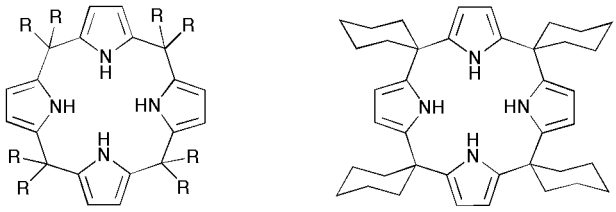

Figure 1.12 Calix[4]pyrroles.

Further investigation revealed that calix[4]pyrrole **28** can function as an ion pair receptor for cesium halides, as Cs^+ cations may be bound in the cone-like cavity formed when the calix[4]pyrrole complexes the anion, both in solution and in the solid state.[62] The crystal structure of **28**.Cs^+Cl^- is shown in **Figure 1.13**. This ion pair complexation prompted a collaborative project between Sessler, and Gale to study the ability of calix[4]pyrroles **28**-**32** to transport ion pairs across lipid bilayers.[63] Compound **28** was

found to efficiently mediate the efflux of chloride from CsCl containing vesicles. This activity was mostly independent of the external anion; only a small increase in transport activity was observed by exchanging the external anion from SO_4^{2-} to NO_3^-. This implied a predominant Cs^+/Cl^- symport mechanism. The transport was highly cation dependent; negligible transport was observed in the absence of Cs^+. This is unsurprising as the smaller group I cations are not bound in the cone-like cavity of calix[4]pyrroles as they are of a less complementary size and are more hydrophilic. The inability of calix[4]pyrroles to facilitate a Cl^-/NO_3^- antiport mechanism in the absence of Cs^+ most likely reflects the poor binding of NO_3^- and the lower lipophilicity of the anion-receptor complex when a cation is not coordinated to provide charge neutrality. Interestingly, calix[4]pyrroles **29-31** showed no Cs^+/Cl^- symport activity, while **32** mediated only small amounts of CsCl flux. This may be due to poorer solubility of these compounds under the conditions of the assay.

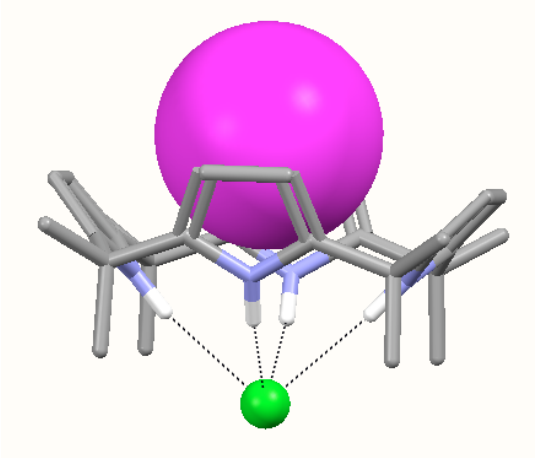

Figure 1.13 The crystal structure of **28**.Cs^+Cl^-. The Cs^+ cation has been drawn in space filling mode for clarity.

There has been intensive study of the synthesis and anion binding properties of strapped calix[4]pyrroles. Many groups have found that strapped calix[4]pyrroles exhibit stronger chloride binding. This is attributed to greater anion encapsulation and, if applicable, the formation of additional hydrogen bonds from the strap. Gale and co-workers report the synthesis of 1,2,3-triazole strapped calix[4]pyrrole **33** (**Figure 1.14**).[64] The binding of TBACl by **33** was investigated by ITC in MeCN and DCM. In both cases, Cl^- was found to be complexed more strongly by **33** than by unmodified calix[4]pyrrole

28. Like compound **28**, compound **30** was found to mediate Cs^+/Cl^- symport. However, it was also found to promote Cl^- efflux from vesicles containing other group I metal chloride salts. In the presence of larger cations such as Cs^+ and Rb^+, the transport rates were less dependent on the nature of the external anion; however, when the internal cations were smaller (K^+ or Na^+) there was a larger reduction in transport rate observed on exchanging the external NO_3^- for SO_4^{2-}. These observations indicated that both M^+/Cl^- symport and Cl^-/NO_3^- antiport processes could be facilitated by **33**. Larger, more charge diffuse cations were preferentially transported by a symport mechanism, thus the rate was less dependent on the external anion; more hydrophilic cations were energetically more difficult to transport, thus a predominant antiport mechanism was observed in these cases. The ability to facilitate an anion antiport mechanism may be due to the stronger anion binding and greater anion encapsulation by strapped calix[4]pyrroles, therefore more effectively screening the charge of the anion from the hydrophobic interior of the bilayer. Importantly, it also demonstrated that functionalization of the calix[4]pyrrole scaffold can result in modulation of transport properties and facilitate alternative transport mechanisms.

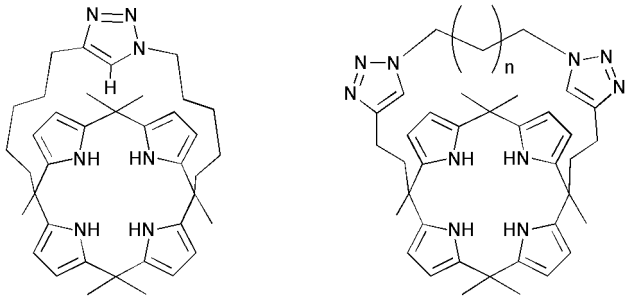

33

34 n = 1
35 n = 2
36 n = 3

Figure 1.14 The triazole strapped calix[4]pyrroles reported by Gale *et al.*

Further to this work, P. A. Gale *et al*. reported the synthesis and anion binding and transport properties of strapped calix[4]pyrroles **34-36**, containing two 1,2,3-triazole groups to aid anion complexation joined with an alkyl chain of varying length (**Figure 1.14**).[65] Binding studies conducted by ITC in MeCN with TBACl indicated that all of these receptors bind Cl^- similarly strongly. The crystal structure of the chloride complex of **36** is shown in **Figure 1.15** and shows that the calix[4]pyrrole has adapted the "cone"

conformation on binding to the anion. In this structure, the 1,2,3-triazole $CH\cdots Cl^-$ bond lengths are 2.788 Å and 2.753 Å, with both of these CH donors orientated towards the anion. Chloride transport studies revealed that a preference for either a Cs^+/Cl^- symport or a Cl^-/NO_3^- antiport mechanism varied across the series, although each receptor seemed to be capable of both. Compounds **34** and **35** operated predominantly by a Cs^+/Cl^- symport system but were able to facilitate low levels of anion antiport. However, the chloride efflux mediated by compound **35** was found to be far less dependent on the encapsulated M^+ cation implying a shift towards a favoured anion antiport mechanism. Chloride transport by compound **35** was also inhibited the most when the external anion was SO_4^{2-}. It was concluded that the observed trends in transport efficiency could be due to the partitioning of the receptor or receptor-anion complex with the aqueous or lipid phase, or the varying mobility of the receptors in the lipid phase, or a combination of these factors. The results did demonstrate that transport efficiency is not only related to anion binding strength.

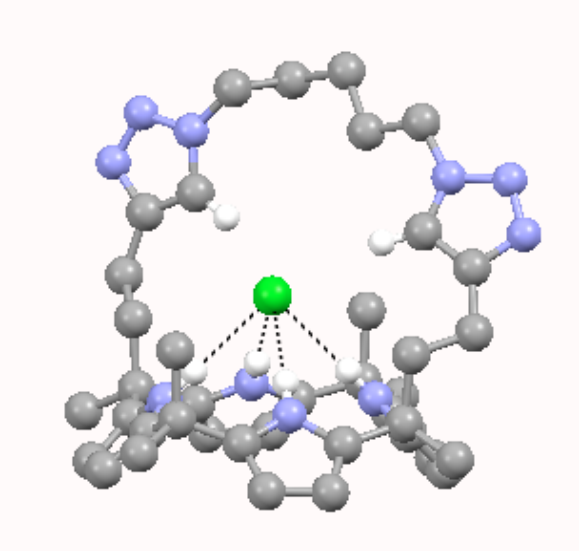

Figure 1.15 The crystal structure of the Cl^- complex of calix[4]pyrrole **35**.

Fluorination of aromatic structures is thought to increase their lipophilicity.[66] Additionally, fluorination of the scaffold of an anion receptor can lead to stronger binding due to the electron withdawing nature of the fluorine substituents. The anion transport activity of octafluorocalix[4]pyrrole **36** was investigated by Sessler and Gale.[67] They found that Cl^- efflux mediated by **36** from vesicles suspended in $NaNO_3$ was almost

completely independent of the encapsulated anion, implying a purely anion antiport mechanism. Compound **36** was also found to mediate Cl^-/HCO_3^- exchange; the first example of a calix[4]pyrrole to facilitate this mechanism.

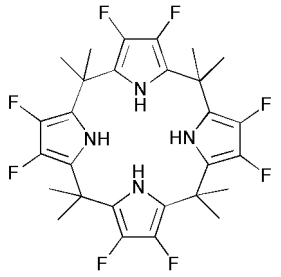

36

Figure 1.16 Octafluorocalix[4]pyrrole **36**.

Gale and co-workers have investigated the anion transport properties of a series of ureas and thioureas based on the tren (tris(2-aminoethyl)amine) scaffold.[68] They found that urea **was** inactive for Cl^- transport, while **38** mediated only low levels of Cl^-/NO_3^- and Cl^-/HCO_3^- exchange. However, thioureas **39** and **40** were effective Cl^-/NO_3^- and Cl^-/HCO_3^- antiporters. As mentioned previously, thioureas have been found to bind anions more strongly than their urea analogues; however, in this case the urea based receptors were found to form stronger 1:1 complexes with TBACl (binding constants of 658, 830, 447 and 191 M^{-1} respectively, calculated by ^{1}H NMR titration in DMSO-d_6/H_2O (0.5 %)). Thus, the better transport activity of the thiourea analogues could not be explained by stronger Cl^- binding. The authors concluded that the greater lipophilicity of the thiourea carriers resulted in better partitioning of the anion- carrier complex with the lipid bilayer.

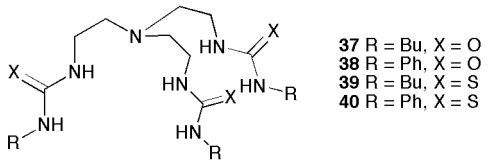

37 R = Bu, X = O
38 R = Ph, X = O
39 R = Bu, X = S
40 R = Ph, X = S

Figure 1.17 Urea and thiourea receptors based on the tren scaffold.

The crystal structure of the carbonate complex of receptor **40** (grown from a DMSO solution of the receptor with $TEAHCO_3$) shows a 2:1 host:guest stoichiometry in the solid state, although the solution phase testing indicated a 1:1 complex formation with

bicarbonate. This structure shows that the anion is almost fully encapsulated by the receptors and is bound by 12 hydrogen bonds and a number of longer range interactions. The anion, which was added as HCO_3^- has presumably been deprotonated by free anion in solution to give the CO_3^{2-} complex. This effect has been previously observed by Gale *et al.*[69-71]

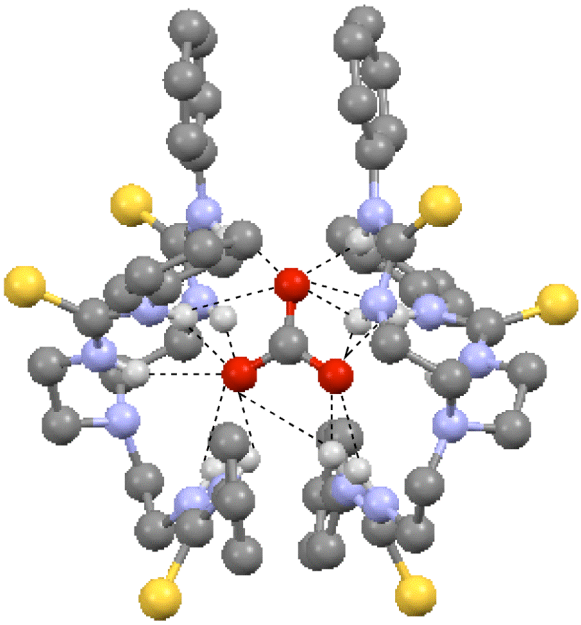

Figure 1.18 The carbonate complex of tren receptor **40**.

One approach to ensure the effective partitioning of a receptor within the lipid bilayer is to choose a naturally occurring scaffold with desirable partitioning properties. B. D. Smith and co-workers have synthesized the urea functionalized phospholipid **41** which can be preincorporated into the vesicle bilayers and facilitate anion antiport *via* a novel "relay" mechanism as represented in **Figure 1.19**.[72] The authors found that Cl^-/NO_3^- antiport was only observed if the receptor was preincorporated into the vesicle membrane, due to the necessity of the receptor locating within both leaflets of the bilayer for this mechanism to occur. This design combines a stationary scaffold with a mobile "arm" which can complex and transport the anion, thus employing effective strategies from both channel and carrier design.

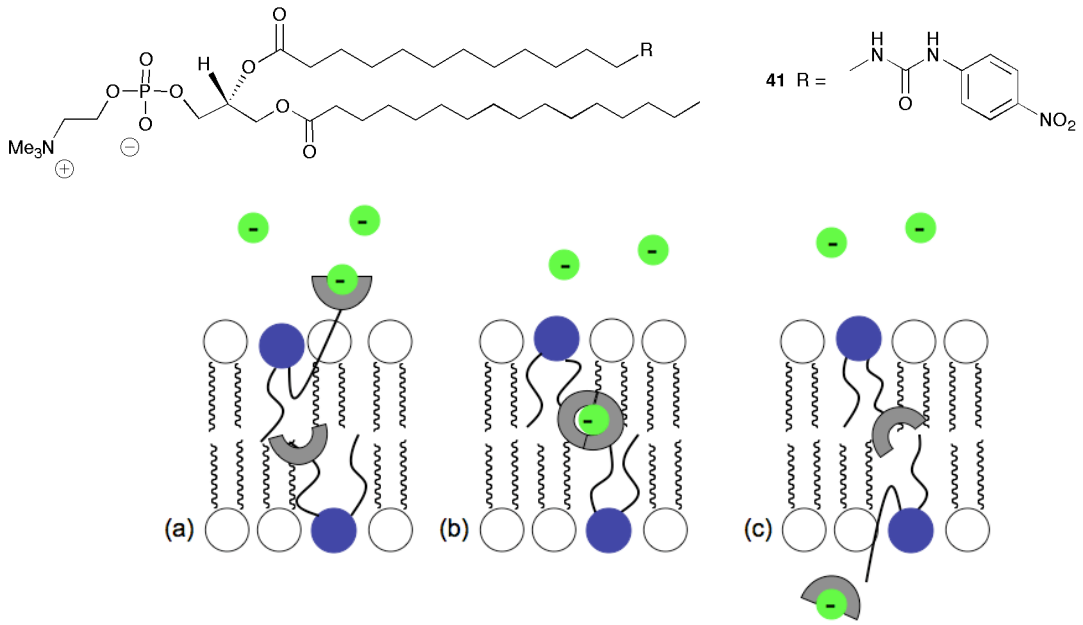

Figure 1.19 A representation of the proposed relay mechanism of Cl^- transport by phospholipid based receptor **41**: (a) Coordination of the anion from the source phase by the urea functionalised arm of **41**; (b) transfer of the anion to a second receptor molecule located in the opposite leaflet of the bilayer; (c) release of the anion into the receiving phase.

Anion receptors which facilitate an anion antiport mechanism are able to bind and transport both components of the antiport process. Similarly, receptors designed to facilitate a symport process often provide a binding site for both the anion and the cation of interest. Calix[4]pyrroles are ditopic Cs^+Cl^- receptors and facilitate a Cs^+/Cl^- symport mechanism. Similarly, B. D. Smith *et al.* have investigated the ion pair binding and transport properties of ditopic macrobicycle **42**.[73] This receptor contains an isophthalamide unit for anion complexation and a crown ether unit for binding an alkali metal cation. It was found to bind K^+Cl^- and Na^+Cl^- as contact ion pairs in DMSO solution; additionally, the binding of Cl^- to the receptor was enhanced if K^+ or Na^+ was already complexed by the receptor. **42** was found to mediate K^+/Cl^- and Na^+/Cl^- symport from vesicles; this process was not dependent on the nature of the external anion. However, no transport was observed in the presence of Cs^+Cl^-, as Cs^+ has been found to be too large to bind within the crown ether unit. Interestingly, addition of the individual cation and anion binding components of this receptor **43** and **44** did not mediate Cl^- transport; thus the ditopic nature of this receptor was shown to be highly important.

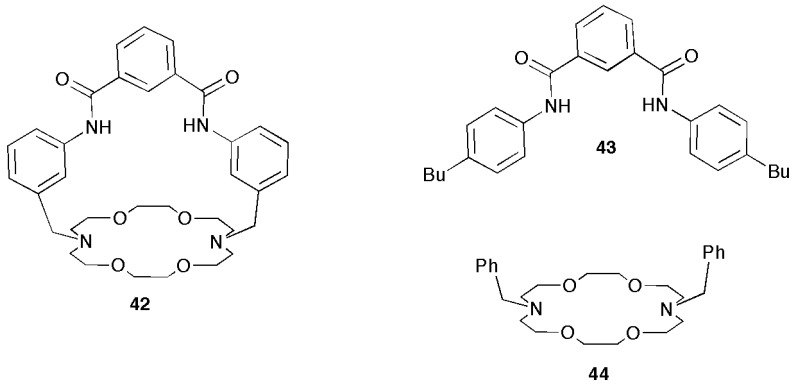

Figure 1.20 Ditopic receptor **42** transports NaCl and KCl as ion pairs.

However, recent work from Gale and co-workers has described a "dual host" approach to salt transport, in which the individual components of a symport pair can be transported by different ionophores in two complementary uniport processes.[74] Valinomycin was chosen as a highly potent K^+ carrier; in combination with known Cl^- transporters, Cl^- efflux from KCl containing vesicles was observed. A mixture of valinomycin and strapped calix[4]pyrroles **33** and **36** was shown to promote K^+/Cl^- more effectively than the sum of the activity of the individual receptors; however, unmodified calix[4]pyrrole **28** was found not to promote this mechanism. The authors reasoned that the transport activity of calix[4]pyrrole **28** is highly dependent on the presence of Cs^+, thus it could not function as a Cl^- uniporter; however, as **33** and **36** are able to facilitate anion antiport, they were thought to be more able to facilitate the movement of a single anion across the bilayer at any one time.

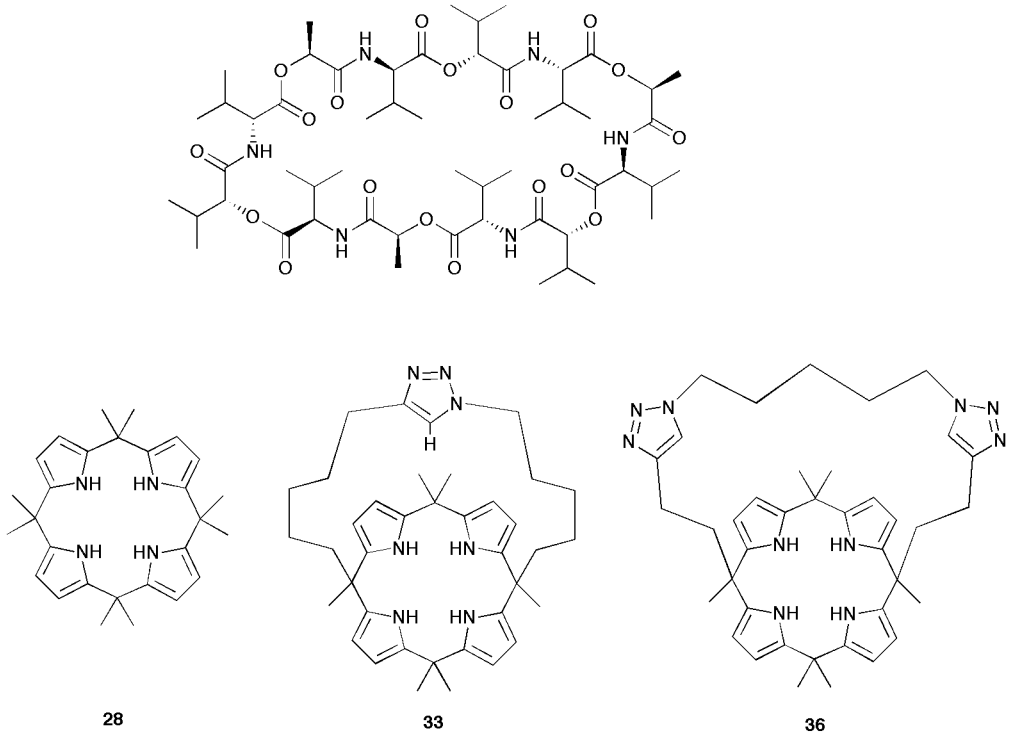

Figure 1.21 Valinomycin and the calix[4]pyrroles used for the dual host transport of K^+/Cl^-.

More recently, Gale *et al.* have applied the dual host approach to the Cl^-/HCO_3^- antiport process.[75] In this work, **33** and **36** were once again employed to mediate Cl^- uniport, although these receptors were not capable of HCO_3^- transport. Based on the previous finding that simple thioureas are effective Cl^-/HCO_3^- antiporters,[76] **45** and **46** were chosen to mediate the transport of HCO_3^-. The Cl^-/HCO_3^- antiport activity of **45** and **46** was enhanced in the presence of **33** and **36**, with the combined action of these receptors mediating more Cl^- flux than the summed activity of the individual receptors. Again, no such enhancement was observed on addition of calix[4]pyrrole **28**.

.

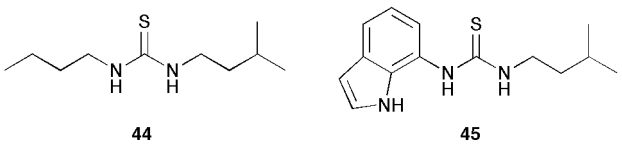

Figure 1.22 The simple thioureas examined as part of a dual host system for Cl^-/HCO_3^- antiport.

The concept of designing symporters which contain a binding site for both components of the transport process can be extended to H^+/Cl^- co-transport. Prodigiosin **1** contains a basic pyrrolic N (a binding site for H^+). This inspired collaborative work from Gale, B. D. Smith and co-workers to investigate the H^+/Cl^- co-transport activity of some receptors containing a methylimidazole group as a basic site for H^+ binding to mimic the action of prodigiosin. Initially, the authors discovered by ^1H NMR titration in CD_3CN that the binding of Cl^- by **47** was enhanced when the receptor was protonated in the presence of 1 equivalent of HPF_6 (K_a was increased from 60 to 397 M^{-1}).[77] However, no such enhancement was observed for receptor **48**, which lacked a basic site. Correspondingly, of these two receptors only **47** was found to mediate Cl^- efflux from vesicles containing NaCl suspended in $NaNO_3$ using an ISE method. This efflux was highly pH dependent. The greatest Cl^- efflux was observed in the presence of a pH gradient (inside = pH 4, outside = pH 6.7), indicating that a H^+/Cl^- co-transport mechanism was operating. However, in the absence of a pH gradient (inside = pH 7.2, outside = pH 7.2) reduced Cl^- efflux was observed, indicating that a Cl^-/NO_3^- mechanism was also possible. When the intra- and extra- vesicular solutions were acidic, no transport was observed. The authors reasoned that, when the external solution was acidic no transport occurred because the externally added receptor would become protonated in the extravesicular solution and become too hydrophilic to pass through the vesicle membrane.

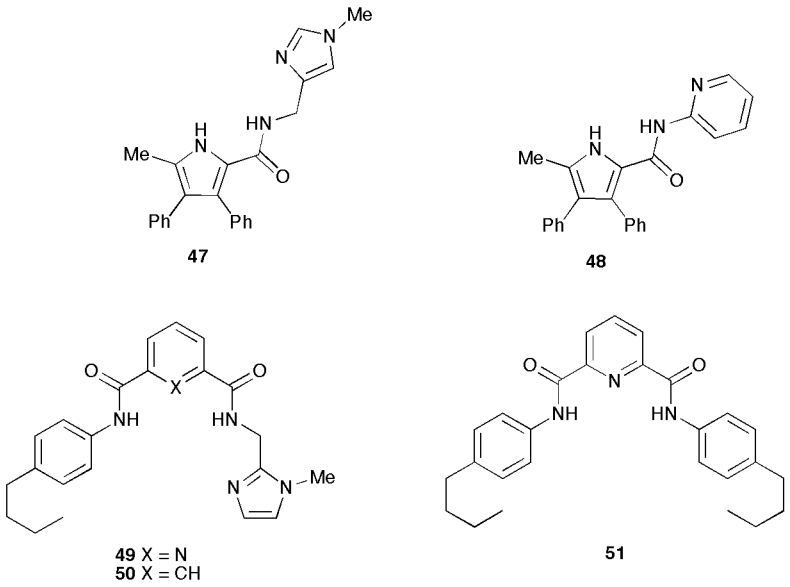

Figure 1.23 The synthetic prodigiosin mimics reported by Gale and co-workers.

Further to this work, the same authors investigated the transport activity of receptors **49** – **51**.[78] They found that receptor **49** exhibited an enhanced affinity for Cl^- in the presence of HPF_6 (in DMSO-d_6/H_2O (0.5 %)). The stronger binding of H^+/Cl^- by **49** over **50** was attributed to the preorganizational effect inferred over the binding site by intramolecular hydrogen bonding as shown in **Figure 1.24**. In the presence of a pH gradient, **49** was found to be the most effective Cl^- transporter from vesicles containing NaCl suspended in $NaNO_3$. **50** was also found to mediate H^+/Cl^- co-transport to a lesser degree, while **51**, which does not contain a protonatable site, did not mediate Cl^- transport under these conditions. In the absence of pH gradient, only **49** was found to mediate Cl^- efflux from vesicles, but less effectively than in the presence of a pH gradient; thus, **49** was the only receptor to also mediate Cl^-/NO_3^- antiport.

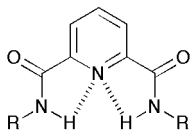

Figure 1.24 The preorganization of the anion binding cleft in diamides of picolinic acid.

D. K. Smith *et al*. have reported that anion receptors based on the tren scaffold can facilitate the transport of H^+/Cl^- through a non-polar phase using a U-tube experiment.[79] The carrier efficiency was found to correlate with the binding site encapsulation, indicating that the most effective carriers could screen the charge of the anion from the hydrophobic organic phase. J. T. Davis and co-workers have also utilized tren as a scaffold for H^+/Cl^- co-transport.[80] They used two convergent catechol groups as hydrogen bond donors to complex the anion. The role and substitution pattern of these OH hydrogen bond donors were found to be highly important, as analogues **55** and **56** exhibited no anion transport activity. The positions of the OH hydrogen bond donors in analogue **56** are less convergent than those in receptor **52**, thus anion binding is less favourable. Receptor **52** was found to mediate a variety of H^+/X^- co-transport processes in the presence of a pH gradient, using vesicles containing HPTS. Analogues **53** and **54** with shorter and longer alkyl substituents were found to be less active. This was attributed to poorer partitioning with the bilayer. The anion selectivity was found to follow the Hofmeister series. The Hofmeister series orders ions according to their ability to cause proteins to precipitate from aqueous solution.[81] The precipitation of the protein is caused by the strong competing interactions between the ion and the water, thus increasing the effective concentration of the protein. Thus, the Hofmeister series can be viewed as ranking the ions according to the strength of their interaction with water. This is a highly relevant concept when considering the transmembrane transport of ionic species, as to cross the lipid bilayer the ion must be dehydrated; the stronger the interaction of the ion with water, the less favourable this process will be.

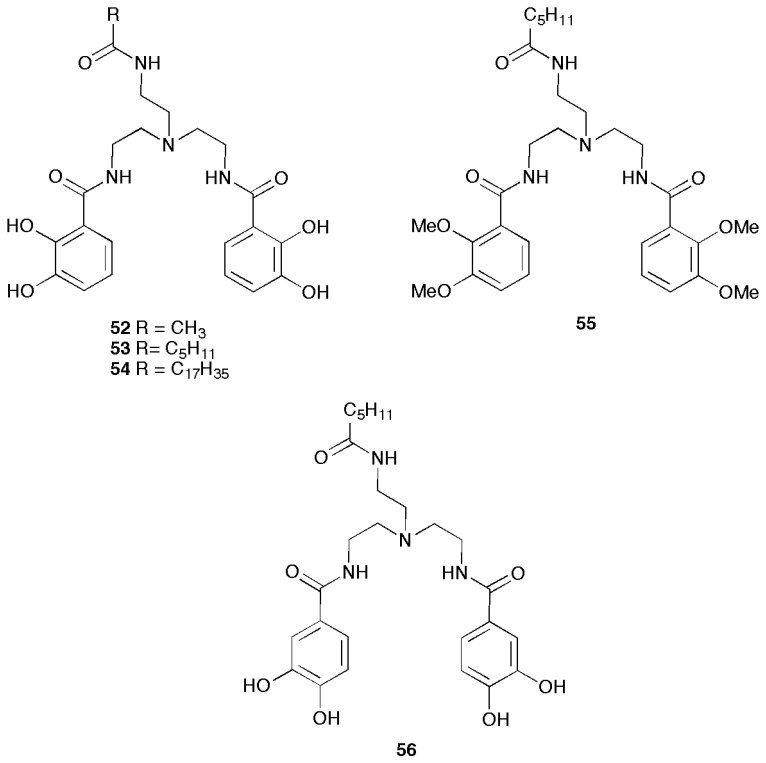

Figure 1.25 The catechol substituted tren receptors reported as H^+/X^- co-transporters.

1.7 Synthetic anion channels

The design of ion channels requires a different approach to that of mobile carrier design. In contrast to mobile carriers, the ability of a synthetic channel to bind the anion of interest is less important. The key function of a channel is to form a structure which will span the membrane, either as a single entity or a self assembled pore, and allow the passage of the anion by a lower energy pathway. CFTR is an example of a membrane spanning chloride channel.

The determination of the crystal structures of several naturally occurring protein based channels has provided insight into their action, as reviewed by Gouax and MacKinnon.[82] Transport proteins have been found to contain water filled pores which function as an entrance to the channel for hydrated ions. The ions must subsequently pass a narrower portion of the channel interior causing dehydration. This also functions as an ion selectivity filter on the basis of size exclusion.

One approach to channel design is to try to mimic the function and structure of naturally occurring peptide based ion channels. The first reported development of a series

of synthetic chloride channels was reported by Tomich *et al*., who have extensively investigated the chloride conducting properties of various membrane spanning amino acid sequences derived from the second transmembrane segment of the brain glycine receptor, M2GlyR (compound **57**, **Figure 1.26**). The unmodified sequence was known to form anion channels in lipid bilayers, single cells and epithelial monolayers;[83, 84] however, the poor aqueous solubility of this species and its propensity to aggregate in solution limited its effectiveness. This prompted Tomich *et al.* to investigate the application of some synthetic analogues of this sequence.[85-90] Over 200 peptides based on this sequence were synthesized by systematic modification of individual amino acids within the sequence, one of which is shown in **Figure 1.26**. These synthetic peptides were analyzed for increased water solubility, decreased aggregation and anion transport capabilities.[85, 91] For example, C-K_4-M2GlyR (compound **58**, **Figure 1.26**) was found to have increased water solubility due to the presence of the additional lysine subunits.

M2GlyR **57** H_2N-PARVG LGITT VLTMT TQSSG SRA-COOH

C-K_4-M2GlyR **58** H_2N-PARVG LGITT VLTMT TQSSG SRAKK KK-COOH

Figure 1.26 The structure of M2GlyR **56** and one synthetic analogue C-K_4-M2GlyR **57** with enhanced water solubility.

The peptides were found to promote an anion dependent current in lipid bilayers, in whole cell patches and in epithelial monolayers.[86, 92-94] They found that the water soluble peptides exist as monomers in solution and form supramolecular assemblies within the bilayer to form bioactive structures. Aggregation of the monomers was found to be inhibited by the addition of an aromatic residue at the C-terminus, thus reducing the formation of high molecular weight associations of the peptide which had no activity. The placement of aromatic and charged amino acids[88] within the acyl core was crucial to the final channel geometry; for example, placement of a tryptophan C-terminally to an arginine resulted in distortion of the helix due the guanido group orientating towards the lipid/water interface. This in depth analysis of structure-activity relationships for a series of synthetic anion transporters highlights that the behavior of a target molecule within a bilayer can be readily modulated synthetically. It also reveals that synthetic systems can

be applied to function effectively in natural systems- an important consideration for the therapeutic application of these species.

Gokel and co-workers have also reported a synthetic peptide for chloride transport based on a naturally occurring amino acid sequnce, which they named SCMTR (synthetic chloride membrane transporter, compound **59**).[95] Based on the observation that all members of the C1C family of channel proteins contain the amino acid sequence GKxGPxxH in the anion pathway, the authors chose to synthesize a heptapeptide; this was combined with a proline residue to introduce an "arch" (the presence of proline in channel forming peptides is known to cause a "hinge-bend" shape[96]), flanked by glycine residues. A long chain dialkylamide terminus was chosen to function as a membrane anchor. The structure of SCMTR is shown if **Figure 1.27**.

$(C_{18}H_{37})_2NCOCH_2OCH_2CO$-GGPGGG-$OCH_2Ph$

Figure 1.27 The structure of SCMTR **59**.

Peptide **59** was found to cause rapid efflux of Cl^- from vesicle systems. However, replacement of the proline in the sequence with leucine resulted in diminished Cl^- transport, thus demonstrating the importance of the structural constraints the proline residue has on peptide shape. A truncated analogue containing a 4-residue peptide sequence, again not containing proline, was also found to be inactive. An anion antiport mechanism was confirmed by the inhibition of Cl^- transport by **59** when the external anion was SO_4^{2-}, and channel activity was demonstrated using voltage clamp techniques. Interestingly, the channel formation by **59** was found to be voltage gated between -3 and 10 mV, as indicated by the transmitted current dependence on membrane potential. Voltage gating is a key feature of naturally occurring ion channels which is challenging to replicate in synthetic systems but crucial for biological control of the open and close behaviour. Further investigation by the same authors revealed that the Cl^- conductance of this type of peptide was enhanced if the chain length of the anchor was decreased.[97] This was attributed to the simpler aggregation equilibria of the shorter analogue formed in the aqueous phase prior to partitioning with the lipid bilayer- thus, insertion of the active dimeric species is faster.

It is not only peptides that can form membrane spanning ion channels. Amphotericin B (**Figure 1.28**) is a natural product isolated from *Streptomyces nodosus*. It has antifungal activity and has been shown to form channels in sterol-containing bilayers which transmit both anions and cations.[98] This indicates that the design of ion channels need not focus purely on synthetic peptides. Additionally, amphotericin B is not long enough to span the bilayer, thus the active channel state is an aggregate formed within the bilayer. This demonstrates that synthetic channels do not need to be large enough to span the bilayer as a single entity.

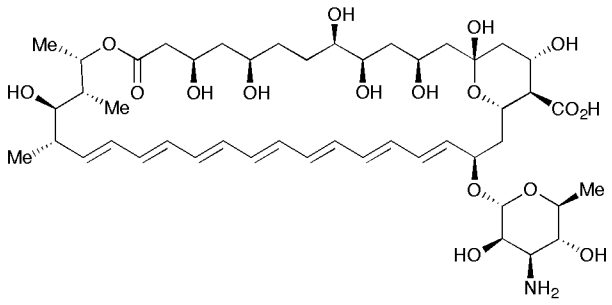

Figure 1.28 Amphotericn B is a naturally occurring non-peptide based ion channel.

The rigid polyene backbone of amphotericn B inspired Matile and co-workers to investigate the ion channel forming ability of some "rigid-rod" molecules.[99] They found that a rigid rod composed of an octa(*p*-phenylene) backbone with protruding glycerol residues functioned as a unimolecular H^+ conducting channel in EYPC vesicles (**Figure 1.29**). They found that this octaphenylene rod **60** was more active than analogous tetraphenyl and hexaphenyl rods. These were speculated to be too short to span the bilayer (the apolar interior of an EYPC bilayer was estimated to be 36 Å). Metal cations were not transported, although H^+/K^+ antiport was observed in the presence of valinomycin. Interestingly, the authors reported that these channels could also mediate OH^-/Cl^- exchange in vesicle systems- a process which can be viewed as analogous to H^+/Cl^- symport. Further work by the same authors explored the effect of adding hydrophobic sidechains to these octaphenylenes in order to compensate the unfavourable interactions between the hydroxyl groups and the apolar membrane interior. This was found to improve proton conductance, but the anion transport properties of these molecules were not investigated.

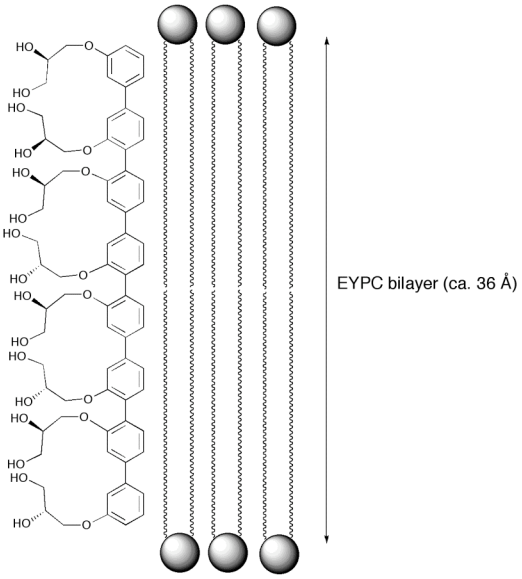

Figure 1.29 Octa(*p*-phenylene) rod **60** is a complementary size to the apolar interior of an EYPC bilayer.

Further to this work, Matile and co-workers reported the synthesis and anion channel formation of oligo-(*p*-phenylene)-*N*,*N*-naphthalenediimide (O-NDI) rods of type **61**.[100] The NDI units were selected due to their π-acidity. It was hoped that anions could be conducted through a bilayer by these species guided by anion-π interactions, thus stabilizing the anion within the bilayer as shown in **Figure 1.30** (a). The rods were named anion-π slides due to this proposed mode of action. These species were found to mediate OH^-/X^- exchange in EYPC vesicles containing the pH sensitive fluorescent dye HPTS. The observed transport was not dependent on the nature of any of the metal cations present, but was found to be highly anion dependent- thus, O-NDI rods function as anion selective channels. O-NDI rods with one cationic terminus were found to be the most active for anion transport. Importantly, this work demonstrates that a transmembrane anion channel need not resemble a classical pore like structure, but should simply provide stabilizing interactions to the anion as it crosses the lipid bilayer. Interestingly, the neutral O-NDI rods showed an anti-Hofmeister selectivity ($Cl^- > F^- > Br^- > I^-$). As an extension of this work, the authors synthetically tethered two O-NDI rods together to form a hairpin structure; this resulted in an even greater Cl^- selectivity.

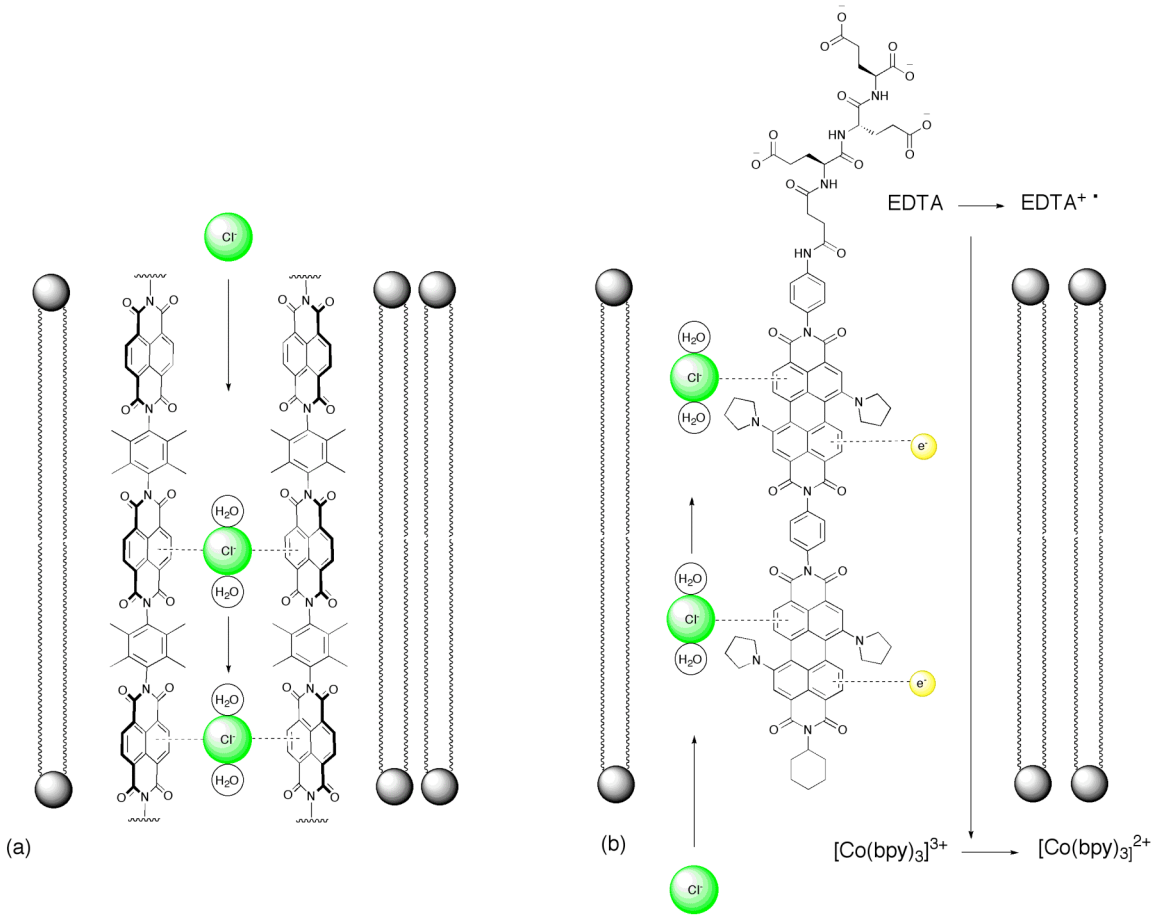

Figure 1.30 (a): O-NDI rods (**61**) reported by Matile to function as anion-π slides, and (b): O-PDI rods (**62**) which facilitate the movement of anions and electrons.

More recent work from Matile *et al.* describes the structure and function of some oligo-*p*-phenyl-*N*,*N*-perylenediimides (O-PDI rods, **62**), shown in **Figure 1.30** (b).[101] PDIs are π-acidic semiconductors. The rods were designed to be long enough to span the membrane, with one anionic terminus to ensure membrane orientation. The O-PDI rods were found to facilitate Cl^-/OH^- exchange and to display the same anion selectivity as the O-NDI rods. The semiconducting ability of PDIs also prompted the authors to examine the ability of these receptors to transport electrons- photosynthetic activity- using the Hurst assay. In this experiment, vesicles are prepared containing $[Co(bpy)_3]^{3+}$, the photoreduction of which can be detected by a change in absorption around 320 nm. The extra-vesicular solution contained EDTA, used as an electron donor. Thus, observed reduction of the $[Co(bpy)_3]^{3+}$ is evidence of the passage of electrons across the bilayer. The O-PDIs were found to exhibit photosynthetic activity under these conditions. The

addition of a proton carrier, FCCP, to the system did not alter this observed activity; this supports the theory that the active transport of an electron is coupled to the passive exchange of an anion. This work represents a novel application for adapted anion transport systems.

Schmitzer and co-workers have described the Cl^- transport activity of a series of imidazolium salts **63**-**65**.[102] Inspired by the work of Matile, the authors proposed that potential anion-π interactions between these molecules and Cl^- should be strong due to the positively charged imidazolium substituent close to the aromatic system. Only compound **65** was found to mediate Cl^-/NO_3^- exchange in lucigenin containing vesicles. Emission spectra of **64** and **65** indicated the existence of eximers in liposomal membranes, thus implying aromatic-aromatic interactions are present. A computational study predicted that compound **65** should form an aggregate of the correct length to span the bilayer. Additionally, the observed transport activity was inhibited by the addition of α-cyclodextrin or cucurbit[7]uril. These species are known to form complexes with imidazolium salts. Their addition was assumed to disrupt channel formation and enhance the partitioning of the transporter in the aqueous phase over the lipid phase.

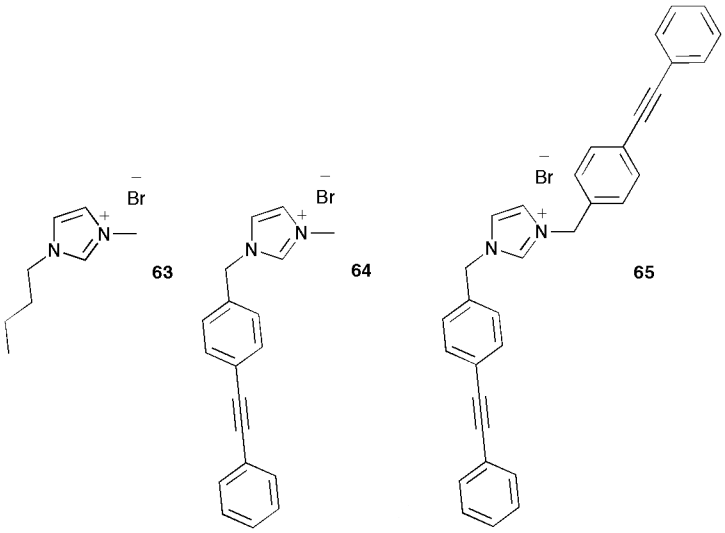

Figure 1.31 The imidazolium salts investigsted by Schmitzer *et al.*

The self assembly of channels from smaller constituent units has also been demonstrated by Yang and co-workers, who report that compound **66** forms chloride selective channels.[103] The design of **66** was chosen to incorporate α-aminooxy hydrogen

bond donors, as this had been previously shown to be effective for the complexation of Cl^-.[104, 105] Cl^-/NO_3^- antiport was demonstrated in unilamellar vesicles containing the halide sensitive dye 6-Methoxy-N-(3-sulfopropyl)quinolinium (SPQ). Using patch clamp techniques, single channel measurements were recorded which proved the presence of channels. Additionally, MDCK cells which had been loaded with SPQ were used to demonstrate Cl^- transport in cells. It is remarkable that such a small compound is able to assemble into membrane spanning channels, and notable that a small scaffold designed to complex Cl^- was found to function as a channel rather than a mobile carrier. The biological potential of this work was further demonstrated when the authors reported that **66** could regulate cell membrane potentials and the action of voltage gated Ca^{2+} channels.[106] This indicates that the action of synthetic anion transporters can regulate other physiological effects and be incorporated into natural processes.

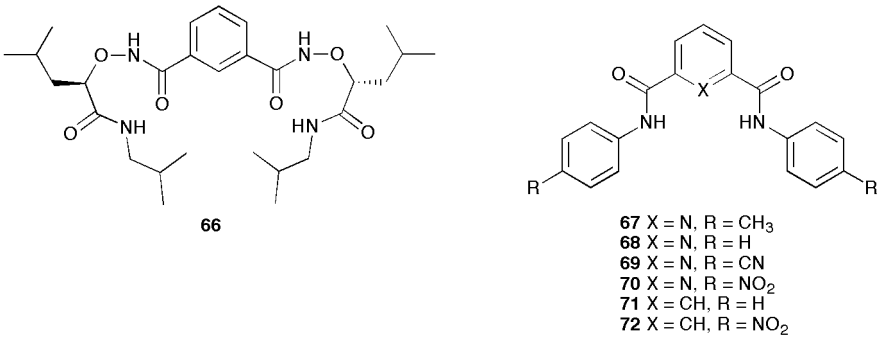

Figure 1.32 Some simple molecules known to assemble into anion channels.

Similarly, Gokel has reported that certain dianilides of picolinic or isophthallic acid are able to assemble into membrane spanning channels.[107] Aromatic substituents containing electron withdrawing groups were found to the most effective anion transporters. **69**, **70** and **72** were shown to efficiently mediate Cl^- influx into DOPC vesicles containing lucigenin as a fluorescent Cl^- sensitive probe, while **67**, **68** and **71** were less active. The planar bilayer conductance technique was used as proof of channel assembly; the authors reasoned that such a membrane spanning structure would require aggregation within the bilayer. Evidence of stacking was obtained by fluorescence measurements in both DMSO and within lipid bilayers, leading the authors to hypothesize that the stacking of multiple monomer units is responsible for the formation

of a pore. This work demonstrates that even small molecules can assemble to form pores, and that prediction of channel *vs.* carrier activity may not always be straightforward as self assembly can be unpredictable.

J. T. Davis and co-workers explored ion transport activity of a calix[4]arene tetrabutylamide **74**.[108] They found that **74** could mediate H^+/Cl^- efflux from HPTS containing vesicles in the presence of a pH gradient. However, when the internal solution was Na_2SO_4 no transport was observed, indicating that HSO_4^- could not be transported in this way. Channel formation was proved using voltage clamp experiments. This transport was not cation dependent. The secondary amide NH groups were found to be essential for anion transport activity. Calix[4]arene **75**, which does not contain amide NH groups to aid anion binding, was found to bind Na^+ and to mediate ion transport which was dependent on the nature of the encapsulated cation but not anion dependent.

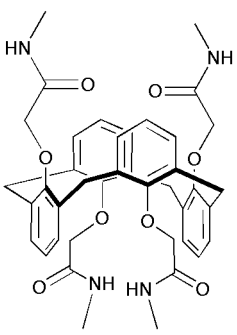

73

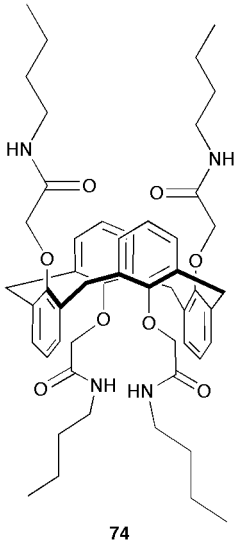

74

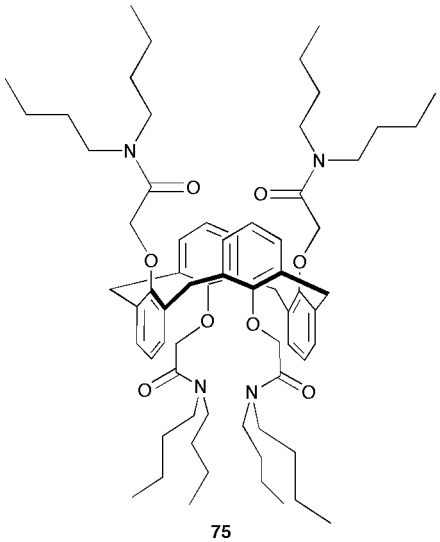

75

The authors failed to crystallize active calix[4]arene **74** but were able to grow crystals of **73**.$H^+/Cl^-.3H_2O$, shown in **Figure 1.33**. Calix[4]arene **73** does not promote membrane ion transport, presumably because it is less lipophilic than **74** and **75**; however, the authors reasoned that it should bind H^+/Cl^- analogously to **74**. The crystal structure indicates that individual calix[4]arenes are bridged by hydrogen bonding to Cl^- and water filled pores.

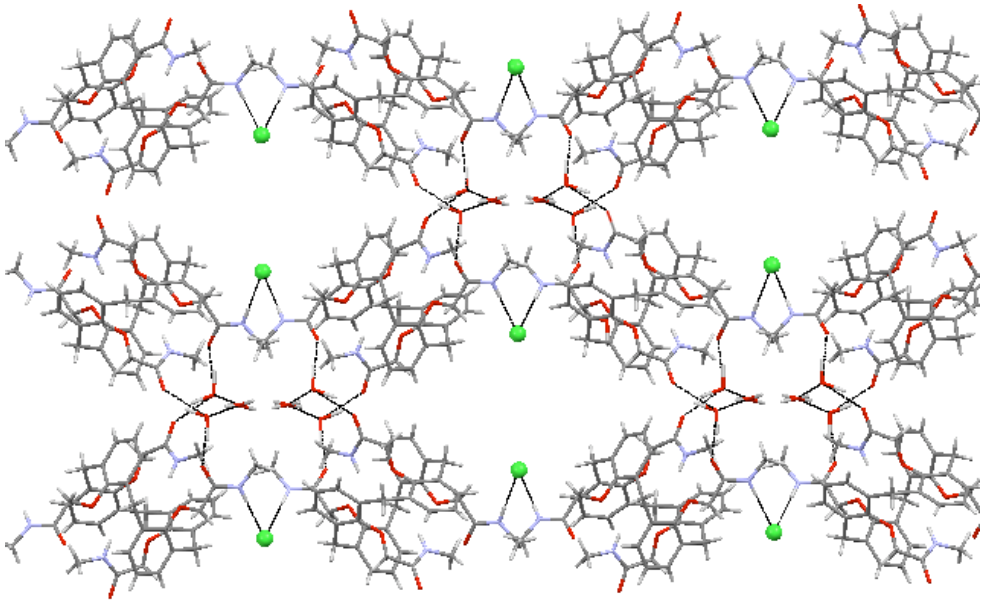

Figure 1.33 The hydrogen bonding array found in the crystal structure of **73**.$H^+Cl^-.3H_2O$.

This solid state structure, while not necessarily representative of channel formation in vesicle bilayers, indicated that the formation of this hydrogen bonded array did not involve complexation of the Cl^- within the cavity of the calix[4]arene and that as such, the calix[4]arene macrocycle may not be directly involved in the anion transport process. This prompted the authors to investigate the ion transport activity of some acyclic oligophenoxyacetamides **76-81**.[109] Using vesicles containing HPTS, they found that trimer **78** was an order of magnitude more active for H^+/Cl^- co-transport than calix[4]arene **74**; meanwhile, analogues **76**, **77** and **79-81** exhibited limited activity. No ion transport was observed if the Cl^- was exchanged for SO_4^{2-}, thus indicating the highly anion dependent nature of this transport process. The transport of Cl^- by **78** was also observed directly using $^{35}Cl^-$ techniques.

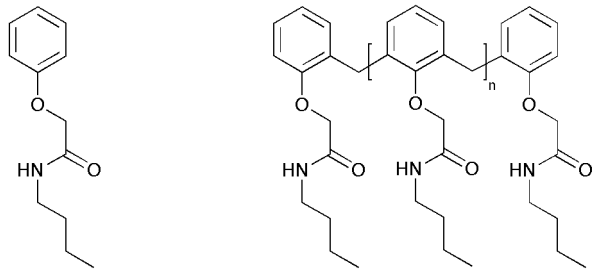

76

77 n = 0
78 n = 1
79 n = 2
80 n = 3
81 n = 4

Figure 1.34 J. T. Davis *et al.* have also explored the anion transport activity of some acyclic calixarene analogues.

J. T. Davis and co-workers have also found that tetraamide substituted calix[4]arenes fixed in a partial cone or a cone conformation can facilitate Cl^-/NO_3^- antiport. They found that partial cone **82** and cone **83** could facilitate Cl^-/NO_3^- antiport under neutral conditions in vesicles containing lucigenin. **82** was found to be twice as active as **83** under the same conditions. The substitution pattern of the calix[4]arene was found to be critical, as **85**, in which one of the amide arms was replaced by an ester, was found to be much less active than the analogous tetramide **83**. However, calixarene **84**, which contained only 3 amide arms was more active than the tetramide. The pH sensitive nature of the free phenolic group prompted the authors to examine **84** as a pH tunable transporter. They found that increasing the pH of the system resulted in a decrease in observed transport activity corresponding to deprotonation of the phenolic OH group. This pH dependence was not observed with tetraamide **83**. Thus, **84** was found to function as a pH gated Cl^- transporter.

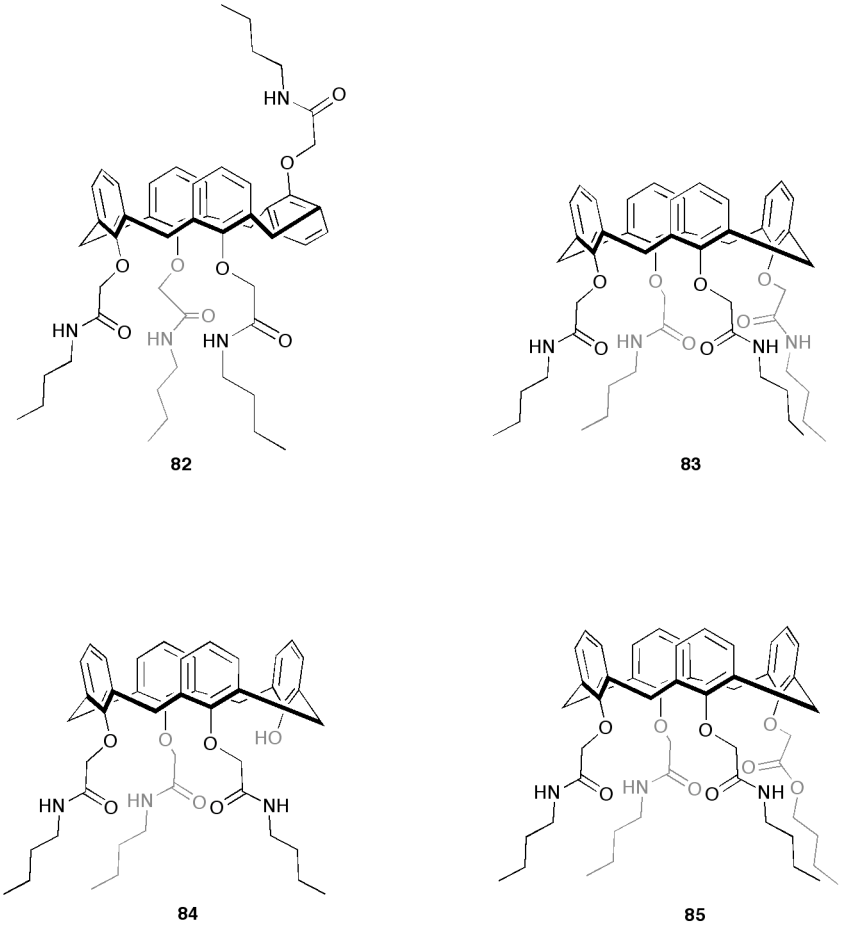

Figure 1.35 Calix[4]arene amides fixed in a cone or partial cone conformation have also been found to mediate Cl^- transport.

Gin and co-workers have explored the ion channel formation by a modified β-cyclodextrin **86**.[110, 111] The oligoether chains were thought to be hydrophobic enough to penetrate the bilayer and long enough to span the bilayer; thus, this design comprises a water soluble head group, presumed to position near the surface of the bilayer, coupled with hydrophobic chains to provide a transmembrane ion pathway. In vesicles containing HPTS they demonstrated that **86** could facilitate Na^+/OH^- influx (or Na^+/H^+ antiport). The observed pH changes were not found to be cation selective; however, the influx of Na^+ was observed directly using ^{23}Na NMR. The anion selectivity of the channel was probed by variation of the counteranion (Cl^-, Br^- and I^-) using Na^+ salts. In this case, a more complex process was found to occur. On addition of NaBr or NaI, the intra-vesicular pH was observed to sharply fall; this was attributed to rapid X^- influx (H^+/X^- symport or X^-/OH^- antiport). The internal pH was then observed to steadily increase, indicative of a

slower Na^+ transport process. The rate of influx of Cl^- was more comparable with the rate of efflux of Na^+ thus producing a gradual decrease in intra-vesicular pH with no observable re-equilibriation process. The anion selectivity followed the Hofmeister sequence (I^- > Br^- > Cl-). Thus, **86** was found to function as a highly selective anion channel.

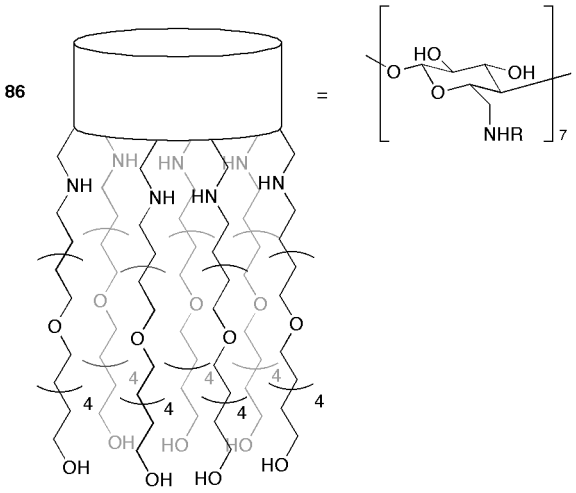

Figure 1.36 A functionalized β-cyclodextrin reported by Gin *et al.* to function as an anion channel.

This design inspired collaborative work from Montesarchio and Tecilla to investigate the ion transport properties of some cyclic phosphate-linked oligosaccharides (CyPLOS) **87**-**91**.[112] The authors hypothesized that the anionic macrocycle could form a pore at he polar membrane surface, with the amphiphilic chains penetrating the inner core of the bilayer in a manner analogous to Gins cyclodextrin based channel.[110, 111] They found using vesicles containing HPTS (internal solution = pH 7.0) that spiking in NaOH after addition of the ionophore resulted in an increase in intra-vesicular pH. The biggest response was exhibited by CyPLOS **87**; analogues **88** and **89** were found to be much less active, indicating the importance of the tetraethylene glycol chains, potentially as these form the polar transmembrane pathway for the ions. CyPLOS **90** and **91** also exhibited ion transport activity. The behaviour of these compounds was similar to that exhibited by Gins β-CD; the observed transport was found not to be cation selective, (although Na^+ trasport was confirmed using $^{23}Na^+$ techniques), but highly dependent on the nature of the counteranion, displaying Hofmeister selectivity.

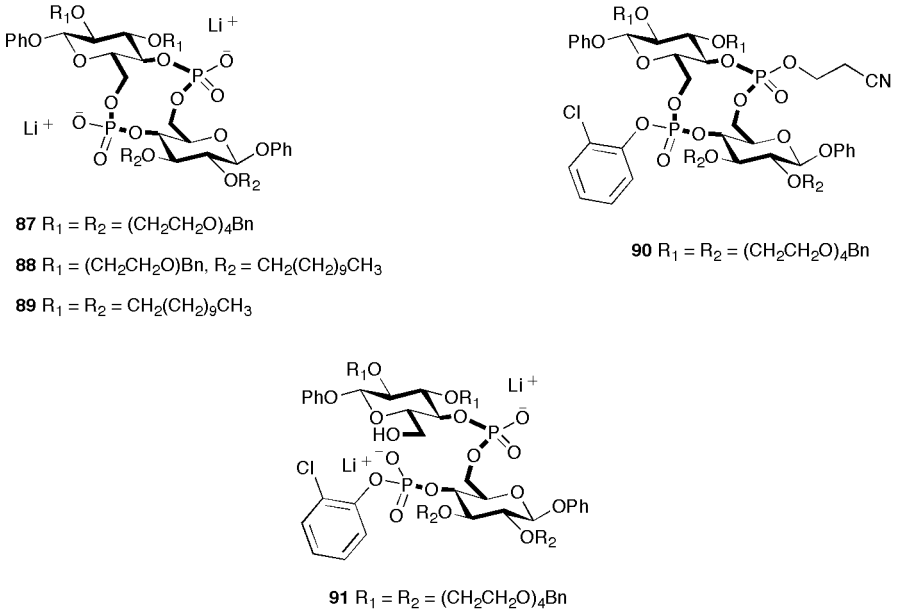

Figure 1.37 CyPLOS macrocycles which form a pore at the surface of the bilayer.

The self-assembly of cyclic D,L-α-peptides has been used to produce self assembled ion channels. Matile *et al.* have investigated the transport activity of peptidomimetic oligourea/amide macrocycles **92-97**.[113] Solution phase aggregation studies indicated that **32** formed hydrogen bonded dimers in $CDCl_3$ or CD_2Cl_2, whereas **92** and **95** formed tubular stacks. The stacks associate *via* dipole-dipole interactions between the macrocycles to form nanotubes. The dipole of the macrocycles is represented in **Figure 1.38**.

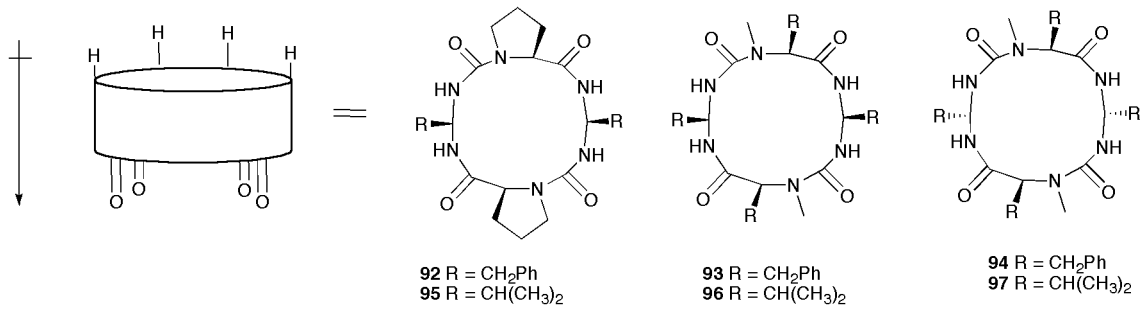

Figure 1.38 The oligourea/amide macrocycles reported by Matile which assemble to form stacks by dipole-dipole interactions.

Using a HPTS assay, the H^+ co-transport of anions including Cl^- was demonstrated. As the macrocycles are too small to complex the ions of interest within the central cavity, a "Jacobs-Ladder" mechanism was proposed. The macrocycles are assumed to stack with their macrodipoles aligned to provide a pathway for ions through the bilayer. Anions may be bound to one face of a macrocycle by the urea and amide hydrogen bond donors. The macrocycles are theorized to rotate 180° and thus facilitate the movement of anions along the ladder. This mechanism is represented in **Figure 1.39** Additionally, macrocycle **92** showed an anti-Hofmister bias, whereas **93** and **94** exhibited anion selectivity according to the Hofmeister sequence; however, both **92** and **93** showed extra selectivity for Cl^-. Macrocycles **92-94** were found to be an order of magnitude more active than alkyl substituted receptors **95-97**.

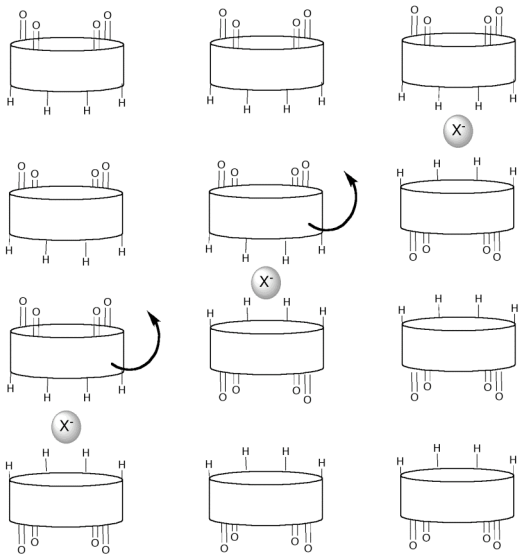

Figure 1.39 The proposed "Jacobs-ladder" mechanism of anion transport mediated by Matile's oligourea/amide macrocycles.

1.8 Experimental techniques to assess anion transport

1.8.1 Vesicles

Laboratory made, unilamellar vesicles serve as a simple and easily reproducable model of a cell membrane. The techniques described within this thesis were developed by B. D. Smith and co-workers.[48, 114] The preparation of the vesicles used in this work is versatile, allowing for careful control of the intra- and extra-vesicular solutions. The vesicles are formed by a freeze thaw and extrusion technique,[115] described in detail within **Chapter 6.2**. There is a criteria that the intra- and extra-vesicular solutions should be isotonic, as transmembrane osmotic imbalances can result in membrane rupture. Solutions are buffered to prevent the build up of undesirable pH gradients. However, it is possible to vary the salt composition of the intra- and extra-vesicular solution within these limits. By systematically varying these salt compositions, it is possible not only to observe anion transport but also to gain important mechanistic insight into the process.

1.8.2 Monitoring the movement of anions

It is possible to observe the transport of various anions by a number of methods. Almost exclusively in this work, the transport of chloride has been monitored using a chloride selective electrode (ISE) as depicted in **Figure 1.40(a)**. The intra-vesicular solution is "invisible" to the ISE; thus, an increase in chloride concentration of the extra-vesicular solution can be monitored and equated to chloride efflux.

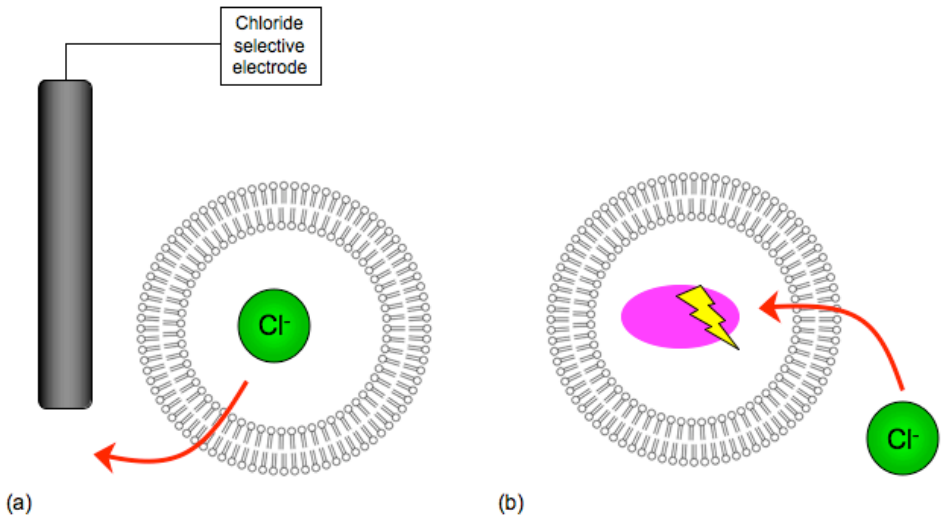

Figure 1.40 The movement of anions across vesicle membranes can be tracked using (a) an ISE technique, or (b) using fluorescent dyes encapsulated within the vesicle.

Alternatively, a number of fluorescent probes may encapsulated within the vesicles and utilized to track the movement of anions (**Figure 1.40(b)**). The structures of some commonly used dyes are shown in **Figure 1.41**. Halide sensitive dyes such as lucigenin and 6-methoxy-N-(3-sulfopropyl)quinolinium (SPQ) may be used to monitor changes in the intra-vesicular chloride concentration as their fluorescence is quenched by chloride.[53] 8-Hydroxypyrene-1,3,6-trisulfonate (HPTS, also known as pyranine) is a pH sensitive dye, which has been used to great effect in monitoring the changes in intra-vesicular pH associated with H^+/Cl^- co-transport.[116] As this technique is independent of the nature of the anion, it has also been utilized to demonstrate the co-transport of anions other than chloride with protons. Safranin-O is a potential sensitive dye that may be used to identify changes in the membrane potential induced by the transport of ions.[117] Meanwhile, J. T. Davis and co-workers have pioneered the use of ^{13}C NMR to monitor the transport of $H^{13}CO_3$.[59] Distinct resonances may be observed for intra- and extra-vesicular $H^{13}CO_3$, allowing the movement of this anion to be assessed. Addition of Mn^{2+} causes broadening of the signal associated with the extra-vesicular $H^{13}CO_3$ but not the intra-vesicular $H^{13}CO_3$, allowing the identity of each resonance to be established. Carboxyfluorescein is an anionic fluorescent dye which is self-quenching; thus, changes in its intra-vesicular concentration can be easily monitored. Anion transporters that can facilitate the transport of carboxyfluorescein anions are often hypothesized to be forming

large, non-selective pores, due to the greater anion selectivity inferred by binding site design in mobile carriers.[2] However, it should be noted that Gokel *et al.* have observed the transport of carboxyfluorescein in a U-tube experiment, thus it is not impossible that the transport of carboxyfluorescein may occur by a mobile carrier mechanism.[2]

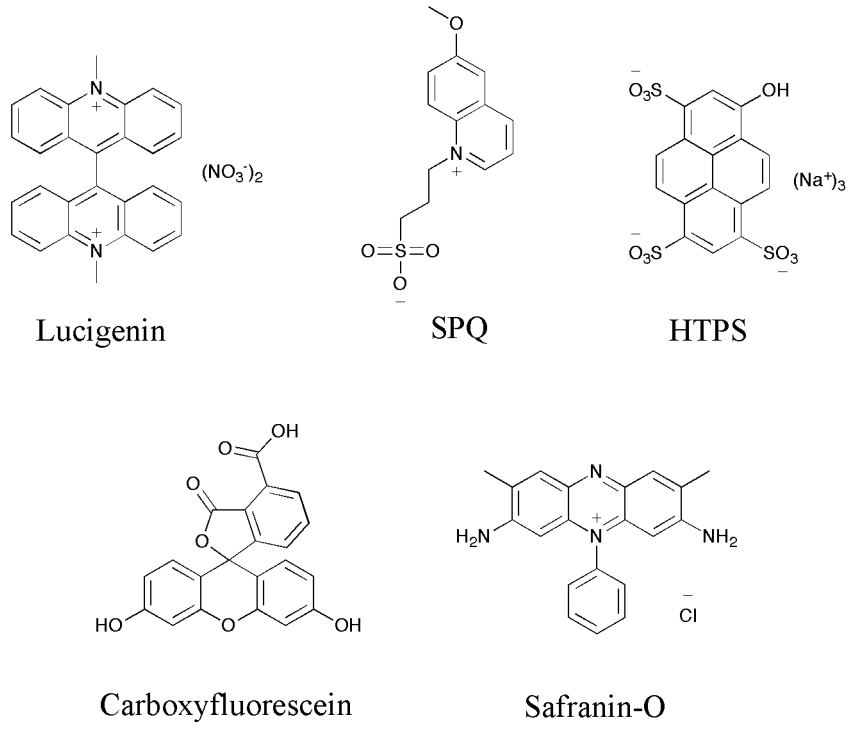

Figure 1.41 The structure of various fluorescent dyes that can be used to track the movement of ions in vesicle studies.

1.8.3 Variation of salt composition

Variation of the intra- and extra-vesicular salt solutions can distinguish between and characterise an antiport or symport mechanism. An initial test for chloride antiport processes uses vesicles containing NaCl suspended in $NaNO_3$. If chloride efflux is promoted by addition of a carrier, it may be *via* a Cl^-/NO_3^- antiport mechanism or a Na^+/Cl^- symport mechanism. Anion antiport mechanisms are dependent on the nature of both the intra- and extra-vesicular anion as both are involved in the transport process. Substituting the external anion for SO_4^{2-} should inhibit an antiport mechanism, as SO_4^{2-} is divalent and highly hydrophillic, and to date there are no known synthetic receptors able to facilitate its transport. If a Cl^-/NO_3^- antiport mechanism is proved, it is then desirable to

establish if the carrier is able to facilitate the antiport of Cl^- and HCO_3^- due to the greater biological relevance of this process. This is investigated using vesicles containing NaCl suspended in Na_2SO_4. The receptor is added and, as the receptor is an antiporter, no chloride efflux should be observed. A pulse of $NaHCO_3$ is then added, and any resulting chloride efflux may be attributed to a Cl^-/HCO_3^- antiport process. HCO_3^- transport may also be directly observed using the ^{13}C NMR technique as detailed above.

Alternatively, if the carrier is able to facilitate M^+/Cl^- symport, the transport will not be dependent on the nature of the extra-vesicular anion. It will however be dependent on the nature of the intra-vesicular cation. Using vesicles suspended in Na_2SO_4 to rule out any antiport activity, the alkali metal cation in the intra-vesicular MCl solution can be varied to establish the preferred cation for the symport process. Meanwhile, a H^+/Cl^- symport process can be evaluated by varying the relative starting pH of the intra- and extra-vesicular solutions. For example, for a solution of vesicles containing NaCl suspended in Na_2SO_4, H^+/Cl^- efflux should be encouraged if the intra-vesicular solution is more acidic than the external solution, and inhibited if the opposite pH gradient is applied.

1.8.4 Choice of lipid

There are a number of different phospholipids commonly utilized for transport experiments. Phosphotidylcholines (PCs) are a major component of cell membranes. POPC is commonly used for transport studies, has been used by Gale and co-workers in all publications to date, and as such has been used most commonly within this thesis. The structure of POPC and some other phospholipids used in similar studies are shown in **Figure 1.42**. EYPC (egg yolk PC) is a phospholipid derived from egg yolks which is predominantly composed of POPC and thus the properties are similar. DOPC and related di-unsaturated PCs have also been used for vesicle formation. In particular, using lipids from this family with different chain lengths has been used as a tool to probe the effect of bilayer thickness on transporter efficiency,[54] as changing this variable should influence the observed activity of a channel and a mobile carrier in different ways. Additionally, the saturated phospholipid DPPC has been used in mobility assays as described below.

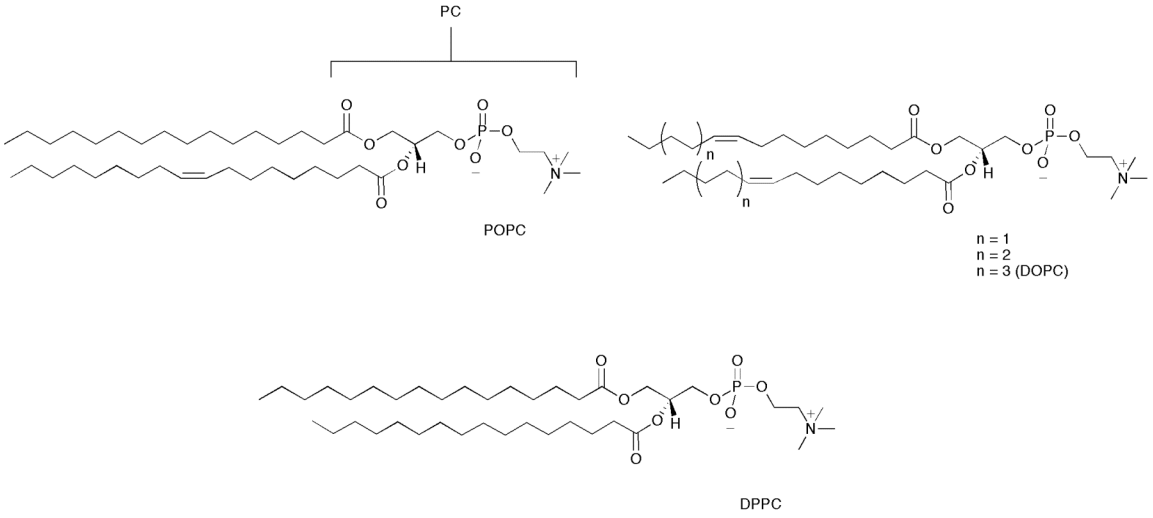

Figure 1.42 Some commonly used phospholipids.

1.8.5 Mobility assays

There are various proofs that have been employed to demonstrate mobile carrier activity over channel formation. It was previously common to use the lipid DPPC in mobility assays. DPPC undergoes a phase transition from the solid gel phase to a liquid crystalline (fluid) phase at 41 °C. The action of a channel- which is relatively stationary once established- should be undisturbed by this transition once the channel has been inserted into the bilayer; however, the action of mobile carriers is dependent on diffusion through the bilayer, and thus should be inhibited if the system is cooled below 41 °C. Inhibition of transport on cooling a system of DPPC vesicles was therefore taken as proof of mobile carrier activity.[118] However, Regen has described the so-called "squeezing out" of an ionophore;[119] that is, that on cooling a system of DPPC vesicles below the transition temperature, the transporter was expelled from the bilayer. Thus, it is now not necessarily accepted that a loss of transport on cooling in this system is proof of a mobile carrier mechanism.

For small molecules which are not large enough to span the bilayer, it has been argued that a first order concentration dependence on observed transport activity is proof that no cooperativity is occurring and that the active species cannot be an aggregate.[48]

Additionally, the inclusion of cholesterol within a membrane reduces its fluidity and thus the rate of transport by mobile carriers should be reduced.[58, 119]

1.8.6 Voltage clamp experiments

While the formation of channels may be implied by various means including carboxyfluorescein transport and variation of the lipid bilayer thickness, according to Fyles, the voltage clamp technique "is the sole method to unequivocally establish the presence of channel-like activity".[120] It is certainly the only known method which can directly observe the action of ion channels. The term "voltage clamp" may refer to planar lipid bilayer studies, in which the current flowing across a painted bilayer is monitored, or patch clamp measurements,[121] which monitor the transmembrane current across a patch of a cell or vesicle membrane. Using these techniques, it is possible to observe a transmembrane current as a result of ion transport. Crucially, it is possible to record "single channel" measurements- the observation of ion transport due to one or a small number of discrete channels.[122] As such, it is possible to observe characteristic open-close behaviour of individual channels as step-wise changes in conductance. In contrast, the action of a mobile carrier might be expected to produce an increase in membrane current but with no such open-close behaviour.

1.8.7 The Hill equation

The Hill equation was first introduced by A. V. Hill in 1910 to describe the cooperativity of oxygen binding to haemoglobin.[123] More specifically, the equation described the relationship between the concentration of a substrate (in this case oxygen), and an observed effect (the % of saturated haemoglobin binding sites). Since then, the Hill equation has been applied to a wide range of systems.[124] It has been often utilized in pharmacodynamics to describe the relationship between drug concentration (C) and observed drug effect (E).[125, 126] A form of the Hill equation that is useful in this context is shown below (**Equation 1.1**), where EC_{50} is the drug concentration for which 50 % of maximum effect is obtained and n is the Hill coefficient of sigmoidality. The Hill

coefficient has been interpreted to represent the number of ligand binding patterns required to mediate the observed effect.

$$E = E_{max}C^n / (EC_{50}{}^n + C^n)$$

Equation 1.1 A form of the Hill equation frequently applied to pharmadynamics.

The Hill equation can been applied to ion transport systems by examining the effect of varying the concentration of transporter (C) on the observed ion flux (E). In this way, a value of EC_{50} can be calculated and used to quantify transport activity- the lower the value of EC_{50}, the more potent the transporter. Calculation of the Hill coefficient can provide mechanistic insight into the transport process, representing the number of transporter molecules required to transport a single ion; either as an aggregate mobile carrier complex, or as a self-assembled channel species. However, Matile reports that the use of the Hill coefficient to study supramolecular self assembly is not always straightforward. The formation of highly stable assemblies may give a Hill coefficient of 1, presumably because the assembly "behaves" as a single entity and can be misinterpreted as a monomer. It has also been suggested that the Hill analysis is only compatible with endergonic self-assembly, thus inconsistencies may arise if the assembly is exergonic.

1.8.8 Testing in real cells

While testing in synthetic bilayers is more commonly used due to the ease at which such bilayers can be produced, there are also examples of synthetic transporters which have been tested in real cells by a number of techniques. The patch clamp technique can be applied to monitor the whole-cell current.[121] This gives no insight into channel *vs* carrier activity but can be used to quantify anion transport. The Ussing chamber technique measures the current across a monolayer of epithelial cells grown on a permeable support.[127] It is also possible to incubate cells with fluorescent dyes such as SPQ; changes in the internal fluorescence of the cells can then be observed as indicative of ion transport.[128]

Experiments using real cells have been reported far more commonly in the testing of synthetic chloride channels. To the authors knowledge, the only reported example of testing a mobile carrier in real cells to date is a cholapod published by A. P. Davis which has shown activity using the Ussing chamber technique.[48]

1.8.9 Comparison of experimental techniques

Little attempt has been made within this introduction to distinguish the relative effectiveness of different transport systems. The small variations in the transport experiments utilized by different research groups makes this an extremely difficult task. Such variations may include:

- The concentrations of salts. The effectiveness of a transporter is linked to the magnitude of the electrochemical gradient that drives the transport process.
- The choice of phospholipid. Commonly used lipids in vesicle based transport studies include POPC, EYPC and DOPC. The composition of the lipid bilayer directly affects the ease of transport through it. Additionally, the activity of several channels has been found to be dependent on the thickness of the bilayer, and thus the structure of the phospholipid.
- The use of cholesterol. The addition of cholesterol to a bilayer causes the lipids to become more ordered and the bilayer to become more viscous. This effect has been used to probe the action of mobile carriers that are diffusion controlled; however, some research groups use vesicles containing cholesterol as standard procedure. Clearly, in the testing of mobile carriers this is a significant factor.
- Preincorporation. If a receptor is too lipophillic to pass through an aqueous phase in order to partition with the vesicle bilayer, its transport activity can still be evaluated by preparing vesicles in which the receptor is already contained within the vesicle membrane. However, these results are incomparable with the results obtained without preincorporation.

Within the experiment reported in this thesis, these factors have been kept constant unless otherwise stated so that the experiments are comparable with each other and with previous publications by the Gale group.

1.9 Aims of this thesis

This chapter has covered the major advances in the development of synthetic anion transporters over recent years. The work in this thesis focuses on the development of new mobile carriers for anions. There are a large variety of structural motifs that have been previously used for this purpose. This work aims not only to identify new anion carriers but also to gain insight into the structure-activity relationships. In short, this work attempts to determine- "what makes a good anion carrier?"

In order to address this challenge, this thesis has been divided such that each chapter examines a different series of structurally related receptors and analyzes the trends that become apparent in their anion binding and transport properties. The anion transport properties of the receptors discussed in this thesis have been investigated using vesicle-based methods. The solution phase anion binding properties of new receptors has also been investigated, along with the solid state anion binding properties where possible.

Chapters 2, 3 and **4** examine a progression in receptor design from structurally simple ureas and thioureas (**Chapter 2**) to a series of bipodal bis-alkyl ureas (**Chapter 3**) and bipodal bis-alkyl thioureas (**Chapter 4**). **Chapter 5** reports the anion transport studies relating to a number of strapped calix[4]pyrroles which were provided by J. L. Sessler and C.- H. Lee.

Chapter 2
Structurally simple transmembrane anion transporters

2.1 Introduction

The use of ureas as hydrogen bond donors for anion complexation was first explored by Wilcox[129] and since then urea and thiourea groups have been successfully incorporated into a vast number of neutral anion receptors.[130] The directionality of the N-H hydrogen bond donors facilitates the effective binding of Y-shaped anions such as carboxylates and the chelation of spherical anions such as Cl^- (**Figure 2.1**).

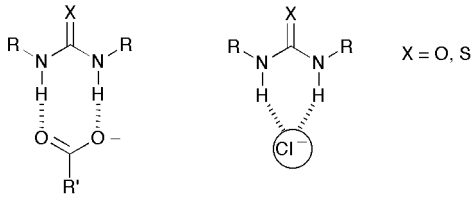

Figure 2.1 The binding of Y-shaped and spherical anions by (thio)urea receptors.

2.1.1 Ureas *vs.* thioureas for anion binding

Thioureas are more acidic than analogous ureas.[52] Steiner has stated that hydrogen bonding can be simplistically viewed as partial proton transfer between the hydrogen bond donor and acceptor.[131] In any case, considering the greater polarization of the N-H bond, it is reasonable to expect that thioureas will form stronger hydrogen bonds with anions, thus making them more potent anion receptors, although this is not always the case.[69, 132] Work by Umezawa and co-workers investigated the anion binding properties

of bis-urea **98** and bis-thiourea **99** (**Figure 2.2**).[133] Binding studies were carried out by ^{1}H NMR titration of the ligands with tetrabutylammonium anion salts in DMSO-d_6. Both receptors were found to be selective for $H_2PO_4^-$ (K_a = 110 and 820 M^{-1} respectively) The interaction of thiourea **99** with $CH_3CO_2^-$ (K_a = 470 M^{-1}) was also found to be stronger than receptor **98** (K_a = 43 M^{-1}). This observation was directly attributed to the formation of stronger hydrogen bonds to the anion by the more acidic thiourea N-H donors. It has also been reported that thioureas have a lower propensity to self associate through intermolecular hydrogen bonding than ureas due to the lower hydrogen bond basicity of the sulfur,[134] so there is less competition for hydrogen bond formation to the anion.

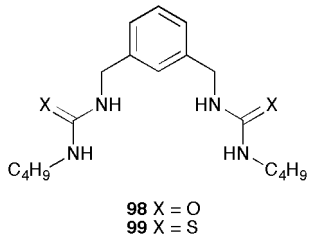

98 X = O
99 X = S

Figure 2.2 The urea and thiourea receptors reported by Umezawa.

However, the higher acidity of thioureas can result in their deprotonation by basic anions. The deprotonation of neutral NH groups in anion receptors by F^- was first reported by Gunlaugsson[135, 136] and Gale.[137-139] Subsequently, Fabbrizzi *et al.* investigated this effect in detail, comparing the interaction of a urea and a thiourea with various anions.[140] Receptors **100** and **101** (**Figure 2.3**) contain a phthalimide substituent as a chromophore to allow the interactions of the receptors with anions to be monitored using UV-vis and NMR techniques in DMSO solution. They found that urea **100** was only deprotonated by F^-, while compound **101** undergoes deprotonation in the presence of F^-, CH_3CO_2, $PhCO_2^-$ and $H_2PO_4^-$. The extent of deprotonation of **101** correlated with the stability of the corresponding hydrogen bridged dianion $[X\text{-}H\text{-}X]^-$ complex. Only Cl^- failed to deprotonate **101** to any extent. Thus, the authors concluded that, while hydrogen bond donor acidity is a desirable property for anion recognition that can lead to strong anion binding, receptors which are too acidic can lead to the formation of complexes which are unstable with respect to the release of HX.

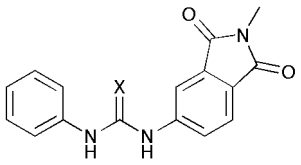

100 X = O
101 X = S

Figure 2.3 Fabbrizzi *et al*. have have studied the deprotonation of (thio)ureas containing a chromophore.

Interesting work from Hayashita and Teramae has investigated binding anions in aqueous solution using thioureas **102-109**, shown in **Figure 2.4**, in cationic vesicles.[141] The authors noted that binding anions in aqueous solution is highly challenging due to the hydration of the anion. Therefore, they proposed that anion recognition in water could be achieved by incorporating the receptor into a vesicle bilayer in order to shield the binding site from water. The receptors were preincorporated into vesicles composed of didodecyldimethylammonium bromide (DDAB), a simple amphiphile.

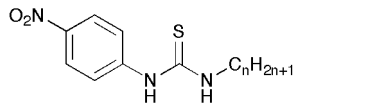

102-109: n = 1 - 8

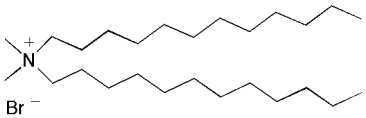

DDAB

Figure 2.4 Thioureas with a lipophilic alkyl substituent can complex anions within a vesicle bilayer.

The UV-vis absorption spectra of the compounds in DDAB indicate that the positioning of the receptor binding site was highly dependent on the length of the receptors alkyl substituent. The λ_{max} of the receptors shifts to higher wavelengths (by comparison to the value in acetonitrile) progressively as the alkyl chain length increases. The authors explain that, for the receptors with a longer alkyl chain, the binding site is located on the surface of the vesicle whereas the receptors with shorter chain lengths position their binding site in the hydrophobic interior of the bilayer. This is because the longer chain analogue can adequately position within the bilayer such that the

hydrophobic alkyl chain resides in the apolar bilayer interior, with the polar binding site located on the vesicle surface. However, the shorter chain analogues are not long enough to facilitate this positioning, resulting in the whole molecule positioning within the hydrophobic bilayer interior. Further evidence was obtained by comparison of the ^{1}H NMR spectra of **102-109** in DMSO-d_6 and in DDAB-D_2O. In DMSO-d_6 the vicinal protons of each receptor appear at similar chemical shift, but in DDAB-D_2O solution the chemical shifts range from 8.00 ppm (compound 1) to 8.22 ppm (compound 8). UV-vis titration of the receptor **102** in DDAB vesicles with various anions resulted in a bathochromic shift in λ_{max} with an enhanced molar absorptivity. These observations were attributed to the formation of the receptor-anion complex and a change in the positioning of the receptor within the vesicle membrane as a result of the hydrophilicity of the anion. The observed anion selectivity followed the Hofmeister bias (Br^- > $H_2PO_4^-$ > Cl^- >> HCO_3^-, $CH_3CO_2^-$). However, compound **109** showed little selectivity and was found to interact weakly with more hydrophilic anions such as acetate, which did not interact with compound **102**. Therefore it was assumed that anion binding by **109** takes place on the surface of the vesicle resulting in weaker binding due to contact with the aqueous phase, while compound **102** binds the anions within the bilayer resulting in a strength of interaction highly dependent on the lipophilicity of the anion. Compounds **103-108** showed a progressive intermediate response between these two extremes. This study demonstrates that thioureas can membrane-solubilize anions including chloride, which is highly relevant to the challenge of transporting the anions across the bilayer. Presumably, this chain length selectivity would be dependent on the thickness of the bilayer relative to the length of the receptor.

2.1.2 Indole substituted ureas and thioureas

Heterocycles such as indole, pyrrole and carbazole are useful functional groups for anion recognition[142] as they contribute an NH hydrogen bond donor which is not accompanied by a hydrogen bond acceptor (as in the case of other functional groups such as amides and ureas which contain a carbonyl C=O). This is an advantageous property for anion complexation as there are consequently no competing inter- or intramolecular

hydrogen bonding interactions associated with the use of indoles. This property is also useful in the design of anion transporters as additional hydrogen bond acceptors make a scaffold less lipophilic, thus making their partitioning with the bilayer less favourable.

As they contribute only one hydrogen bond donor, indoles are frequently used in combination with adjacent urea moieties to produce a convergent hydrogen bonding cleft. Pfeffer *et al.* have reported receptors **109-111** (**Figure 2.5**)[143] The anion binding properties of these receptors were investigated by ^{1}H NMR titration with the tetrabutylammonium salts of interest. By examining the change in chemical shifts of each hydrogen bond donor on the addition of aliquots of anion, the authors were able to determine the involvement of each NH proton in anion complexation. Titration of host **110** with TBA^+AcO^- revealed that only the thiourea NHs were found to significantly shift, thus implying that the indole and amide NHs did not contribute to the binding process. This may be due to the strong binding of Y-shaped anions by the (thio)urea motif. Titration of host **109** with $TBA^+H_2PO_4^-$ revealed that all of the hydrogen bond donors were involved in anion complexation. Binding constants were determined, revealing that smaller receptors **109** and **110** were selective for $H_2PO_4^-$, most likely due to the more convergent binding sites thus allowing all of the hydrogen bond donors to contribute anion binding. Receptor **111** was selective for AcO^-, as the longer spacer between the thiourea and the indole and amide moieties reduced the favourability of the cooperative binding of $H_2PO_4^-$.

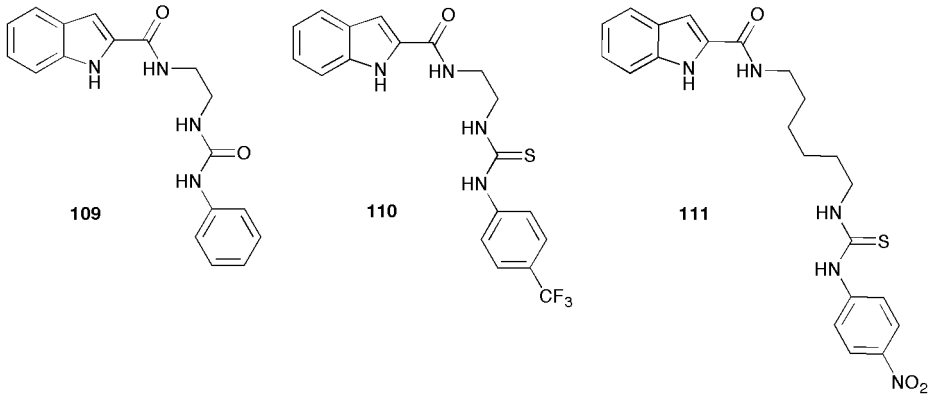

Figure 2.5 The indole containing receptors reported by Pfeffer *et al.*

Gale and co-workers have also used a combination of indoles and ureas to yield highly effective scaffolds for anion recognition. Di-indolylurea **112** (**Figure 2.6**) was found to selectively bind $H_2PO_4^-$ (by ^1H NMR titration with the TBA^+ salt).[69] A 1:1 binding stoichiometry was confirmed for this process by Job plot analysis. Remarkably, interaction was observable in DMSO-d_6/H_2O mixture of increasing polarity; binding constants were calculated as 5170 M^{-1} in DMSO-d_6/H_2O-10 % and 160 M^{-1} in DMSO-d_6/H_2O-25 %. The strength of this interaction in highly competitive solvent systems indicates that the diindolylurea cleft is well suited to binding the $H_2PO_4^-$ anion. Further to this work, Gale *et al.* found that increasing the number of hydrogen bond donors on the diindolyl urea scaffold (receptor **113**, **Figure 2.6**) resulted in hosts which could complex a range of anions extremely strongly in DMSO-d_6/H_2O mixtures.[70] Interestingly, the titration of **113** with $TBAH_2PO_4$ in DMSO-d_6/H_2O-0.5 % resulted in the appearance of new peaks, apparently in slow exchange, after the addition of 1.4 eq. anion. The authors found that these peaks indicated the deprotonation of the bound $H_2PO_4^-$ anion to HPO_4^{2-}. They reasoned that the strong complexation of the anion by 6 hydrogen bond donors could modify the pK_a of the bound anion by stabilizing the deprotonated form. The deprotonation of a bound anion had been previously observed in the solid state;[69] however, this was the first reported example of this effect in solution.

Further to this work, the same authors described the synthetic modification of the diindolylurea scaffold to incorporate pendant indole substituents (receptor **114**, **Figure 2.6**).[71] This receptor contains 8 hydrogen bond donors which could potentially complex a single anion. In DMSO-d_6/H_2O 0.5%, receptor **114** facilitated the deprotonation of bound $H_2PO_4^-$ and HCO_3^- by free anion in solution. The interactions towards TBA_2SO_4 were also investigated by ^1H NMR titration under the same conditions. The binding of SO_4^{2-} was judged to be strong based on the shape of the binding curves; however, the binding curves could not be fitted to a 1:1 or 2:1 profile. The data indicated initial strong 1:1 complexation followed by the formation of higher order complexes at higher SO_4^{2-} concentrations. In the solid state, the crystal structure of **114**.SO_4^{2-} showed a 1:1 stoichiometry in which the anion was bound by 8 hydrogen bonds. However, other anions including benzoate were bound in a 3:1 manner in which the pendant indole groups

rotated away from the binding cleft to facilitate the binding of further equivalents of anion.

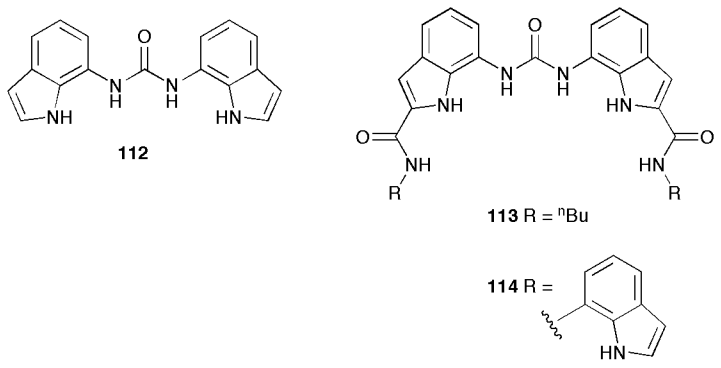

Figure 2.6 Gale and co-workers have extensively studied a progression of di-indolylureas.

Prior to this work, Gale and *et al.* had reported that receptors of the form **115** (**Figure 2.7**) bound Cl^-, $H_2PO_4^-$, AcO^- and $PhCO_2^-$ in DMSO-d_6/ H_2O 0.5 %.[144] On binding to oxoanions, the ^1H NMR titration showed that all of the NH hydrogen bond donors undergwent a downfield shift consistent with hydrogen bonding to the anion. This prompted Plavec and co-workers to investigate the conformational changed that occur when these receptors interact with anions by a combination of heteronuclear NMR spectroscopy and *ab initio* quantum mechanical calculations.[145] They found that the free receptors preferentially adopt an *anti-anti* conformation (**Figure 2.7**); however, interaction with anions such as AcO^- and Cl^- causes a conformational change to the *syn-syn* conformation, allowing the NH hydrogen bond donors to converge and contribute to binding the anion.

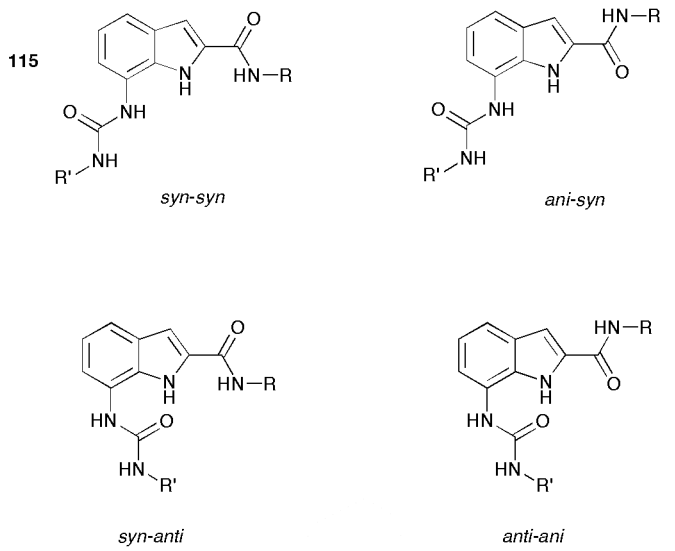

Figure 2.7 The different conformations that receptors of type **115** can adopt.

Jeong and co-workers have investigated the anion binding properties of bis-indolylurea receptor **117** by comparison to the analogous bis-amide **116**, shown in **Figure 2.8**.[146] UV-vis titration with the tetrabutylammonium salts in DMSO revealed that **116** and **117** bind $H_2PO_4^-$ (K_a = 1.4 x 10^5 M^{-1} and 3.9 x 10^5 M^{-1} respectively) more strongly than AcO^- (K_a = 4.3 x 10^4 M^{-1} and 7.5 x 10^4 M^{-1} respectively) These anions were bound similarly strongly by **116** and **117**, indicating that the additionally hydrogen bond donors in **117** contribute little to the binding of these anions. However, bis-urea **117** was found to bind $HP_2O_7^{3-}$ much more strongly than bis-amide **116** (K_a > 5 x 10^6 M^{-1} and 5.2 x 10^5 M^{-1} respectively). This indicates that the additional hydrogen bond donors were beneficial in the complexation of a larger anion, possibly due to a better fit to the binding cleft. Additionally, the authors found that a number of dicarboxylates were also bound strongly by **117** (UV-vis titration in 10 % MeOH/DMSO), which showed the greatest affinity for adipate (K_a = 8.1 x 10^5 M^{-1}).

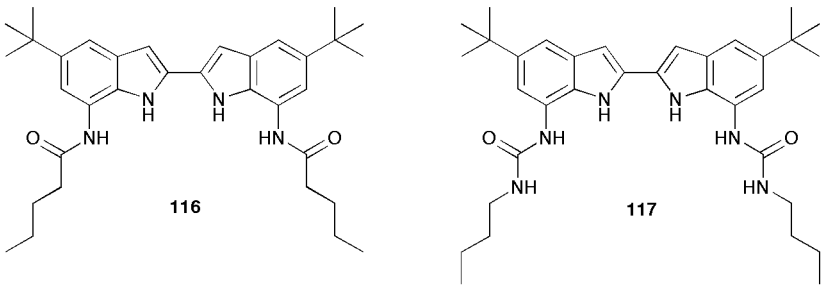

Figure 2.8 Jeong has incorporated the bi-indole scaffold into receptor design.

Jurczak and co-workers have also utilized a combination of indole and urea NH hydrogen bond donors in their design of receptors **118-120** (**Figure 2.9**).[147] They found by ^{1}H NMR titration that these receptors interacted with various anions in MeOH-d_3, a highly competitive and protic solvent. All of the anions tested were complexed in a 1:1 binding mode except for the larger $HP_2O_7^{3-}$ facilitated a 2:1 host:guest binding mode. Receptors **118-120** were found to interact most strongly with tetrahedral oxoanions such as $H_2PO_4^-$ (K_a = 135 M^{-1}, 535 M^{-1} and 265 M^{-1} respectively following the urea NH signal). Interestingly, these ligands interact as strongly with Cl^- as they do with benzoate, a much more basic anion. This may be due to the steric hinderance of binding benzoate. The stronger anion binding by **119** over **118** was attributed to the greater acidity of the hydrogen bond donors due to the enhanced electron withdrawing effect of the phenyl substituents. The additional indole group in **120** does not result in increased binding of the anions tested; however, the selectivity is improved. Receptor **119** binds HSO_4^- similarly strongly to $H_2PO_4^-$ (K_a = 280 M^{-1} and 535 M^{-1}), whereas the affinity of **120** for HSO_4^- (K_a = 90 M^{-1}) is greatly reduced by comparison to $H_2PO_4^-$ (K_a = 265 M^{-1}).

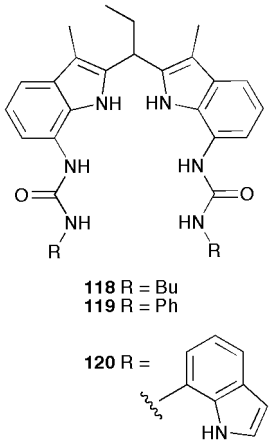

Figure 2.9 The indolylureas reported by Jurczak *et al.*

2.1.3 Ureas *vs.* thioureas for anion transport

Amongst the most successful anion carriers reported to date are the cholapods developed by A. P. Davis and co-workers.[48, 53-56] The key features of these carriers are the lipophilic cholic acid scaffold and, most commonly, the use of ureas as an anion binding motif. However, within the same work, A. P. Davis *et al.* have found that analogous thiourea substituted cholapods function as more efficient anion carriers. This observation was attributed to the stronger Cl^- binding by the thiourea receptors. For example, compound **20** binds chloride more strongly than compound **14** (K_a (**14**) = 5.2 x 10^8 M^{-1}, K_a(**20**) = 2.0 x 10^9 M^{-1}) and is also a more effective anion carrier. However, these two cholapods could only be tested comparatively by pre-incorporating the receptors into the vesicle membrane, as the thiourea analogue was found to precipitate if added externally. This highlights the greater hydrophobicity of the thiourea group if compared to the urea group.

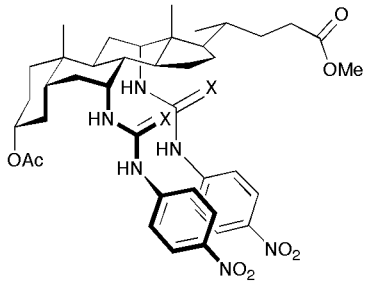

14 X = O
20 X = S

Figure 2.10 A. P. Davis and co-workers have used urea and thiourea derivatised cholapods.

A. P. Davis *et al.* also investigated the anion transport activity of urea **121**, shown in **Figure 2.11**, as a simple analogue of the cholapods.[54] When preincorporated into the lipid bilayer, **121** was found to mediate Cl^-/NO_3^- exchange although it was, unsurprisingly, much less active than cholapod **14**. Additionally, B. D. Smith and co-workers have described a functionalised phospholipid which facilitates anion transport by a relay mechanism.[72] The anion binding domain of this transporter is a *p*-nitrophenyl urea.

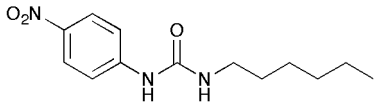

121

Figure 2.11 A simple urea is a structural analogue of the binding site of a cholapod.

Gale and co-workers have also investigated the anion transport properties of a series of tripodal ureas and thioureas based on the tren scaffold **37- 40** (**Figure 2.12**) In this work, the urea substituted ionophores were inactive for anion transport, while the thioureas were found to be efficient Cl^-/NO_3^- and Cl^-/HCO_3^- antiporters. In this work, binding studies were carried out by ^1H NMR titration in DMSO-d_6/H_2O (0.5 %) and little correlation between anion binding strengths and transport efficiencies was observed. The greater anion transport activity of the thiourea based molecules was attributed to their greater lipophilicity, thus better enabling the partitioning of the anion-receptor complex within the bilayer.

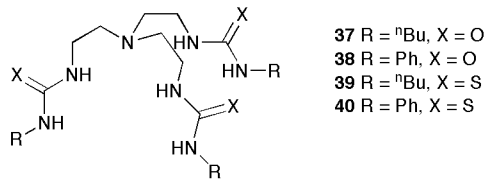

Figure 2.12 The (thio)urea receptors based on tren reported by Gale *et al.*

2.2 Structurally simple anion transporters for chloride

Inspired by the excellent transport activity exhibited by the bis-urea or thiourea functionalised cholapods and by Gale's tripodal thioureas, a series of structurally simple ureas and thioureas **122-127** (**Figure 2.13**) were synthesized to allow their comparative anion transport properties to be investigated.[68] The simplicity of the structures was chosen to allow for the straightforward assessment of substituent effects, and to allow comparison to the simple *p*-nitrophenyl urea **121**. The investigation of the tren based carriers had studied the effect of alkyl *vs.* aromatic (thio)urea substitution and found them to be similarly effective. Drawing on this, butyl- and phenyl- substituted ureas and thioureas **122-125** were synthesized. Indolyl- substituted urea and thiourea **126** and **127** were synthesized to investigate the effect of incorporating an additional indole hydrogen bond donor into the receptor design. The *i*-pentyl substituent common to all of the carriers was chosen as a general alkyl chain that had been previously incorporated into successful carrier design.[59]

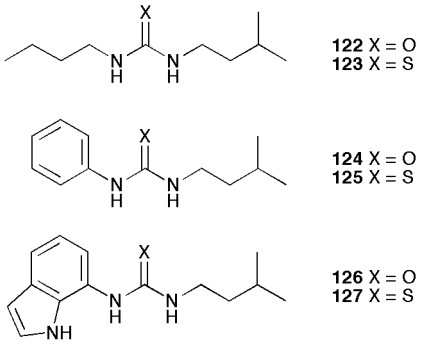

Figure 2.13 The structures of the anion carriers reported in this study.

The work discussed in this chapter was published in 2011.[76]

2.2.1 Synthesis

Compounds **122** and **126** were synthesized by SJM. Compounds **124** and **125** were synthesized by NA. Compound **123** was synthesized by CCT. Details of these synthetic procedures can be found elsewhere.[76] (A list of the full names of any contributing authors may be found in the abbreviations section. Where applicable, the contributions of these authors have been highlighted in the text.)

Thiourea **127** was synthesized as shown in **Scheme 2.1**. 7-Nitroindole was reduced using a Pd/C catalyst under an atmosphere of H_2 in EtOH, and subsequently the amine was converted to the corresponding isothiocyanate by reaction with thiophosgene in a two phase mixture of DCM and sat. $NaHCO_{3\,(aq)}$.[69] Finally, the isothiocyanate was reacted with ^{i}pentylamine in DCM to give compound **127** in 25 % yield after purification. Full experimental details may be found in **Chapter 6.4**.

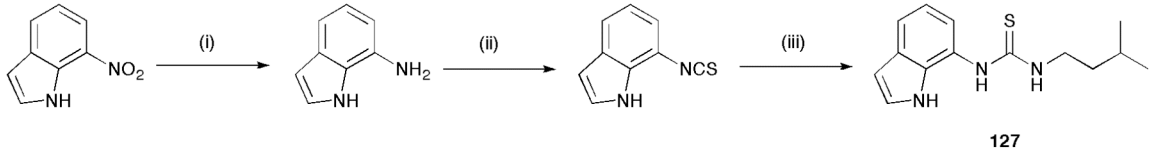

127

Scheme 2.1 The synthesis of thiourea **6**. Reagents and conditions: (i) H_2, Pd/C, EtOH, 2 h, RT, assumed 100 % yield; (ii) thiophosgene, DCM/ sat. $NaHCO_{3\,(aq)}$, overnight, RT, assumed 100 % yield; (iii) ^{i}pentylamine, DCM, overnight, RT, 25 % overall yield.

Crystals of compound **127** suitable for X-ray crystallography were grown from a DCM/ Et_2O (50:50) solution by slow evaporation. The structure is shown in **Figure 2.14**. Full details of the X-ray diffraction analysis can be found in the appendix section **A3.1**.

(a)

(b)

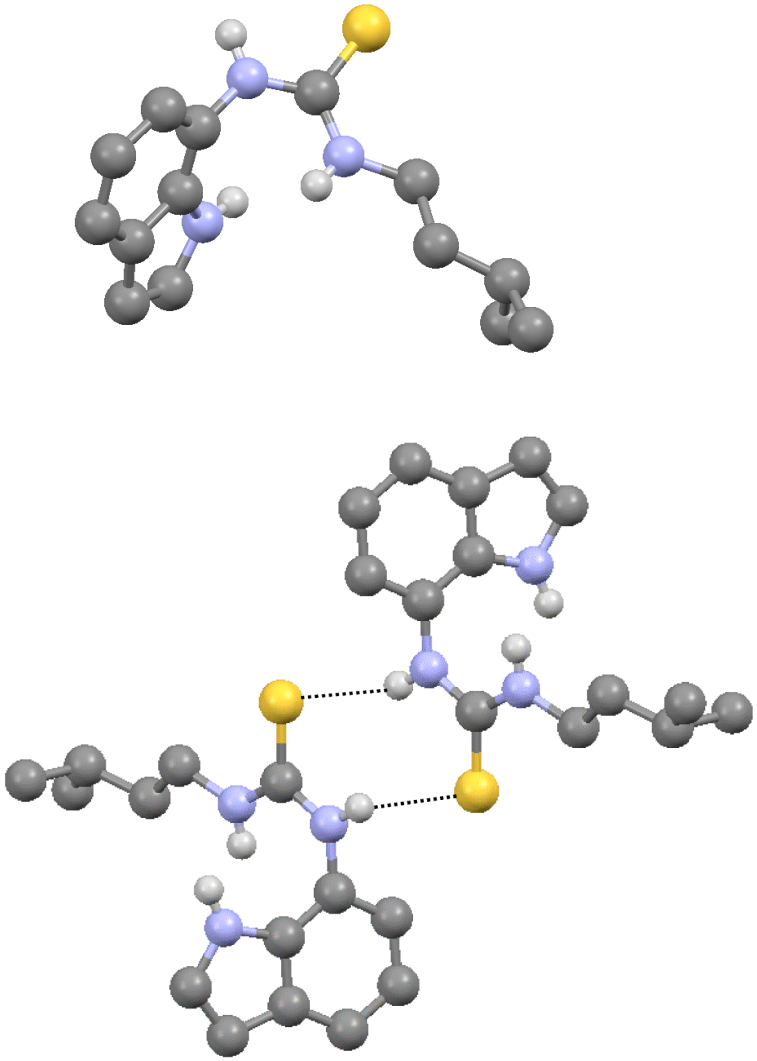

Figure 2.14 The crystal structure of (a) a single molecule of receptor **127** and (b) intermolecular hydrogen bonding between two receptor molecules. Non-acidic hydrogen atoms have been omitted for clarity.

The structure shows that in the solid state the receptor is not preorganised for anion binding, as the thiourea NH adjacent to the indole group is orientated away from the binding cleft. However, this is not a reliable indication of the favoured conformation of this receptor in solution. In the solid state, a hydrogen bonding interaction between the NH and the S atom of another receptor molecule dictates this conformation (**Figure 2.14**(b)).

2.2.2 Chloride transport studies

The ability of compounds **122-127** to facilitate Cl^-/NO_3^- antiport was investigated as follows. A solution of the receptor in DMSO (final receptor concentration 0.02 mM, or 2 mol% with respect to lipid) was added to a suspension of unilamellar POPC vesicles containing 489 mM NaCl suspended in 489 mM $NaNO_3$. All of the solutions were buffered to pH 7.2 with 5 mM sodium phosphate salts. The lipid concentration in the sample was 1 mM. The chloride concentration of the external solution was monitored using a chloride selective electrode. After 300 s the vesicles were lysed by the addition of octaethylene glycol monodecyl ether solution (H_2O/DMSO 7:1 *v*/*v*) to calibrate 100 % chloride efflux. Full details of the vesicle preparation and transport experiments may be found in the **Chapter 6.2** The results are shown in **Figure 2.15**.

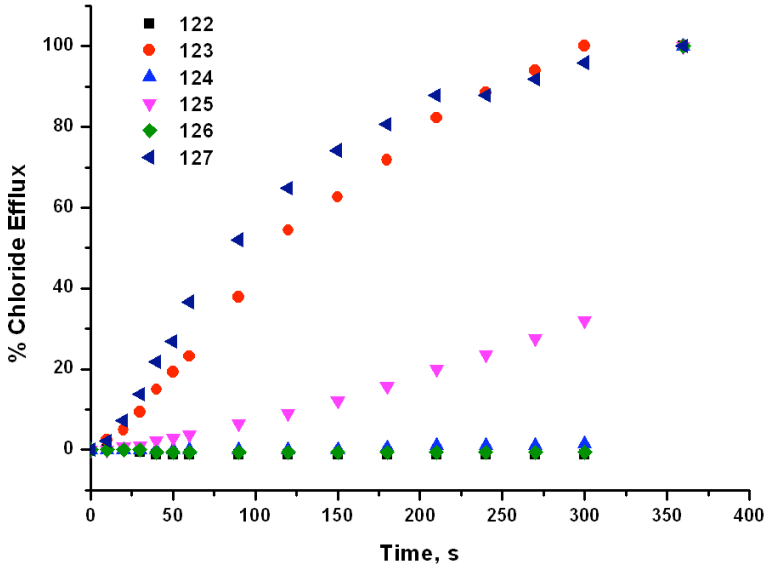

Figure 2.15 Chloride efflux promoted by receptors **122-127** (2 mol% with respect to lipid) from unilamellar POPC vesicles containing 489 mM NaCl buffered to pH 7.2 with 5 mM sodium phosphate salts. The vesicles were suspended in 489 mM $NaNO_3$ buffered to pH 7.2 with 5 mM sodium phosphate salts. At the end of the experiment, the vesicles were lysed to calibrate 100 % chloride efflux. Each point represents the average of 3 trials.

Thioureas **123**, **125** and **127** were found to facilitate Cl^-/NO_3^- antiport, while the corresponding ureas were completely inactive. Compounds **123** and **127** were the most active, and under these conditions they mediate a similarly high level of Cl^- efflux. Work

by SJM showed that the activity diminished in vesicles composed of POPC:cholesterol (7:3), thus implying a mobile carrier mechanism for these receptors. To confirm that the observed chloride efflux was due to an anion antiport mechanism, the chloride efflux mediated by **122-127** was monitored from vesicles containing NaCl suspended in Na_2SO_4. The results are shown in **Figure 2.16**.

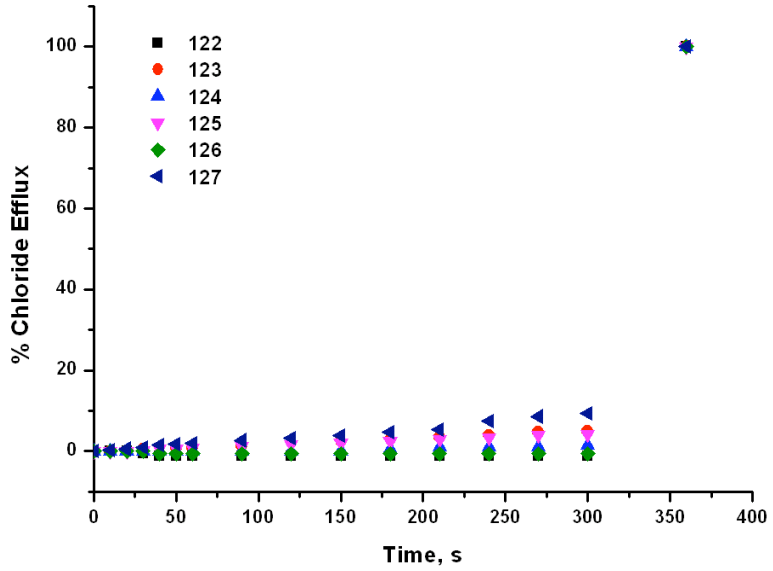

Figure 2.16 Chloride efflux promoted by receptors **122-127** (2 mol% with respect to lipid) from unilamellar POPC vesicles containing 489 mM NaCl buffered to pH 7.2 with 5 mM sodium phosphate salts. The vesicles were suspended in 167 mM Na_2SO_4 buffered to pH 7.2 with 5 mM sodium phosphate salts. At the end of the experiment the vesicles were lysed to calibrate 100 % chloride efflux. Each point represents the average of 3 trials.

When the external anion was exchanged for SO_4^{2-} the observed Cl^- transport was inhibited. This dependence on the external anion indicates that the thiourea receptors **123**, **125** and **127** mediate Cl^- transport by an antiport mechanism.

2.2.3 The Hill analysis

The data in **Figure 2.15** indicates that ^{n}butyl thiourea **123** and 7-indolyl thiourea **127** are similarly effective anion transporters. However, at lower carrier concentrations it becomes apparent that receptor **127** is more potent. For example, the chloride efflux

mediated by each receptor at a concentration of 0.05 mol% (with respect to lipid) is shown in **Figure 2.17**.

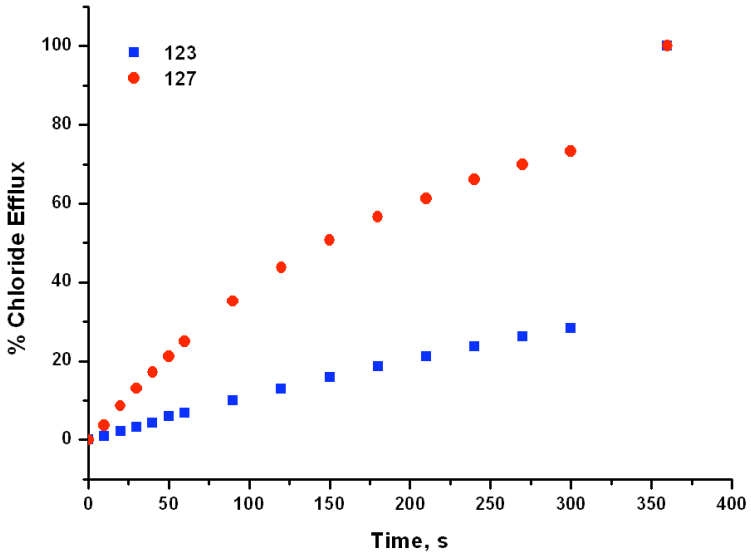

Figure 2.17 Chloride efflux mediate by receptors **123** and **127** (0.05 mol% with respect to lipid) from unilamellar POPC vesicles containing 489 mM NaCl buffered to pH 7.2 with 5 mM sodium phosphate salts. The vesicles were suspended in 489 mM $NaNO_3$ buffered to pH 7.2 with 5 mM sodium phosphate salts. At the end of the experiment, the vesicles were lysed to calibrate 100 % chloride efflux. Each point represents the average of 3 trials.

This data clearly indicates that receptor **127** is a more efficient carrier at lower concentrations. This highlights that testing at a single concentration is not sufficient to fully examine the relative efficiencies of two carriers.

In order to further investigate and quantify the observed Cl^-/NO_3^- antiport activity, a Hill analysis was performed for this process. The full analysis for compound **123** is shown below as an example of this procedure; all other Hill analyses may be found in the Appendix (section **A1.1**). A more detailed explanation of this analysis may be found in **Chapter 1**.

$$y = V_{max}x^n / (k^n + x^n)$$

Equation 2.1 A form of the Hill equation where y is the % chloride efflux at 270 s, V_{max} is the maximum chloride efflux (100%), x is the carrier loading, k is the EC_{50} (the carrier loading required to promote 50 % total chloride efflux at 270 s, measured in mol% with respect to lipid) and n is the Hill coefficient, representing the number of carriers required to transport a single anion.

The Cl^-/NO_3^- antiport promoted by different concentrations of compound **123** was investigated. The results are shown below. The corresponding graphs for **125** and **127** may be found in the appendix (section **A1.1**).

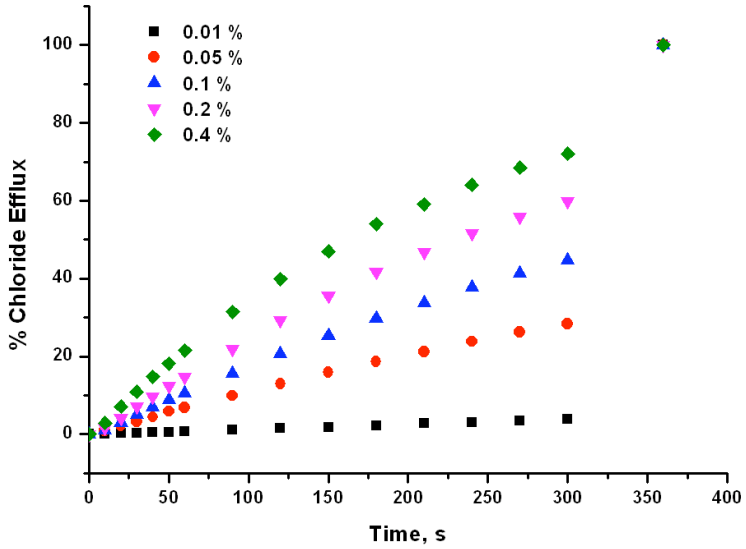

Figure 2.18 Chloride efflux promoted by various concentrations of **123** from unilamellar POPC vesicles containgng 489 mM NaCl buffered to pH 7.2 with 5 mM sodium phosphate salts. The vesicles were suspended in 489 mM $NaNO_3$ buffered to pH 7.2 with 5 mM sodium phosphate salts. At the end of the experiment, the vesicles were lysed to calibrate 100 % chloride efflux. Each point represents the average of 3 trials.

The total chloride efflux after 270 s was plotted against the carrier concentration and this data was fitted to the Hill equation (**Equation 2.1**) using Origin® 8.1. This analysis is shown below.

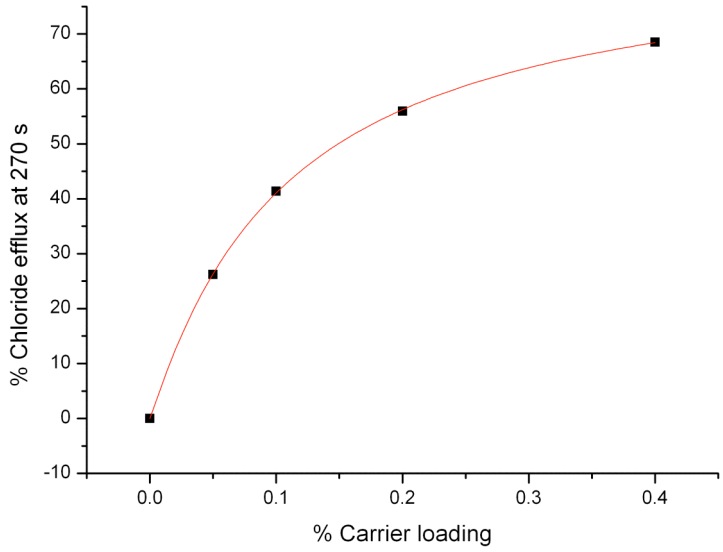

Figure 2.19 The Hill analysis for Cl^-/NO_3^- antiport mediated by compound **123**. The data was fitted to **Equation 2.1** using Origin. $R^2 = 0.99977$. $k = 0.110 \pm 0.006$, $n = 1.05 \pm 0.04$.

The relevant constants from the Hill analyses are shown in **Table 2.1**.

Table 2.1 The EC_{50} at 270 s for the Cl^-/NO_3^- antiport by **123**, **125** and **127** and the Hill coefficient (n) calculated by the Hill analysis.

Compound	**EC_{50} at 270 s (Cl^-/NO_3^-)/ mol%**	**n**
123	0.11	1.0
125	3.05	1.36
127	0.03	1.52

The $EC_{50\ 270\ s}$ values demonstrate that the most potent receptor is indole substituted thiourea **127**. This receptor exhibited similar transport activity to compound **123** at 2 mol% loading (**Figure 2.15**); however, it mediates chloride transport at much lower concentrations than compound **123** which is reflected in the significantly lower $EC_{50\ 270\ s}$ value. In fact, compound **127** is able to facilitate Cl^-/NO_3^- exchange at a loading of 0.004 mol% or 1:25 000 (carrier to lipid). The most active carrier which had been reported prior to this work was a cholapod reported by A. P. Davis to function at a loading of 1:250 000 (carrier to lipid), but only if preincorporated into the lipid bilayer.[54] The potency of receptor **127** is remarkable considering its simplicity. Compound **123** also

functions as an efficient Cl^-/NO_3^- antiporter, while compound **125** is the least efficient of the thioureas tested. The Hill coefficient (n) values indicate that the transport process by each receptor is unimolecular, i.e that each anion is transported by a single receptor. This offers further evidence of a mobile carrier process rather than the possible assembly of pores.

2.2.4 Bicarbonate transport and binding studies

Work by SJM demonstrated that compounds **123**, **125** and **127** can also mediate Cl^-/HCO_3^- exchange. $EC_{50\ 270\ s}$ values for this process are shown in **Table 2.2**, along with binding constants for **122-127** with relevant anions (determined by SJM by titration with tetrabutylammonium or tetraethylammonium salts in DMSO-d_6/H_2O 0.5 %) and the clogP (calculated octanol-water partition coefficient, a measure of lipophilicty) and polar surface area (PSA) of the receptors (calculated using Spartan '08 for Macintosh).

Table 2.2 EC_{50} values for Cl^-/HCO_3^- antiport calculated by Hill analysis by SJM. Anion binding constants determined by ^1H NMR titration with the tetrabutylammonium or tetraethylammonium anion salts in DMSO-d_6/H_2O (0.5 %), performed by SJM. Errors on binding constants are < 10 %. clogP and PSA values were calculated using Spartan '08 for Macintosh. In the case of compounds **126-127** a range of PSA values is quoted, representing the different rotational conformations that the indole can adopt.

Compound	EC_{50} at 270 s (Cl^-/HCO_3^-)	K_a (Cl^-)/ M^{-1}	K_a (NO_3^-)/ M^{-1}	K_a (HCO_3^-)/ M^{-1}	clogP	PSA/ $Å^2$
122	-	< 10	[a]	18	1.99	37.0
123	0.30	10	[a]	58	3.14	22.2
124	-	21	[a]	135	2.42	34.8
125	2.08	22	[a]	343	3.57	21.5
126	-	96	[a]	1170	2.02	44.6-47.7
127	0.04	28	[a]	516	3.16	31.3-35.5

Again, receptor **127** is also the most potent carrier for Cl^-/HCO_3^- exchange, while **123** and **125** are also active. The values of EC_{50} for this exchange process are higher than for Cl^-/NO_3^- antiport. This is commonly observed for 2 reasons: (i) HCO_3^- is more hydrophilic than NO_3^- and is therefore expected to be more difficult to transport across a bilayer;[1] (ii) the nature of the Cl^-/HCO_3^- assay provides a smaller HCO_3^- gradient (40 mM external HCO_3^-) than the NO_3^- gradient present in the Cl^-/NO_3^- assay (489 mM external NO_3^-) thus there is a smaller electrochemical gradient to drive the transport process.

The binding constants obtained do not reveal a strong correlation between anion affinity and the transport activity. The greater transport activity of the thiourea receptors by comparison to their urea analogues is attributed to their greater lipophilicity, as demonstrated by their higher clogP and lower PSA values. However, it is postulated that the indolyl thiourea **127** is the most active carrier as it combines the lipophilic thiourea scaffold with an additional NH hydrogen bond donor for anion complexation.

2.2.5 Amides and thioamides

A series of amides and thioamides **128-133** were synthesized as analogues of **122-127** in order to investigate the importance of the (thio)urea functionality compared to a receptor containing only one hydrogen bond donor.

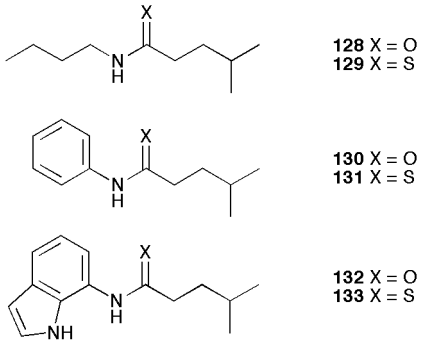

Figure 2.20 The amides and thioamides studied as analogues of receptors **122-127**.

Compound **130** was synthesized by the activation of 4-methylvaleric acid with 1,1'-carbonyldiimdazole (CDI) in $CHCl_3$, followed by reaction with aniline.

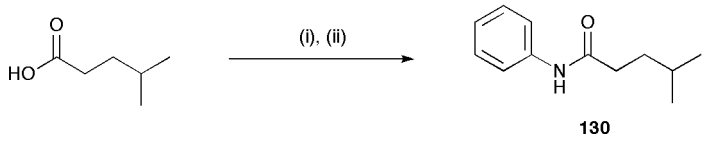

130

Scheme 2.2 Reagents and conditions: (i) CDI, $CHCl_3$, reflux, 2 h; (ii) aniline, $CHCl_3$, reflux, overnight, 76 % yield.

Thioamides **129** and **131** were synthesized by reaction of the corresponding amide with Lawesson's reagent in THF.

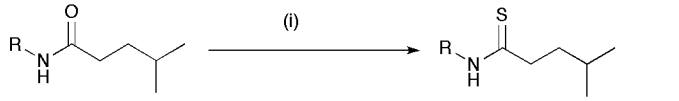

128 R = ^{n}Bu
130 R = Ph

129 R = ^{n}Bu, 75 % yield
131 R = Ph, 62 % yield

Scheme 2.3 Reagents and conditions: (i) Lawesson's reagent, THF, reflux, overnight.

Compounds **128**, **132** and **133** were synthesized by SJM by similar procedures. The Cl^-/NO_3^- antiport activity of **128-133** was investigated by SJM. Unsurprisingly, amides **128**, **130** and **132** were found to be inactive. The transport activity of the thioamides **129**, **131** and **133** was found to be greatly diminished by comparison to the thioureas. This highlights the importance of the chelating ability of the thiourea NHs to anion transport.

2.3 Conclusions

The work discussed in this chapter demonstrates that structurally simple thiourea based anion receptors function as highly potent anion antiporters. The key feature of the thiourea scaffold which makes it more effective than an analogous urea is proposed to be the enhanced lipophilicity and reduced PSA, both of which factors aid the partitioning of the receptor and the formed receptor-anion complex within the lipid bilayer. Indolyl thiourea **127** was found to be a remarkably potent anion carrier considering the simplicity of its structure. At the time when this work was completed, it was the most potent synthetic anion carrier that had been developed by the Gale group. This indicates that 7-indoles are a useful structural motif in the design of anion carriers, and that the reduction

in lipophilicity associated with the inclusion of an additional hydrogen bond donor into a receptor scaffold does not necessarily cause a corresponding decrease in transport activity if the hydrogen bond donor is of use in anion complexation. Additionally, this work shows that even very simple anion receptors can function as highly potent transporters and gives evidence that encapsulation of the anion is not necessary for efficient transport.

The development of anion carriers which function at low concentrations is an important target as the target of this research is to produce carriers with potential application as drugs for the treatment of various diseases. High potency is a desirable target in the synthesis of new pharmaceuticals as it allows the administration of lower concentrations and potentially reduces the risk of other harmful side effects.

Chapter 3
Bis-indolylureas as tunable chloride transport agents

3.1 Introduction

It is well established that anion receptors based on urea and thiourea hydrogen bond donors can also function as highly efficient anion antiporters.[53-56, 68, 76] In the studies reported in **Chapter 2**, it was demonstrated that structurally simple thiourea carriers were more active than their urea analogues. This observation was attributed to the higher lipophilicity of these species. The most active compound studied was indolyl thiourea **127**, implying that inclusion of the indole moiety in transporter scaffolds may be a useful design strategy. However, A. P. Davis *et al.* have effectively demonstrated that urea based molecules can also function as extremely active transporters.[48, 54-56] The key features of the cholapod design seem to be the lipophilicity of the cholic acid skeleton and the chelating ability of the pendant urea arms.

3.1.1 Bis-ureas for anion binding

Lin and co-workers have investigated the anion binding properties of the series of (bis)-*p*-nitrophenylureas **134-136** shown in **Figure 3.1**.[148] Investigation of the anion binding properties of these receptors by UV-vis titration in DMSO indicated that compound **134** was selective for F^- (log K_a = 5.31) over $H_2PO_4^-$ and AcO^-, while the addition of other halides resulted in little or no spectral response. Receptor **135** was found to be selective for $H_2PO_4^-$ with log K_a = 4.35, while receptor **136** displayed little selectivity. Job plot analyses showed that the anions were bound in a 1:1 receptor:anion

stoichiometry. The trends in binding selectivity were explained as a result of increasing the length of the central alkyl chain. Receptor **134** (with the shortest chain) was selective for the comparatively small F^- anion, whereas receptor **135** was selective for the larger $H_2PO_4^-$ as a result of the longer alkyl linker between the urea groups. Upon further extension of this central alkyl chain (compound **136**), any selectivity due to size complementarity was lost.

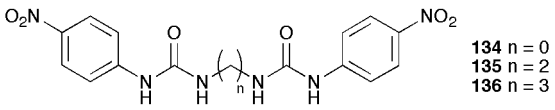

Figure 3.1 The bis-ureas **134-136** synthesized by Lin and co-workers.

Beer and co-workers have investigated the anion binding properties of some mono- and bis- urea substituted ferrocenes **137-140** as shown in **Figure 3.2**.[149] ^{1}H NMR titrations in CD_3CN were used to demonstrate that the bis- urea substituted receptors **139** and **140** bound Cl^- and $H_2PO_4^-$ more strongly than their monosubstituted analogues. A 1:1 binding stoichiometry for these binding events was confirmed by Job plot analyses, indicating that the bis-urea receptors were chelating the anion- a likely cause of the observed higher binding constants by comparison to the mono-urea receptors. Receptors **137** and **139** were found to be selective for $H_2PO_4^-$ over Cl^-, while receptors **138** and **140** displayed the opposite binding preference. This observation was attributed to the bulky substituents of receptors **138** and **140**, which sterically disfavoured the binding of the larger $H_2PO_4^-$ anion.

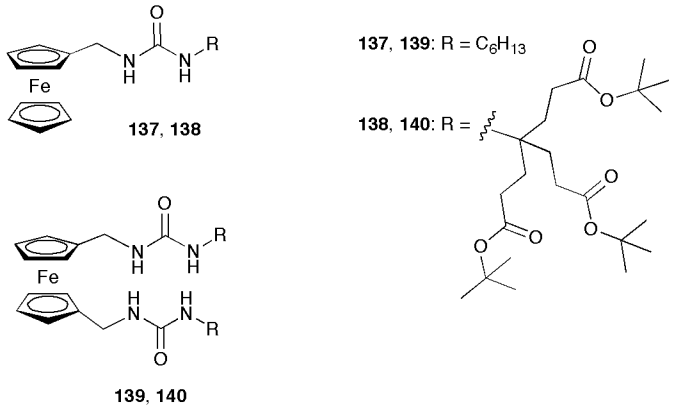

Figure 3.2 The mono- and bis- urea substituted ferrocenes reported by Beer.

Gale, Loeb and co-workers have investigated the anion complexation behaviour of a Pt(II) complex bearing urea containing ligands.[150] They used ^{1}H NMR titrations to investigate the binding mode of receptor **141** (**Scheme 3.1**) with TBACl and K_2SO_4 in DMSO-d_6. They found that Cl^- was complexed in a 1:2 receptor to anion stoichiometry, with each Cl^- coordinated *via* 4 hydrogen bond donors from 2 urea groups. However, SO_4^{2-}, as a larger anion with a higher charge, was bound in a 1:1 stoichiometry and complexed by all 8 hydrogen bond donors simultaneously. These binding modes are shown in **Scheme 3.1**, and were confirmed in the solid state by X-ray crystallography. This demonstrates that for a multi-urea containing receptor, if conformational flexibility exists, the binding mode will be dependent on the nature of the anion.

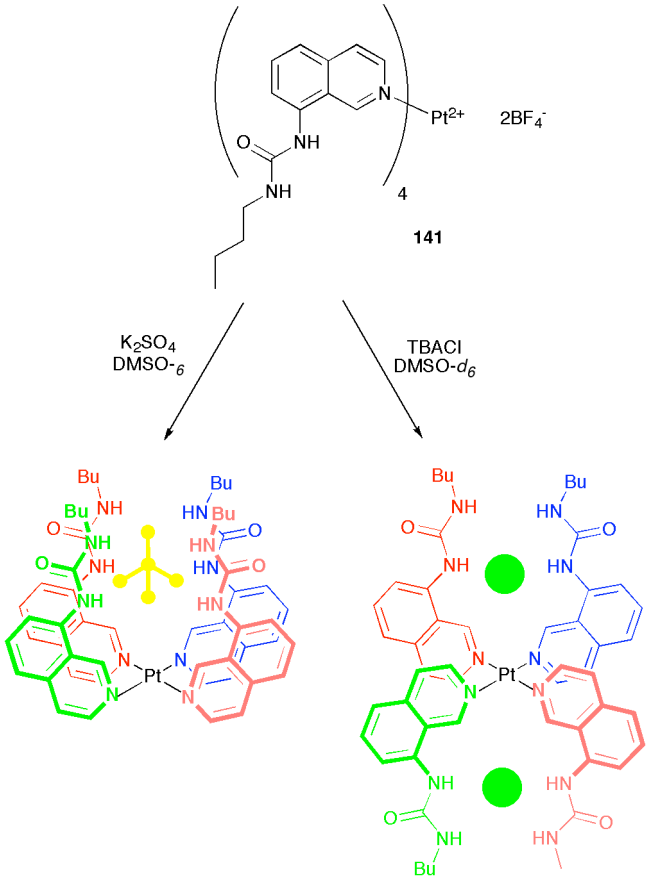

Scheme 3.1 Tetra-urea receptor **141** adopts different receptor:anion stoichiometries depending on the anion.

3.1.2 Self assembly of bis-ureas

The propensity of bis-ureas to self assemble is well documented as urea moieties are often found to form a network of hydrogen bonding interactions as shown in **Figure 3.3**.[151] As such, bis-ureas have commonly been found to act as gelators for organic solvents. [152-156]

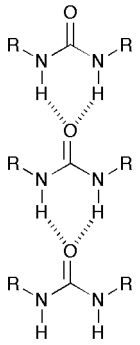

Figure 3.3 Hydrogen bonding interactions between urea moieties.

Work by Steed and co-workers has utilized this behaviour in their studies on the series of bis-ureas **142-148**.[157] They found that compounds **142**, **144**, **146** and **148**, in which n = even, functioned as low molecular weight gelators (LMWGs) forming organogels in a variety of solvents, whereas the remaining compounds (**143**, **145** and **147**) in which n = odd exhibited no gelation behaviour. This was attributed to the relative orientations of the two urea groups in these sets of molecules; if n = odd, the urea groups should be orientated in the same direction, while if n = even, the urea groups should be orientated in opposite directions, which was found to be preferable for gelation. Interestingly, the gel strength of compounds **142**, **144**, **146** and **148** was found to be reduced and in some cases completely inhibited in the presence of small amounts AcO^-, Cl^- and Br^- and NO_3^- (added as their TBA^+ salts). This modulation of gel strength was not observed upon addition of BF_4^-. These observations were attributed to disruption of the urea hydrogen bonding networks in the presence of anions that could compete for hydrogen bonding interactions.

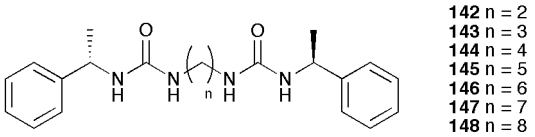

Figure 3.4 The LMWGs reported by Steed *et al.*

3.1.3 Self assembly of ureas for ion transport

Fyles *et al.* report the dynamic self assembly of a series of crown ether substitued ureas such as **149** into alkali metal cation conducting pores.[158] Individually, these molecules function as ditopic receptors in which an anion is bound by the urea moiety and a cation may be bound within the crown ether. On first appearances then, these molecules may be expected to function as discrete ion carriers. However, their self assembly within liquid membrane phases led to consideration of the possibility that they could form potentially membrane spanning superstructures. Planar bilayer conductance studies proved single channel behaviour of the assembled structures. It was proposed that the assembled structures were formed by intermolecular hydrogen bonding interactions between urea groups as depicted in **Figure 3.5** which would bring the crown ether moieties into close proximity and allow the passage of a cation through the assembled network.

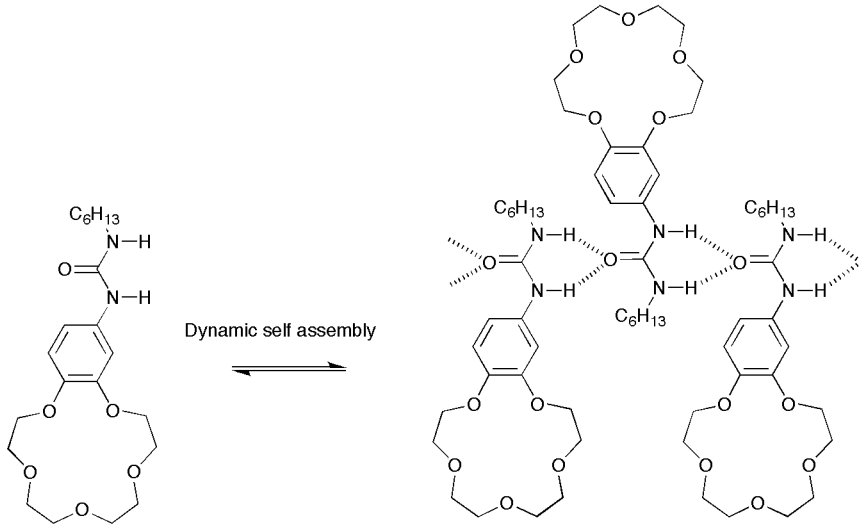

149

Figure 3.5 The proposed dynamic self assembly of crown ether substituted urea **149** reported by Fyles *et al.*

3.1.4 Variation of ion transporter length

The optimum design of transmembrane ion channels relies on the channel being of a complementary size to span the membrane. Fyles and co-workers report the cation channel formation of compound **151**, while compounds **150** and **152** with shorter and longer alkyl chains respectively were found to be almost completely inactive under the same conditions (**Figure 3.6**).[120] Voltage clamp techniques were used to demonstrate single channel activity. It was reasoned to be unlikely that a single molecule of **151** could form a pore and therefore assumed that an aggregate structure must assemble within the bilayer. As the alkyl chains of compound **151** are significantly shorter than the fatty acid components of phospholipids (on average C_{16}) it was reasoned that the aromatic groups would most likely reside in the midpolar region of the bilayer, allowing interaction with the fatty acid-phosphocholine carbonyl groups.

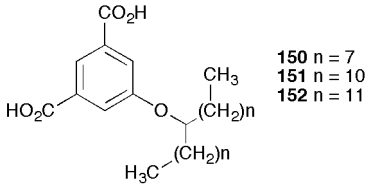

Figure 3.6 The cation channels reported by Fyles.

Regen and co-workers have reported a Na^+ channel forming derivative of spermine and cholic acid, **153**.[159] The ion transport activity of this channel was found to be strongly dependent on the thickness of the bilayer, providing evidence that the molecule was spanning the membrane. This compound was studied in comparison to compound **154** (a pre-existing Na^+ channel). It was found that **153** showed the highest Na^+ conductance in membranes containing lipids with fatty acid residues that were 2 carbons longer than the membranes in which **154** promoted the highest Na^+ flux. This was attributed to the fact that **153** is longer than **154** by 2 methylene units.

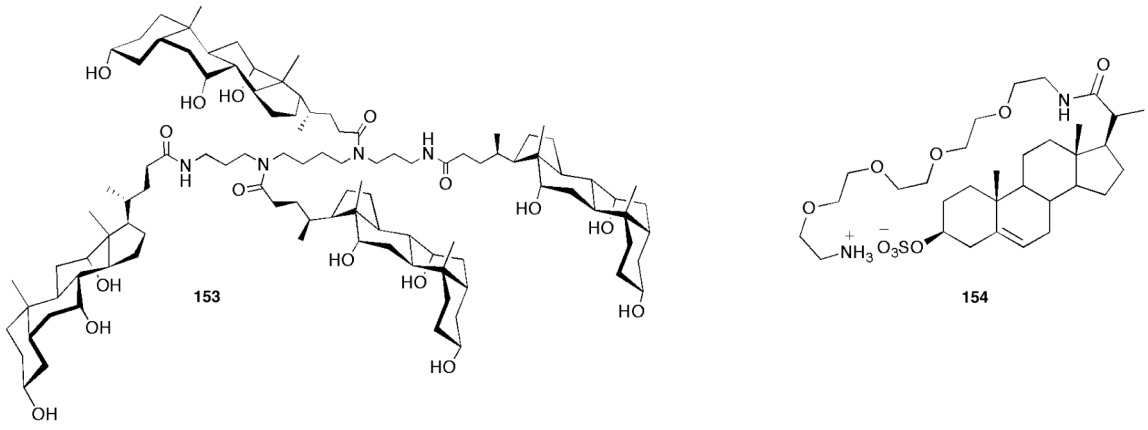

Figure 3.7 The channel forming ability of **153** and **154** is dependent on the bilayer thickness as they span the membrane.

This principle has also been extensively explored by Gokel and co-workers in their studies of the series of peptides shown in **Figure 3.8**.[160] Systematic variation of the substitution of both the C- and N-terminus (R' and R respectively) of these peptides allowed the optimum channel length to be determined.

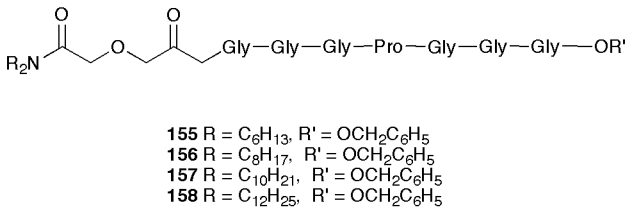

Figure 3.8 The basic structure of the series of heptapeptides studied by Gokel *et al*. with various alkyl substitution at the N- and C-terminus.

It was found that variation of the structure of these molecules had a large effect on their chloride transport efficiency. Variation of the length of the alkyl chain at the N-terminus (compounds **155**-**158**) revealed that the optimum N-substituent was C8 (**156**). In general, increasing the chain length up to C8 resulted in an increase in transport activity; however, after this point the activity was found to decrease with increasing chain length. Similarly, an optimum chain length for the C-terminus substituent was also observed. The authors attributed this finding to a balance between the hydrophilicity and the lipophilicity of the molecule, and that pore formation by dimeric pairs might be inhibited if the chains were too long.

3.2 Bis-indolylureas

The series of receptors discussed in the following chapter are shown in **Figure 3.9**.

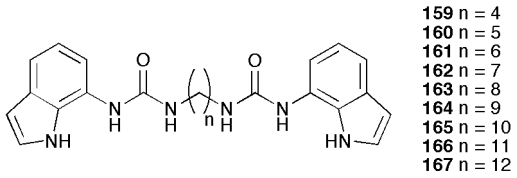

Figure 3.9 The bis-indolyl ureas discussed in this chapter.

The design of these carriers was based on the following principles:

- Thioureas have been shown to be excellent anion transporters. However, thioureas are often found to be toxic[161] which may limit their applicability for biological application. Ureas are less commonly toxic and thus might be more suited to this goal.

- However, in **Chaper 2** simple mono-ureas were found to be inactive for anion transport, thus the complexity of the system must be increased. There are many literature examples in which the use of multiple urea units has lead to enhanced anion recognition properties. This principle could be applied to anion transport.
- The indolyl (thio)urea hydrogen bond donor motif has been incorporated into a highly successful anion carrier (receptor **127**). Therefore, indole was chosen as a substituent in this series of carriers.
- The lipophilicity of anion carriers has been implicated as an important structural consideration in the design of new targets. The bis-alkylurea scaffold allows the straightforward modification of the lipophilicity of these carriers in a stepwise manner by simply increasing the length of the central alkyl chain.

3.3 Synthesis

The series of symmetrical bis-indolylureas **159-167** were synthesized as shown in **Scheme 1**. The reduction of 7-nitroindole was achieved by stirring in EtOH under an atmosphere of H_2 using catalytic Pd/C (10%). The corresponding amine was reacted with CDI in DCM; the intermediate thus formed (**3.1**) was converted to the desired product by reflux with the corresponding diamine in a DCM:DMF mixture (99:1) to give compounds **159-167** in 24-82 % overall yield. Full synthetic details can be found in **Chapter 6.4**.

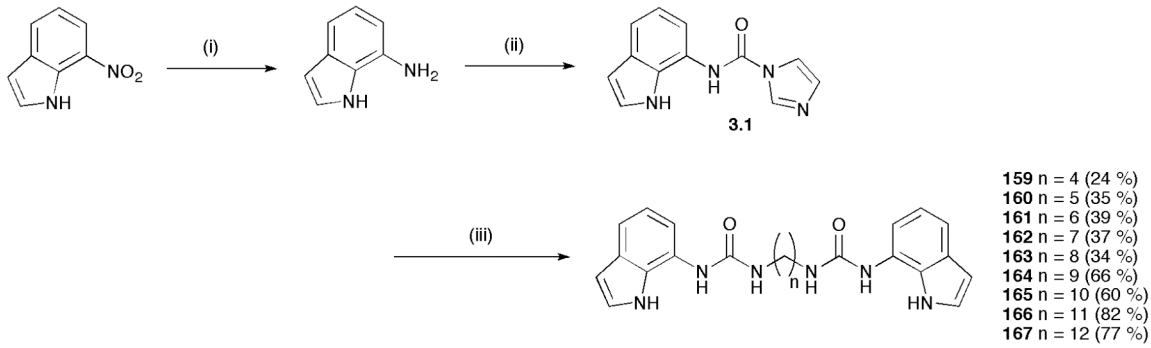

Scheme 3.2 Reagents and conditions: (i) H_2, Pd/ C, EtOH, 3 h, RT; (ii) CDI, DCM, N_2, RT, overnight; (iii) ½ equivalent diamine, DCM:DMF (99:1), N_2, reflux, overnight. The yields quoted are overall yields starting from 7-nitroindole.

3.4 Anion transport studies

3.4.1 Chloride transport activity

Compounds **159-167** were tested for Cl^-/NO_3^- antiport activity. The results are shown in **Figure 3.10**.

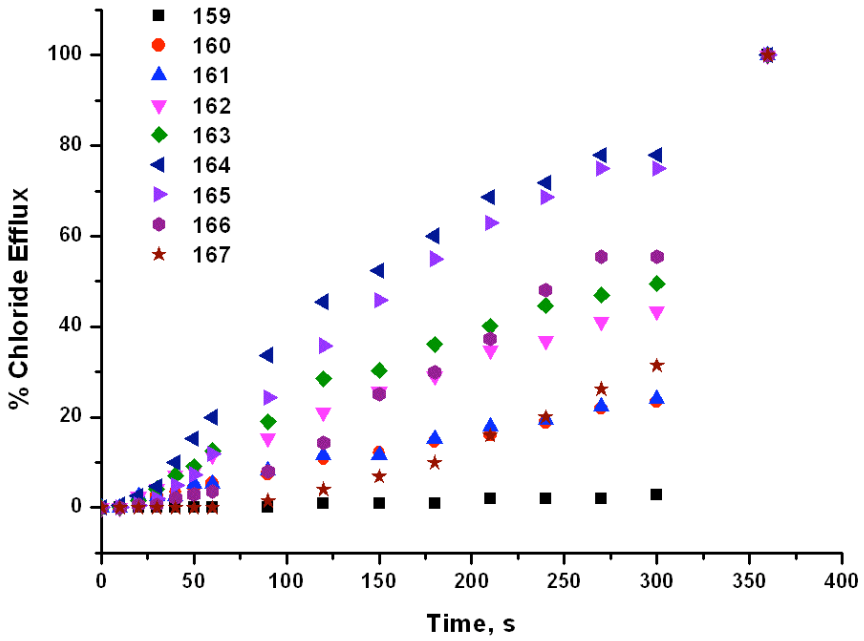

Figure 3.10 Chloride efflux promoted by compounds **159-167** (2 mol% with respect to lipid) from unilamellar vesicles containing 489 mM NaCl buffered to pH 7.2 with 5 mM sodium phosphate salts. The vesicles were suspended in 489 mM $NaNO_3$ buffered to pH 7.2 with 5 mM sodium phosphate salts. At the end of the experiment, the vesicles were lysed by addition of detergent to calibrate 100 % chloride efflux. Each point represents the average of 3 trials.

The results show that compounds **159-167** exhibit a range of chloride transport activity. The maximum activity under these conditions was observed for compounds **164** and **165** with n = 9 and 10 respectively. Between compounds **159-165**, transport activity was found to increase with the increasing length of the central alkyl chain; after this point, transport activity is reduced with increasing chain length.

Chloride transport was demonstrated to occur *via* a Cl^-/NO_3^- antiport mechanism as chloride efflux was inhibited when the external solution was replaced with Na_2SO_4.

Compounds **159-167** were also found mediate only low levels of Cl^-/HCO_3^- antiport (see Section **A1.2** in the appendix).

A Hill analysis was performed for each compound in order to examine the mediated Cl^-/NO_3^- exchange process in more detail. The relevant constants from the Hill analysis are shown in **Table 3.1**. The full Hill analyses can be found in the appendix (section **A1.2**).

Table 3.1 $EC50_{270\ s}$ values and Hill coefficients (*n*) were derived from the Hill analyses of mediated chloride efflux by compounds **159-167** from unilamellar vesicles in a Cl^-/NO_3^- exchange process. Values of clogP and PSA were calculated using Spartan '10 for Macintosh. The range of PSA values given reflects the different conformations of the indolyl urea unit. [a] These compounds were not active enough to perform the Hill analysis ($EC_{50\ 270\ s}$ > 4 mol%).

Compound	$EC_{50\ 270\ s}$ (mol% carrier:lipid)	*n*	clogP	PSA/ (Å^2)
159	[a]	-	-0.97	89.2-94.7
160	[a]	-	-0.55	89.2-94.7
161	[a]	-	-0.13	89.1-94.5
162	2.78	1.93	0.29	90.0-94.0
163	2.53	1.56	0.70	89.3-94.8
164	1.33	2.41	1.12	89.2-94.8
165	1.46	2.26	1.54	89.2-94.7
166	2.07	2.14	1.95	89.9-94.7
167	3.37	2.36	2.37	89.9-95.5

The results of the Hill analysis confirm the order of transporter efficiency observed in **Figure 3.10**. Increasing the length of the central alkyl chain from receptors **159** (n = 4) and **164** (n = 9) results in an increase in chloride transport activity. This correlates with an increase in the lipophilicity of the receptors, as evidenced by the increasing clogP values, thus enhancing the interaction of the receptor and the receptor-anion complex with the hydrophobic interior of the lipid bilayer. However, between receptors **164** (n = 9) and **167** (n = 12) a decrease in transport activity is observed on increasing the alkyl chain length. In order to investigate this effect, the differences in the initial rate of chloride efflux promoted by these receptors was investigated.

3.4.2 Partitioning kinetics

Closer analysis of the data from the Cl^-/NO_3^- antiport assays revealed that compound **167** (n = 12) promotes slower *initial* chloride efflux than its shorter chain analogues. However, after a short period of time an increased transport rate is observed. For example, a comparison between compound **167** (n = 12) and compound **162** (n = 7) is shown in **Figure 3.11**. The same trend is observed at all carrier loadings; the loadings shown below were selected, as the trend is more pronounced at higher loadings.

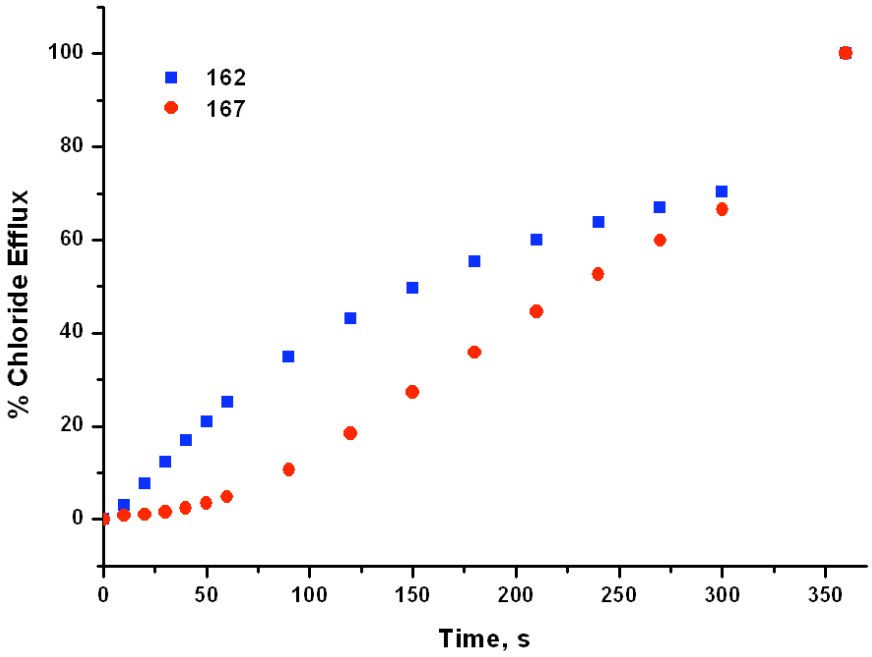

Figure 3.11 Chloride efflux promoted by receptors **162** and **167** (4 mol% w.r.t. lipid) from unilamellar vesicles containing 489 mM NaCl buffered to pH 7.2 with 5 mM sodium phosphate salts. The vesicles were suspended in 489 mM $NaNO_3$ buffered to pH 7.2 with 5 mM sodium phosphate salts. At the end of the experiment, the vesicles were lysed by addition of detergent to calibrate 100 % chloride efflux. Each point represents the average of 3 trials.

By the end of the experiment (300 s) these receptors have achieved a comparable % chloride efflux; however, it is clear that the initial rate of chloride efflux is very different. This demonstrates that the initial rate of chloride efflux mediated by the longer chain compounds is slower. This may be an explanation for their reduced overall transport activity.

A reason for the slower initial transport rate might be that the longer chain analogues take longer to partition into the lipid bilayer and begin mediating chloride flux. In order to investigate this hypothesis, an experiment was designed to allow the receptors to partition with the vesicle bilayer before the anion transport was initiated. Receptors **162** and **167** (4 mol% with respect to lipid) were added to a suspension of vesicles containing NaCl suspended in Na_2SO_4. Little chloride efflux was observed, as these conditions do not support an antiport mechanism. After 2 minutes, a pulse of $NaNO_3$ was

added and the resulting chloride efflux was monitored using a chloride ISE. The results are shown in **Figure 3.12**.

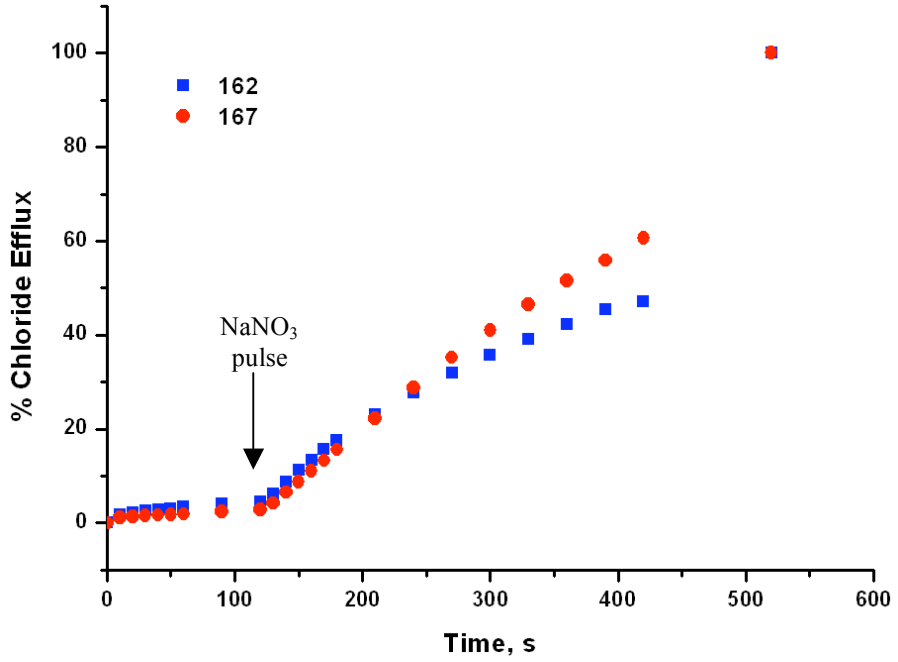

Figure 3.12 Chloride efflux promoted by receptors **162** and **167** (4 mol% w.r.t. lipid) from unilamllar POPC vesicles containing 489 mM NaCl buffered to pH 7.2 with 5 mM sodium phosphate salts. The vesicles were dispersed in 167 mM Na_2SO_4 buffered to pH 7.2 with 5 mM sodium phosphate salts. At t =120 s a pulse of $NaNO_3$ was added such that the final NO_3^- concentration was 40 mM. At the end of the experiment the vesicles were lysed to calibrate 100 % chloride efflux. Each point represents the average of 3 trials.

In this experiment, the chloride efflux promoted by receptors **162** and **167** appears to start at a comparable rate. There is no lag phase for the chloride transport by **167**, which indicates that in the previous experiment poor partitioning kinetics are responsible for this behaviour. By the end of the experiment, compound **167** has mediated a greater amount of chloride efflux than **162**, whereas in the previous experiment these values were similar. This indicates that the partitioning kinetics may be partially responsible for the observed reduction in transport activity on increasing the chain length > n = 9.

A value of the initial rate of chloride efflux was calculated for each receptor based on the chloride efflux mediated within the first 30 s of the experiment (2 mol% carrier loading with respect to lipid). The graph in **Figure 3.13** shows the correlation between this initial rate of transport and the total chloride efflux at 270 s mediated by each of the

receptors according to the central alkyl chain length. These values are tabulated in the appendix.

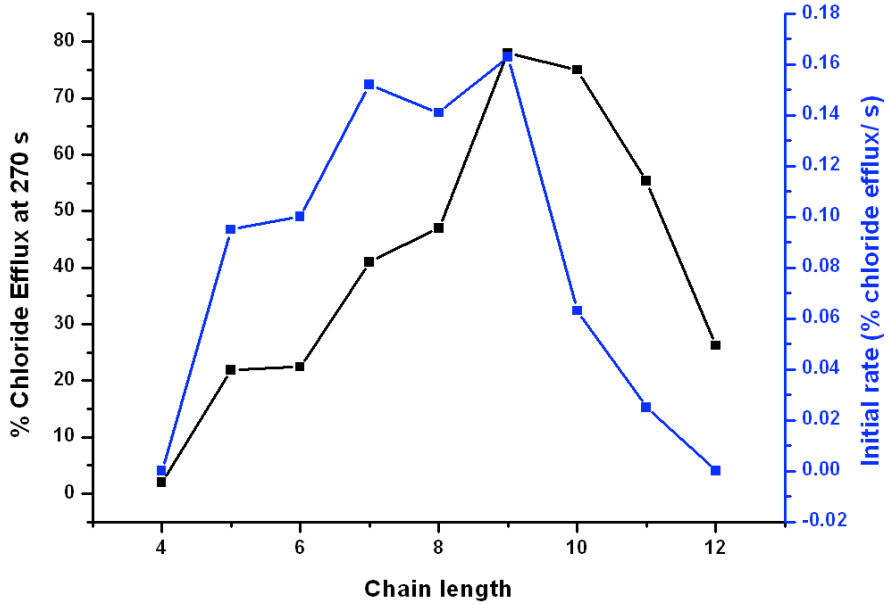

Figure 3.13 The chloride efflux at 270 s (black line and axis) and the initial rate of chloride efflux in the first 30 s (blue line and axis) mediated by compounds **159**-**167** (2 mol% w.r.t. lipid) from unilamellar POPC vesicles containing 489 mM NaCl buffered to pH 7.2 with 5 mM sodium phosphate salts. The vesicles were suspended in 489 mM $NaNO_3$ buffered to pH 7.2 with 5 mM sodium phosphate salts.

In general, there is good correlation between the amount of chloride efflux mediated in 270 s (a measure of the overall activity of the transporter) and the initial rate of chloride efflux. However, the biggest discrepancy in this trend is observed for compound **165** (n = 10). The transport efficiency of **165** is only slightly reduced compared to **164** (n = 9); however, there is a large reduction in the initial rate of transport. This implies that it is at this point that the partitioning kinetics becomes a limiting factor in the mediated chloride efflux. Correspondingly, this is also the point at which transport efficiency begins to decrease with increasing chain length. Compound **164** is the most efficient carrier as it represents the best balance between lipophilicity and mobility through the aqueous phase.

3.4.3 Water solubility

The clogP values listed in **Table 3.1** imply that compounds **159**-**161** are hydrophilic. For compounds with clogP > 0, it is expected that in a water:octanol system the majority

of the compound will reside in the water phase. However, injection of a DMSO solution of receptor **159** into water resulted in the receptor visibly precipitating. To investigate this further, a sample of **159** (theoretically the most hydrophilic receptor) in DMSO-d_6 (10 μl, 10 mM) was added to 0.5 ml D_2O. The sample was sonicated for 30 mins, after which a ^{1}H NMR spectrum of the sample was recorded with ~4000 scans in order to attempt to detect low concentrations of dissolved **159**. The spectrum recorded is shown in **Figure 3.14**.

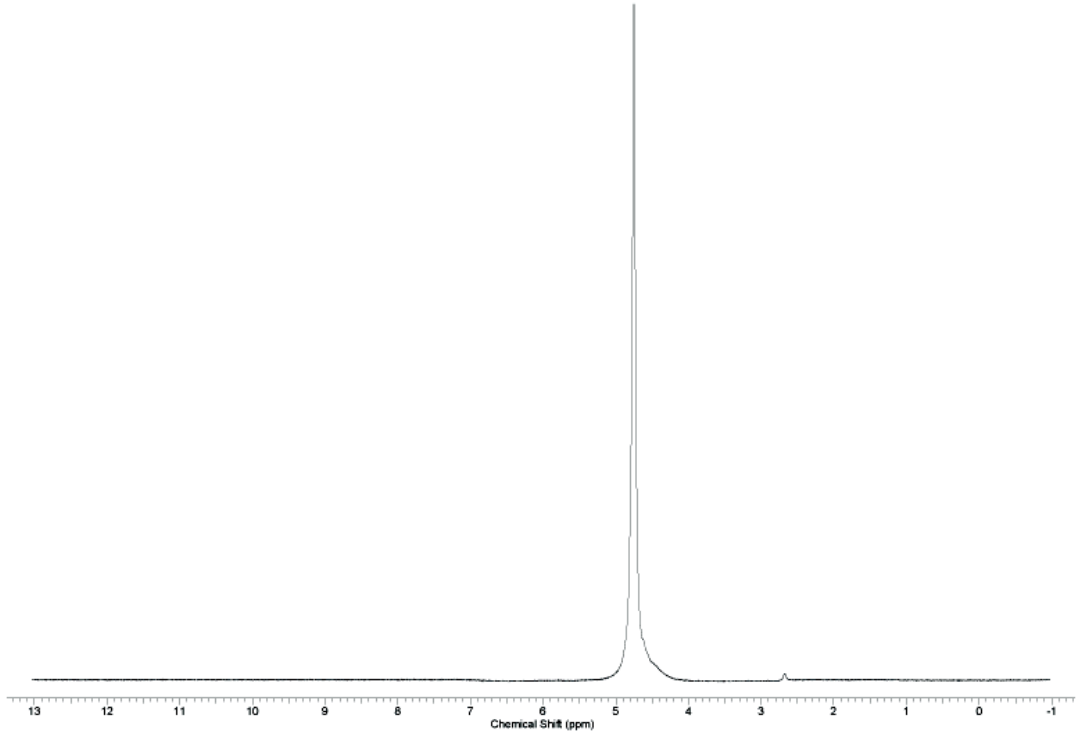

Figure 3.14 The ^{1}H NMR spectrum recorded of a sample of receptor **159** (10 μl of a 10 mM solution in DMSO-d_6) injected into 0.5 ml D_2O after ~4000 scans.

There are no visible resonances in the aromatic region of this spectrum. This implies that the amount of dissolved receptor is too low to be detected by this means, and that receptor **159** is highly insoluble in water. This shows that, while the clogP values may be useful to investigate a relative trend in the lipophilicity across a series of molecules, they should not be taken as an absolute value. In this perspective, compound **159** is more hydrophilic than compound **160** but it is not soluble in water.

This finding is significant when considering the partitioning of receptors **159-167** between the aqueous and lipid phases. Clearly, the level of receptor contained within the water phase will be small. Therefore the observed trends in anion transport activity are not due to the increased localization of the receptor within the membrane as the chain length increases, as all of these receptors would be expected to be fully contained within the lipid bilayer. However, the increasing chain length would also result in the increased lipophilicity of the receptor-anion complex. It is likely that the increased lipophilicity of the receptor-anion complex is responsible for the enhanced transport activity as the chain length increases.

This finding also indicates that the poorer partitioning kinetics displayed by the longer chain analogues is not a result of their aqueous insolubility, as all of these compounds are insoluble in water. However, it is possible that these compounds have a higher tendency to aggregate on passing through the aqueous phase which may limit their activity.

3.4.4 Analogous mono-indolylureas

A series of analogous mono-indolylureas **168-176** shown in **Figure 3.15** were synthesized by SJM.

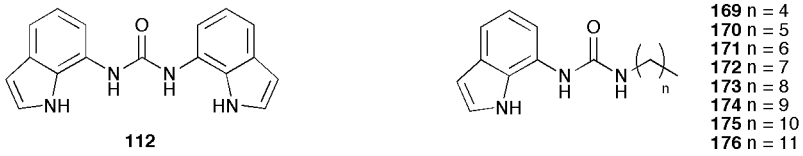

Figure 3.15 The series of analogous mono-indolylureas **10-18**, synthesized by SJM.

Work by SJM demonstrated that these compounds mediate low levels of Cl^-/NO_3^- antiport, but that this is greatly reduced compared to compounds **160-167**. Additionally, di-indolylurea **112**, which has been previously reported as an anion receptor by the Gale group, was found to mediate very low levels of Cl^-/NO_3^- exchange. This highlights the importance of the bis-urea scaffold.

3.4.5 Transporter mechanism-mobility assays

To investigate if **159-167** were transporting anions *via* a mobile carrier mechanism, their Cl^-/NO_3^- antiport ability was tested in unilamellar vesicles composed of POPC:cholesterol (7:3). This is a commonly used proof of mobile carrier activity. Cholesterol organises the membrane resulting in higher viscosity; this will significantly reduce the rate of transport of a mobile carrier as this activity is controlled by the diffusion of the receptor-anion complex through the lipid bilayer.

However, a reduction in the rate of chloride transport by **159-167** was not observed in this experiment. As shown in the comparative graph for compound **164** (**Figure 3.16**), a comparable rate is observed in vesicles containing cholesterol. The corresponding graphs for the other compounds in this series may be found in the appendix (**Section A1.2**).

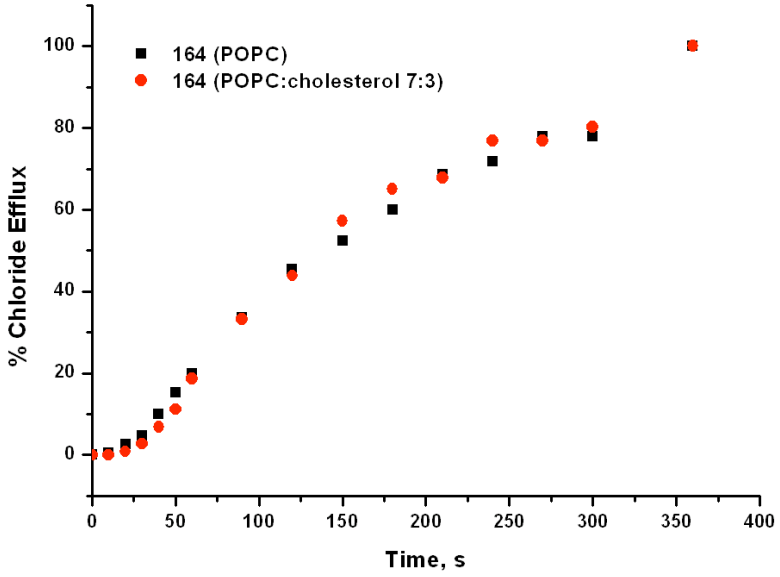

Figure 3.16 Chloride efflux mediated by receptor **164** (2 mol% w.r.t. lipid) from unilamellar vesicles composed of POPC or POPC:cholesterol (7:3) containing 489 mM NaCl buffered to pH 7.2 with 5 mM sodium phosphate salts. The vesicles were suspended in 489 mM $NaNO_3$ buffered to pH 7.2 with 5 mM sodium phosphate salts. At the end of the experiment, the vesicles were lysed to calibrate 100 % chloride efflux. Each point represents the average of 3 trials.

This finding is not proof of channel formation by these compounds; however, channel formation could not be disproved by this method. Zhao has reported increased glucose transport by synthetic receptors in the presence of cholesterol;[162] this observation

was rationalized as follows. POPC bilayers with comparable levels of cholesterol are known to phase separate into cholesterol-rich and cholesterol-deficient domains. This may cause greater aggregation of receptors that interact more favourably with one of these domains as they are more likely to accumulate in these areas. The action of mobile carriers has been found in the past to be unperturbed by the addition of cholesterol in the membrane- for example, Gale *et al.* found that fluorocalix[4]pyrrole **36** exhibited comparable transport rates in both POPC and POPC:cholesterol (7:3) membranes.[67] The mobile carrier activity of fluorocalix[4]pyrole was implied by its observed Cl^- transport in a U-tube experiment. However, the poor solubility of compounds **159-167** in solvents that are immiscible with water prevented the use of similar experiments.

It has previously been inferred that a first order, or linear dependence of transport activity on receptor concentration is indicative of mobile carrier activity if the molecule is too small to span the bilayer.[54] The Hill analyses for Cl^-/NO_3^- antiport by **162-165** demonstrate a linear relationship between receptor concentration and % chloride efflux at 270 s. The data for compound **163** is shown below.

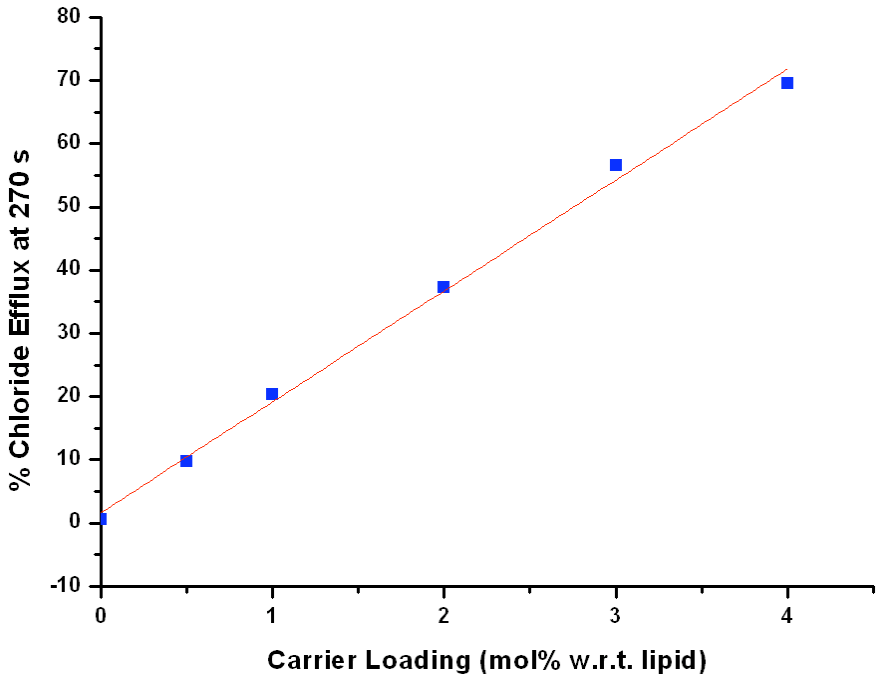

Figure 3.17 The chloride efflux after 270 s promoted by receptor **163** from unilamellar POPC vesicles containing 489 mM NaCl buffered to pH 7.2 with 5 mM sodium phosphate salts. The vesicles were dispersed in 489 mM$NaNO_3$ buffered to pH 7.2 with 5 mM sodium phosphate salts.

This observation implies that a mobile carrier mechanism is operational. However, given the well-documented propensity of ureas to self associate, with examples of this known within the bilayer,[158] further proof of mechanism was sought.

A. P. Davis *et al*. have reported that examining the behaviour of a series of compounds in bilayers of varying thickness can be used to distinguish between anion channel or carrier activity.[54] When testing a series of cholapods, they found a simple correlation between membrane thickness and transport rates. A similar relationship has been demonstrated by Läuger for K^+ transport by valinomycin.[163] As the membrane thickness increases, the rate of transport by a mobile carrier will decrease as there is a greater distance across which the ion must be transported. However, as discussed in section **3.1.3**, the correlation between the activity of a channel and the bilayer thickness is more complex. Similar rates should be observed for a range of bilayer thicknesses, but this should reduce dramatically once the channel can no longer span the membrane.

Additionally, considering the Hill coefficients for the Cl^- transport by **161**-**167** are ~2 for each transporter, therefore it is unlikely that channels are formed by large aggregates of these receptors. These receptors are not large enough to span the bilayer as a single entity, but a structure composed of two receptors may be long enough. Matile has reported that the thickness of the hydrophobic interior of an EYPC bilayer (mainly composed of POPC) is approximately 36 Å.[99] The crystal structure of **159** (**Figure 3.30**, discussed in section **3.5**) indicates that the length of this receptor is 17.825 Å from C2 to C10 (shown in **Figure 3.18**).

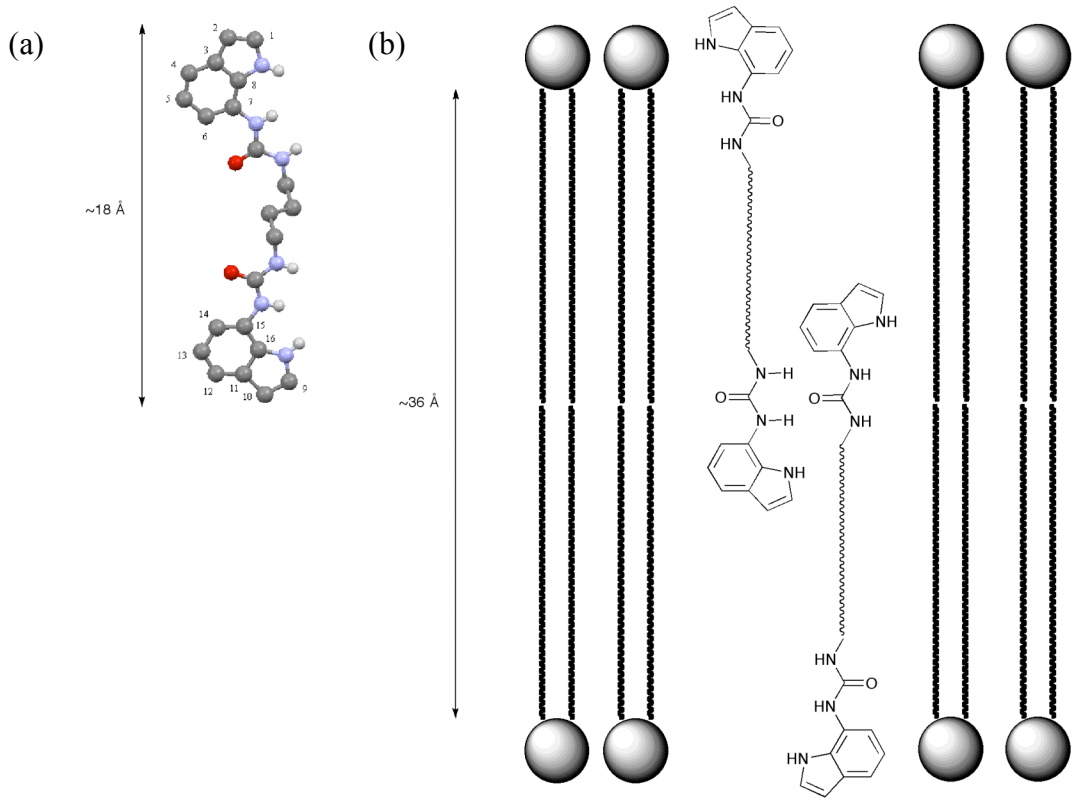

Figure 3.18 A comparison of (a) the approximate length of receptor **159** by comparison to the thickness of the hydrophobic interior of a POPC bilayer, and (b) a possible 2-receptor assembly which could theoretically span the bilayer. The crystal structure image was taken from the **159**.K_2[oxalate][18-crown-6]$_2$ structure depicted in **Figure 3.30**. Non-acidic protons and both anions and cations have been removed for clarity.

Although the alkyl chain of the receptor is kinked in this structure, this can be used as an estimate of the dimensions of this molecule. Thus, it may be possible that as the chain length increases, the receptors may be able to form membrane spanning assemblies as shown in **Figure 3.18(b)**. The propensity of ureas to self assemble *via* hydrogen bonding interactions could provide a route to this assembly. This would also explain the observed trend in Cl^- transport activity across the series, as it may be possible that compound **164** is of the optimum length to form this type of structure in a bilayer of this thickness. Therefore, an experiment was undertaken to examine the effect of changing the bilayer thickness on the trends in transport activity across the series.

The lipids used for this experiment were C_{18}(1)PC (DOPC) and C_{16}(1)PC, shown in **Figure 3.19**. These lipids were previously utilized in a similar assay by A. P. Davis *et al.*[54] and were selected as they contain unsaturated acyl chains, which maintain the fluid

phase at room temperature. Like POPC they contain a phosphocholine (PC) head group, but the two appending acyl chains are of the same length and are both mono-unsaturated. The lipid bilayer thickness is known to vary linearly with acyl chain length in PC vesicles.[164] The bilayer thickness of $C_{18}(1)$PC is reported to be 32 Å.[165] As $C_{16}(1)$PC is a less commonly used lipid, an experimental value for this parameter is not available, although it will be smaller than for $C_{18}(1)$PC. The effect of reducing the length of a phospholipid acyl chain by 2 methylene units may be estimated by the difference in thickness of bilayers composed of the saturated acyl chain lipids $C_{16}(0)$PC and $C_{14}(0)$PC, (7.6 Å);[165] a similar difference in bilayer thickness may be expected for $C_{18}(1)$PC and $C_{16}(1)$PC.

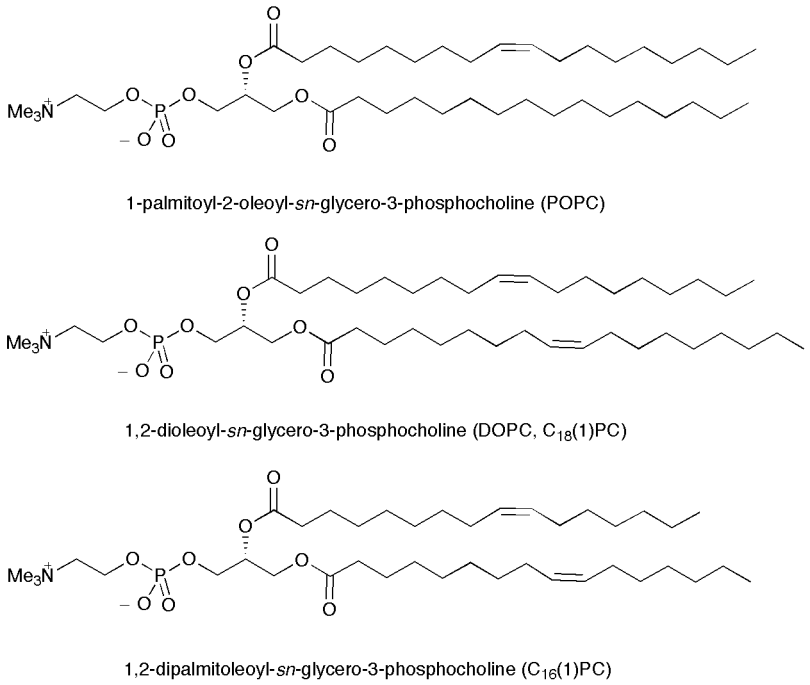

Figure 3.19 The structures of the phospholipids used in these studies.

The Cl^-/NO_3^- antiport activity of **159-167** was investigated in vesicles composed of $C_{16}(1)$PC and $C_{18}(1)$PC. The results are shown in **Figure 3.20**.

(a)

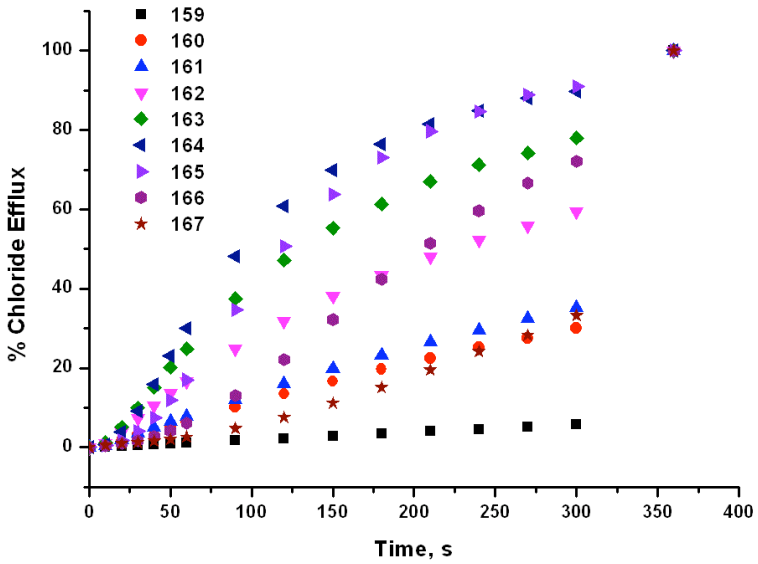

(b)

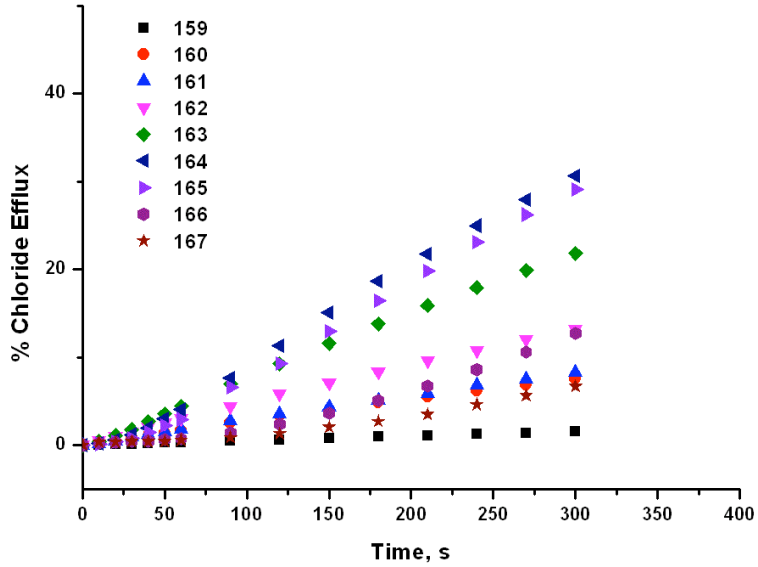

Figure 3.20 Chloride efflux promoted by receptors **159-167** (2 mol% w.r.t. lipid) from unilamllar vesicles composed of (a) C_{16}PC or (b) C_{18}PC containing 489 mM NaCl buffered to pH 7.2 with 5 mM sodium phosphate salts. The vesicles were suspended in 489 mM $NaNO_3$ buffered to pH 7.2 with 5 mM sodium phosphate salts. At the end of the experiment the vesicles were lysed to calibrate 100 % chloride efflux. Each point represents the average of 3 trials.

As expected, the transport activity of **159-167** was reduced in vesicles composed of C_{18}(1)PC by comparison to C_{16}(1)PC. This is due to the increasing bilayer thickness and thus a larger transmembrane distance for the receptor-anion complex to travel. As a

measure of the anion transport activity of **159-167** in these experiments, the chloride efflux after 270 s is shown in **Figure 3.21**.

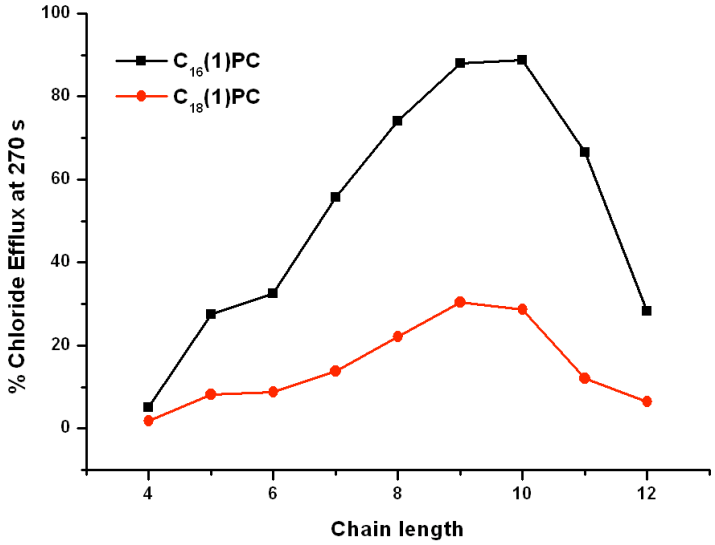

Figure 3.21 The chloride efflux after 270 s promoted by receptors **159-167** (2 mol% w.r.t. lipid) from unilamellar vesicles composed of C_{16}PC or C_{18}PC containing 489 mM NaCl buffered to pH 7.2 with 5 mM sodium phosphate salts. The vesicles were suspended in 489 mM $NaNO_3$ buffered to pH 7.2 with 5 mM sodium phosphate salts.

The data in **Figure 3.21** demonstrates that the trend in anion transport activity across the series **159-167** is the same in both sets of vesicles, despite the variation in bilayer thickness. This trend is also the same as observed in POPC vesicles. If these receptors were forming membrane spanning structures, it would be expected that reducing the thickness of the bilayer should favour channel formation by a shorter chain receptor. As this is not the case, these results indicates that a mobile carrier mechanism is operational.

3.4.6 Summary of anion transport results

Compounds **159-167** show a range of chloride transport activity, which is dependent on the length of the central alkyl chain. The best Cl^-/NO_3^- antiporter is compound **164** (n = 9). This optimum chain length may be explained as a balance between the lipophilicity of the carrier, a favourable characteristic for ion transport which increases with increasing

chain length, and the kinetics of the receptor passing through the aqueous phase and partitioning within the bilayer, which appears to decrease for the longest chain lengths. Mobile carrier activity has been demonstrated by comparing the transport activity in bilayers of varying thickness. Additionally, the greatly reduced Cl^-/NO_3^- antiport activity of mono-ureas **168-176** demonstrates that the bis-urea scaffold facilitates anion transport by a mechanism in which the two urea groups are not functioning independently. This implies that their transport capability is not solely due to lipophilicity arguments and that the inclusion of two urea moieties in receptor design is advantageous for transmembrane anion transport.

3.5 Solution phase anion binding

3.5.1 ^{1}H NMR titrations

The solution phase anion binding properties of compounds **159-167** with a selection of anions relevant to the transport experiments and in biological systems were investigated by ^{1}H NMR titration in DMSO-d_6/ 0.5 % H_2O. **Figure 3.22** shows the change in chemical shift of the urea NH proton adjacent to the indole moiety on titration with various anions. Across the series **159-167**, similar binding profiles were observed for each anion tested, therefore each analysis is representative of all of the receptors in this series. The full analysis for each receptor can be found in the appendix (section **A2.1**).

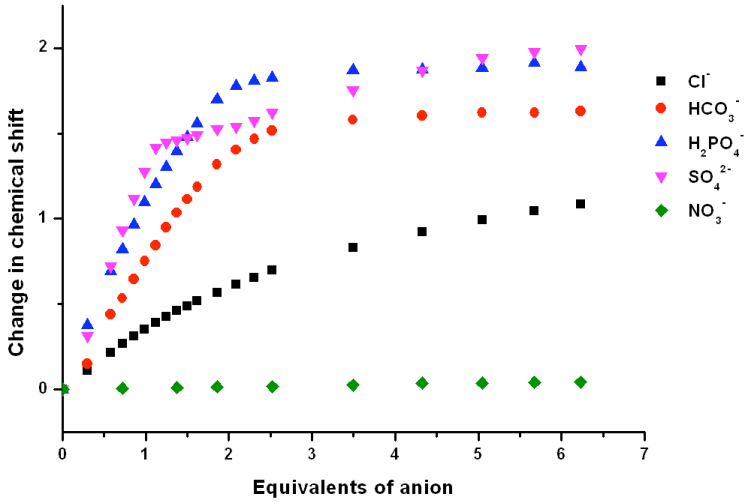

Figure 3.22 The change in chemical shift of the indolyl urea NH proton (starting at ~ 8.3 ppm) of receptor **159** during the ^{1}H NMR titration with various anions (added as the tetrabutylammonim or tetraethylammonium salts) in DMSO-d_6/H_2O 0.5 %.

Across the series **159-167**, none of the receptors were observed to interact with $TBANO_3$. On titration with TBACl, the indolyl urea NH resonance at ~8.3 ppm is observed to gradually shift downfield for the duration of the experiment, consistent with hydrogen bond formation to the anion. This is observed for all of the NH hydrogen bond donors in this receptor, as shown in **Figure 3.23(a)**, which indicates that all of the NH groups participate in the anion binding.

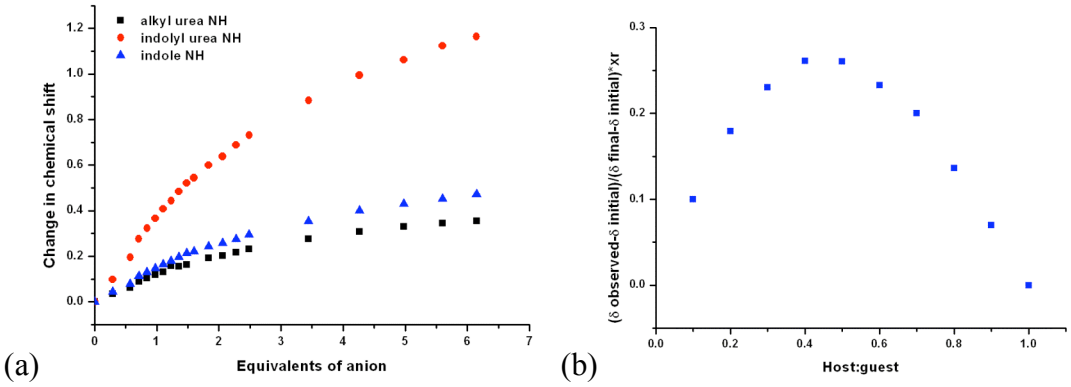

Figure 3.23 (a) The change in chemical shift of the NH hydrogen bond donors of receptor **159** on titration with TBACl in DMSO-d_6/ H_2O 0.5 %; (b) The Job plot analysis for this process following the indolyl urea NH resonance at ~8.3 ppm.

A Job plot analysis, shown in **Figure 3.23(b)**, confirmed a 1:1 binding mode for this process. This implies that a weak 1:1 complex with chloride is formed. However, it should be noted that the formation of a 2:2 complex, as shown in **Figure 3.24**, is also theoretically possible and would be indistinguishable from a 1:1 complex by these means.

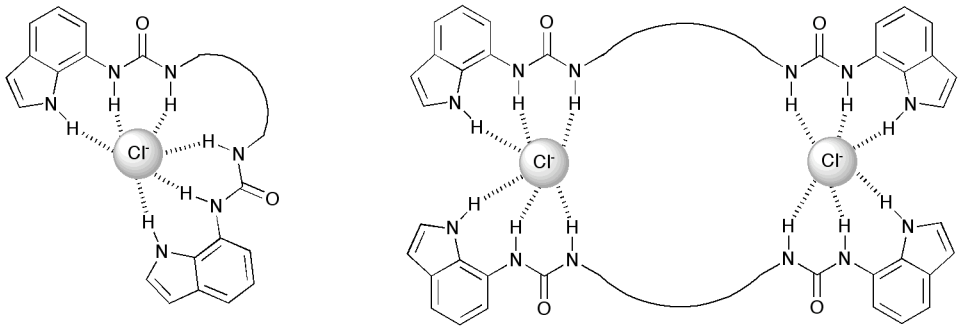

Figure 3.24 A representation of the possible 1:1 and 2:2 binding modes for the complexation of Cl^- by bis-indolylureas receptors **159-167**.

The titration data was fitted to a 1:1 binding model using WinEQNMR 2.[166] The binding constants obtained are shown in **Table 3.2**. These results show that increasing the length of the alkyl chain across the series has no observable effect on the Cl^- binding strengths under these conditions. Thus, there is no observable correlation between the Cl^- binding strengths of these receptors and their Cl^- transport activity.

Table 3.2 Binding constants (M^{-1}) obtained from the ^1H NMR titration of **159-167** with TBACl in DMSO-d_6/H_2O 0.5% following the urea NH resonance at ~8.3 ppm. The data was fitted to a 1:1 binding model using WinEQNMR 2. All errors are < 10 %.

	159	**160**	**161**	**162**	**163**	**164**	**165**	**166**	**167**
K_a	37	35	37	32	39	38	37	32	42

On titration with TBA_2SO_4, the urea NH resonance is observed to rapidly shift downfield until approximately 1 equivalent of anion. After this point, the curve plateaus briefly, followed by a gradual downfield shift. As shown in **Figure 3.25(a)**, similar behaviour is observed for the other NH hydrogen bond donors of these receptors. This profile is indicative of strong binding to 1 equivalent of SO_4^{2-}, followed by a much weaker complexation of a second equivalent of anion. The high negative charge of SO_4^{2-}

results in strong binding of the first equivalent, but also makes the binding of a second anion electrostatically unfavourable. The Job plot analysis for this process, shown in **Figure 3.25(b)**, indicates that the 1:1 complex was the most prevalent. This reflects the much stronger binding of the first equivalent. The titration data was fitted to a 1:2 binding model using WinEQNMR 2, as the data could not be adequately fit to a 1:1 binding model. The binding constants calculated are shown in **Table 3.3**. Although the errors associated with the 1:2 model were large in some cases, this is a consequence of the shape of the binding curves, in particular the plateau after the addition of 1 equivalent of anion. This in itself is likely to be a consequence of the much stronger binding of the first equivalent of anion. There is a general trend across the series that K_1 decreases and K_2 increases. This reflects the decreasing favourability of the formation of a 1:1 complex of the form shown for Cl^- in **Figure 3.24** due to increasing the chain length. The binding of the second equivalent is therefore more favourable as dissociation of the 1:1 complex is less unfavourable.

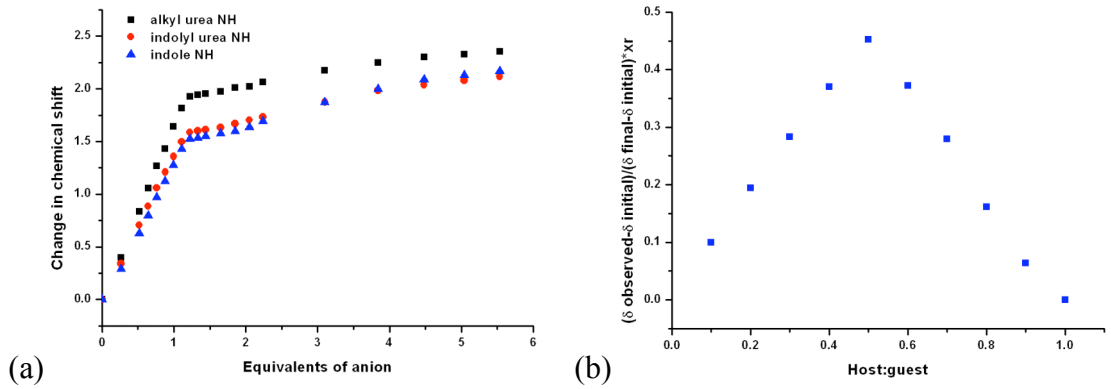

Figure 3.25 (a) The change in chemical shift of the NH hydrogen bond donors of receptor **159** on titration with TBA_2SO_4 in DMSO-d_6/ H_2O 0.5 %; (b) The Job plot analysis for this process following the indolyl urea NH resonance at ~ 8.3 ppm.

Table 3.3 Binding constants (M^{-1}) obtained from the ^1H NMR titration of **159-167** with TBA_2SO_4 in DMSO-d_6/H_2O 0.5% following the urea NH resonance at ~8.3 ppm. The data was fitted to a 1:2 binding model using WinEQNMR 2. The errors are reported in brackets as a percentage of the value.

	159	**160**	**161**	**162**	**163**	**164**	**165**	**166**	**167**
K_1	$> 10^4$	$> 10^4$	9768 (20 %)	7171 (17 %)	8560 (13 %)	3280 (20 %)	3320 (20 %)	1267 (27 %)	2230 (9 %)
K_2	16 (25 %)	22 (27 %)	19 (32 %)	72 (21 %)	72 (14 %)	110 (23 %)	124 (26 %)	163 (35 %)	182 (22 %)

The binding profiles from the titration of **159-167** with $TEAHCO_3$ and $TBAH_2PO_4$ were similar in appearance. The continuous downfield shift of the urea NH resonances until approximately 2.4 equivalents of anion is indicative of a predominantly 1:2 binding mode (as shown in **Figure 3.26(a)** and **Figure 3.27(b)**). The data in these figures indicates that HCO_3^- is bound most strongly by the urea NH hydrogen bond donors, as expected for a Y-shaped anion. In contrast, $H_2PO_4^-$ is bound most strongly by the indole and indolyl urea NH donors. When the data was fitted to a 1:2 binding model using WinEQNMR 2, in some cases the calculated binding constants had large errors. These binding constants are shown in **Table 3.4** and **Table 3.5**. Further to this, a Job plot analysis indicated that the binding of HCO_3^- does not proceed by a purely 1:2 binding mode as the Job plot peaked at 0.4 (**Figure 3.26(b)**). This could be a result of a mixture of 1:1 and 1:2 binding, or it could alternatively be representative of the presence of multiple equilibria. The Job plot analysis for the binding of $H_2PO_4^-$ does peak at approximately 0.33 (as expected for a 1:2 binding model, shown in **Figure 3.27(b)**). However, the large errors associated with the binding constants calculated using this model, and the similarity to the HCO_3^- binding profile may indicate that a purely 1:2 binding mode does not exist under these conditions.

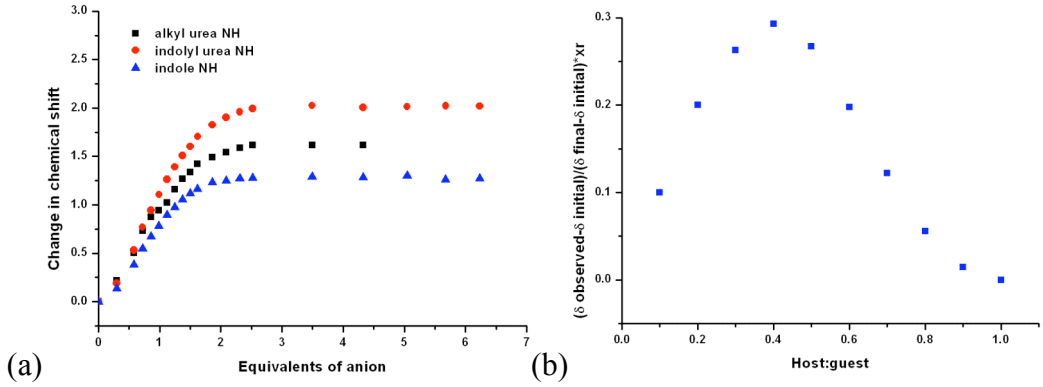

Figure 3.26 (a) The change in chemical shift of the NH hydrogen bond donors of receptor **159** on titration with $TEAHCO_3$ in DMSO-d_6/ H_2O 0.5 %; (b) The Job plot analysis for this process following the indolyl urea NH resonance at ~ 8.3 ppm.

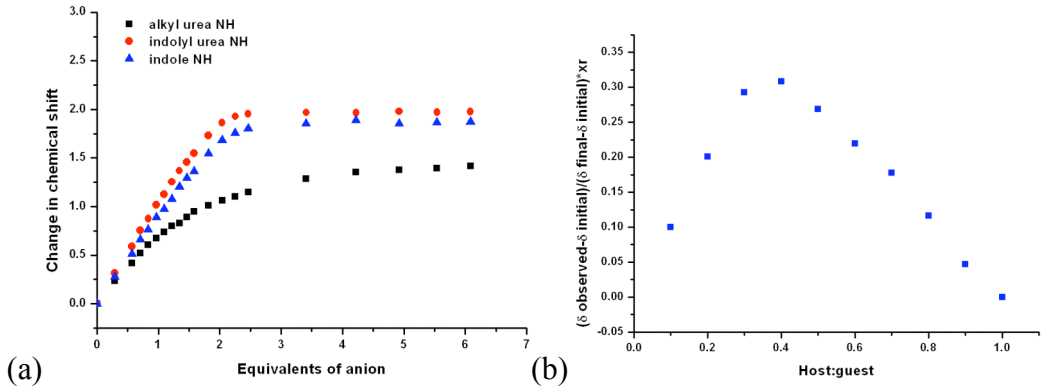

Figure 3.27 (a) The change in chemical shift of the NH hydrogen bond donors of receptor **159** on titration with $TBAH_2PO_4$ in DMSO-d_6/ H_2O 0.5 %; (b) The Job plot analysis for this process following the indolyl urea NH resonance at ~ 8.3 ppm.

Table 3.4 Binding constants (M^{-1}) obtained from the ^1H NMR titration of **159-167** with $TEAHCO_3$ in DMSO-d_6/H_2O 0.5% following the urea NH resonance at ~8.3 ppm. The data was fitted to a 1:2 binding model using WinEQNMR 2. The errors are reported in brackets as a percentage of the value.

	159	**160**	**161**	**162**	**163**	**164**	**165**	**166**	**167**
K_1	802 (13 %)	1118 (27 %)	813 (22 %)	584 (11 %)	1101 (15 %)	560 (11 %)	1328 (21 %)	290 (10 %)	1026 (7 %)
K_2	823 (13 %)	955 (27 %)	1090 (23 %)	798 (12 %)	761 (16 %)	104 (12 %)	656 (22 %)	848 (12 %)	721 (7 %)

Table 3.5 Binding constants (M^{-1}) obtained from the ^1H NMR titration of **159-167** with $TBAH_2PO_4$ in DMSO-d_6/H_2O 0.5% following the urea NH resonance at ~8.3 ppm. The data was fitted to a 1:2 binding model using WinEQNMR 2. The errors are reported in brackets as a percentage of the value.

	159	**160**	**161**	**162**	**163**	**164**	**165**	**166**	**167**
K_1	722 (15 %)	1542 (9 %)	386 (28 %)	341 (20 %)	420 (23 %)	572 (18 %)	635 (10 %)	508 (23 %)	899 (9 %)
K_2	1042 (16 %)	455 (9 %)	1623 (31 %)	2317 (20 %)	1349 (24 %)	1023 (19 %)	830 (10 %)	406 (25 %)	498 (10 %)

The binding of the second equivalent of HCO_3^- or $H_2PO_4^-$ is generally of similar strength to the binding of the first equivalent. This indicates that the two anion binding sites are able to bind anions almost independently if the anions are only singly charged and thus the electrostatic repulsions are not too strong. There is no observable trend in binding strengths across the series. In some cases, the value of K_2 is observed to be higher than K_1. This result would normally be indicative of a cooperative binding effect. However, in this case it is more likely that this unusual observation is merely an artefact of the poor fit of the data to the binding model, as the cooperative binding of two anionic species is improbable.

3.5.2 Bis-urea receptors and the 1:2 binding model

While the binding curves from the titrations of receptors **159-167** with $TEAHCO_3$ and $TBAH_2PO_4$ indicate that a predominately 1:2 binding mode is operational, the

imperfect fit of the titration data to a simple 1:2 binding model implies the existence of multiple equilibria. In order to investigate whether the binding of $H_2PO_4^-$ by these receptors could facilitate its deprotonation by free anions in solution, as has been previously observed for other indolylurea receptors reported by the Gale group,[70, 71] a sample of **161** was titrated with 1.4 equivalents of $H_2PO_4^-$ followed by up to 2 equivalents of TBAOH (1M in MeOH). The results were unlike any of the previously reported titration data (see the appendix for details), thus indicating that this process is not occurring. However, this does not rule out multiple binding equilibria.

A simple 1:2 binding model between a receptor L and an anion X examines the general equilibria as shown below.

$$L \rightleftharpoons LX \rightleftharpoons LX_2$$

However, the binding of 1 or 2 equivalents of anion (X) to a bis-urea receptor (L) may result in multiple equilibria as there are two forms that the 1:1 complex can adopt: one in which the anion interacts with a single binding site, and one in which the receptor curves and both urea groups interact with the anion. As mentioned previously, a 2:2 complex (L_2X_2) is also theoretically possible. These equilibria are represented in **Figure 3.28**.

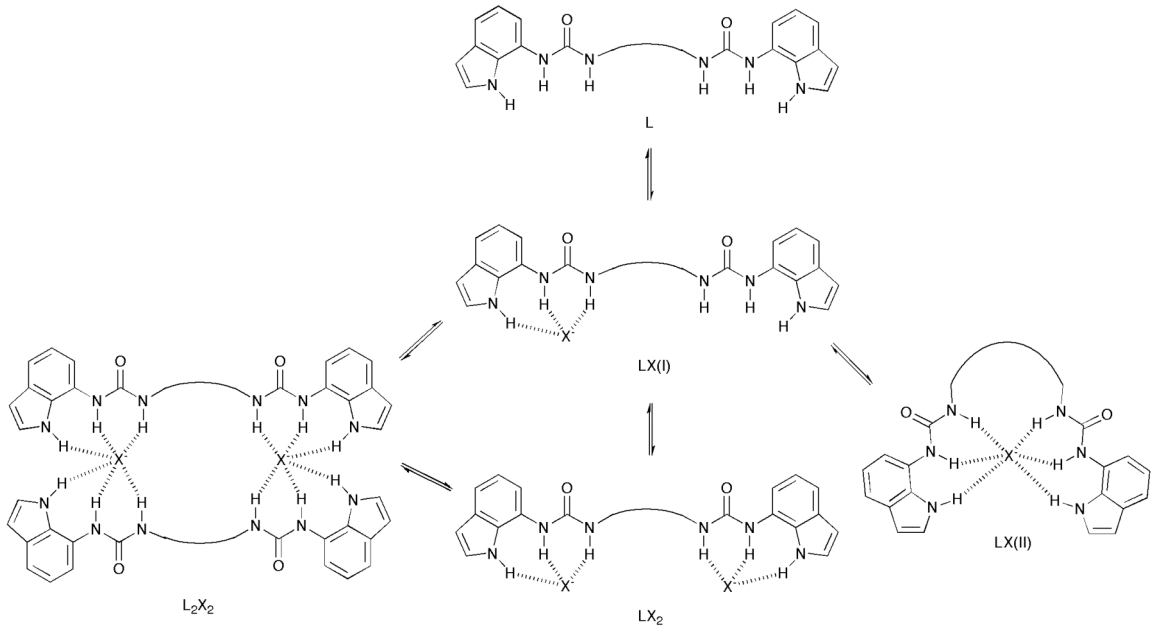

Figure 3.28 Possible solution phase binding equilibria for anion complexation by bis-ureas **159-167**.

If the most stable form of the 1:1 complex is LX(II), there is an additional equilibrium to consider on moving from the 1:1 complex to the 1:2 complex as one of the urea groups must dissociate from the first anion in order to bind the second. If a 2:2 complex is possible, this further complicates the system. This additional equilibium may explain the imperfect fit of this data to a 1:2 binding model.

3.6 X-ray crystallography

Crystals of compounds **159-167** proved to be extremely difficult to grow, as did crystals of their anion complexes. This is most likely due to the high flexibility of the receptors, indicating that the molecules are likely to be disordered in the solid state. Additionally, the poor solubility of these receptors in the majority of organic solvents prevented the straightforward control of crystallization by variation of the mother liquor. Often, any crystalline material obtained was not of suitable quality for single crystal X-ray analysis.

Crystals of the $H_2PO_4^-$ complex of **161** were grown by slow evaporation of a DMSO solution of the receptor with an excess of $TBAH_2PO_4$. The structure was

elucidated by single crystal X-ray diffraction and is shown in **Figure 3.29**. Full details of the X-ray diffraction analysis can be found in the appendix (section **A3.2**).

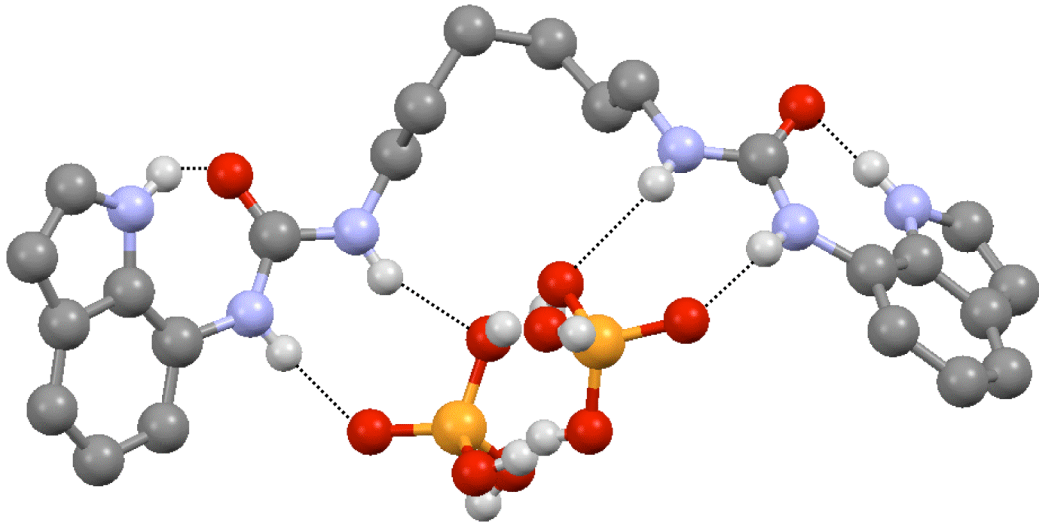

Figure 3.29(a) The X-ray structure of the crystals grown from a DMSO solution of **161** and $TBAH_2PO_4$ adopts a pseudo 1:2 stoichiometry due to oligomerisation of the phosphate anions. Counterions and non-interacting hydrogen atoms have been removed for clarity.

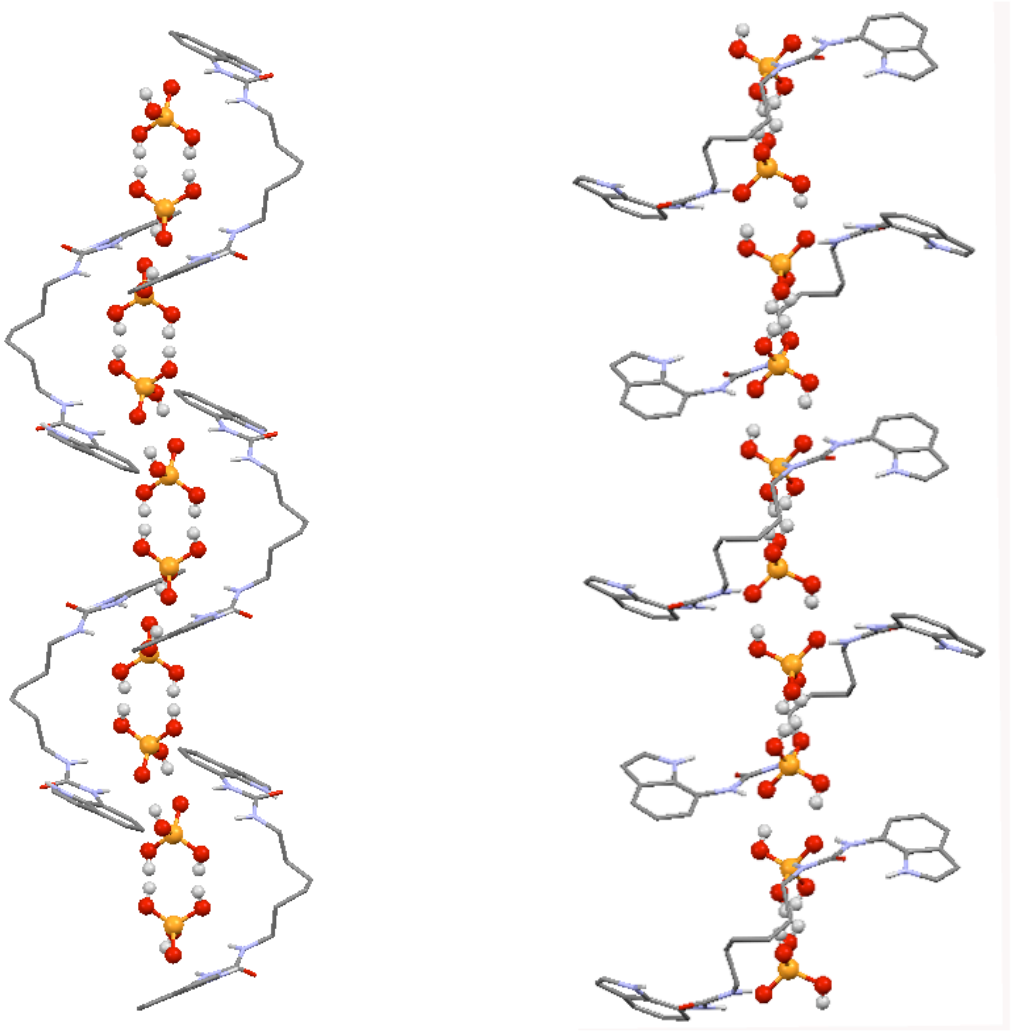

Figure 3.29(b) Two views of the expanded crystal structure of **161** binding to an oligomerised phosphate rod. The receptors wrap around the rod in a helical fashion. Counterions and non-interacting hydrogen atoms have been removed for clarity.

The structure shows that the phosphate anions have oligomerised into a rigid rod *via* hydrogen bonding interactions between the anions. The receptor- anion complex adopts a pseudo 1:2 stoichiometry, with each indolylurea unit coordinating 1 anion *via* two urea NH···O hydrogen bonds (**Figure 3.29(a)**). The indole NHs are orientated out of the binding cleft due to intramolecular hydrogen bonding to the urea C=O (as shown in **Figure 3.29(a)**), thus are not contributing to binding the anion. This is in contrast to the solution phase binding studies, in which the downfield shift of the indole NH resonance indicates hydrogen bonding to the $H_2PO_4^-$. The receptors wrap around the oligomerised

phosphate rod in a helical manner, as illustrated in **Figure 3.29(b)**. Some bond lengths and angles of interest are shown in **Table 3.6**.

Table 3.6 Some bond lengths and angles of interest relating to the crystal structure of **161**·$TBAH_2PO_4$.

d(NH···O_{anion})	1.912-2.260 Å
d(N···O_{anion})	2.750-2.989 Å
∠ (N-H-O_{anion})	141-158 °
d(NHindole···Ourea)	1.961 Å
∠ (N_{indole}-H-O_{urea})	135 °
d(P···P)	4.196 Å
d(OHphosphate···Ophosphate$_2$)	1.675-1.758 Å
d(Ophosphate···Ophosphate$_2$)	2.474-2.553 Å
∠ (N_{indole}-H-O_{urea})	157-159 °

Single crystals of the oxalate complex of compound **159** were grown by slow evaporation of a DMSO solution of **159** containing 18-crown-6 and potassium oxalate. 18-crown-6 was included in this experiment to enhance the low solubility of potassium oxalate in DMSO. Compound **159** and 18-crown-6 (1:1) were dissolved in hot DMSO, and potassium oxalate was added. The solution was agitated with further heating and filtered while still hot. The sample was allowed to stand for 6 weeks. The structure of the resulting crystals is shown in **Figure 3.30**. Full details of the X-ray diffraction analysis can be found in the appendix (section **A3.3**).

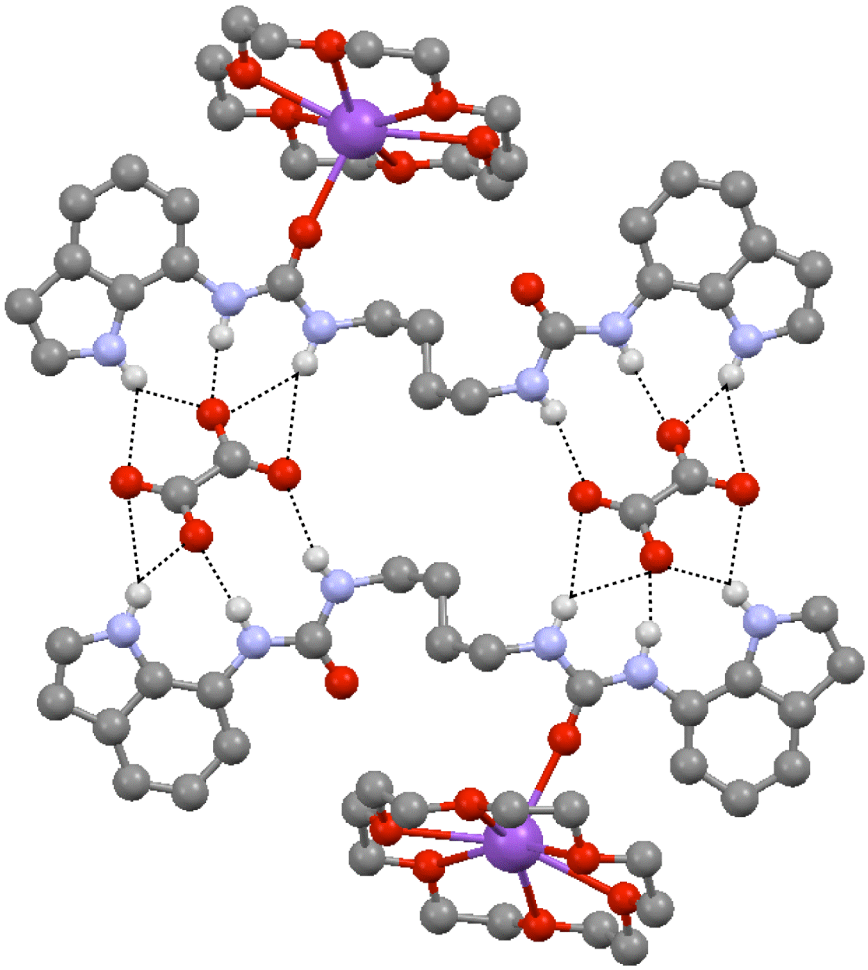

Figure 3.30(a) The crystal structure of **159**·K_2[oxalate][18-crown-6]$_2$. Non-interacting hydrogen atoms and additional K^+[18-crown-6] units have been omitted for clarity.

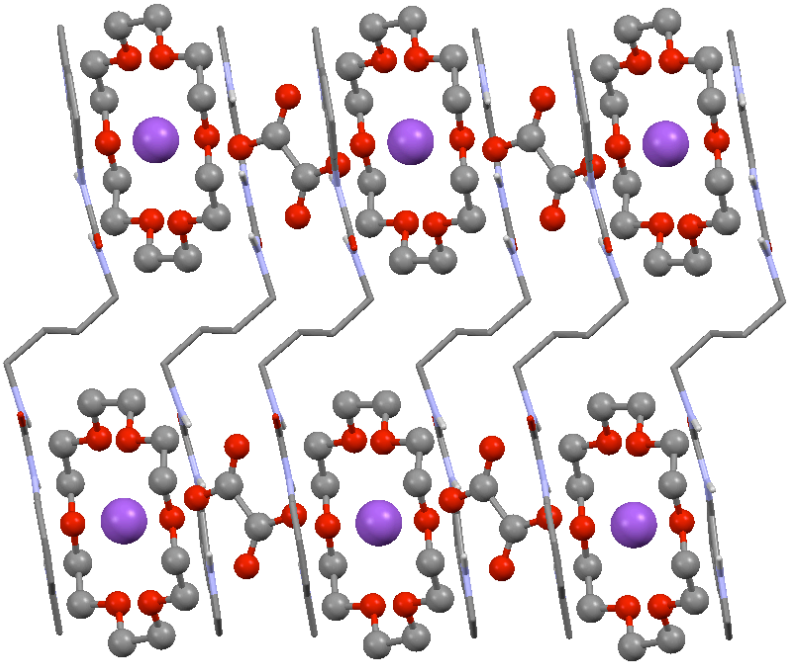

Figure 3.30(b) The packing in the crystal structure of **159**.K_2[oxalate]. Non-interacting hydrogen atoms and additional counterions have been omitted for clarity.

The oxalate anions are coordinated in a 2:2 host:guest stoichiometry as shown in **Figure 3.30(a)**. Each oxalate anion is coordinated by two indolylurea units from two different receptors by a total of 9 hydrogen bonding interactions. The K^+ counterions are bound by 18-crown-6. Two of the K^+[18-crown-6] units are coordinated to the oxygen donors of the urea groups; the other two K^+[18-crown-6] required for complex neutrality can be found coordinated to the oxalate anions as shown in **Figure 3.30(b)**. The NH···$O_{oxalate}$ bond lengths are in the range of 1.876 – 2.703 Å. While this structure cannot be interpreted as evidence of the mode of binding any anions in solution, it is evidence that a discrete 2:2 complex is possible in the solid state using receptors of this type.

3.7 Conclusions

The work in this chapter demonstrates that the bis-urea scaffold has been used to yield effective anion transporters, while variation of the central alkyl chain length allows for the straightforward modulation of transport activity. The bis-urea scaffold has also been demonstrated to be more effective for carrier design that the equivalent mono-urea scaffold. Carriers **159-167** contain anion binding clefts inspired by literature anion receptor designs. However, it is worth noting that from a purely anion complexation perspective, the design of these receptors may be considered to be relatively poor. The increasing length and flexibility of the central alkyl chain which separates the two distinct binding sites results in the binding sites becoming increasingly likely to function individually. The lack of rigidity in the receptor design means that there is little preorganization towards anion complexation, leading to multiple possible binding modes and complex binding equilibria. There is also little difference between the binding properties of the receptors across the whole series. However, the increasing carrier efficiency across the series serves to highlight that a theoretically poor anion receptor can effectively facilitate anion transport. Thus, the design of future carriers should consider both the interactions between the host and the guest and the interactions between the resulting complex and the lipid bilayer.

Chapter 4
Bis-phenylthioureas as tunable transporters for chloride and bicarbonate

4.1 Introduction

The receptors described in **Chapter 3** were found to function as Cl^-/NO_3^- antiporters with varying anion transport activity that was highly dependent on the length of the central alkyl chain. This observed trend allows for the straightforward control of transport activity. The receptors were also found to be significantly more active than their analogous monosubstituted indolylureas, thus implying that the bis-urea scaffold facilitates anion transport not just by providing two discrete urea subunits instead of one, but that the two urea groups function complementarily.

The bis-(alkyl)-urea scaffold is easily synthesized and thus can be used as a model for improved systems. One particular area for improvement is the lack of Cl^-/HCO_3^- antiport activity. While the observed Cl^-/NO_3^- antiport trends can be partially attributed to the variations in lipophilicity across the series, this lack of HCO_3^- transport implies that either the receptors are not inherently lipophilic enough to facilitate the transmembrane transport of the more hydrophilic HCO_3^- anion, or that the receptors do not interact with HCO_3^- sufficiently strongly to transport it. Considering the stronger binding of HCO_3^- than Cl^- or NO_3^- by these receptors in polar DMSO-d_6/H_2O (0.5 %) solution, the first explanation is the most likely. Therefore, inspired by the generally greater Cl^-/HCO_3^- antiport activity of thioureas over ureas (as described in **Chapter 2** and documented elsewhere), a series of bis-phenylthioureas **177-182** were synthesized in order to investigate whether the dependency of the length of the central alkyl chain to transport

efficiency could be applied to the transmembrane transport of HCO_3^-, and if the bis-thiourea scaffold could mediate more efficient anion transport than the analogous mono-thioureas. For comparison, the transport activity of bis-indolylthiourea **183** and bis-phenylurea **184** were also investigated. The carriers described in this chapter are shown in **Figure 4.1.**

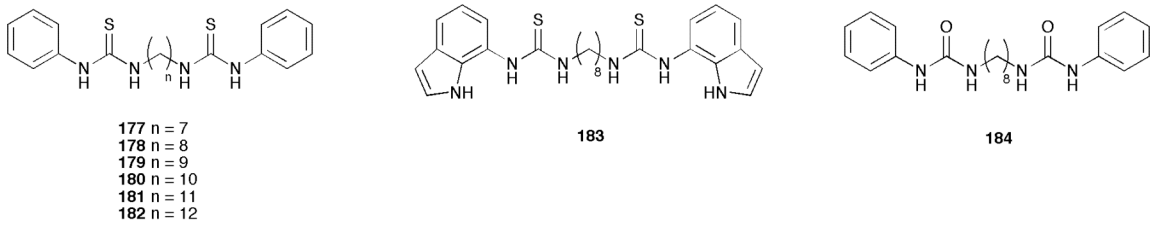

Figure 4.1 The bis-(thio)urea carriers described in this chapter.

4.2 Synthesis

Thioureas **177-182** were synthesized by refluxing a solution of phenylisothiocyanate with the corresponding diamine in DCM/DMF (1 %) as shown in scheme 3.1.

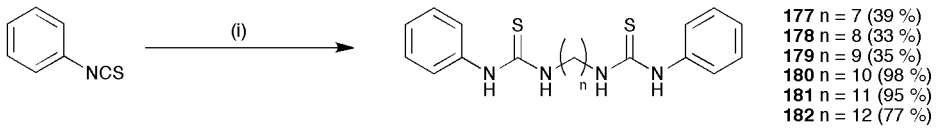

Scheme 4.1 Reagents and conditions: ½ eq. diamine, DCM/DMF (1 %), reflux, N_2, overnight.

Compound **183** was synthesized by the reflux of 7-isothiocyanato-1*H*-indole (synthesized by a literature procedure as described in **Chapter 2**[69]) with 1,8-diaminooctane in DCM/DMF (1%).

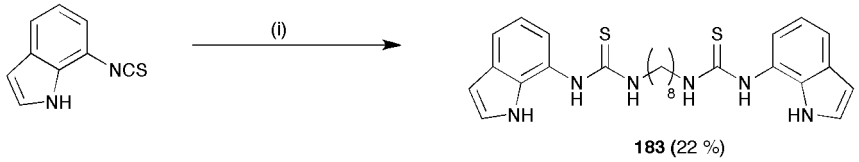

Scheme 4.2 Reagents and conditions: (i) ½ eq. 1,8-diaminooctane, DCM/DMF (1 %), reflux, N_2, overnight.

Compound **184** was synthesized by the room temperature reaction of phenylisocyanate with 1,8-diaminooctane in DCM.

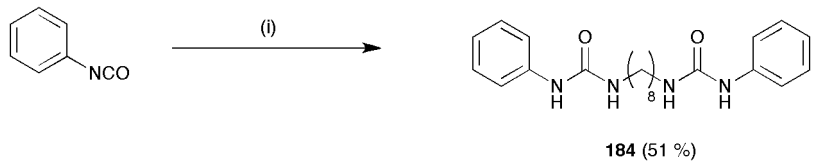

184 (51 %)

Scheme 4.3 Reagents and conditions: (i) ½ eq. 1,8-diaminooctane, DCM, RT, 2 h.

Full synthetic procedures can be found in **Chapter 6.4**.

4.3 Anion transport studies

4.3.1 Results

Initially, the Cl^-/NO_3^- antiport activity of **177-182** was investigated. A solution of each receptor in DMSO was added to a suspension of unilamellar vesicles containing NaCl suspended in $NaNO_3$. The results are shown below.

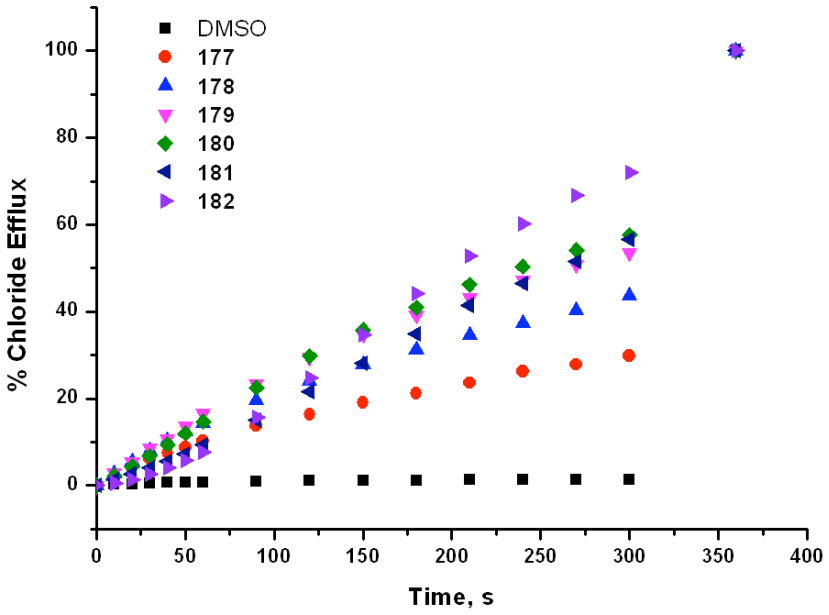

Figure 4.2 Chloride efflux promoted by receptors **177-182** (2 mol% w.r.t lipid) from unilamellar POPC vesicles containing 489 mM NaCl buffered to pH 7.2 with 5 mM sodium phosphate salts. The vesicles were suspended in 489 mM $NaNO_3$ buffered to pH 7.2 with 5 mM sodium phosphate salts. At the end of the experiment the vesicles were lysed to calibrate 100 % chloride efflux. Each point represents the average of 3 trials.

The results showed that under these conditions, **177-182** exhibited a range of transport activities and that increasing the length of the alkyl chain resulted in an increase in the total chloride efflux. Interestingly, the highest transport activity was observed for **182** (n = 12); unlike the series of receptors described in **Chapter 3**, there is no maximum chain length for increased efficiency observed within this series.

The Cl^-/HCO_3^- antiport activity of **177-182** was also investigated by addition of a DMSO solution of the receptor to vesicles containing NaCl suspended in Na_2SO_4. After 120 s, a solution of $NaHCO_3$ was added such that the total HCO_3^- concentration was 40 mM. The results are shown in **Figure 4.3**.

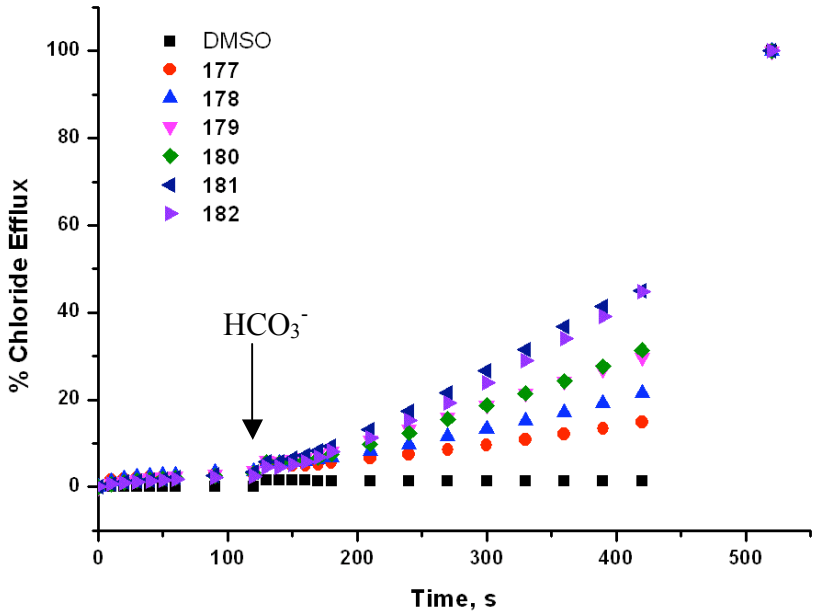

Figure 4.3 Chloride efflux mediated by **177-182** (2 mol% w.r.t. lipid) from unilamellar POPC vesicles containing 489 mM NaCl buffered to pH 7.2 with 20 mM sodium phosphate salts. The vesicles were suspended in 167 mM Na_2SO_4 buffered to pH 7.2 with 20 mM sodium phosphate salts. At t = 120 s, a pulse of $NaHCO_3$ was added such that the final HCO_3^- concentration was 40 mM. At the end of the experiment, the vesicles were lysed to calibrate 100 % chloride efflux. Each point represents the average of 3 trials.

These results show that bis-thioureas **177-182** are able to mediate Cl^-/HCO_3^- antiport. Under these conditions, a similar trend is observed as for the Cl^-/NO_3^- antiport by these receptors. The longest receptors **181** and **182** (n = 11 and 12) are the most active anion carriers.

Hill analyses were performed for the Cl^-/NO_3^- and Cl^-/HCO_3^- antiport by **177-182** and for bis-indolylthiourea **183**. Bis-phenylurea **184** was found to be inactive for both transport modes and was observed to precipitate during the experiment. **Table 4.1** contains the relevant constants from the Hill analyses and the clogP and PSA values for each compound (calculated using Spartan '10 for Macintosh). The full Hill analyses can be found in the appendix (section **A1.3**). The values determined for compound **125** and **127** (as discussed in **chapter 2**) and compound **163** (discussed in **chapter 3**) have been included for comparison. The structures of these carriers is shown in **Figure 4.4**.

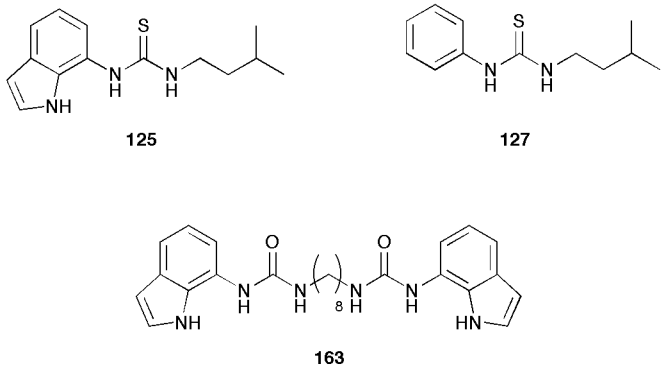

Figure 4.4 The structures of receptors **125**, **127** and **163** included in this study for comparison from other chapters.

Table 4.1 Values of EC_{50} for Cl^-/NO_3^- and Cl^-/HCO_3^- exchange and clogP and PSA values for compounds **177-182** and some structurally related analogues for comparison. Values of $EC_{50\ 270\ s}$ for Cl^-/NO_3^- and Cl^-/HCO_3^- antiport were calculated by a Hill analysis. clogP values were calculated using Spartan '10 for Macintosh [Ghose Crippen model]). The receptors were minimized using AMI semi-emperical methods with the two urea or thiourea NH groups parallel and the clogP and PSA values calculated. For the indole containing species, two conformations were minimized-one with the indole NH forming a convergent array with the urea NH groups and the other with the indole NH orientated towards the urea or thiourea O or S atom (hence a range of values for PSA is given). [a] The observed transport activity was too low to allow the determination of $EC_{50\ 270\ s}$ by a Hill analysis (EC_{50} > 4 mol%) ; [b] determined by SJM.

Compound	EC_{50} (Cl^-/NO_3^-) / mol%	EC_{50} (Cl^-/HCO_3^-) / mol%	clogP	PSA/ Å
177	[a]	[a]	4.37	43.8
178	2.29	[a]	4.79	42.9
179	1.75	[a]	5.21	43.3
180	1.69	3.66	5.63	42.9
181	1.16	1.13	6.04	43.4
182	0.93	0.42	6.46	42.7
183	0.52	[a]	2.99	62.0-67.3
184	Precipitates	Precipitates	2.50	69.2
127	0.029	0.036	3.16	31.1-35.5
125	3.07	2.08[b]	3.57	21.5
163	2.47	Not active	0.70	89.3-94.8

These results confirm that the most effective bis-thiourea for Cl^-/NO_3^- and Cl^-/HCO_3^- antiport agent is compound **182**, and that in general, increasing the length of the alkyl chain results in improved transport activity. This correlates with the increased clogP value and hence higher lipophilicity associated with increasing the length of the central aliphatic chain. Across the series **177-182** there is little change in the PSA. This is because the most polar regions of the molecule are the binding sites and increasing the length of the aliphatic chain has little bearing on this.

4.3.2 Analysis of structure-activity relationships

4.3.2.1 Substituent effects

The anion antiport properties of bis-indolylthiourea **183** are shown by comparison to the analogous bis-phenylthiourea **178** in **Figure 4.5(a)** and **(b)**.

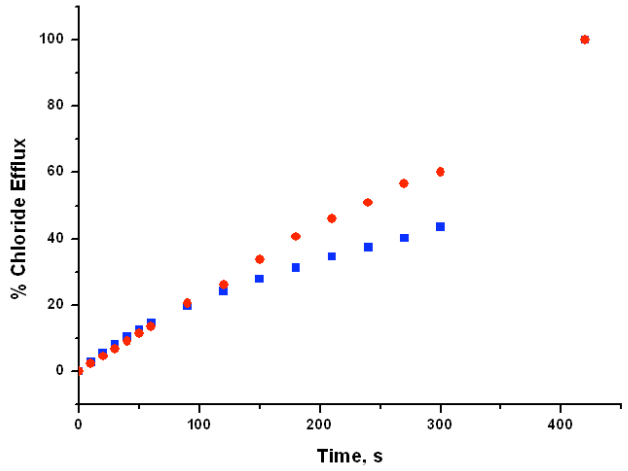

Figure 4.5(a) Chloride efflux promoted by **178** (blue) and **183** (red) (2 mol% with respect to lipid) from unilamellar POPC vesicles containing NaCl suspended in $NaNO_3$.

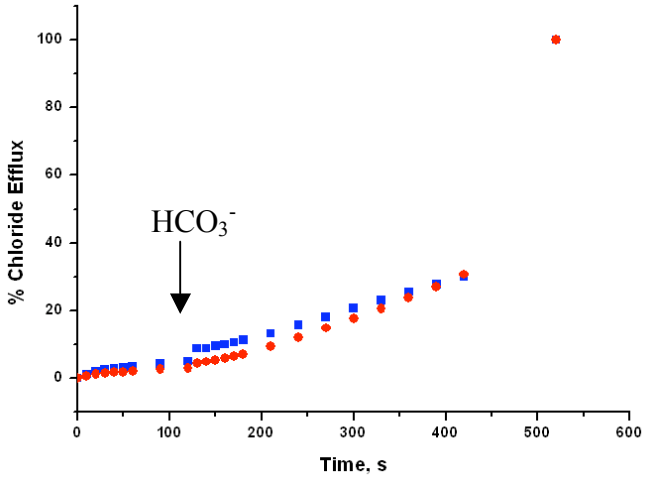

Figure 5(b) Chloride efflux promoted by **178** (blue) and **183** (red) (2 mol% with respect to lipid) from unilamellar POPC vesicles containing NaCl suspended in Na_2SO_4. At t = 120 s, a pulse of $NaHCO_3$ was added such that the final HCO_3^- concentration was 40 mM.

Compound **183** was more active for Cl^-/NO_3^- antiport than **178** as represented by the EC_{50} values and as shown in **Figure 4.5(a)**. This correlates with the finding from **Chapter 2** that a mono-indolylthiourea **127** was more active than a mono-phenylthiourea

125, possibly due to the better anion binding by a receptor with more hydrogen bond donors. However, at 2 mol% loading, the Cl^-/HCO_3^- antiport activity of **178** and **183** appear to be similar (**Figure 4.5(b)**). While these activities were too low to be quantified by a Hill analysis, it seems that in this case there is little advantage to the indolyl substituent by comparison to a phenyl substituent.

Bis-indolylurea **163** was more active for Cl^-/NO_3^- antiport than bis-phenylurea **184**, which precipitated during the experiment. Compound **163** is more hydrophilic than **184** (as judged by the clogP values) and also has a higher PSA, which may aid its passage through the aqueous phase. However, it is unlikely that lipophilicity is the sole reason that **184** precipitates, as it is less lipophilic than all of the listed thiourea compounds which are active. It is possible that **184** forms very strong intermolecular hydrogen bonds with itself, thus making its precipitation energetically favourable. Thioureas are known to be less likely to self associate by hydrogen bonding due to the lesser H-bonding basicity of the C=S group by comparison to C=O.[134]

4.3.2.2 Ureas *vs* thioureas

As mentioned above, bis-phenylurea **184** is completely inactive for anion transport, thus it is less active than the analogous thiourea **178**. Compound **183** was also found to be more active for Cl^-/NO_3^- antiport than the analogous bis-urea **163**, as evidenced by the values of EC_{50}. These observations correlate with the finding discussed in **Chapter 2** that thioureas tend to be more active than their urea analogues, previously argued on the basis of their greater lipophilicity.

4.3.2.3 The advantage of the bis-thiourea scaffold

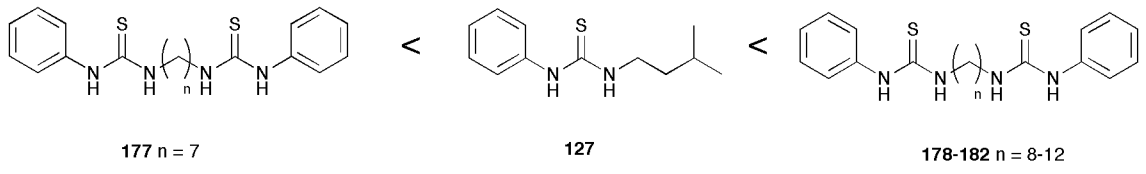

Figure 4.6 A comparison of the Cl^-/NO_3^- antiport activity of the phenylthiourea based carriers.

Compound **177** (n = 7) was found to be less active for Cl^-/NO_3^- exchange than mono-phenylthiourea **125** despite containing two thiourea binding sites. The presence of a second binding site makes the carrier less lipophillic as it contains a second polar region. The clogP values are significantly reduced, and the PSA approximately doubles. Thus, the activity is reduced compared to the mono-thiourea. Increasing the central alkyl chain length compensates this, as the longer chain bis-thioureas (compounds **178-182**, n = 8-12) were found to be more active than mono-thiourea **125**. Compounds **177-180** (n = 7-10) were also found to be less active for Cl^-/HCO_3^- antiport than **125**; however, the longest and most active analogues **181** and **182** (n = 11 and 12) were more active than **125** for both transport modes. These trends are summarised in **Figure 4.6**.

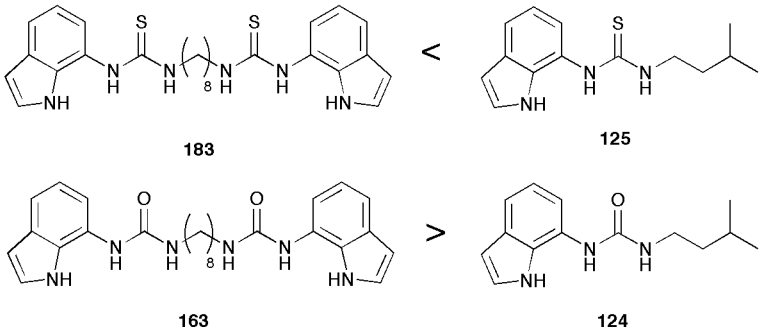

Figure 4.7 A comparison of the Cl^-/NO_3^- antiport activity of the indoly(thio)urea based carriers.

In **Chapter 3**, it was found that bis-indolylurea **163** was more active than analogous mono-ureas such as **126** (which exhibits no anion transport activity). However, when considering bis-thiourea **183** this trend is reversed, as it is significantly less active than **127**. The trends for the indole containing carriers are illustrated in **Figure 4.7**.

4.3.3 Mobility Assay

A mobile carrier mechanism for carriers **177-183** was confirmed by examining their Cl^-/NO_3^- antiport activity in vesicles composed of POPC:cholesterol (7:3). The comparative graph for receptor **182** is shown in **Figure 4.8**. The other analyses may be found in the appendix (section **A1.3**).

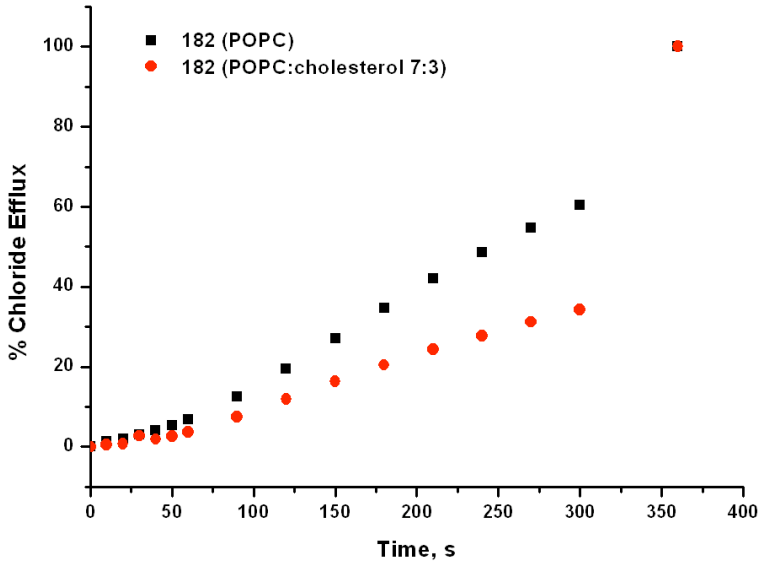

Figure 4.8 Chloride efflux mediated by receptor **182** from unilamellar vesicles composed of POPC or POPC:cholesterol (7:3) containing 489 mM NaCl buffered to pH 7.2 with 5 mM sodium phosphate salts. The vesicles were suspended in 489 mM $NaNO_3$ buffered to pH 7.2 with 5 mM sodium phosphate salts. At the end of the experiment the vesicles were lysed to calibrate 100 % chloride efflux. Each point represents the average of 3 trials.

A reduction in transport rate was observed for all of **177-183** compounds in membranes containing 30 % cholesterol; this indicates that the transport is diffusion controlled and confirms that these compounds function as mobile carriers rather than channels.

4.4 Solution phase anion binding studies

The solution phase anion binding properties of **177-184** with various anions was investigated by ^{1}H NMR titration in DMSO-d_6/H_2O 0.5 %. The H-atoms discussed in this section are assigned as shown in **Figure 4.9**.

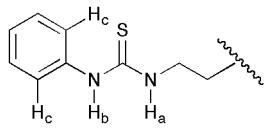

Figure 4.9 The phenylthiourea moiety of receptors **177-182** with the protons relevant to the ^{1}H NMR titrations labelled.

None of the series **177-184** were observed to interact with $TBANO_3$ in these experiments. The receptors were found to interact weakly with TBACl under these conditions. The binding curves were similar across the series. As shown in **Figure 4.10(a)**, both of the thiourea NH protons (H_a and H_b) participate in hydrogen bonding. A doublet centered at ~7.4 ppm, which corresponds to aromatic CH_c, was also observed to undergo a small downfield shift. This implies that there may be a small hydrogen bonding contribution from this CH donor. A Job plot analysis (**Figure 4.10(b)**) indicated that the binding stoichiometry was predominantly 1:1, and the data was fitted to a 1:1 binding model using WinEQNMR 2. The binding constants are shown in **Table 4.2**. This data indicates that the binding of Cl^- by these receptors is weak under these conditions, and that there is no trend across the series. Attempts to fit the binding curves from aromatic CH_c to a 1:1 model gave binding constants which were below the lower limit of detection by this method (< 10 M^{-1}). This trend is similar to that observed for receptors **159-167**, discussed in **Chapter 3**, although the binding is comparatively slightly weaker. Again, there is no correlation between the Cl^- binding strengths and transport activity.

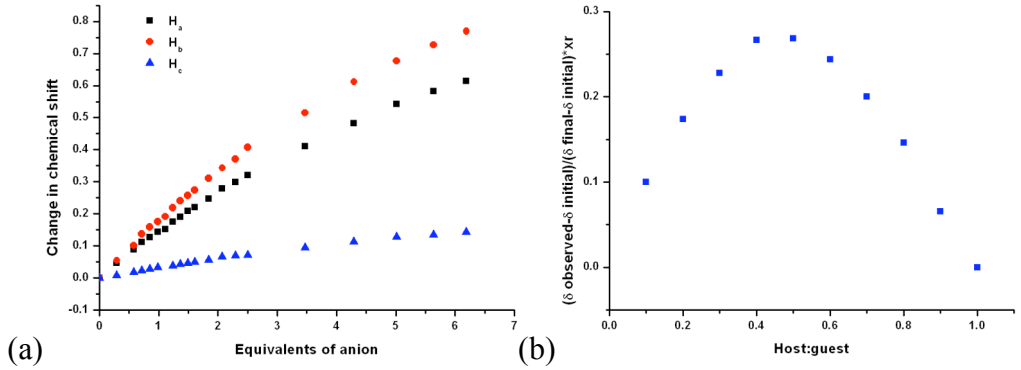

Figure 4.10 (a) The change in chemical shift of H_a, H_b and H_c of receptor **180** on titration with TBACl in DMSO-d_6/H_2O 0.5 %; (b) The Job plot analysis for this process following H_a.

Table 4.2 Binding constants (M^{-1}) obtained from the ^1H NMR titration of **177-181** with TEACl in DMSO-d_6/H_2O 0.5% following the thiourea NH resonance at ~7.4 ppm. The data was fitted to a 1:1 binding model using WinEQNMR 2. The errors are reported in brackets as a percentage of the value. All errors are < 10 %.

	177	**178**	**179**	**180**	**181**	**182**
K_a	16	14	9	11	16	11

During the titration of receptors **177-182** with $TEAHCO_3$, the thiourea NH resonances were observed to immediately broaden. This prevented the investigation of HCO_3^- binding by following these resonances. However, the aromatic CH_c resonance was observed to shift downfield. This shift is shown in **Figure 4.11(a)**. The shift of the CH_c resonance indicates hydrogen bond formation to the anion, and the shape of the curve indicates that a 1:2 complex is likely to be the predominant species in solution. The Job plot analysis for this process, shown in **Figure 4.11(b)** indicated that the stoichiometry was potentially a mixture of 1:1 and 1:2 binding.

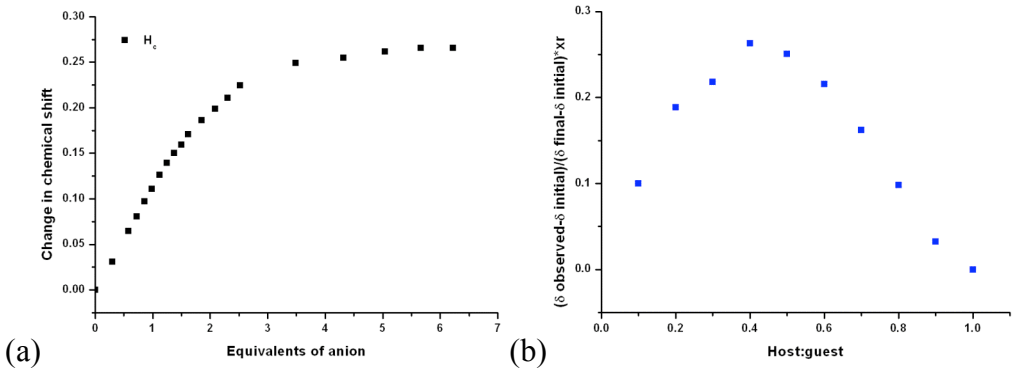

Figure 4.11 (a) The change in chemical shift of the aromatic CH_c resonance of receptor **180** on titration with $TEAHCO_3$ in DMSO-d_6/H_2O 0.5 %; (b) The Job plot analysis for this process following H_c.

The binding curves from the CH_c resonance were fitted to a 1:2 binding model using WinEQNMR 2. The binding constants obtained are shown in **Table 4.3**.

Table 4.3 Binding constants (M^{-1}) obtained from the ^1H NMR titration of **177-181** with $TEAHCO_3$ in DMSO-d_6/H_2O 0.5% following the aromatic CH_c resonance at ~7.4 ppm. The data was fitted to a 1:2 binding model using WinEQNMR 2. The errors are reported in brackets as a percentage of the value.

	177	**178**	**179**	**180**	**181**	**182**
K_1	384 (27 %)	128 (13 %)	114 (18 %)	264 (2 %)	189 (24 %)	247 (13 %)
K_2	413 (28 %)	182 (14 %)	190 (18 %)	227 (7 %)	290 (26 %)	137 (17 %)

The large errors associated with some of these binding constants implies that, as with receptors **159-167** (**Chapter 3**), the simple 1:2 binding model does not perfectly

describe the equilibria present in these systems. There is no observable trend in binding strength across the series.

During the titration of **177-182** with $TBAH_2PO_4$, the thiourea NH_b was observed to broaden throughout the experiment and therefore could not be tracked for the entire titration. The change in chemical shift of thiourea NH_a and aromatic CH_c is shown in **Figure 4.12**.

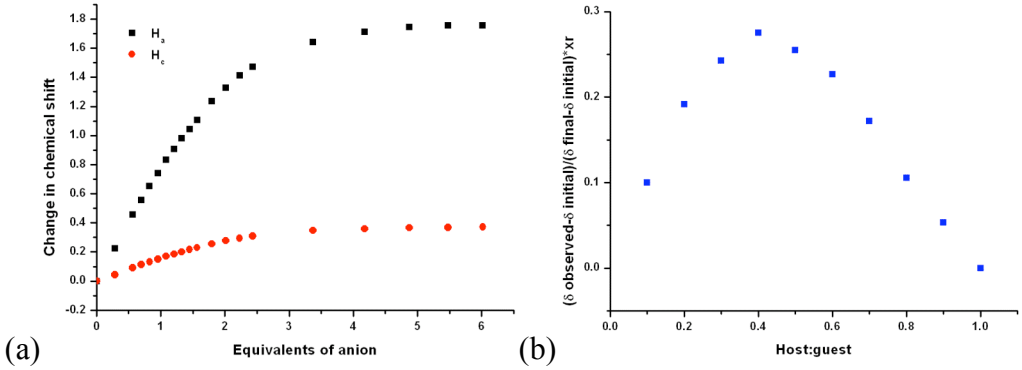

Figure 4.12 (a) The change in chemical shift of H_a and H_c of receptor **180** on titration with $TBAH_2PO_4$ in DMSO-d_6/H_2O 0.5 %; (b) The Job plot analysis for this process following H_a.

These binding curves were fitted to a 1:2 binding model using WinEQNMR 2. The calculated binding constants are shown in **Table 4.4** and **Table 4.5**.

Table 4.4 Binding constants (M^{-1}) obtained from the ^1H NMR titration of **177-181** with $TBAH_2PO_4$ in DMSO-d_6/H_2O 0.5% following the thiourea NH_a resonance at ~7.7 ppm. The data was fitted to a 1:2 binding model using WinEQNMR 2. The errors are reported in brackets as a percentage of the value.

	177	**178**	**179**	**180**	**181**	**182**
K_1	718 (7 %)	806 (9 %)	157 (41 %)	343 (24 %)	458 (10 %)	676 (23 %)
K_2	274 (12 %)	207 (11 %)	221 (41 %)	255 (24 %)	110 (18 %)	102 (37 %)

Table 4.5 Binding constants (M^{-1}) obtained from the ^1H NMR titration of **177-181** with $TBAH_2PO_4$ in DMSO-d_6/H_2O 0.5% following the aromatic CH_c resonance at ~7.4 ppm. The data was fitted to a 1:2 binding model using WinEQNMR 2. The errors are reported in brackets as a percentage of the value.

	177	**178**	**179**	**180**	**181**	**182**
K_1	714 (34 %)	716 (5 %)	346 (11 %)	308 (13 %)	516 (15 %)	473 (4 %)
K_2	258 (34 %)	216 (5 %)	255 (13 %)	313 (14 %)	204 (17 %)	101 (7 %)

Again, there is no observable trend in binding strengths across the series. The binding of $H_2PO_4^-$ seems to be of similar strength to the binding of HCO_3^-. In some cases the errors on these values are large, implying that a simple 1:2 model does not accurately describe the equilibria that are present. The binding constants obtained from following H_a and H_c are similar, and can therefore be compared to the HCO_3^- binding constants. The binding of HCO_3^- by these receptors is similarly strong as the binding of $H_2PO_4^-$.

In order to investigate whether the observed peak broadening effects were due to the receptor being deprotonated by basic anions, a control titration was performed with receptor **180** and TBAOH (1 M in MeOH) under the same conditions. The stack plot for this titration is shown in **Figure 4.13**.

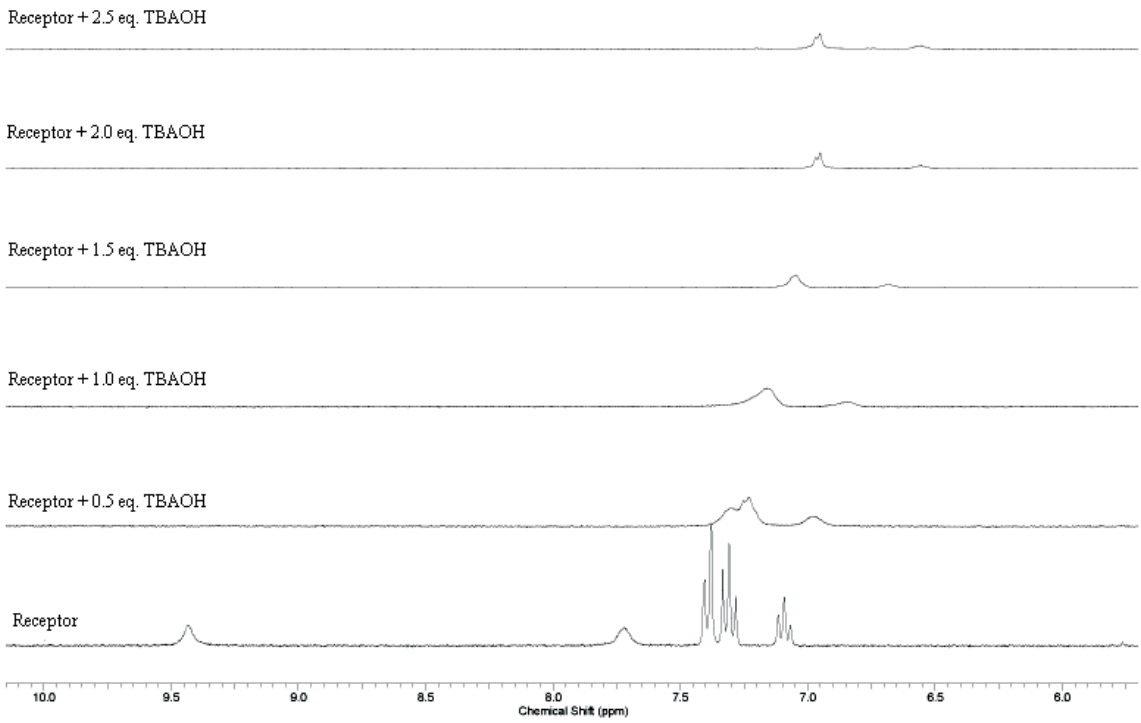

Figure 4.13 Stack plot showing the titration of receptor **180** with a methanolic solution of TBAOH in DMSO-d_6/ H_2O 0.5 %).

This titration shows that when these receptors are deprotonated, the aromatic CH resonances shift upfield. As this behaviour is not observed in the titrations with HCO_3^- and $H_2PO_4^-$, this suggests that deprotonation of the receptor by these anions is not occurring.

During the titration of **177-182** with TBA_2SO_4, the H_a, H_b and H_c resonances were observed to shift downfield until the addition of 1 equivalent of anion, as shown in **Figure 4.14(a)**; at this point, the downfield shift slowed and a clear turning point was observed, but the resonances continued to slowly shift throughout the rest of the experiment. This behaviour is analogous to the SO_4^{2-} binding by receptors **159-167**, which were found to strongly complex one equivalent of SO_4^{2-} and to weakly complex the second equivalent of anion. The Job plot analysis shown in **Figure 4.14(b)** indicates that the binding stoichiometry is potentially a mixture of 1:1 and 1:2. This is in contrast to the Job plot obtained from the SO_4^{2-} binding by bis-indolylureas **159-167**, which appeared to show 1:1 binding as the second binding event was so weak. The binding curves following H_a were fitted to a 1:2 binding model using WinEQNMR 2. The binding

constants thus obtained are shown in **Table 4.6**. The binding curves following the aromatic CH_c fitted best to a 1:1 binding model as the change in chemical shift throughout the titration was much less, and the change in chemical shift after the addition of 1 equivalent of anion was almost negligible. The binding constants obtained from this analysis are shown in **Table 4.7**.

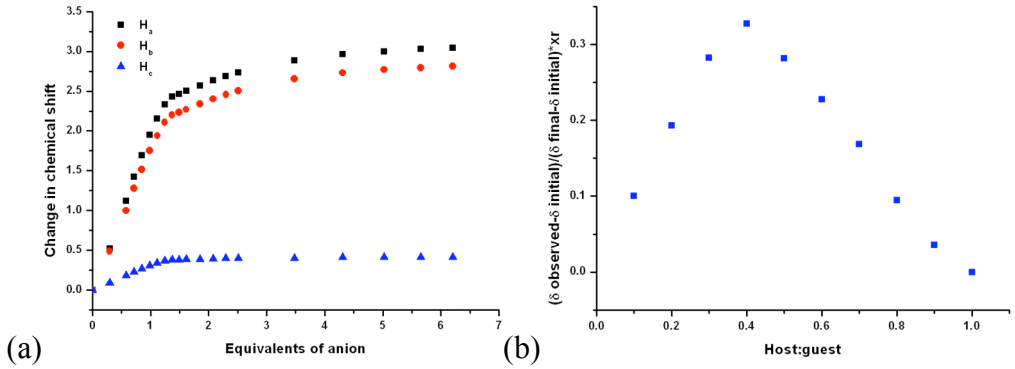

Figure 4.14 (a) The change in chemical shift of H_a, H_b and H_c of receptor **180** on titration with TBA_2SO_4 in DMSO-d_6/H_2O 0.5 %; (b) The Job plot analysis for this process following H_a.

Table 4.6 Binding constants (M^{-1}) obtained from the ^1H NMR titration of **177-181** with TBA_2SO_4 in DMSO-d_6/H_2O 0.5% following the thiourea NH resonance at ~7.7 ppm. The data was fitted to a 1:2 binding model using WinEQNMR 2. The errors are reported in brackets as a percentage of the value.

	177	**178**	**179**	**180**	**181**	**182**
K_1	4612 (30 %)	5248 (30 %)	6339 (18 %)	3195 (24 %)	5179 (4 %)	3427 (16 %)
K_2	53 (44 %)	36 (59 %)	70 (21 %)	69 (41 %)	61 (11 %)	90 (22 %)

Table 4.7 Binding constants (M^{-1}) obtained from the ^1H NMR titration of **177-181** with TBA_2SO_4 in DMSO-d_6/H_2O 0.5% following the aromatic CH resonance at ~7.4 ppm (centre of a doublet). The data was fitted to a 1:1 binding model using WinEQNMR 2. The errors are reported in brackets as a percentage of the value.

	177	**178**	**179**	**180**	**181**	**182**
K_a	129 (7 %)	338 (14 %)	209 (13 %)	176 (4 %)	259 (12 %)	153 (11 %)

The anion binding by compounds **183** and **184** was also investigated by ^{1}H NMR titration in DMSO-d_6/ H_2O 0.5 %. The change in chemical shift of the thiourea NH resonance of receptor **183** and the urea NH resonance of receptor **184** on titration with a variety of anions is shown in **Figure 4.15**.

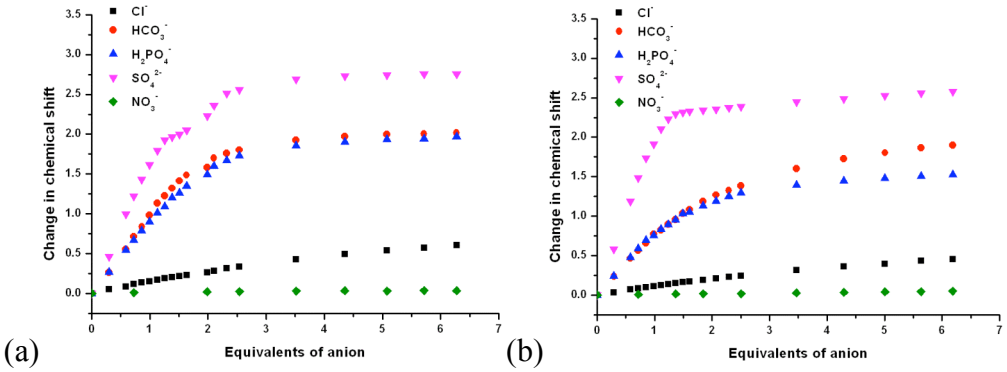

Figure 4.15 The change in chemical shift of (a) the thiourea NH resonance of **183** at ~7.5 ppm, and (b) the urea NH resonance of **184** at ~6.1 ppm during the ^{1}H NMR titration with various anions (added as he tetrabutylammonium or tetraethylammonium salts) in DMSO-d_6/ H_2O.

Like the previously discussed receptors, **183** and **184** do not interact with $TBANO_3$ under these conditions. The binding profiles for the interaction of **183** and **184** with Cl^-, HCO_3^- and $H_2PO_4^-$ are similar to those obtained from bis-indolylureas **159-167** (**Chapter 3**) and bis-phenylthioureas **177-182** which implies that they exhibit similar binding modes. The shape of the binding curve from the titration of **184** with TBA_2SO_4 seems to increase only very slightly after the addition of 1 equivalent of anion. This implies that either a 1:1 binding mode is prevalent, or that the binding of the second equivalent of anion is extremely weak. In contrast, the binding curve from the titration of **183** with TBA_2SO_4 indicates that a second equivalent of anion is bound, resulting in a two-step binding curve. This implies that the binding of the second SO_4^{2-} anion by **183** is correspondingly stronger than by **184**. The binding curves obtained were fitted to an appropriate binding model. The corresponding Job plot analyses may be found in the appendix (section **A2.2**) The binding constants obtained are shown in **Table 4.8**.

Table 4.8 Binding constants (M^{-1}) obtained from the ^1H NMR titration of **183** and **184** with various anions (added as their tetrabutylammonium or tetraethylammonium salt) in DMSO-d_6/H_2O 0.5% following the thiourea NH resonance of **183** at ~7.4 ppm and the urea NH resonance of **184** at ~6.1 ppm. The data was fitted to a 1:1 or 1:2 binding model using WinEQNMR 2. The errors are reported in brackets as a percentage of the value.

		183	**184**
Cl^-	K_a	17 (5 %)	15 (3 %)
HCO_3^-	K_1	2907 (9 %)	3882 (9 %)
	K_2	338 (9 %)	55 (12 %)
$H_2PO_4^-$	K_1	2281 (7 %)	3584 (7 %)
	K_2	344 (7 %)	135 (8 %)
SO_4^{2-}	K_1	5632 (7 %)	$> 10^4$
	K_2	217 (11 %)	29 (19 %)

This data shows that, like **159-167** and **177-182**, Cl^- is weakly complexed in a 1:1 binding mode. HCO_3^- and $H_2PO_4^-$ are complexed in a predominantly 1:2 fashion, and the binding strengths of the first and second equivalent of anion for each receptor is similar. Receptors **183** and **184** bind SO_4^{2-} in a 1:2 binding mode; however, the second equivalent of SO_4^{2-} is bound more strongly by **183**.

4.5 Conclusions

The work in this chapter demonstrates that the bis-urea scaffold reported in **Chapter 3** can be readily modified to yield new successful anion carriers. The bis-phenylthiourea scaffold was found to be more active for anion transport than an analogous mono-thiourea at longer chain lengths. This shows that the bis-thiourea scaffold becomes more advantageous as the lipophilicity of the carrier increases. An analogous bis-phenylurea **184** was found to be completely inactive for anion transport. Unlike the series of bis-indolylthioureas **159-167** reported in **Chapter 3**, the greatest transport activity is observed for compound **182**, the longest receptor in the series. This implies that the bis-phenylthiourea receptors do not suffer reduced mobility through the aqueous phase as the longer chain analogues do not mediate reduced transport activity as a result of their slower membrane partitioning. This may be a result of the lesser hydrogen bond basicity of the C=S group,[134] meaning that the receptors are less likely to aggregate in the water phase, despite their greater lipophilicity. This greater lipophilicity of the bis-thiourea scaffold may be the cause of their Cl^-/HCO_3^- antiport activity, a transport mode which the bis-indolylureas **159-167** can not facilitate. Additionally, a bis-indolylthiourea **183** was found to be more active for anion transport than its phenyl-substituted analogue, again highlighting the advantages of including the indole moiety in receptor design.

As anion receptors, the anion complexation behaviour of the carriers reported in this chapter is similar to the bis-indolylureas **159-167**. This demonstrates that the observed complex anion binding behaviour is not specific to a single group of bis-(thio)ureas but is a general consequence of the flexibility of this type of scaffold. These results further confirm that more active anion carriers may be synthesised without consideration of improving their anion binding strengths. These results also reiterate that it is becoming increasingly evident that the interaction of the receptor-anion complex within the hydrophobic interior of the lipid bilayer is a more important parameter in the design of new transporters than the anion binding strength. The design of new anion carriers could be based on structures with predicted clogP values in an optimum range for anion transport, providing they contain a suitable anion binding site.

Chapter 5
Anion transport by strapped calix[4]pyrroles

5.1 Introduction

In 2008 Gale and co-workers first described the use of calix[4]pyrrole **28** (**Figure 5.1**) as a Cs^+/Cl^- symporter.[63] This behaviour was attributed to the function of **28** as an ion pair receptor for CsCl, in which binding of the Cl^- organises the macrocycle into a cone conformation, allowing the Cs^+ to be complexed within the cup-like cavity thus created.[62] Cs^+ is a large, charge diffuse cation and is bound by the calix[4]pyrrole cup due to effective size complemetarity. Cs^+ is also the least hydrophilic of the stable alkali metal cations, and as such would be expected to be the least energetically unfavourable cation in this group to transport across a lipid bilayer. However, Cs^+ is not a biologically relevant cation, so the potential application of **28** as a biological chloride transport agent is limited as no transport can occur in the absence of Cs^+. There is currently much academic interest in the synthetic modification of the calix[4]pyrrole framework in order to create receptors to facilitate anion transport under biological conditions.

5.1.1 Anion binding by modified calixpyrroles

Since Sessler *et al.* first reported the use of calix[4]pyrroles (such as **28**) as anion receptors in 1996,[61] there has been extensive work dedicated to the modification of this scaffold to yield alternative anion selectivites and enhanced anion binding strengths. Early efforts focused on functionalizing the β-pyrrolic positions or the *meso*-substituents as these changes are synthetically the most straightforward.

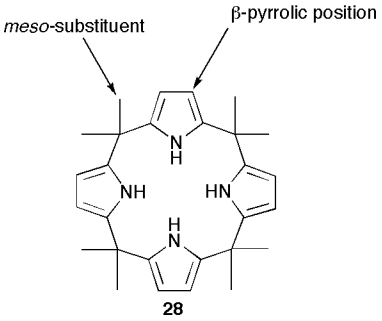

Figure 5.1 Parent macrocycle *meso*-octamethylcalix[4]pyrrole (**28**).

β-fluorination of the calix[4]pyrrole scaffold leads to enhanced anion binding due to the increased aciditiy of the pyrrole NHs. Sessler and co-workers have reported the synthesis and anion binding studies of some fluorinated calix[n]pyrroles **36** and **185-188** as shown in **Figure 5.2**.[167] Binding studies were undertaken using ITC in MeCN (2 % H_2O *v*/*v*) and revealed that fluorocalix[4]pyrrole **36** bound TBACl more strongly than unmodified calix[4]pyrrole **28** (K_a = 31000 M^{-1} and 5400 M^{-1} respectively). A number of binding studies were completed by ITC in MeCN and DMSO. The results showed that increasing the size of the cavity resulted in an increased selectivity for Br^- over Cl^-. The binding of larger anions such as $H_2PO_4^-$ was also enhanced as the cavity size increased across the series.

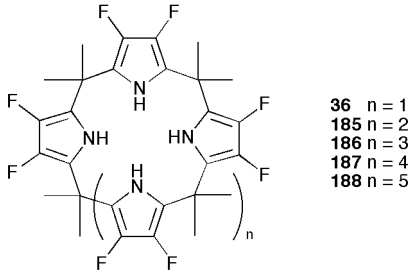

Figure 5.2 Fluorinated expanded calix[4]pyrroles.

Sessler and co-workers have also reported the expansion of the calix[4]pyrrole cavity by employing bipyrrole in place of pyrrole, yielding calix[n]bipyrroles such as **189** (**Figure 5.3**).[168] By a combination of ^{1}H NMR titration and ITC in MeCN and DMSO (or deuterated equivalents) they found that **189**, like calix[4]pyrrole **28**, displayed selectivity for Cl^- over Br^- and I^- (F^- was not tested), although **28** was the stronger chloride receptor.

However, **189** was found to bind Br^- and I^- more strongly than **28** as a result of the expanded cavity. Subsequently, the same authors reported that calix[2]bipyrrole[2]furan **190** and calix[2]bipyrrole[2]thiophene **191** (**Figure 5.3**) were weaker receptors for all of the anions tested than **28** and **189**.[169] However, **190** and **191** were found to be selective for carboxylates such as benzoate (K_a = 63000 M^{-1} and 139000 M^{-1} respectively), while **28** was found to complex benzoate similarly strongly to Cl^- (115000 M^{-1} and 140000 M^{-1} respectively) and was thus less selective. The relatively weaker binding of the spherical Cl^- anion by these receptors with a larger, non-symmetrical binding cleft was attributed to the poorer size complementarity of the cavity.

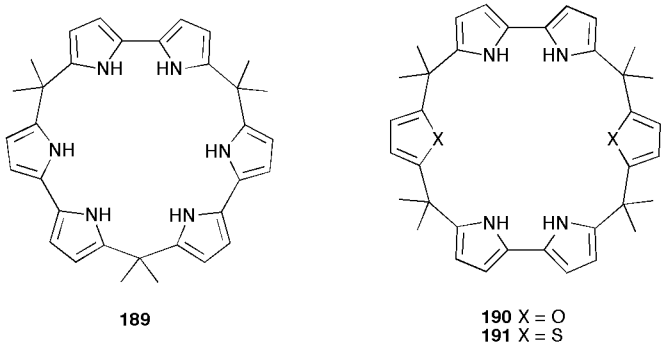

Figure 5.3 The expanded calixbipyrroles reported by Sessler *et al.*

Modification of the binding properties of the calix[4]pyrrole scaffold can also be achieved by the so-called "strapping" of the macrocycle to give receptors of the general form shown in **Figure 5.4**.[170] This structural modification should yield a receptor with a more preorganized binding site, as the calix[4]pyrrole cleft will be better shielded from solvent molecules. Variation of the length of the strap can allow control of size selectivity, and inclusion of additional hydrogen bond donors into the strap can also contribute to the binding of the anion.

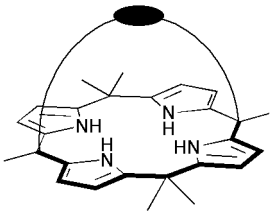

Figure 5.4 A general representation of a strapped calix[4]pyrrole. The calix[4]pyrrole framework is not planar but has been represented as such for clarity.

The first example of a strapped calix[4]pyrrole (compound **192**) was reported by Lee and co-workers in 2002.[171] Subsequently, the same authors described the synthesis and comparative anion binding studies of **193** and **194**.[172] These receptors are shown in **Figure 5.5**.

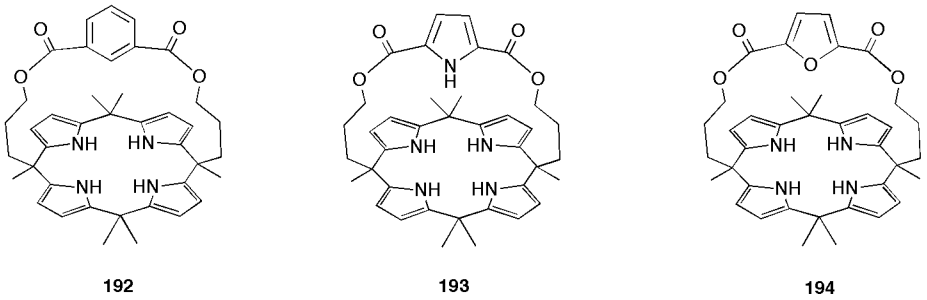

Figure 5.5 A series of strapped calix[4]pyrroles reported by Lee *et al.*

Attempts to determine the chloride binding constants of these receptors by ^{1}H NMR were unsuccessful as slow exchange kinetics were observed. Consequently, binding constants were determined by ITC in dry MeCN for **192-194** with TBACl. By comparison to un-strapped calix[4]pyrrole **28**, (K_a = 2.2 x 10^5 M^{-1}), compound **192** bound chloride 10 times more strongly (K_a = 2.2 x 10^6 M^{-1}). The strongest chloride binding was observed with compound **193** (K_a = 1.8 x 10^7 M^{-1}), while compound **194** (K_a = 1.9 x 10^5 M^{-1}) did not exhibit enhanced chloride binding compared to **28**. This suggests that additional hydrogen bonding interactions from the pyrrole NH of **193** and the phenyl CH of **192** contributed to stronger binding. Single crystal X-ray diffraction studies of the chloride complexes of **192** and **193** provided evidence of these hydrogen bonding interactions in the solid state, whilst evidence for this in solution was obtained from the corresponding downfield shift of the resonances of these protons in the ^{1}H NMR titration

of these molecules with TBACl in DMSO-d_6. This highlights the advantages of inclusion of additional hydrogen bond donors into the strap.

There are a large variety of functional groups that can be incorporated into the strap in order to achieve desirable properties. For example, compounds **195**[173] and **196**[174] contain a chromophore and a fluorophore respectively, which is of use for anion sensing. Meanwhile, the strap of calix[4]pyrrole **197** contains a Ni(II) capped porphyrin which can enhance anion binding *via* Lewis acid interaction with the bound metal cation.[175] Receptors **197***R* and **197***S* contain a chiral strap.[176] Correspondingly, they were found to bind chiral carboxylates with high affinity in MeCN, with the strongest complexes formed between the (*S*)-guest-(*S*)-host pair and the (*R*)-guest-(*R*)-host pair.

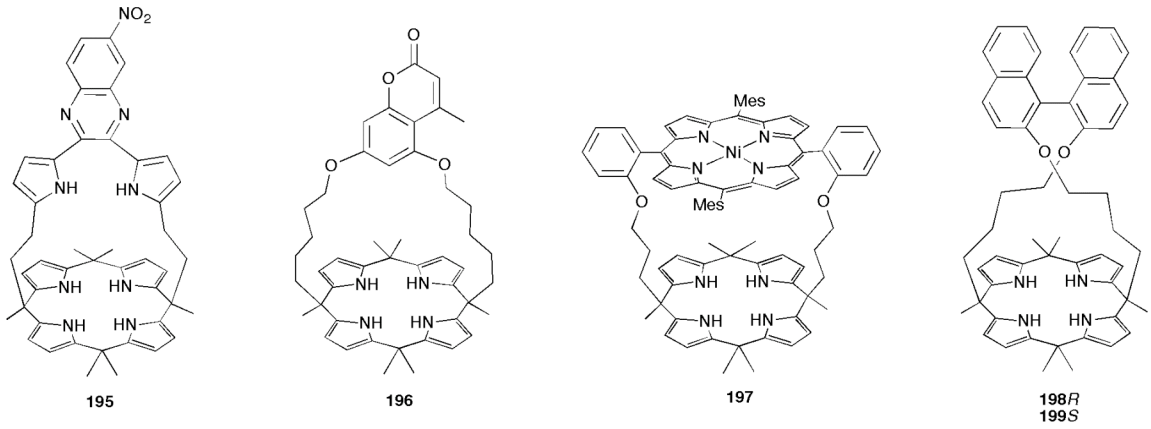

Figure 5.6 The incorporation of a wide variety of structural motifs can result in novel binding and sensing properties.

5.1.2 Modified calix[4]pyrroles as anion transport agents

Calix[4]pyrrole based carriers may be of use biologically if their transport activity can function in the absence of Cs^+. This has been achieved in the past by synthetic modification of the calix[4]pyrrole scaffold. For example fluorocalix[4]pyrrole **36** functions as a Cl^-/NO_3^- and Cl^-/HCO_3^- antiporter but is unable to facilitate any symport mechanisms.[67] In general, anions are bound more strongly by **36** in comparison to **28**. It is possible that a stronger interaction with the secondary anion (NO_3^- or HCO_3^-) is the route of the observed antiport activity of **36**. Unlike **28**, compound **36** does not mediate

Cs^+/Cl^- symport. This may be due to the electron withdrawing fluorine substituents resulting in a reduction in electron density of the pyrrole-π-system, reducing the affinity of the macrocycle for cesium. Additionally, fluorinated aromatic structures are known to be more lipophilic than non-fluorinated analogues;[66] this may contribute to the effective partitioning of the receptor-anion complex within the bilayer.

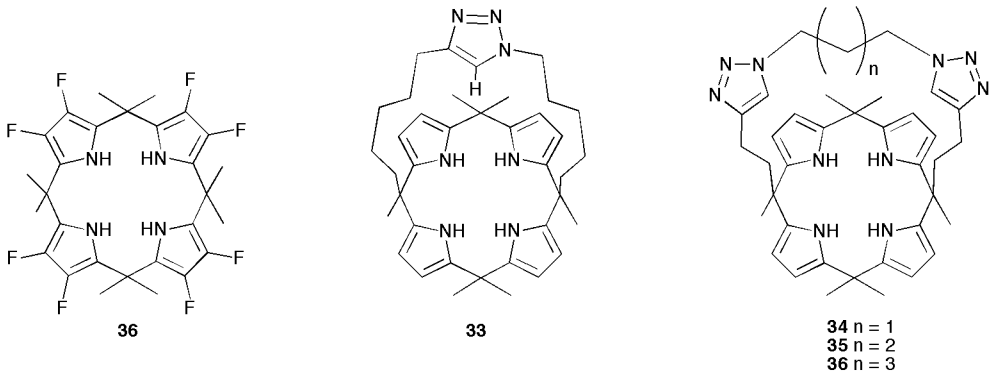

Figure 5.7 The structurally modified calix[4]pyrroles which have been reported to facilitate Cl^- transport in the absence of Cs^+.

Strapping the calix[4]pyrrole framework has also led to anion carriers which can function both in the presence and in the absence of Cs^+. Gale and co-workers have reported a series of 1,2,3-triazole strapped calix[4pyrroles **33-36**.[64, 65] These carriers can function as Cs^+/Cl^- symporters, but can also facilitate Cl^-/NO_3^- exchange. The preferred transport pathway differs across the series, but this is further proof that strapping the calix[4]pyrrole framework can encourage an antiport mechanism. Additionally, carriers **31** and **36** have also been shown to function as part of dual host system, in which they are though to facilitate the uniport of Cl^-, which is coupled to a second transport event mediated by a different carrier.[74, 75]

5.2 New calix[4]pyrrole based carriers

The design of new calix[4]pyrrole based transporters can utilize the chloride complexation behaviour of the calix[4]pyrrole core. An anion antiport mechanism may be encouraged by the inclusion of additional hydrogen bond donors into the strap, thus

providing greater stabilization of the receptor with the second anion of interest. Alternatively, it is hoped that if the strap facilitates the binding of a metal cation other than Cs^+, the symport of a biologically relevant ion pair may be encouraged. In particular, the groups of J. L. Sessler and C.-H. Lee have been at the forefront of this research and, in collaboration with the Gale group, have been working towards the synthesis of calix[4]pyrroles for biological applications. In particular, the goal of synthesizing new K^+/Cl^- symporters has been highlighted by these authors. Some typical intra- and extracellular ion concentrations are shown in **Table 5.1**.[4] It is hoped that the passive transport of Cl^- out of cells (against the electrochemical gradient) may be achieved by co-transport with K^+, for which there is a favourable gradient.

Table 5.1 Typical intracellular and extracellular ion concentrations in mammalian (vertebrate) cells.

Ion	Cell (mM)	Blood (mM)
Cl^-	4	116
HCO_3^-	12	29
Na^+	12	145
K^+	139	4

5.3 Calix[4]pyrrole-crown-6: anion transport by an ion pair receptor

Calix[4]pyrrole **200** was provided by the groups of J. L. Sessler and C.-H. Lee. It was designed as an ion pair receptor to facilitate the binding of a metal cation by the polyethyleneglycol strap, based on the well-documented complexation of group (I) metal cations by crown ethers.[177] In unpublished work, **200** was found to complex Cl^- and F^- in MeCN. Treatment of the chloride complex of **200** with group (I) metal cations revealed that no significant complexation of Na^+ or K^+ occurred. Treatment with Li^+ resulted in a tightly bound ion pair in which the Li^+ was complexed by the crown ether strap. Conversely, Cs^+ was bound in the cup-like cavity of the calix[4]pyrrole analogously to parent macrocycle **28**, giving rise to a host separated ion pair.

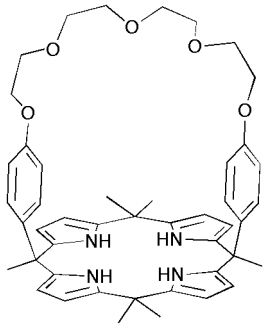

200

Figure 5.8 Calix[4]pyrrole-crown-6 **200**.

5.3.1 Anion transport studies

Due to the metal cation coordination properties of **200**, initial anion transport studies were conducted to investigate its M^+/Cl^- symport activity. The chloride efflux from vesicles containing MCl suspended in Na_2SO_4 mediated by **200** was monitored. The intra- and extra-vesicular solutions were chosen to ensure that the observed chloride efflux could only occur *via* a symport mechanism. The results are shown in **Figure 5.9**.

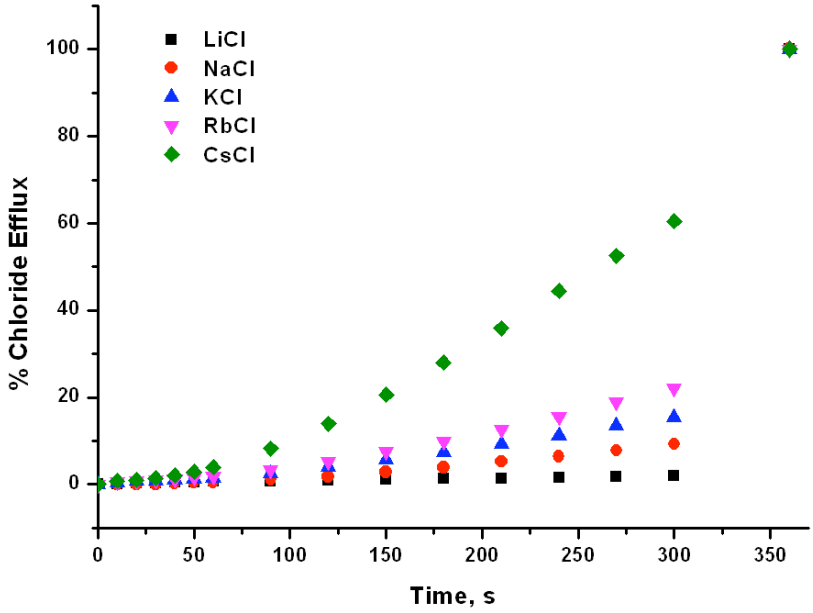

Figure 5.9 Chloride efflux mediated by receptor **200** (4 mol% w.r.t. lipid) from POPC vesicles containing 489 mM MCl buffered to pH 7.2 with 5 mM sodium phosphate salts (M = group (I) cations). The vesicles were suspended in 167 mM Na_2SO_4 buffered to pH 7.2 with 5 mM sodium phosphate salts. At the end of the experiment, the vesicles were lysed to calibrate 100 % chloride efflux. Each point represents the average of 3 trials.

It was found that **200** can mediate Cs^+/Cl^- symport; however, the symport of other group (I) cations was greatly reduced (and generally mirrors the increasing lipophilicity of the cations with increasing ionic radius). This is unsurprising, as the binding studies conducted by Sessler *et al.* revealed that Na^+ and K^+ are not complexed as part of a chloride ion pair. Li^+ is small and highly charge dense, thus its transport across a lipid phase is highly unfavourable.

The Cl^-/NO_3^- antiport activity of **200** was investigated by monitoring chloride efflux mediated by **200** from vesicles containing NaCl or CsCl suspended in $NaNO_3$. A comparative graph showing the effect of replacing the external SO_4^{2-} with NO_3^- is shown in **Figure 5.10**.

(a)

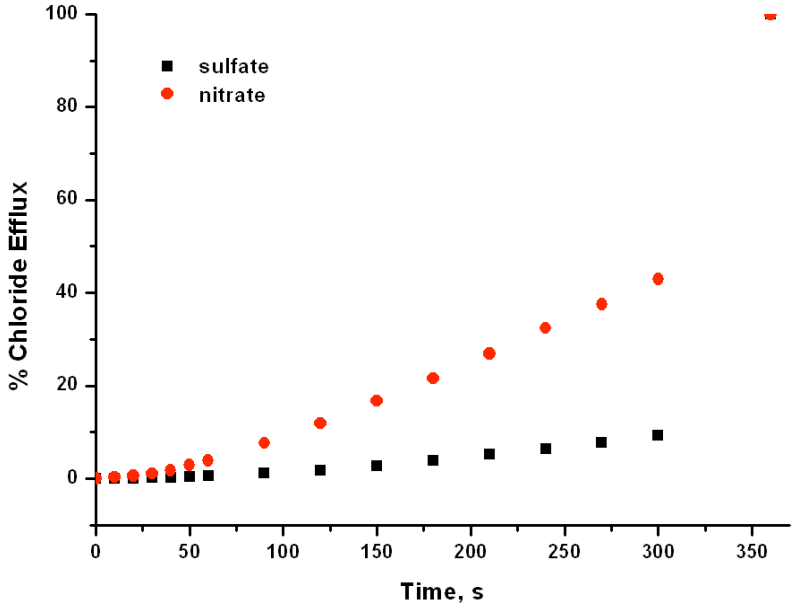

(b)

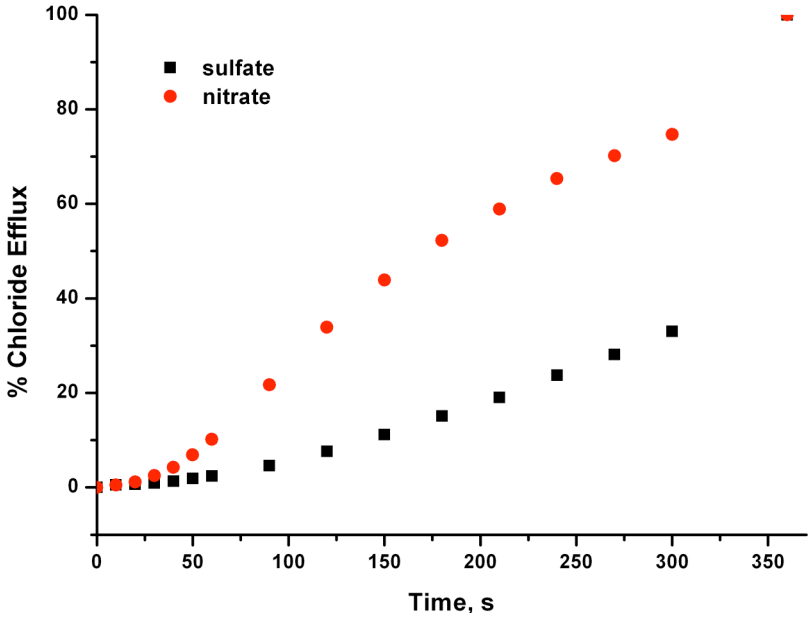

Figure 5.10 Chloride efflux mediated by receptor **200** from vesicles containing 489 mM NaCl (graph (a), 4 mol% carrier loading) or 489 mM CsCl (graph (b), 2 mol% carrier loading) buffered to pH 7.2 with 5 mM sodium phosphate salts. The vesicles were suspended in 167 mM Na_2SO_4 or 489 mM $NaNO_3$ buffered to pH 7.2 with 5 mM sodium phosphate salts. At the end of the experiment, the vesicles were lysed to calibrate 100 % chloride efflux. Each point represents the average of 3 trials.

The results show that receptor **200** can mediate Cl^-/NO_3^- antiport, although this is less efficient than the Cs^+/Cl^- symport pathway. When both pathways are available (CsCl/ $NaNO_3$) the highest chloride efflux is observed, indicating a likely combination of these transport pathways. Hill analyses for these processes were performed. While the Cl^-/NO_3^- antiport activity of **200** is too low to yield a reliable EC_{50} value, the EC_{50} value for Cs^+/Cl^- symport is 1.94 mol%, while when both pathways are possible the observed EC_{50} value is lower at 1.17 mol%, thus reflecting this enhancement. (The full Hill analyses can be found in section **A1.4** in the appendix).

In order to verify whether **200** was functioning as a mobile carrier, chloride efflux from CsCl contaning vesicles composed of POPC:cholesterol (7:3) suspended in Na_2SO_4 was measured. Calix[4]pyrroles have only been reported to function as mobile carriers in the past. However, no reduction in transport rate was observed by comparison to vesicles which were composed of 100 % POPC. Despite this finding, in light of U-tube experiments conducted by J. L. Sessler *et al.* which showed that **200** is capable of transporting various ions across an apolar phase, it was concluded that it most likely functions as a mobile carrier.

5.3.2 Conclusions

Receptor **200** was designed as a ditopic ion pair receptor. However, it fails to transport any ion pairs except for CsCl. This is most likely because the size of the crown ether cavity is too small to facilitate the binding of any cation except Li^+, which is extremely hydrophilic and thus difficult to transport. CsCl may be bound as a host separated ion pair and is most likely transported in this manner, analogously to unmodified calix[4]pyrrole **28**. A promising route towards the development of a similar receptor for the symport of NaCl or KCl would be to expand the crown ether moiety in order to favour the binding of these larger cations.

5.4 Pyridyl strapped calix[4]pyrroles

Compounds **201**-**203** were provided by the groups of J. L. Sessler and C.-H. Lee. Calix[4]pyrrole **201** contains an amide linked pyridyl strap, providing additional hydrogen bond donors for anion complexation. In particular, unpublished work by J. L. Sessler *et al.* has demonstrated that this receptor is capable of binding HCO_3^- utilizing these hydrogen bond donors in combination with the calix[4]pyrrole core. By contrast, calix[4]pyrrole **202** contains an analogous ester linked strap, which does not provide these additional hydrogen bond donors. Compound **203** was also investigated as a control to determine if any observed results for compound **201** could be attributed to the strap alone. Significantly, compound **201** has been recently found to exhibit *in vitro* anticancer activity, while control compounds **202** and **203** are not effective. Previous work from Sessler *et al.* has found correlation between the H^+/Cl^- co-transport activity of a series of synthetic prodigiosins and their anticancer activity.[178] It was hoped that in this study, the anticancer activity of **201** could be correlated to a biologically relevant transport process.

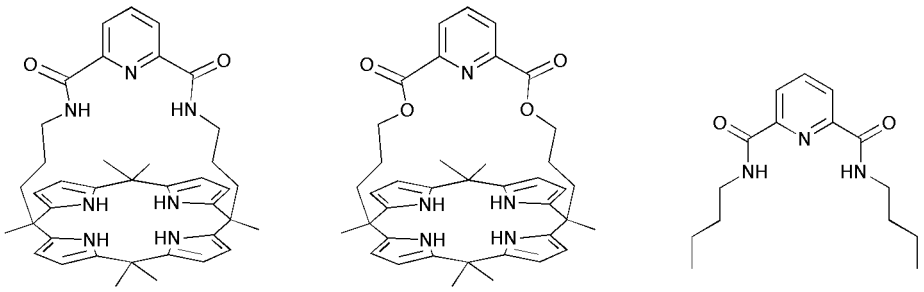

Figure 5.11 Pyridyl strapped calix[4]pyrroles **201** and **202**, and control compound **203**.

5.4.1 Anion transport studies

The design of receptor **201** facilitates stronger anion binding due to hydrogen bonding contributions from the strap. Therefore, the anion antiport activity of these compounds was initially investigated. In particular, the HCO_3^- affinity of **201** prompted the investigation of it's Cl^-/HCO_3^- antiport activity. The results are shown below.

(a)

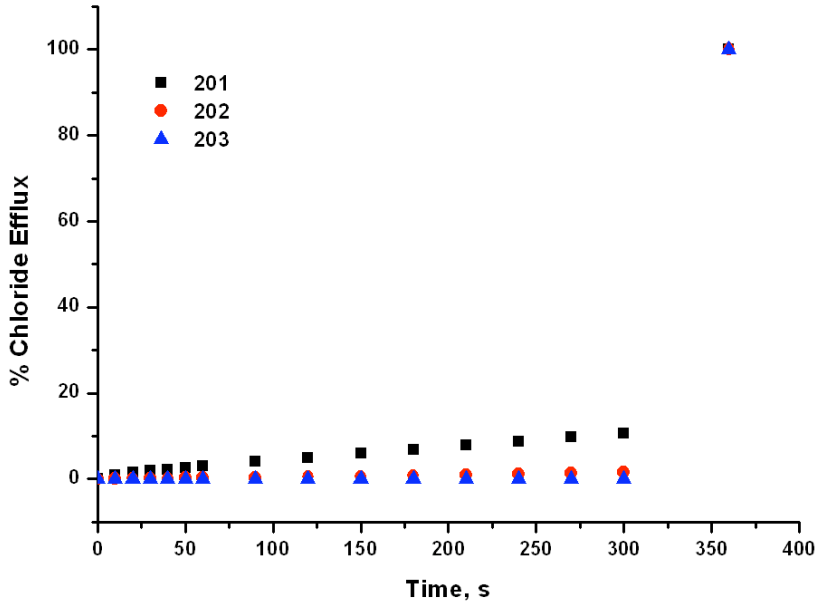

(b)

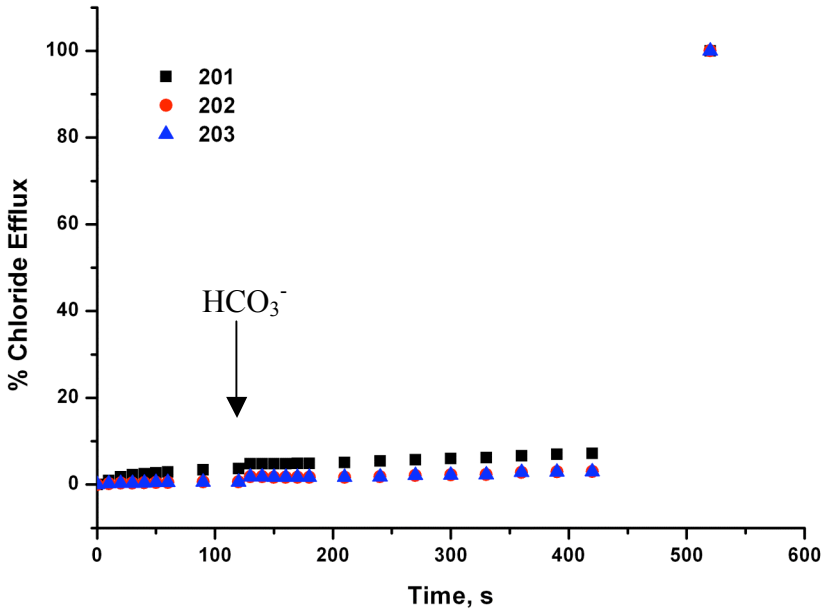

Figure 5.12 Chloride efflux mediated by receptors **201**-**203** (4 mol% w.r.t. lipid) from unilamellar POPC vesicles containing NaCl buffered to pH 7.2 with (a) 5 mM sodium phosphate salts, or (b) 20 mM sodium phosphate salts. (a) The vesicles were suspended in 489 mM $NaNO_3$ buffered to pH 7.2 with 5 mM sodium phosphate salts; (b) the vesicles were suspended in 167 mM Na_2SO_4 buffered to pH 7.2 with 20 mM sodium phosphate salts, at t = 120 s, a pulse of $NaHCO_3$ was added such that the final HCO_3^- concentration was 40 mM. At the end of each experiment, the vesicles were lysed to calibrate 100 % chloride efflux. Each point represents the average of 3 trials.

Compound **201** was found to mediate only extremely low levels of Cl^-/NO_3^- exchange and Cl^-/HCO_3^- exchange. Control compounds **202** and **203** were also found to be largely inactive for these transport modes.

The M^+/Cl^- symport activity of compound **201** was investigated for a range of group (I) metal cations. The results are shown in **Figure 5.13**.

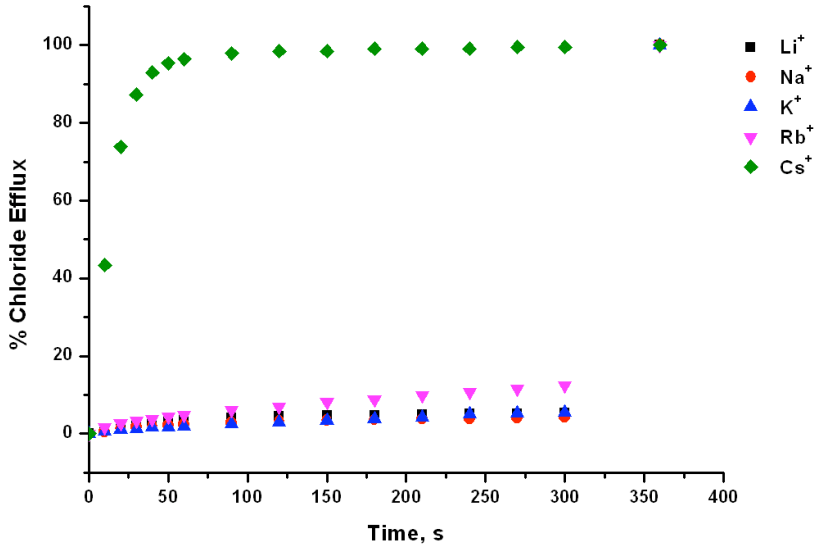

Figure 5.13 Chloride efflux promoted by receptor **201** (4 mol% w.r.t. lipid) from unilamellar POPC vesicles containing 489 mM MCl buffered to pH 7.2 with 5 mM sodium phosphate salts. The vesicles were suspended in 167 mM Na_2SO_4 buffered to pH 7.2 with 5 mM sodium phosphate salts. At the end of the experiment, the vesicles were lysed to calibrate 100 % chloride efflux. Each point represents the average of 3 trials.

Calix[4]pyrrole **201** was found to function as an efficient Cs^+/Cl^- symporter, but was found to have significantly lower activity in the presence of other alkali metal cations. In this way, calix[4]pyrrole **201** has similar transport activity to unmodified calix[4]pyrrole **28**. A Hill analysis was performed for the Cs^+/Cl^- transport mediated by **201** which yielded an $EC_{50\ 270\ s}$ value of 1.01 mol%. The full Hill analysis may be found in the appendix (section **A1.4**). The M^+/Cl^- symport activity of **202** and **203** were also investigated under the same conditions. The results are shown in **Figure 5.14**.

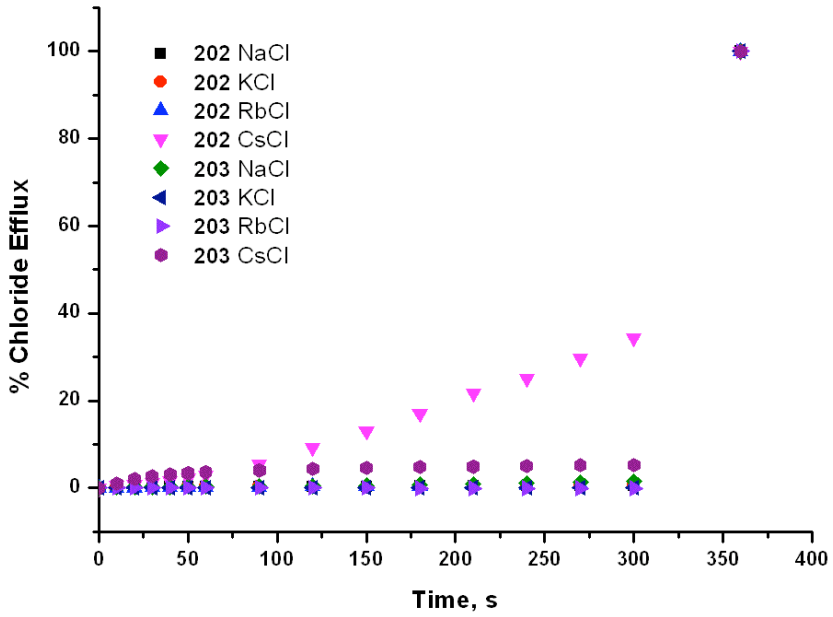

Figure 5.14 Chloride efflux promoted by receptors **202** and **203** from unilamellar POPC vesicles containing 489 mM MCl buffered to pH 7.2 with 5 mM sodium phosphate salts. The vesicles were suspended in 167 mM Na_2SO_4 buffered to pH 7.2 with 5 mM sodium phosphate salts. At the end of the experiment, the vesicles were lysed to calibrate 100 % chloride efflux. Each point represents the average of 3 trials.

Calix[4]pyrrole **202** was found to symport Cs^+/Cl^-, but significantly less efficiently than parent calix[4]pyrrole **28** (reported to mediate ~ 80 % CsCl efflux after 270 s under the same conditions)[67] or compound **201**. Control compound **203** did not mediate chloride transport under any of the conditions tested.

5.4.2 Conclusions

The results of the anion transport assays do not give insight into the observed biological activity of compound **201** by comparison to **202** and **203**. While compound **201** is significantly more active for the symport of Cs^+/Cl^- than the control compounds, the absence of Cs^+ in the cellular environment makes this process biologically irrelevant and thus it cannot be the cause of the observed anticancer activity. Compound **201** cannot symport chloride with a biologically relevant cation or antiport chloride with a biologically relevant anion; thus, it cannot facilitate charge neutral transport of biologically prevalent species. However, as discussed in **Chapter 1**, ion transport

processes in cells are complicated and are often closely linked. It is possible that in the cellular environment, the uniport of chloride by **201** is electrochemically mediated for by the action of a naturally occurring membrane protein.

Chapter 6
Experimental methods

6.1 General remarks

^{1}H NMR (300 MHz) and ^{13}C{^{1}H} NMR (75 MHz) were determined on a Bruker AV300 spectrometer. Chemical shifts for ^{1}H NMR are reported in parts per million (ppm), calibrated to the solvent peak set. The following abbreviations are used for spin multiplicity: s = singlet, d = doublet, t = triplet, m = multiplet. Chemical shifts for ^{13}C{^{1}H} NMR are reported in ppm, relative to the central line of a septet at δ = 39.52 ppm for DMSO-d_6. Infrared (IR) spectra were recorded on a Matterson Satellite (ATR). FTIR are reported in wavenumbers (cm^{-1}). HRMS(ES) spectra were recorded using a Bruker Apex III spectrometer and reported as *m/z* (relative intensity). All solvents and starting materials were purchased from commercial sources and used without further purification unless otherwise stated. Dry DCM was obtained by distillation over CaH_2 and degassed for 15 min prior to use. Aniline was distilled prior to use. POPC was supplied by Genzyme. Other phospholipids were supplied by Avanti. Chloride concentrations during transport experiments were determined using an Accumet or Cole-Parmer chloride selective electrode.

6.2 Vesicle studies

6.2.1 General remarks

The vesicles used in the transport studies were prepared by a standard literature procedure.[115] The ionic strengths of the intra- and extra-vesicular solutions were chosen

to be isotonic during vesicle preparation to avoid the rupturing of the vesicle membranes. All solutions were buffered to pH 7.2 with 5 mM or 20 mM (in the case of the HCO_3^- assays) sodium phosphate salts unless otherwise stated. The ionic strength of the solutions was controlled at 500 mM with the desired internal salt (most commonly NaCl) or external salt (most commonly $NaNO_3$ or Na_2SO_4) as applicable.

6.2.2 Preparation of vesicles

A lipid film was prepared by evaporation of a chloroform solution of POPC (1 ml containing ~ 28 mg POPC) was evaporated using a rotary evaporator and dried under high vacuum overnight. The lipid was suspended in the required internal solution (1 ml) using a lab dancer. 9 freeze-thaw cycles were completed on the suspension- freezing using liquid nitrogen followed by warming to room temperature- after which the suspension was allowed to stand for 30 minutes. The vesicles thus formed were extruded 25 times through 200 nm polycarbonate membranes. The vesicles were subjected to dialysis in the desired external solution for a minimum of 2 h to remove unencapsulated internal salts. The lipid was then diluted to a concentration of 1 mM using the desired external solution.

6.2.3 Transport experiments

Unilamellar POPC vesicles, prepared as described above, were suspended in 489 mM $NaNO_3$ or 167 mM Na_2SO_4 solution buffered to pH 7.2 with sodium phosphate salts. The lipid concentration per sample was 1 mM. A DMSO solution of the carrier molecule (10 mM) was added to start the experiment and the chloride efflux was monitored using a chloride sensitive electrode. At 5 min, the vesicles were lysed with 50 μl of polyoxyethylene(8)lauryl ether (0.232 mM in 7:1 water:DMSO v/v) and a total chloride reading was taken at 7 min. In the case of the Cl^-/HCO_3^- antiport assays, after 2 min a solution of $NaHCO_3$ in 167 mM Na_2SO_4 was added such that the total HCO_3^- concentration was 40 mM. The vesicles were then lysed after 7 min.

6.3 Titration and Job plot methods

6.3.1 ^{1}H NMR titrations

1.5 ml of a 0.01 M solution of the receptor was prepared. Of this solution, 0.5 ml was added to an NMR tube which was then sealed with an air tight suber seal. The remaining 1 ml of the receptor solution was used to make a 0.15 M solution of the desired guest. The anion/receptor solution was titrated into the NMR tube in small aliquots and a ^{1}H NMR spectrum was recorded after each addition. This resulted in an increasing concentration of guest throughout the experiment while the receptor concentration was kept constant. Chemical shifts for each peak were calibrated to the solvent peak. The data was fitted to a relevant binding model using WinEQNMR 2[166] in order to generate values for the binding constant(s).

6.3.2 ^{1}H NMR Job plots

Two solutions were prepared; the first was a 3 ml, 0.01 M solution of the receptor and the second was a 3 ml, 0.01 M of the guest. 0.5 ml of the receptor solution was added to an NMR tube. The volume of receptor solution was then decreased by 0.05 ml and the amount of guest solution was increased by 0.05 ml for each successive NMR tube until a 9:1 anion:receptor ratio was reached. A ^{1}H NMR spectrum was recorded for each of the ten samples, and calibrated to the solvent peak. This data was used to produce a Job plot in accordance with the methods described by Job.[179] The molar fraction of the receptor (χ_r) was plotted against the values given by the formula given in **Equation 1**.

$$y = \frac{\delta_{obs} - \delta_{int}}{\delta_{fin} - \delta_{int}} \times \chi_r$$

Equation 6.1 The formula used to generate a Job plot, where δ_{obs} is the observed chemical shift, δ_{int} is the initial chemical shift and δ_{fin} is the final chemical shift.

6.4 Synthetic procedures

6.4.1 Synthesis for chapter 2

7-aminoindole

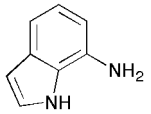

7-aminoindole was prepared according to a literature procedure as follows.[69] 7-nitroindole (, 1.5 mmol) was dissolved in EtOH and Pd/C (10 % by mass, catalytic) was added. The solution was stirred under atmosphere of H_2 for 3 h at RT until the colour had changed from yellow to colourless. The Pd/C was removed by filtration through celite, and the solvent was removed to yield 7-aminoindole as a white solid.

Assumed 100 % yield. This compound was used without characterisaton due to its assumed instability.

7-isothiocyanato-1*H*-indole

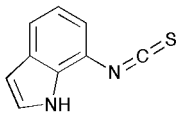

7-isothiocyanato-1*H*-indole was prepared according to a literature procedure.[69] 7-aminoindole (prepared as described above, 1.5 mmol) was dissolved in a 2-phase mixture of DCM (75 ml) and sat. $NaHCO_{3\ (aq)}$ (75 ml) and stirred vigorously. Thiophosgene, (0.171 g, 0.114 ml, 1.5 mmol) was added and the reaction was stirred overnight at room temperature. The organic layer was isolated and washed with 2 x 100 ml water. The organic layer was dried over $MgSO_4$ and the solvent was removed under reduced pressure to leave a brown residue. The residue was triturated in hexane to afford 7-isothiocyanato-1*H*-indole as a brown solid which was isolated by filtration.

Assumed 100 % yield. This intermediate was not characterized due to its assumed high reactivity.

1-(1*H*-indol-7-yl)-3-isopentylthiourea 127

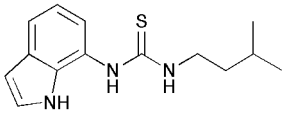

7-isothiocyanato-1*H*-indole (1.5 mmol) was dissolved in 100 ml DCM and *i*-pentylamine (0.131 g, 1.5 mmol) was added. The reaction was stirred at room temperature overnight under nitrogen. The solution was washed with 2 x 100 ml water and the organic layer was dried over $MgSO_4$. The crude mixture was subjected to column chromatography on silica (eluent DCM/MeOH 4%). The solvent was removed to leave an orange residue. Hexane (10 ml) was added causing an off white solid to form which was isolated by filtration and recrystallized from DCM to give compound **127** as a white solid.

Total yield (from 7-nitroindole): 89 mg (24 %); ^{1}H NMR (300 MHz, DMSO-d_6): δ= 10.88 (br s, 1H, NH), 9.20 (br s, 1H, NH), 7.42 (m, 2H, 2 x overlapping aromatic CH), 7.28 (t, 1H, J=2.8 Hz, aromatic CH), 6.97 (m, 2H, 2 x overlapping aromatic CH), 6.46 (dd, 1H, J_1=2.6 Hz, J_2=1.9 Hz, NH), 3.48 (m, 2H, CH_2), 1.56 (m, 1H, alkyl CH), 1.42 (q, 2H, J=6.9 Hz, CH_2); ^{13}C NMR (75 MHz, DMSO-d_6): δ= 180.6 (thiourea C=S), 129.4 (aromatic CH), 125.6 (aromatic CH), 119.0 (aromatic CH), 118.0 (aromatic CH), 42.6 (CH_2), 25.6 (alkyl), 22.5 (alkyl); LRMS(ESI-): *m/z* = 260.2 ([M-H]$^-$), 274.2 ([M.MeOH-H]$^-$); HRMS(ES): for $C_{14}H_{20}N_3S$ [M + H]$^+$ *m/z*= 262.1378 (calculated), 262.1378 (found); for $C_{14}H_{19}N_3SNa$ [M + Na]$^+$ *m/z* = 284.1197 (calculated), 284.1195 (found); for $C_{28}H_{38}N_6S_2Na$ [2M + Na]$^+$ *m/z* = 545.2497 (calculated), 545.2509 (found); IR (film): ν= 3370 (indole NH stretching), 3310 (urea NH stretching), 3180 (urea NH stretching); M_p: 88-90 °C.

***N*-butyl-4-methylpentanethioamide 129**

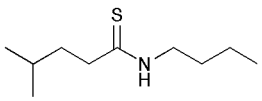

128 (prepared by SJM, 300 mg, 1.75 mmol) was dissolved in THF and Lawesson's reagent (710 mg, 1.76 mmol) was added. The reaction was refluxed overnight. On cooling, the solvent was removed *in situ* and the oily residue obtained was re-dissolved in

DCM. The product was washed with 2 x 100 ml of brine followed by 2 x 100 ml of 0.1 M HCl and 2 x 100 ml sat. $NaHCO_3$. The product was further purified by column chromatography on silica (elution with DCM). This afforded the product as a colourless oil.

Yield: 245 mg (75 %); ^{1}H NMR (300 MHz, DMSO-d_6): δ= 7.15 (br.s, 1H, NH), 3.66 (td, 2H, J_1=7.3 Hz, J_2=5.5 Hz, CH_2), 2.66 (m, 2H, CH_2), 1.65 (m, 5H, alkyl CH + 2 x CH_2), 1.41 (m, 2H, CH_2), 0.95 (m, 9H, 3 x CH_3); ^{13}C NMR (75 MHz, DMSO-d_6): δ=203.8 (carbonyl CO), 44.8 (alkyl), 43.2 (alkyl), 38.2 (alkyl), 29.2 (alkyl), 27.0 (alkyl), 22.3 (alkyl), 19.6 (alkyl), 13.6 (alkyl); LRMS(ESI+): *m/z* = 188.3 ($[M + H]^+$); HRMS(ES): for $C_9H_{19}NSNa$ $[M + Na]^+$ *m/z*= 210.1292 (calculated), 210.1287 (found); IR (film): ν= 3240 (amide NH stretching);.

4-methyl-*N*-phenylpentanamide 130

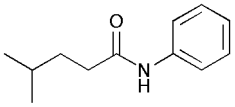

This compound has been previously reported.[180-184]

4-methyl valeric acid (500 mg, 4.30 mmol) was activated by reflux in chloroform (100 ml) with CDI (700 mg, 4.30 mmol). After 2 hours, aniline (440 mg, 4.73 mmol) was added and the reaction was refluxed overnight. On cooling the product was washed with 2 x 100 ml water followed by 2 x 100 ml 0.1 M HCl and 2 x 100 ml sat. $NaHCO_3$. The combined organic layers were dried over $MgSO_4$ and the solvent was removed to give an off-white solid. This was triturated in hexane to afford the product as a white solid.

Yield: 623 mg (76%); ^{1}H NMR (300 MHz, DMSO-d_6): δ= 9.86 (s, 1H, NH), 7.59 (d, 2H, J=8.7 Hz, aromatic CH), 7.28 (t, 2H, J=7.9 Hz, aromatic CH), 7.01 (m, 1H, aromatic CH), 2.30 (m, 2H, CH_2), 1.52 (m, 3H, Alkyl CH + CH_2); 0.90 (d, 6H, J=6.4 Hz, 2 x CH_3); ^{13}C NMR (75 MHz, DMSO-d_6): δ= 171.4 (carbonyl CO), 139.3 (aromatic CH), 128.6 (aromatic CH), 122.8 (aromatic CH), 119.0 (aromatic CH), 34.5 (aromatic CH), 34.0 (aromatic CH), 27.2 (aromatic CH), 22.2 (aromatic CH); LRMS(ESI-): *m/z* = 190.2 ($[M – H]^-$); HRMS(ES): for $C_{11}H_{16}NONa$ $[M + Na]^+$ *m/z*= 214.1208 (calculated), 214.1202

(found); IR (film): ν= 3250 (amide NH stretching), 1650 (carbonyl C=O stretching); M_p: 109-110 °C.

4-methyl-*N*-phenylpentanethioamide 131

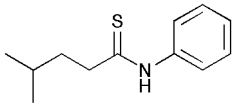

This compound has been previously reported.[183]

130 (300 mg, 1.57 mmol) was dissolved in THF and Lawesson's reagent (634 mg, 1.57 mmol) was added. The reaction was refluxed overnight. On cooling, the solvent was removed *in situ* and the oily residue obtained was re-dissolved in DCM. The product was washed with 2 x 100 ml of brine followed by 2 x 100 ml of 0.1 M HCl and 2 x 100 ml sat. $NaHCO_3$. The organic layer was dried over $MgSO_4$ and the solvent removed to give compound **131** as an off white solid.

Yield: 201 mg (62%); ^{1}H NMR (300 MHz, DMSO-d_6): δ= 11.49 (s, 1H, NH), 7.77 (d, 2H, J=8.1 Hz, aromatic CH), 7.39 (t, 2H, J=7.9 Hz, aromatic CH), 7.22 (m, 1H, aromatic CH), 2.75 (m, 2H, CH_2), 1.64 (m, 3H, alkyl CH + CH_2), 0.92 (d, 6H, J=6.2 Hz, 2 x CH_3); ^{13}C NMR (75 MHz, DMSO-d_6): δ= 204.3 (thiourea C=S), 139.6 (aromatic CH), 128.4 (aromatic CH), 125.8 (aromatic CH), 123.3 (aromatic CH), 45.1 (alkyl CH_2), 27.1 (alkyl), 22.4 (alkyl); LRMS(ESI-): *m/z* = 206.2 ($[M - H]^-$); HRMS(ES): for $C_{11}H_{17}N$ $[M + H]^+$ *m/z*= 208.1160 (calculated), 208.1154 (found); IR (film): ν= 3180 (amide NH stretching); M_p: 61-62 °C.

6.4.2 Synthesis for chapter 3

***N*-(1*H*-indol-7-yl)-1*H*-imidazole-1-carboxamide (Intermediate 3.1)**

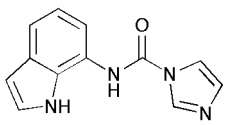

Intermediate **3.1** was prepared according to a literature procedure.[76] 7-aminoindole[69] (1.5 mmol) was dissolved in dry DCM (50 ml) and CDI (0.75 g, 4.5 mmol) was added. The

reaction was stirred under N_2 at RT overnight. The white precipitate thus formed was isolated by filtration and used without further purification.

The bis-indolylureas **159-167** were synthesized according to the same general procedure as follows:

1,1'-(butane-1,4-diyl)bis(3-(1*H*-indol-7-yl)urea) 159

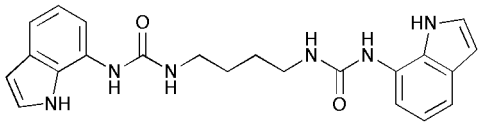

Intermediate **3.1** (200 mg, ~0.8 mmol) was dissolved in dry DCM:DMF (50:1, DCM dried over molecular sieves prior to use). 1,4-Diaminobutane (7.1 mg, 0.44 mmol) was added and the mixture was heated to reflux under N_2 and stirred overnight. The mixture was cooled and the white precipitate was collected by filtration. The solid was washed with 3 x 10 ml of water and 3 x 10 ml diethyl ether and dried under vacuum to give **159** as a white solid.

Yield: 43 mg (24 %); ^{1}H NMR (300 MHz, DMSO-d_6): δ= 10.68 (s, 2H, NH), 8.35 (s, 2H, NH), 7.29 (t, 2H, J=2.56 Hz, aromatic CH), 7.20 (d, 2H, J=7.68 Hz, aromatic CH), 7.07 (d, 2H, J=7.32 Hz, aromatic CH), 6.88 (t, 2H, J=7.68 Hz, aromatic CH), 6.39 (m, 2H, aromatic CH), 6.26 (t, 2H, J=5.49 Hz, aromatic CH), 3.18 (br m, 4H, 2x eq CH_2), 1.53 (br m, 4H, 2x eq CH_2); ^{13}C NMR (75 MHz, DMSO-d_6): δ=155.7 (CO), 129.1 (aromatic CH), 127.9 (aromatic CH), 124.9 (aromatic CH), 124.8 (aromatic CH), 119.1 (aromatic CH), 114.5 (aromatic CH), 111.8 (aromatic CH), 101.4 (aromatic CH), 27.4 (multiple overlapping CH_2); LRMS (ESI-): *m/z* = 403.1 ([M-H]$^-$); HRMS (ES): for $C_{22}H_{25}N_6O_2$ [M + H]$^+$ *m/z* = 405.2039 (calculated), 405.2032 (found); IR (film): ν= 3390 (indole NH stretching), 3310 (urea NH stretching); decomposes above 240 °C.

1,1'-(pentane-1,5-diyl)bis(3-(1*H*-indol-7-yl)urea) 160

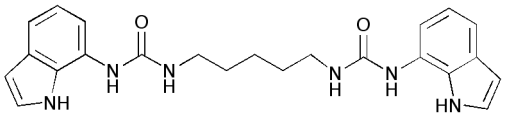

Yield: 63 mg (34 %); ^{1}H NMR (300 MHz, DMSO-d_6): δ= 10.67 (s, 2H, NH), 8.32 (s, 2H, NH), 7.29 (t, 2H, J=2.56 Hz, NH), 7.20 (d, 2H, J=7.68 Hz, aromatic CH), 7.06 (d, 2H, J=6.95 Hz, aromatic CH), 6.88 (t, 2H, J=7.68 Hz, aromatic CH), 6.39 (m, 2H, aromatic CH), 6.24 (t, 2H, J=5.49 Hz, aromatic CH), 3.16 (q, 4H, J_1=6.59 Hz, J_2=6.22 Hz, 2x eq CH_2), 1.52 (m, 4H, 2x eq CH_2), 1.38 (m, 2H, CH_2); ^{13}C NMR (75 MHz, DMSO-d_6): δ= 155.6 (CO), 129.1 (aromatic CH), 127.8 (aromatic CH), 125.0 (aromatic CH), 124.8 (aromatic CH), 119.1 (aromatic CH), 114.5 (aromatic CH), 111.7 (aromatic CH), 101.4 (aromatic CH), 29.6 (CH_2), 23.8 (CH_2); LRMS (ESI+): *m/z* = 419.1 ($[M + H]^+$), 441.2 ($[M + Na]^+$); HRMS (ES): for $C_{23}H_{27}N_6O_2$ $[M + H]^+$ *m/z* = 419.2195 (calculated), 419.2190 (found); IR (film): ν= 3390 (indole NH stretching), 3390 (urea NH stretching), 3310 (urea NH stretching); decomposes above 240 °C.

1,1'-(hexane-1,6-diyl)bis(3-(1*H*-indol-7-yl)urea) 161

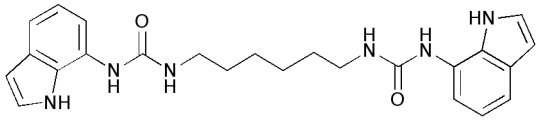

Yield: 75 mg (39 %); ^{1}H NMR (300 MHz, DMSO-d_6): δ= 10.67 (s, 2H, NH), 8.31 (s, 2H, NH), 7.29 (t, 2H, J= 2.93 Hz, NH), 7.20 (d, 2H, J=7.68 Hz,, aromatic CH), 7.06 (d, 2H, J=7.32 Hz, aromatic CH), 6.88 (t, 2H, J=7.68 Hz, aromatic CH), 6.40 (m, 2H, aromatic CH), 6.22 (t, 2H, J=5.49 Hz, aromatic CH), 3.15 (q, 4H, J_1=6.59 Hz, J_2=6.22 Hz, 2x eq CH_2), 1.50 (br m, 4H, 2x eq CH_2), 1.36 (br m, 4H, 2x eq CH_2); ^{13}C NMR (75 MHz, DMSO-d_6): δ= 155.6 (CO), 129.1 (aromatic CH), 127.8 (aromatic CH), 125.0 (aromatic CH), 124.8 (aromatic CH), 119.1 (aromatic CH), 114.5 (aromatic CH), 111.8 (aromatic CH), 101.4 (aromatic CH), 29.8 (CH_2), 26.2 (CH_2); LRMS (ESI+): *m/z* = 455.2 ($[M + Na]^+$); HRMS (ES): for $C_{24}H_{29}N_6O_2$ $[M + H]^+$ *m/z* = 433.2352 (calculated), 433.2348 (found); IR (film): ν= 3390 (indole NH stretching), 3310 (urea NH stretching); decomposes above 240 °C.

1,1'-(septane-1,7-diyl)bis(3-(1*H*-indol-7-yl)urea) 162

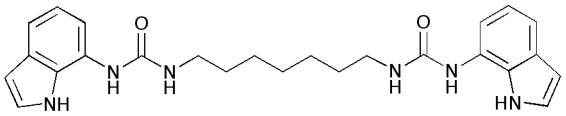

Yield: 73 mg (37 %); ^{1}H NMR (300 MHz, DMSO-d_6): δ= 10.67 (br s, 2H, NH), 8.30 (s, 2H, NH), 7.29 (t, 2H, J=2.93 Hz, NH), 7.20 (d, 2H, J=8.05 Hz, aromatic CH), 7.05 (d, 2H, J=7.32 Hz, aromatic CH), 6.88 (t, 2H, J=7.68 Hz, aromatic CH), 6.39 (m, 2H, aromatic CH), 6.21 (t, 2H, J=5.85 Hz, aromatic CH), 3.14 (q, 4H, J_1= 6.59 Hz, J_2=6.22 Hz, 2x eq CH_2), 1.49 (m, 4H, 2x eq CH_2), 1.34 (br m, 6H, 3 x CH_2); ^{13}C NMR (75 MHz, DMSO-d_6): δ= 155.6 (CO), 129.1 (aromatic CH), 127.8 (aromatic CH), 125.0 (aromatic CH), 124.8 (aromatic CH), 119.1 (aromatic CH), 114.5 (aromatic CH), 111.7 (aromatic CH), 29.8 (CH_2), 28.6 (CH_2), 26.4 (CH_2); LRMS (ESI+): *m/z* = 470.3 ([M + Na]$^+$); HRMS (ES+): for $C_{25}H_{31}N_6O_2$ [M + H]$^+$ *m/z* = calculated 447.2508, found 447.2498; IR (film): ν= 3390 (indole NH stretching), 3320 (urea NH stretching); decomposes above 240 °C.

1,1'-(octane-1,8-diyl)bis(3-(1*H*-indol-7-yl)urea) 163

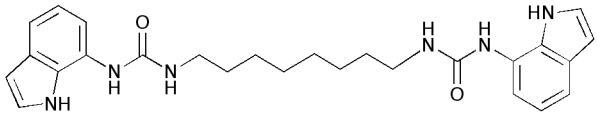

Yield: 70 mg (34 %); ^{1}H NMR (300 MHz, DMSO-d_6): δ= 10.67 (br s, 2H, NH), 8.29 (s, 2H, NH), 7.30 (t, 2H, J=2.56 Hz, NH), 7.20 (d, 2H, J=7.68 Hz, aromatic CH), 7.04 (d, 2H, J=7.32 Hz, aromatic CH), 6.88 (t, 2H, J=7.68 Hz, aromatic CH), 6.39 (m, 2H, aromatic CH), 6.20 (t, 2H, J= 5.85 Hz, aromatic CH), 3.13 (q, 4H, J_1=6.59 Hz, J_2=5.85 Hz, 2x eq CH_2), 1.48 (m, 4H, 2x eq CH_2), 1.32 (br m, 8H, 4x CH_2); ^{13}C NMR (75 MHz, DMSO-d_6): δ= 155.6 (CO), 129.1 (aromatic CH), 127.8 (aromatic CH), 124.8 (aromatic CH), 119.2 (aromatic CH), 114.5 (aromatic CH), 111.7 (aromatic CH), 108.7 (aromatic CH), 101.4 (aromatic CH), 29.8 (CH_2), 28.8 (CH_2), 26.40 (CH_2); LRMS (ESI+): *m/z* = 483.2 ([M + Na]$^+$); HRMS (ES): for $C_{26}H_{33}N_6O_2$ [M + H]$^+$ 461.2665 (calculated), 461.2659 (found); IR (film): ν= 3390 (indole NH stretching), 3320 (urea NH stretching); decomposes above 240 °C.

1,1'-(nonane-1,9-diyl)bis(3-(1*H*-indol-7-yl)urea) 164

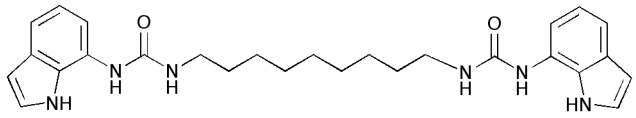

Yield: 104 mg (66 %); ^{1}H NMR (300 MHz, DMSO-d_6): δ= 10.68 (s, 2H, NH), 8.35 (s, 2H, NH), 7.29 (t, 2H, J=2.56 Hz, aromatic CH), 7.20 (d, 2H, J=7.68 Hz, aromatic CH), 7.07 (d, 2H, J=7.32 Hz, aromatic CH), 6.88 (t, 2H, J=7.68 Hz, aromatic CH), 6.39 (m, 2H, aromatic CH), 6.26 (t, 2H, J=5.49 Hz, aromatic CH), 3.14 (q, J= 6.6 Hz, 4H, 2x eq CH_2), 1.46 (br m, 4H, 2x eq CH_2), 1.31 (br s, 10 H, 5x CH_2); ^{13}C NMR (75 MHz, DMSO-d_6): δ= 155.6 (CO), 129.1 (aromatic CH), 127.8 (aromatic CH), 125.0 (aromatic CH), 124.8 (aromatic CH), 119.1 (aromatic CH), 114.5 (aromatic CH), 111.715 (aromatic CH), 101.4 (aromatic CH), 29.8 (CH_2), 29.1 (CH_2), 28.8 (CH_2), 26.4 (CH_2); LRMS (ESI+): *m/z* = 497.2 ([M + Na]$^+$); HRMS (ES): for $C_{27}H_{34}N_6O_2$ *m/z* = [M + H]$^+$ calculated 475.2821, found 475.2820; IR (film): ν= 3390 (indole NH stretching), 3320 (urea NH stretching); decomposes above 227 °C.

1,1'-(decane-1,10-diyl)bis(3-(1*H*-indol-7-yl)urea) 165

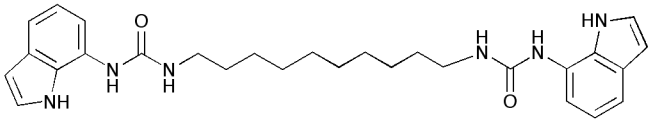

Yield: 97 mg (60 %); ^{1}H NMR (300 MHz, DMSO-d_6): δ= 10.67 (s, 2H, NH), 8.35 (s, 2H, NH), 7.29 (t, 2H, J=2.56 Hz, aromatic CH), 7.20 (d, 2H, J=7.68 Hz, aromatic CH), 7.07 (d, 2H, J=7.32 Hz, aromatic CH), 6.88 (t, 2H, J=7.68 Hz, aromatic CH), 6.39 (m, 2H, aromatic CH), 6.26 (t, 2H, J=5.49 Hz, aromatic CH), 3.14 (q, J= 6.6 Hz, 4H, 2x eq CH_2), 1.46 (br m, 4H, 2x eq CH_2), 1.31 (br s, 12 H, 6x CH_2); ^{13}C NMR (75 MHz, DMSO-d_6): δ= 155.6 (CO), 129.1 (aromatic CH), 127.8 (aromatic CH), 125.0 (aromatic CH), 124.8 (aromatic CH), 119.1 (aromatic CH), 114.5 (aromatic CH), 111.7 (aromatic CH), 101.4 (aromatic CH), 29.8 (CH_2), 29.0 (CH_2), 28.8 (CH_2), 26.4 (CH_2); LRMS (ESI+): *m/z*= 511.2 ([M + Na]$^+$); HRMS (ES): for $C_{28}H_{37}N_6O_2$ *m/z* = [M + H]$^+$ calculated 489.2978, found 489.2982; IR (film): ν= 3390 (indole NH stretching), 3320 (urea NH stretching); decomposes above 225 °C.

1,1'-(undecane-1,11-diyl)bis(3-(1*H*-indol-7-yl)urea) 166

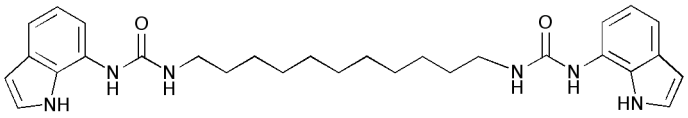

Yield; 137 mg (82 %); ^{1}H NMR (300 MHz, DMSO-d_6): δ= 10.67 (s, 2H, NH), 8.35 (s, 2H, NH), 7.29 (t, 2H, J=2.56 Hz, aromatic CH), 7.20 (d, 2H, J=7.68 Hz, aromatic CH), 7.07 (d, 2H, J=7.32 Hz, aromatic CH), 6.88 (t, 2H, J=7.68 Hz, aromatic CH), 6.39 (m, 2H, aromatic CH), 6.26 (t, 2H, J=5.49 Hz, aromatic CH), 3.14 (q, J= 6.6 Hz, 4H, 2x eq CH_2), 1.46 (br m, 4H, 2x eq CH_2), 1.31 (br s, 14 H, 7x CH_2); ^{13}C NMR (75 MHz, DMSO-d_6): δ= 155.6, (CO), 129.1 (aromatic CH), 127.8, (aromatic CH), 125.0 ((aromatic CH), 119.1 (aromatic CH), 114.5 (aromatic CH), 111.7 (aromatic CH), 101.4 (aromatic CH), 29.8 (CH_2), 29.0 (CH_2), 28.8 (CH_2), 26.4 (CH_2); LRMS (ESI+) *m/z*= 525.3 ($[M + Na]^+$, 16.99%), 503.3 ($[M + H]^+$, 4.97%); LRMS (ESI-): *m/z* = 501.7 ($[M-H]^-$); HRMS (ES+): for $C_{29}H_{38}N_6O_2Na$ $[M + Na]^+$ *m/z* = calculated 525.2954, found 525.2957; IR (film): ν= 3390 (indole NH stretching), 3320 (urea NH stretching); decomposes above 215 °C.

1,1'-(dodecane-1,12-diyl)bis(3-(1*H*-indol-7-yl)urea) 167

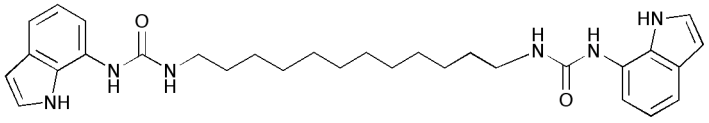

Yield: 125 mg (77 %); ^{1}H NMR (300 MHz, DMSO-d_6): δ= 10.67 (s, 2H, NH), 8.35 (s, 2H, NH), 7.29 (t, 2H, J=2.56 Hz, aromatic CH), 7.20 (d, 2H, J=7.68 Hz, aromatic CH), 7.07 (d, 2H, J=7.32 Hz, aromatic CH), 6.88 (t, 2H, J=7.68 Hz, aromatic CH), 6.39 (m, 2H, aromatic CH), 6.26 (t, 2H, J=5.49 Hz, aromatic CH), 3.14 (q, J= 6.6 Hz, 4H, 2x eq CH_2), 1.46 (br m, 4H, 2x eq CH_2), 1.31 (br s, 14 H, 7x CH_2); ^{13}C NMR (75 MHz, DMSO-d_6): δ= 155.6 (CO), 129.1 (aromatic CH), 127.8 (aromatic CH), 125.0 (aromatic CH), 124.8 (aromatic CH), 119.1 (aromatic CH), 114.5 (aromatic CH), 111.7 (aromatic CH), 101.4 (aromatic CH), 29.8 (CH_2), 29.0 (CH_2), 26.4 (CH_2); LRMS (ESI-) *m/z*= 515.2 ($[M-H]^-$); HRMS (ES): for $C_{30}H_{41}N_6O_2$ $[M + H]^+$ *m/z* = calculated 517.3291, found 517.3281; IR (film): ν= 3390 (indole NH stretching), 3320 (urea NH stretching); decomposes above 221 °C.

6.4.3 Synthesis for chapter 4

The bis-phenylthioureas **177-182** were synthesized according to the same general procedure as follows:

1,1'-(septane-1,7-diyl)bis(3-phenylthiourea) 177

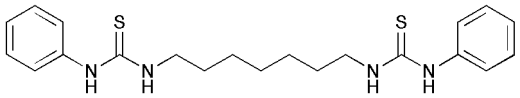

Phenyl isothiocyanate (0.5 g, 3.7 mmol) was dissolved in 75 ml DCM/DMF (1%) and 1, 7-diaminoheptane (241 mg, 1.8 mmol) was added. The mixture was refluxed overnight under nitrogen. On cooling, the mixture was washed with water (150 ml), dilute HCl (100 ml) and sat. $NaHCO_{3\ (aq)}$ (100 ml). The organic layer was dried over $MgSO_4$ and concentrated to approximately 5 ml in volume. The DCM solution was cooled to -5 ºC to induce recrystallisation. The resulting precipitate was isolated by filtration and washed with cold DCM to give compound **177** as on off white solid.

Yield: 291 mg (39 %); ^{1}H NMR (300 MHz, DMSO-d_6): δ= 9.41 (br s, 2H, NH), 7.71 (br s, 2H, NH), 7.41 (m, 4H, aromatic CH), 7.31 (m, 4H, aromatic CH), 7.09 (m, 2H, aromatic CH), 3.45 (br m, 4H, CH_2), 1.54 (br m, 4H, CH_2), 1.32 (br m, 6H, CH_2); ^{13}C NMR (75 MHz, DMSO-d_6): δ= 180.2 (CS), 139.3 (aromatic CH), 128.5 (aromatic CH), 124.0 (aromatic CH), 122.9 (aromatic CH), 43.8 (CH_2), 28.5 (CH_2), 28.4 (CH_2), 26.4 (CH_2); LRMS(ESI+): *m/z* = 401.2 ($[M + H]^+$); HRMS(ES): for $C_{21}H_{29}N_4S_2$ $[M + H]^+$ *m/z* = 401.1234 (calculated), 401.1813 (found); IR (film): ν= 3240 (NH stretching), 3060 (NH stretching), 2920 (alkyl CH stretching), 2850 (alkyl CH stretching); M_p: 82-85 °C.

1,1'-(octane-1,8-diyl)bis(3-phenylthiourea) 178

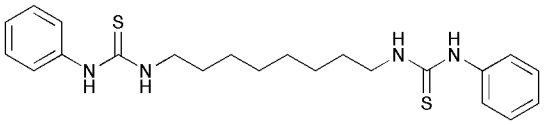

Yield: 268 mg (35 %); ^{1}H NMR (300 MHz, DMSO-d_6): δ= 9.40 (br s, 1H, NH), 7.71 (br s, 1H, NH), 7.41 (m, 2H, aromatic CH), 7.30 (m, 2H, aromatic CH), 7.09 (m, 1H, aromatic CH), 3.45 (br m, 2H, CH_2), 1.54 (br m, 2H, CH_2), 1.31 (br m, 4H, 2 x CH_2); ^{13}C NMR (75 MHz, DMSO-d_6): δ= 180.2 (CO), 139.3 (aromatic CH), 128.5 (aromatic CH), 124.0 (aromatic CH), 122.9 (aromatic CH), 43.8 (CH_2), 28.7 (CH_2), 28.4 (CH_2), 26.4 (CH_2); LRMS(ESI-): *m/z* = 413.1 ([M - H]$^-$); HRMS(ES): for $C_{22}H_{31}N_4S_2$ [M + H]$^+$ *m/z*= 415.1990 (calculated), 415.1992 (found); IR (film): ν= 3240 (NH stretching), 3060 (NH stretching), 2920 (alkyl CH stretching), 2850 (alkyl CH stretching); M_p: 115-117 °C.

1,1'-(nonane-1,9-diyl)bis(3-phenylthiourea) 179

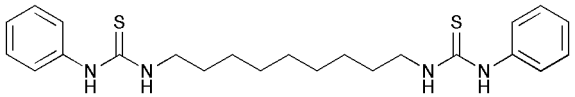

Yield: 272 mg (35 %); ^{1}H NMR (300 MHz, DMSO-d_6): δ= 9.48 (br s, 2H, NH), 7.77 (br s, 2H, NH), 7.45 (m, 4H, aromatic CH), 7.37 (m, 4H, aromatic CH), 7.15 (m, 2H, aromatic CH), 3.50 (br m, 4H, CH_2), 1.59 (br m, 4H, CH_2), 1.36 (br m, 10H, CH_2); ^{13}C NMR (75 MHz, DMSO-d_6): δ= 180.2 (CS), 139.3 (aromatic CH), 128.5 (aromatic CH), 124.0 (aromatic CH), 122.9 (aromatic CH), 43.8 (CH_2), 28.9 (CH_2), 28.7 (CH_2), 28.4 (CH_2), 26.4 (CH_2); LRMS(ESI+): *m/z* = 429.2 ([M + H]$^+$); HRMS(ES): for $C_{23}H_{33}N_4S_2$ [M + H]$^+$ *m/z* = 429.2147 (calculated), 429.2146 (found); IR (film): ν= 3250 (NH stretching), 3060 (NH stretching), 2920 (alkyl CH stretching), 2850 (alkyl CH stretching); M_p: 82-85 °C.

1,1'-(decane-1,10-diyl)bis(3-phenylthiourea) 180

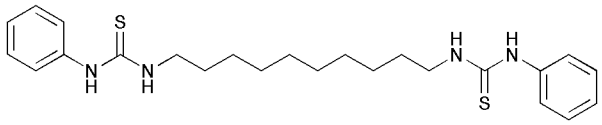

Yield: 792 mg (98 %); ^{1}H NMR (300 MHz, DMSO-d_6): δ= 9.40 (br s, 2H, NH), 7.70 (br s, 2H, NH), 7.40 (m, 4H, aromatic CH), 7.31 (m, 4H, aromatic CH), 7.09 (m, 2H, aromatic CH), 3.44 (br m, 4H, CH_2), 1.53 (br m, 4H, CH_2), 1.29 (br m, 12H, CH_2); ^{13}C NMR (75 MHz, DMSO-d_6): δ= 180.2 (CS), 139.3 (aromatic CH), 128.5 (aromatic CH), 124.0 (aromatic CH), 122.9 (aromatic CH), 43.8 (CH_2), 28.9 ($CH2_2$), 28.7 (CH_2), 28.4 (CH_2), 26.4 (CH_2); LRMS(ESI+): *m/z* = 443.2 ([M + H]$^+$); HRMS(ES): for $C_{24}H_{37}N_4S_2$ [M + H]$^+$ *m/z*= 443.2303 (calculated), 443.2298 (found); IR (film): ν= 3240 (NH stretching), 3070 (NH stretching), 2920 (alkyl CH stretching), 2850 (alkyl CH stretching); M_p: 91-93 °C.

1,1'-(undecane-1,11-diyl)bis(3-phenylthiourea) 181

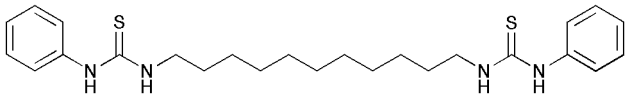

Yield: 807 mg (95 %); ^{1}H NMR (300 MHz, DMSO-d_6): δ= 9.40 (br s, 2H, NH), 7.70 (br s, 2H, NH), 7.40 (m, 4H, aromatic CH), 7.31 (m, 4H, aromatic CH), 7.09 (m, 2H, aromatic CH), 3.44 (br m, 4H, CH_2), 1.53 (br m, 4H, CH_2), 1.29 (br m, 14H, CH_2); ^{13}C NMR (75 MHz, DMSO-d_6): δ= 180.2 (CS), 139.3 (aromatic CH), 128.5 (aromatic CH), 124.0 (aromatic CH), 122.9 (aromatic CH), 43.8 (CH_2), 29.0 ($CH2_2$), 28.8 (CH_2), 28.4 (CH_2), 26.4 (CH_2); LRMS(ESI+): *m/z* = 457.2 ([M + H]$^+$); HRMS(ES): for $C_{25}H_{37}N_4S_2$ [M + H]$^+$ *m/z*= 457.2460 (calculated), 457.2457 (found); IR (film): ν= 3240 (NH stretching), 3060 (NH stretching), 2910 (alkyl CH stretching), 2850 (alkyl CH stretching); M_p: 120-124 °C.

1,1'-(dodecane-1,12-diyl)bis(3-phenylthiourea) 182

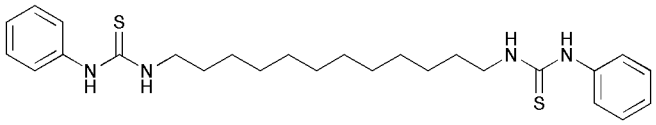

182 was prepared by the general procedure described above. The reaction mixture was washed with 100 ml water which resulted in precipitation of the product in the organic phase. The precipitate was isolated by filtration and washed with cold DCM to give the product as an off white solid.

Yield: 813 mg (77 %); ^{1}H NMR (300 MHz, DMSO-d_6): δ= 9.40 (br s, 2H, NH), 7.70 (br s, 2H, NH), 7.40 (m, 4H, aromatic CH), 7.31 (m, 4H, aromatic CH), 7.09 (m, 2H, aromatic CH), 3.45 (br m, 4H, CH_2), 1.54 (br m, 4H, CH_2), 1.28 (br m, 16H, CH_2); ^{13}C NMR (75 MHz, DMSO-d_6): δ= 180.2 (CS), 139.3 (aromatic CH), 128.5 (aromatic CH), 123.96 (aromatic CH), 122.9 (aromatic CH), 43.8 (CH_2), 29.0 ($CH2_2$), 28.7 (CH_2), 28.4 (CH_2), 26.4 (CH_2); LRMS(ESI+): *m/z* = 471.3 ($[M + H]^+$); HRMS(ES): for $C_{26}H_{39}N_4S_2$ $[M + H]^+$ *m/z*= 471.2616 (calculated), 471.2621 (found); IR (film): ν= 3240 (NH stretching), 3070 (NH stretching), 2910 (alkyl CH stretching), 2850 (alkyl CH stretching); M_p: 118-120 °C.

1,1'-(octane-1,8-diyl)bis(3-(1*H*-indol-7-yl)thiourea)183

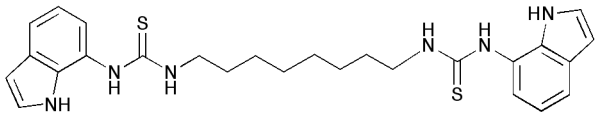

7-isothiocyanato-1*H*-indole[69] was dissolved in 75 ml DCM/DMF (1%) and 1,8-diaminooctane (111 mg, 7.7 x 10^{-4} mol) was added and the mixture was refluxed overnight. On cooling, the organic layer was washed with 2 x 100 ml water and the organic layer was dried over $MgSO_4$. The DCM solution was concentrated and cooled to -5 °C to induce recrystallization. The resulting precipitate was isolated by filtration and washed with cold DCM. Compound **183** was isolated as an off white solid.

Yield: 170 mg (22 %); ^{1}H NMR (300 MHz, DMSO-d_6): δ= 10.89 (br s, 1H, NH), 9.23 (br s, 1H, NH), 7.43 (m, 2H, aromatic CH), 7.28 (m, 1H, aromatic CH), 6.98 (m, 2H,

aromatic CH), 6.46 (m, 1H, NH), 3.45 (m, 2H, CH_2), 1.52 (br m, 2H, CH_2), 1.27 (br m, 4H, 2 x CH_2); ^{13}C NMR (75 MHz, DMSO-d_6): δ= 180.6 (CO), 131.2 (aromatic CH), 129.4 (aromatic CH), 125.6 (aromatic CH), 123.0 (aromatic CH), 119.0 (aromatic CH), 118.0 (aromatic CH), 101.6 (aromatic CH), 44.3 (CH_2), 28.7 (CH_2), 28.5 (CH_2), 26.4 (CH_2); LRMS(ESI-): *m/z* = 491.2 ([M - H]$^-$); HRMS(ES): for $C_{26}H_{33}N_6S_2$ [M + H]$^+$ *m/z*= 493.2208 (calculated), 493.2201 (found); IR (film): ν= 3370 (NH stretching), 3340 (NH stretching), 3170, (NH stretching), 2990 (alkyl CH stretching), 2930 (alkyl CH stretching), 2860 (alkyl CH stretching); M_p: 170-172 °C.

1,1'-(octane-1,8-diyl)bis(3-phenylurea)184

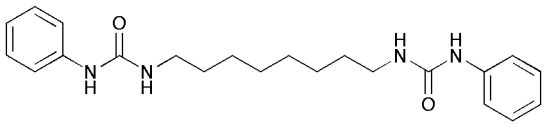

Phenyl isocyanate (0.826 g, 6.94 mmol) was dissolved in 75 ml DCM and 1,8-diaminooctane (0.5g, 3.47 mmol) was added. The mixture was stirred for 2 hours under N_2 during which time a white precipitate formed. The precipitate was isolated by filtration and the solid was washed with 10 ml water and 10 ml Et_2O. Compound **11** was isolated as a white solid (1.36 g, 51% yield).

Yield: 1.36 g (51 %); ^{1}H NMR (300 MHz, DMSO-d_6): δ= 8.34 (s, 1H, NH), 7.37 (d, 2H, J= 8.7 Hz, aromatic CH), 7.20 (t, 2H, J= 7.5 Hz, aromatic CH), 6.87 (m, 1H, aromatic CH), 6.09 (t, 1H, J= 5.7 Hz, NH), 3.06 (q, 2H, J= 6.4 Hz, CH_2), 1.42 (m, 2H, CH_2), 1.29 (br m, 4H, 2 x CH_2) ^{13}C NMR (75 MHz, DMSO-d_6): δ= 155.2 (CO), 140.6 (aromatic CH), 128.6 (aromatic CH), 120.8 (aromatic CH), 117.5 (aromatic CH), 29.3 (CH2), 28.8 (CH2), 26.3 (CH2); LRMS(ESI-): *m/z* = 381.2 ([M - H]$^-$); HRMS(ES): for $C_{22}H_{31}N_4O_2$ [M + H]$^+$ *m/z*= 383.2447 (calculated), 383.2443 (found); for $C_{22}H_{30}N_4O_2$ *m/z* = 405.2267 (calculated), 405.2262 (found); IR (film): ν= 3330 (NH stretching), 3310, (NH stretching) 2930 (alkyl CH stretching), 2850 (alkyl CH stretching); M_p: 215-217 °C.

References

1. A. P. Davis, D. N. Sheppard and B. D. Smith, *Chem. Soc. Rev.*, 2007, **36**, 348-357.
2. G. W. Gokel and N. Barkey, *New J. Chem.*, 2009, **33**, 947-963.
3. J. T. Davis, O. Okunola and R. Quesada, *Chem. Soc. Rev.*, 2010, **39**, 3843-3862.
4. H. F. Lodish, *Molecular cell biology*, W.H. Freeman, New York, 2008.
5. B. Hille, *Ion channels of excitable membranes*, Sinauer, Sunderland, Mass., 2001.
6. F. M. Ashcroft, *Ion channels and disease : channelopathies*, Academic Press, San Diego, 2000.
7. T. M. Fyles, *Chem. Soc. Rev.*, 2007, **36**, 335-347.
8. D. N. Sheppard and M. J. Welsh, *Physiol. Rev.*, 1999, **79**, S23-45.
9. T. J. Jentsch, T. Maritzen and A. A. Zdebik, *J. Clin. Inves.*, 2005, **115**, 2039-2046.
10. D. C. Gadsby, P. Vergani and L. Csanady, *Nature*, 2006, **440**, 477-483.
11. C. F. Foundation, *Patient Registry 2009 Annual Data Report*, 2009.
12. J. A. Dodge, P. A. Lewis, M. Stanton and J. Wilsher, *Eur. Respir. J.*, 2007, **29**, 522-526.
13. P. M. Quinton, *Nature*, 1983, **301**, 421-422.
14. R. Busch, *Acta Univ. Carol. Med. (Praha)*, 1990, **36**, 13-15.
15. P. M. Quinton, *Physiol. Rev.*, 1999, **79**, S3-S22.
16. J. R. Yankaskas, B. C. Marshall, B. Sufian, R. H. Simon and D. Rodman, *Chest*, 2004, **125**, 1s-39s.
17. R. C. Boucher, *Annu. Rev. Med.*, 2007, **58**, 157-170.
18. P. M. Quinton, *Lancet*, 2008, **372**, 415-417.
19. G. L. Patrick and J. Spencer, *An introduction to medicinal chemistry*, Oxford University Press, New York, 2009.
20. A. Furstner, *Angew. Chem. Int. Ed.*, 2003, **42**, 3582-3603.
21. A. J. Castro, *Nature*, 1967, **213**, 903-904.
22. J. E. H. Lazaro, J. Nitcheu, R. Z. Predicala, G. C. Mangalindan, F. Nesslany, D. Marzin, G. P. Concepcion and B. Diquet, *J. Nat. Tox.*, 2002, **11**, 367-377.
23. S. Jenkins, C. D. Incarvito, J. Parr and H. H. Wasserman, *Cryst. Eng. Commun.*, 2009, **11**, 242-245.
24. T. Sato, H. Konno, Y. Tanaka, T. Kataoka, K. Nagai, H. H. Wasserman and S. Ohkuma, *J. Biol. Chem.*, 1998, **273**, 21455-21462.
25. S. Ohkuma, T. Sato, M. Okamoto, H. Matsuya, K. Arai, T. Kataoka, K. Nagai and H. H. Wasserman, *Biochem. J.*, 1998, **334**, 731-741.
26. M. S. Melvin, D. C. Ferguson, N. Lindquist and R. A. Manderville, *J. Org. Chem.*, 1999, **64**, 6861-6869.
27. M. S. Melvin, J. T. Tomlinson, G. R. Saluta, G. L. Kucera, N. Lindquist and R. A. Manderville, *J. Am. Chem. Soc.*, 2000, **122**, 6333-6334.

28. G. Park, J. T. Tomlinson, M. S. Melvin, M. W. Wright, C. S. Day and R. A. Manderville, *Org. Lett.*, 2003, **5**, 113-116.
29. A. Furstner and E. J. Grabowski, *ChemBioChem*, 2001, **2**, 706-709.
30. Y. Chen, M. Schindler and S. M. Simon, *J. Biol. Chem.*, 1999, **274**, 18364-18373.
31. P. I. Hernandez, D. Moreno, A. A. Javier, T. Torroba, R. Perez-Tomas and R. Quesada, *Chem. Commun.*, 2011, DOI: 10.1039/c1031cc11300c.
32. W. A. Harrell, M. L. Bergmeyer, P. Y. Zavalij and J. T. Davis, *Chem. Commun.*, 2010, **46**, 3950-3952.
33. L. J. Siskind and M. Colombini, *Biophys. J.*, 2001, **80**, 499A-499A.
34. P. D. Beer and P. A. Gale, *Angew. Chem. Int. Ed.*, 2001, **40**, 486-516.
35. P. A. Gale, *Coord. Chem. Rev.*, 2001, **213**, 79-128.
36. P. A. Gale, *Coord. Chem. Rev.*, 2003, **240**, 1-1.
37. P. A. Gale, *Coord. Chem. Rev.*, 2003, **240**, 191-221.
38. P. A. Gale and R. Quesada, *Coord. Chem. Rev.*, 2006, **250**, 3219-3244.
39. J. L. Sessler, P. A. Gale and W.-S. Cho, *Anion receptor chemistry*, Royal Society of Chemistry, Cambridge, UK, 2006.
40. P. A. Gale and C. Caltagirone, *Chem. Soc. Rev.*, 2009, **38**, 520-563.
41. P. A. Gale, *Chem. Soc. Rev.*, 2010, **39**, 3746-3771.
42. P. A. Gale, *Chem. Commun.*, 2011, **47**, 82-86.
43. M. R. Ghadiri, W. S. Horne, M. K. Yadav and C. D. Stout, *J. Am. Chem. Soc.*, 2004, **126**, 15366-15367.
44. A. P. Davis, J. J. Perry and R. P. Williams, *J. Am. Chem. Soc.*, 1997, **119**, 1793-1794.
45. A. J. Ayling, S. Broderick, J. P. Clare, A. P. Davis, M. N. Perez-Payan, M. Lahtinen, M. J. Nissinen and K. Rissanen, *Chem. Eur. J.*, 2002, **8**, 2197-2203.
46. T. N. Lambert, J. M. Boon, B. D. Smith, M. N. Perez-Payan and A. P. Davis, *J. Am. Chem. Soc.*, 2002, **124**, 5276-5277.
47. J. M. Boon, T. N. Lambert, A. L. Sisson, A. P. Davis and B. D. Smith, *J. Am. Chem. Soc.*, 2003, **125**, 8195-8201.
48. A. V. Koulov, T. N. Lambert, R. Shukla, M. Jain, J. M. Boon, B. D. Smith, H. Y. Li, D. N. Sheppard, J. B. Joos, J. P. Clare and A. P. Davis, *Angew. Chem. Int. Ed.*, 2003, **42**, 4931-4933.
49. E. P. Kyba, R. C. Helgeson, K. Madan, G. W. Gokel, T. L. Tarnowski, S. S. Moore and D. J. Cram, *J. Am. Chem. Soc.*, 1977, **99**, 2564-2571.
50. J. M. Timko, S. S. Moore, D. M. Walba, P. C. Hiberty and D. J. Cram, *J. Am. Chem. Soc.*, 1977, **99**, 4207-4219.
51. P. Buhlmann, S. Nishizawa, K. P. Xiao and Y. Umezawa, *Tetrahedron*, 1997, **53**, 1647-1654.
52. F. G. Bordwell, *Acc. Chem. Res.*, 1988, **21**, 456-463.
53. B. A. McNally, A. V. Koulov, B. D. Smith, J. B. Joos and A. P. Davis, *Chem. Commun.*, 2005, 1087-1089.
54. B. A. McNally, A. V. Koulov, T. N. Lambert, B. D. Smith, J. B. Joos, A. L. Sisson, J. P. Clare, V. Sgarlata, L. W. Judd, G. Magro and A. P. Davis, *Chem. Eur. J.*, 2008, **14**, 9599-9606.
55. L. W. Judd and A. P. Davis, *Chem. Commun.*, 2010, **46**, 2227-2229.

56. S. Hussain, P. R. Brotherhood, L. W. Judd and A. P. Davis, *J. Am. Chem. Soc.*, 2011, **133**, 1614-1617.
57. D. J. Cram, *Angew. Chem. Int. Edit.*, 1986, **25**, 1039-1057.
58. P. V. Santacroce, J. T. Davis, M. E. Light, P. A. Gale, J. C. Iglesias-Sanchez, P. Prados and R. Quesada, *J. Am. Chem. Soc.*, 2007, **129**, 1886-1887.
59. J. T. Davis, P. A. Gale, O. A. Okunola, P. Prados, J. C. Iglesias-Sanchez, T. Torroba and R. Quesada, *Nature Chem.*, 2009, **1**, 138-144.
60. A. Baeyer, *Ber. Dtsch. Chem. Ges.*, 1886, **19**, 2184.
61. P. A. Gale, J. L. Sessler, V. Kral and V. Lynch, *J. Am. Chem. Soc.*, 1996, **118**, 5140-5141.
62. R. Custelcean, L. H. Delmau, B. A. Moyer, J. L. Sessler, W. S. Cho, D. Gross, G. W. Bates, S. J. Brooks, M. E. Light and P. A. Gale, *Angew. Chem. Int. Ed.*, 2005, **44**, 2537-2542.
63. C. C. Tong, R. Quesada, J. L. Sessler and P. A. Gale, *Chem. Commun.*, 2008, 6321-6323.
64. M. G. Fisher, P. A. Gale, J. R. Hiscock, M. B. Hursthouse, M. E. Light, F. P. Schmidtchen and C. C. Tong, *Chem. Commun.*, 2009, 3017-3019.
65. M. Yano, C. C. Tong, M. E. Light, F. P. Schmidtchen and P. A. Gale, *Org. Biomol. Chem.*, 2010, **8**, 5701-5701.
66. B. E. Smart, *J. Fluorine Chem.*, 2001, **109**, 3-11.
67. P. A. Gale, C. C. Tong, C. J. E. Haynes, O. Adeosun, D. E. Gross, E. Karnas, E. M. Sedenberg, R. Quesada and J. L. Sessler, *J. Am. Chem. Soc.*, 2010, **132**, 3240-3241.
68. N. Busschaert, P. A. Gale, C. J. E. Haynes, M. E. Light, S. J. Moore, C. C. Tong, J. T. Davis and W. A. Harrell, *Chem. Commun.*, 2010, **46**, 6252-6254.
69. C. Caltagirone, J. R. Hiscock, M. B. Hursthouse, M. E. Light and P. A. Gale, *Chem. Eur. J.*, 2008, **14**, 10236-10243.
70. P. A. Gale, J. R. Hiscock, S. J. Moore, C. Caltagirone, M. B. Hursthouse and M. E. Light, *Chem. Asian J.*, 2010, **5**, 555-561.
71. P. A. Gale, J. R. Hiscock, C. Z. Jie, M. B. Hursthouse and M. E. Light, *Chem. Sci.*, 2010, **1**, 215-220.
72. B. A. McNally, E. J. O'Neil, A. Nguyen and B. D. Smith, *J. Am. Chem. Soc.*, 2008, **130**, 17274-17275.
73. A. V. Koulov, J. M. Mahoney and B. D. Smith, *Org. Biomol. Chem.*, 2003, **1**, 27-29.
74. S. J. Moore, M. G. Fisher, M. Yano, C. C. Tong and P. A. Gale, *Chem. Commun.*, 2011, **47**, 689-691.
75. S. J. Moore, M. G. Fisher, M. Yano, C. C. Tong and P. A. Gale, *Dalton Trans.*, 2011, DOI: 10.1039/c1031dt10213c.
76. N. J. Andrews, C. J. E. Haynes, M. E. Light, S. J. Moore, C. C. Tong, J. T. Davis, W. A. Harrell and P. A. Gale, *Chem. Sci.*, 2011, **2**, 256-260.
77. P. A. Gale, M. E. Light, B. McNally, K. Navakhun, K. E. Sliwinski and B. D. Smith, *Chem. Commun.*, 2005, 3773-3775.
78. P. A. Gale, J. Garric, M. E. Light, B. A. McNally and B. D. Smith, *Chem. Commun.*, 2007, 1736-1738.
79. K. J. Winstanley, S. J. Allen and D. K. Smith, *Chem. Commun.*, 2009, 4299-4301.

80. S. K. Berezin and J. T. Davis, *J. Am. Chem. Soc.*, 2009, **131**, 2458-2459.
81. F. Hofmeister, *Arch. Exp. Pathol. Pharmacol.*, 1888, **22**, 247-260.
82. E. Gouaux and R. MacKinnon, *Science*, 2005, **310**, 1461-1465.
83. G. L. Reddy, T. Iwamoto, J. M. Tomich and M. Montal, *J. Biol. Chem.*, 1993, **268**, 14608-14615.
84. D. P. Wallace, J. M. Tomich, T. Iwamoto, K. Henderson, J. J. Grantham and L. P. Sullivan, *Am. J. Physiol. Cell Ph.*, 1997, **272**, C1672-C1679.
85. D. Wallace, K. Henderson, J. Tomich, T. Iwamoto, J. Grantham and L. Sullivan, *J. Am. Soc. Nephrol.*, 1996, **7**, A0236-A0236.
86. D. P. Wallace, J. M. Tomich, T. Iwamoto, K. Henderson, J. J. Grantham and L. P. Sullivan, *Am. J. Physiol. Cell Ph.*, 1997, **41**, C1672-C1679.
87. J. R. Broughman, K. E. Mitchell, R. L. Sedlacek, T. Iwamoto, J. M. Tomich and B. D. Schultz, *Am. J. Physiol. Cell Ph.*, 2001, **280**, C451-C458.
88. J. R. Broughman, L. P. Shank, O. Prakash, B. D. Schultz, T. Iwamoto, J. M. Tomich and K. Mitchell, *J. Membrane Biol.*, 2002, **190**, 93-103.
89. G. A. Cook, O. Prakash, K. Zhang, L. P. Shank, W. A. Takeguchi, A. Robbins, Y. X. Gong, T. Iwamoto, B. D. Schultz and J. M. Tomich, *Biophys. J.*, 2004, **86**, 1424-1435.
90. L. P. Shank, J. R. Broughman, W. Takeguchi, G. Cook, A. S. Robbins, L. Hahn, G. Radke, T. Iwamoto, B. D. Schultz and J. M. Tomich, *Biophys. J.*, 2006, **90**, 2138-2150.
91. J. M. Tomich, D. Wallace, K. Henderson, K. E. Mitchell, G. Radke, R. Brandt, C. A. Ambler, A. J. Scott, J. Grantham, L. Sullivan and T. Iwamoto, *Biophys. J.*, 1998, **74**, 256-267.
92. K. E. Mitchell, L. C. Freeman, L. Sullivan, T. Iwamoto, C. A. Ambler and J. Tomich, *Mol. Biol. Cell.*, 1997, **8**, 1101-1101.
93. K. E. Mitchell, J. Tomich, T. Iwamoto and L. Freeman, *Biophys. J.*, 1998, **74**, A388-A388.
94. K. E. Mitchell, T. Iwamoto, J. Tomich and L. C. Freeman, *Bba-Biomembranes*, 2000, **1466**, 47-60.
95. P. H. Schlesinger, R. Ferdani, J. Liu, J. Pajewska, R. Pajewski, M. Saito, H. Shabany and G. W. Gokel, *J. Am. Chem. Soc.*, 2002, **124**, 1848-1849.
96. N. Gibbs, R. B. Sessions, P. B. Williams and C. E. Dempsey, *Biophys. J.*, 1997, **72**, 2490-2495.
97. P. H. Schlesinger, N. K. Djedovic, R. Ferdani, J. Pajewska, R. Pajewski and G. W. Gokel, *Chem. Commun.*, 2003, 308-309.
98. G. Fujii, J. E. Chang, T. Coley and B. Steere, *Biochem.*, 1997, **36**, 4959-4968.
99. L. A. Weiss, N. Sakai, B. Ghebremariam, C. Y. Ni and S. Matile, *J. Am. Chem. Soc.*, 1997, **119**, 12142-12149.
100. V. Gorteau, G. Bollot, J. Mareda, A. Perez-Velasco and S. Matile, *J. Am. Chem. Soc.*, 2006, **128**, 14788-14789.
101. A. Perez-Velasco, V. Gorteau and S. Matile, *Angew. Chem. Int. Ed.*, 2008, **47**, 921-923.
102. A. R. Schmitzer, C. R. Elie, N. Noujeim and C. Pardin, *Chem. Commun.*, 2011, **47**, 1788-1790.

103. X. Li, B. Shen, X. Q. Yao and D. Yang, *J. Am. Chem. Soc.*, 2007, **129**, 7264-7265.
104. D. Yang, J. Qu, W. Li, Y. H. Zhang, Y. Ren, D. P. Wang and Y. D. Wu, *J. Am. Chem. Soc.*, 2002, **124**, 12410-12411.
105. D. Yang, X. Li, Y. Sha and Y. D. Wu, *Chem. Eur. J.*, 2005, **11**, 3005-3009.
106. X. Li, B. Shen, X. Q. Yao and D. Yang, *J. Am. Chem. Soc.*, 2009, **131**, 13676-13680.
107. C. R. Yamnitz, S. Negin, I. A. Carasel, R. K. Winter and G. W. Gokel, *Chem. Commun.*, 2010, **46**, 2838-2840.
108. V. Sidorov, F. W. Kotch, G. Abdrakhmanova, R. Mizani, J. C. Fettinger and J. T. Davis, *J. Am. Chem. Soc.*, 2002, **124**, 2267-2278.
109. V. Sidorov, F. W. Kotch, J. L. Kuebler, Y. F. Lam and J. T. Davis, *J. Am. Chem. Soc.*, 2003, **125**, 2840-2841.
110. N. Madhavan, E. C. Robert and M. S. Gin, *Angew. Chem. Int. Ed.*, 2005, **44**, 7584-7587.
111. M. S. Gin and N. Madhavan, *ChemBioChem*, 2007, **8**, 1834-1840.
112. D. Montesarchio, S. Licen, C. Coppola, J. D'Onofrio and P. Tecilla, *Org. Biomol. Chem.*, 2009, **7**, 1060-1063.
113. G. Guichard, A. Hennig, L. Fischer and S. Matile, *J. Am. Chem. Soc.*, 2009, **131**, 16889-16895.
114. B. D. Smith and T. N. Lambert, *Chem. Commun.*, 2003, 2261-2268.
115. R. C. Macdonald, R. I. Macdonald, B. P. M. Menco, K. Takeshita, N. K. Subbarao and L. R. Hu, *Biochim. Biophys. Acta.*, 1991, **1061**, 297-303.
116. K. Kano and J. H. Fendler, *Biochim. Biophys. Acta.*, 1978, **509**, 289-299.
117. N. Sakai, D. Houdebert and S. Matile, *Chem. Eur. J.*, 2003, **9**, 223-232.
118. M. J. Pregel, L. Jullien, J. Canceill, L. Lacombe and J. M. Lehn, *J. Chem. Soc. Perk. Trans. 2*, 1995, 417-426.
119. S. Otto, M. Osifchin and S. L. Regen, *J. Am. Chem. Soc.*, 1999, **121**, 10440-10441.
120. T. M. Fyles, R. Knoy, K. Mullen and M. Sieffert, *Langmuir*, 2001, **17**, 6669-6674.
121. D. Ogden and D. Stanfield, *Currents*, 1981, 53.
122. B. Sackmann and E. Neher, *Single-Channel Recording*, Plenum Press, New York, 1981.
123. A. V. Hill, *The Journal of Physiology*, 1910, **40**, i-vii.
124. S. Goutelle, M. Maurin, F. Rougier, X. Barbaut, L. Bourguignon, M. Ducher and P. Maire, *Fund. Clin. Pharmacol.*, 2008, **22**, 633-648.
125. N. H. Holford and L. B. Sheiner, *Critical Reviews in Bioengineering*, 1981, **5**, 273-322.
126. N. H. Holford and L. B. Sheiner, *Clin. Pharmacokinet.*, 1981, **6**, 429-453.
127. D. N. Sheppard, M. R. Carson, L. S. Ostedgaard, G. M. Denning and M. J. Welsh, *Am. J. Physiol.*, 1994, **266**, L405-413.
128. A. C. Chao, J. A. Dix, M. C. Sellers and A. S. Verkman, *Biophys. J.*, 1989, **56**, 1071-1081.
129. P. J. Smith, M. V. Reddington and C. S. Wilcox, *Tetrahedron Lett.*, 1992, **33**, 6085-6088.

130. A. F. Li, J. H. Wang, F. Wang and Y. B. Jiang, *Chem. Soc. Rev.*, 2010, **39**, 3729-3745.
131. T. Steiner, *Angew. Chem. Int. Ed.*, 2002, **41**, 48-76.
132. S. J. Brooks, P. R. Edwards, P. A. Gale and M. E. Light, *New J. Chem.*, 2006, **30**, 65-70.
133. S. Nishizawa, P. Buhlmann, M. Iwao and Y. Umezawa, *Tetrahedron Lett.*, 1995, **36**, 6483-6486.
134. C. Laurence, M. Berthelot, J. Y. Lequestel and M. J. Elghomari, *J. Chem. Soc. Perk. Trans. 2*, 1995, 2075-2079.
135. T. Gunnlaugsson, P. E. Kruger, P. Jensen, F. M. Pfeffer and G. M. Hussey, *Tetrahedron Lett.*, 2003, **44**, 8909-8913.
136. T. Gunnlaugsson, P. E. Kruger, T. C. Lee, R. Parkesh, F. M. Pfeffer and G. M. Hussey, *Tetrahedron Lett.*, 2003, **44**, 6575-6578.
137. S. Camiolo, P. A. Gale, M. B. Hursthouse, M. E. Light and A. J. Shi, *Chem. Commun.*, 2002, 758-759.
138. P. A. Gale, K. Navakhun, S. Camiolo, M. E. Light and M. B. Hursthouse, *J. Am. Chem. Soc.*, 2002, **124**, 11228-11229.
139. S. Camiolo, P. A. Gale, M. B. Hursthouse and M. E. Light, *Org. Biomol. Chem.*, 2003, **1**, 741-744.
140. D. E. Gomez, L. Fabbrizzi, M. Licchelli and E. Monzani, *Org. Biomol. Chem.*, 2005, **3**, 1495-1500.
141. T. Hayashita, T. Onodera, R. Kato, S. Nishizawa and N. Teramae, *Chem. Commun.*, 2000, 755-756.
142. H. Juwarker, J.-M. Suk and K.-S. Jeong, in *Anion Recognition in Supramolecular Chemistry*, eds. P. A. Gale and W. Dehaen, Springer-Verlag, Berlin Heidelberg, 2010, pp. 177-204.
143. F. M. Pfeffer, K. F. Lim and K. J. Sedgwick, *Org. Biomol. Chem.*, 2007, **5**, 1795-1799.
144. M. Albrecht, G. W. Bates, Triyanti, M. E. Light and P. A. Gale, *J. Org. Chem.*, 2007, **72**, 8921-8927.
145. J. Plavec, D. Makuc and M. Albrecht, *Supramol. Chem.*, 2010, **22**, 603-611.
146. J. Y. Lee, M. H. Lee and K. S. Jeong, *Supramol. Chem.*, 2007, **19**, 257-263.
147. J. Jurczak, P. Dydio and T. Zielinski, *Org. Lett.*, 2010, **12**, 1076-1078.
148. W. W. Huang, J. W. Li, H. Lin and H. K. Lin, *J. Incl. Phenom. Macro.*, 2011, **69**, 101-106.
149. M. D. Pratt and P. D. Beer, *Polyhedron*, 2003, **22**, 649-653.
150. C. R. Bondy, P. A. Gale and S. J. Loeb, *J. Am. Chem. Soc.*, 2004, **126**, 5030-5031.
151. M. D. Hollingsworth and K. D. M. Harris, *Solid-State Supramolecular Chemistry: Crystal Engineering, in Comprehensive Supramolecular Chemistry*, Pergamon, Oxford, 1996.
152. J. Brinksma, B. L. Feringa, R. M. Kellogg, R. Vreeker and J. van Esch, *Langmuir*, 2000, **16**, 9249-9255.
153. M. de Loos, A. G. J. Ligtenbarg, J. van Esch, H. Kooijman, A. L. Spek, R. Hage, R. M. Kellogg and B. L. Feringa, *Eur. J. Org. Chem.*, 2000, 3675-3678.
154. Y. Jeong, K. Hanabusa, H. Masunaga, I. Akiba, K. Miyoshi, S. Sakurai and K. Sakurai, *Langmuir*, 2005, **21**, 586-594.

155. F. S. Schoonbeek, J. H. van Esch, R. Hulst, R. M. Kellogg and B. L. Feringa, *Chem. Eur. J.*, 2000, **6**, 2633-2643.
156. J. van Esch, F. Schoonbeek, M. de Loos, H. Kooijman, A. L. Spek, R. M. Kellogg and B. L. Feringa, *Chem. Eur. J.*, 1999, **5**, 937-950.
157. M. O. M. Piepenbrock, G. O. Lloyd, N. Clarke and J. W. Steed, *Chem. Commun.*, 2008, 2644-2646.
158. A. Cazacu, C. Tong, A. van der Lee, T. M. Fyles and M. Barboiu, *J. Am. Chem. Soc.*, 2006, **128**, 9541-9548.
159. P. Bandyopadhyay, V. Janout, L. H. Zhang, J. A. Sawko and S. L. Regen, *J. Am. Chem. Soc.*, 2000, **122**, 12888-12889.
160. N. Djedovic, R. Ferdani, E. Harder, J. Pajewska, R. Pajewski, M. E. Weber, P. H. Schlesinger and G. W. Gokel, *New J. Chem.*, 2005, **29**, 291-305.
161. T. W. Schultz and V. A. Tucker, *B. Environ. Contam. Tox.*, 2003, **70**, 1251-1258.
162. H. Cho and Y. Zhao, *Chem. Commun.*, 2011, DOI:10.1039/c1031cc00092f.
163. R. Benz, O. Frohlich and P. Lauger, *Biochim. Biophys. Acta*, 1977, **464**, 465.
164. B. A. Lewis and D. M. Engelman, *J. Mol. Biol.*, 1983, **166**, 211-217.
165. D. Marsh, *CRC handbook of lipid bilayers*, CRC Press, Boca Raton, Fla., 1990.
166. M. J. Hynes, *J. Chem. Soc. Dalton*, 1993, 311-312.
167. J. L. Sessler, W. S. Cho, D. E. Gross, J. A. Shriver, V. M. Lynch and M. Marquez, *J. Org. Chem.*, 2005, **70**, 5982-5986.
168. J. L. Sessler, D. Q. An, W. S. Cho and V. Lynch, *Angew. Chem. Int. Ed.*, 2003, **42**, 2278-2281.
169. J. L. Sessler, D. Q. An, W. S. Cho and V. Lynch, *J. Am. Chem. Soc.*, 2003, **125**, 13646-13647.
170. C. H. Lee, H. Miyaji, D. W. Yoon and J. L. Sessler, *Chem. Commun.*, 2008, 24-34.
171. D. W. Yoon, H. Hwang and C. H. Lee, *Angew. Chem. Int. Ed.*, 2002, **41**, 1757-1759.
172. D. W. Yoon, D. E. Gross, V. M. Lynch, J. L. Sessler, B. P. Hay and C. H. Lee, *Angew. Chem. Int. Ed.*, 2008, **47**, 5038-5042.
173. J. D. Yoo, M. S. Kim, S. J. Hong, J. L. Sessler and C. H. Lee, *J. Org. Chem.*, 2009, **74**, 1065-1069.
174. H. Miyaji, H. K. Kim, E. K. Sim, C. K. Lee, W. S. Cho, J. L. Sessler and C. H. Lee, *J. Am. Chem. Soc.*, 2005, **127**, 12510-12512.
175. P. K. Panda and C. H. Lee, *Org. Lett.*, 2004, **6**, 671-674.
176. H. Miyaji, S. J. Hong, S. D. Jeong, D. W. Yoon, H. K. Na, J. Hong, S. Ham, J. L. Sessler and C. H. Lee, *Angew. Chem. Int. Ed.*, 2007, **46**, 2508-2511.
177. C. J. Pedersen, *J. Am. Chem. Soc.*, 1967, **89**, 7017-7036.
178. J. L. Sessler, L. R. Eller, W. S. Cho, S. Nicolaou, A. Aguilar, J. T. Lee, V. M. Lynch and D. J. Magda, *Angew. Chem. Int. Ed.*, 2005, **44**, 5989-5992.
179. P. Job, *Ann. Chim. App.*, 1928, **9**, 113-203.
180. L. N. Heydorn, L. M. Carter, R. D. Bowen and J. K. Terlouw, *Eur. J. Mass Spec.*, 2003, **9**, 343-350.
181. K. Ito, T. Iida, T. Fujita and S. Tsuji, *Synthesis*, 1981, **4**, 287.
182. A. Jart, *Acta Polytech. Scand.*, 1965, **44**, 54.
183. W. Geiger, *Spectrochim. Acta*, 1966, **22**, 459-499.

184. F. W. Matthews and J. H. Michell, *Ind. Eng. Chem.*, 1946, **18**, 662-665.

Appendix

A1 Anion transport studies

In this section, the additional vesicles studies relevant to the results reported in **Chapters 2-5** are listed. The vesicles were prepared by the procedure reported in **Chapter 6.2**. Transport studies were performed using an ISE method monitoring chloride efflux from unilamellar vesicles composed of POPC unless otherwise stated. The Hill analysis is described in **Chapter 1.8.7**, and the general procedure is outlined in **Chapter 2.2.3**.

A1.1 Additional transport studies from Chapter 2

A1.1.1 Hill analyses

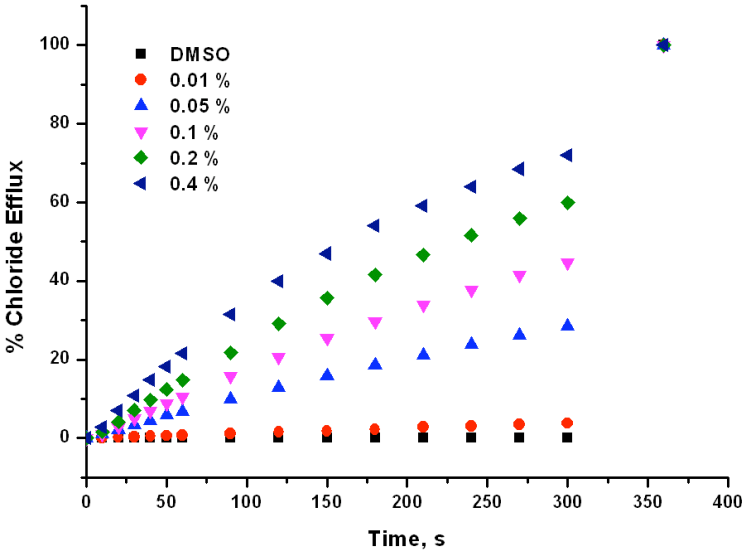

Figure A1.1 Chloride efflux promoted by various concentrations receptor **123** from unilamllar POPC vesicles containing 489 mM NaCl buffered to pH 7.2 with 5 mM sodium phosphate salts. The vesicles were suspended in 489 mM $NaNO_3$ buffered to pH 7.2 with 5 mM sodium phosphate salts. At the end of the experiment, the vesicles were lysed to calibrate 100 % chloride efflux. Each point represents the average of 3 trials. All standard deviations are < 5 %.

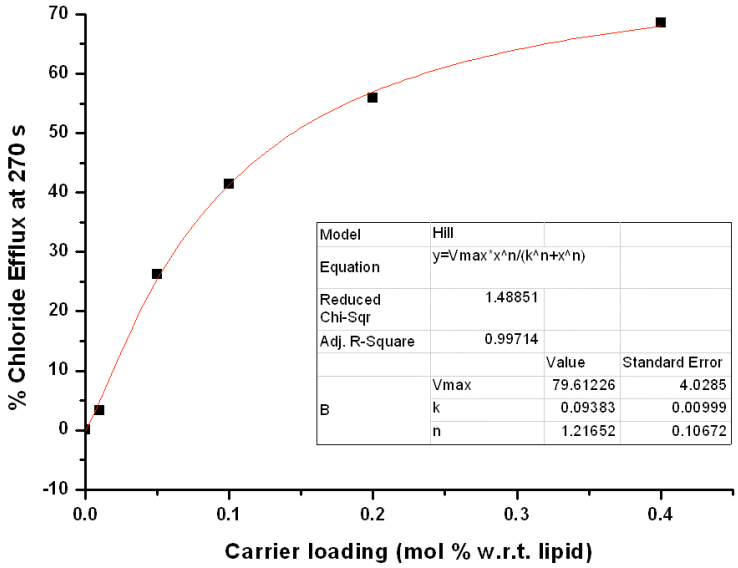

Figure A1.2 Hill plot for the Cl^-/NO_3^- antiport promoted by receptor **123**. The data was fitted to the Hill equation using Origin® 8.1.

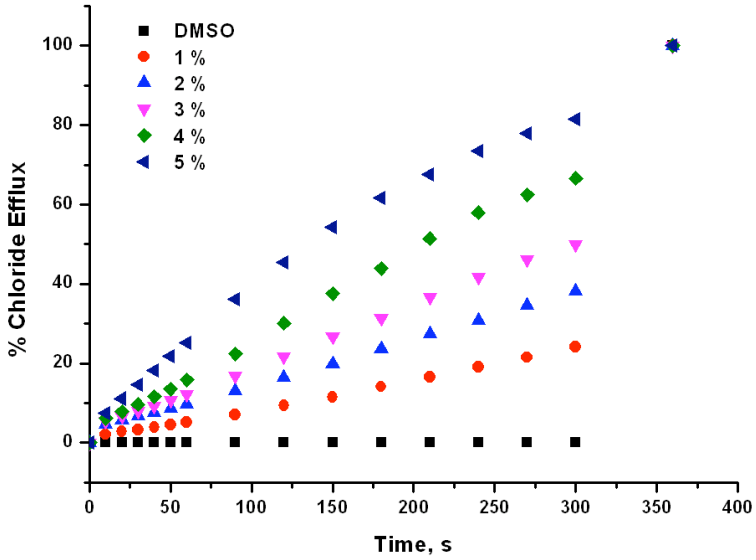

Figure A1.3 Chloride efflux promoted by various concentrations receptor **125** from unilamllar POPC vesicles containing 489 mM NaCl buffered to pH 7.2 with 5 mM sodium phosphate salts. The vesicles were suspended in 489 mM $NaNO_3$ buffered to pH 7.2 with 5 mM sodium phosphate salts. At the end of the experiment, the vesicles were lysed to calibrate 100 % chloride efflux. Each point represents the average of 3 trials. All standard deviations are < 5 %.

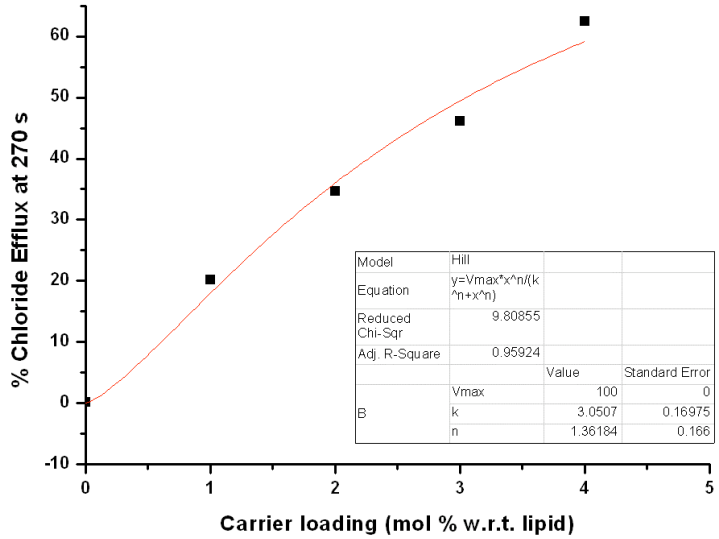

Figure A1.4 Hill plot for the Cl^-/NO_3^- antiport promoted by receptor **125**. The data was fitted to the Hill equation using Origin® 8.1.

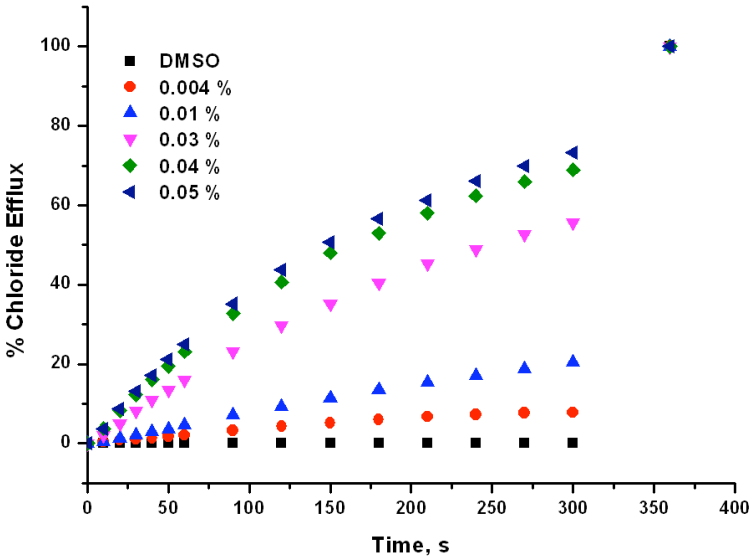

Figure A1.5 Chloride efflux promoted by various concentrations receptor **127** from unilamllar POPC vesicles containing 489 mM NaCl buffered to pH 7.2 with 5 mM sodium phosphate salts. The vesicles were suspended in 489 mM $NaNO_3$ buffered to pH 7.2 with 5 mM sodium phosphate salts. At the end of the experiment, the vesicles were lysed to calibrate 100 % chloride efflux. Each point represents the average of 3 trials. All standard deviations are < 5 %.

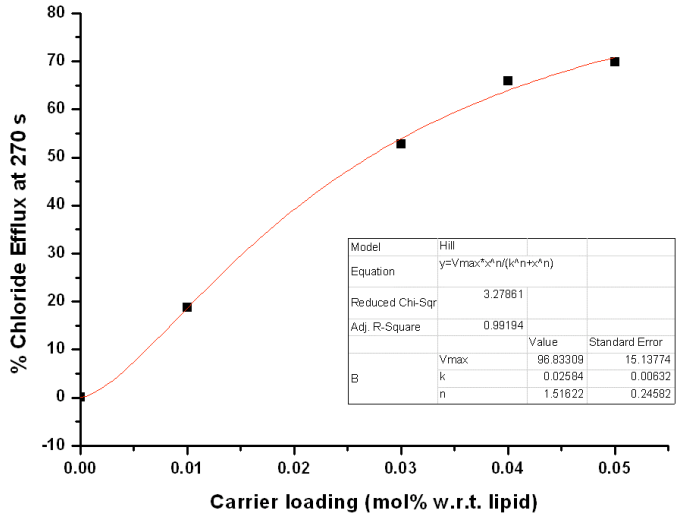

Figure A1.6 Hill plot for the Cl^-/NO_3^- antiport promoted by receptor **127**. The data was fitted to the Hill equation using Origin® 8.1.

A1.2 Additional transport studies from Chapter 3

A1.2.1 Mechanistic studies

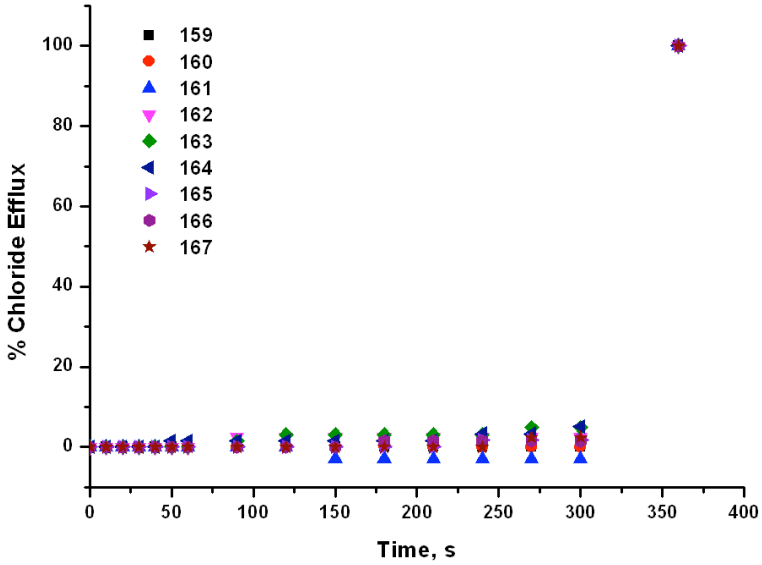

Figure A1.7 Chloride efflux promoted by receptors **159-167** (4 mol% w.r.t. lipid) from unilamllar POPC vesicles containing 489 mM NaCl buffered to pH 7.2 with 5 mM sodium phosphate salts. The vesicles were suspended in 167 mM Na_2SO_4 buffered to pH 7.2 with 5 mM sodium phosphate salts. At the end of the experiment, the vesicles were lysed to calibrate 100 % chloride efflux. Each point represents the average of 3 trials. All standard deviations are < 5 %.

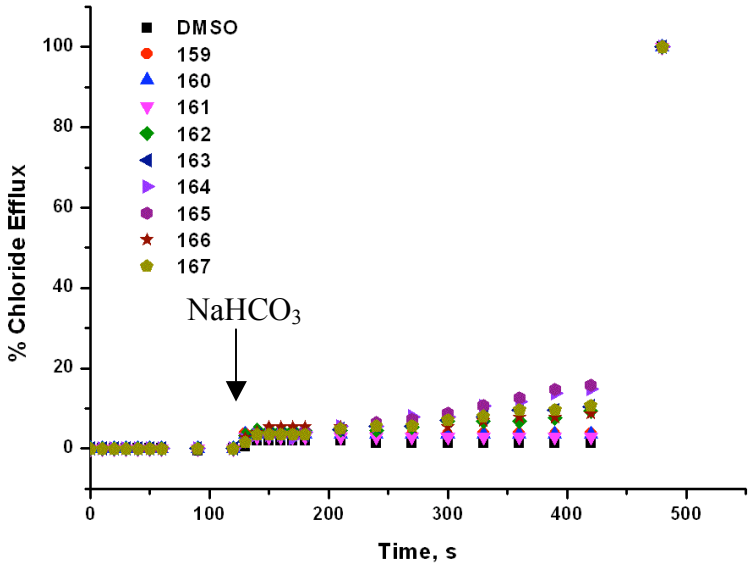

Figure A1.8 Chloride efflux promoted by receptors **159-167** (4 mol% w.r.t. lipid) from unilamllar POPC vesicles containing 489 mM NaCl buffered to pH 7.2 with 20 mM sodium phosphate salts. The vesicles were suspended in 167 mM Na_2SO_4 buffered to pH 7.2 with 20 mM sodium phosphate salts. At t = 120 s, a pulse of $NaHCO_3$ was added such that the final HCO_3^- concentration was 40 mM. At the end of the experiment, the vesicles were lysed to calibrate 100 % chloride efflux. Each point represents the average of 3 trials. All standard deviations are < 5 %.

A1.2.2 Hill analyses

Receptors which failed to mediate > 50 % total chloride efflux after 270 s at a loading of 4 mol% (w.r.t. lipid) were deemed not active enough to warrant a full Hill analysis.

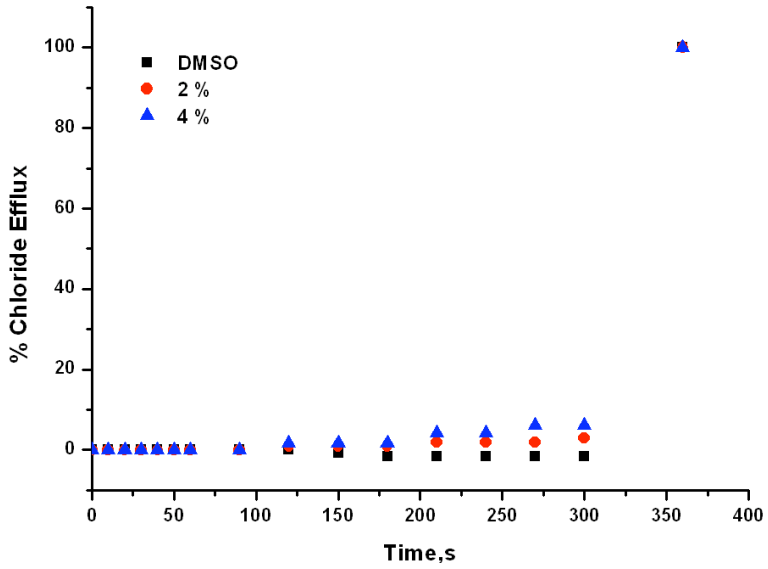

Figure A1.9 Chloride efflux promoted by various concentrations receptor **159** from unilamllar POPC vesicles containing 489 mM NaCl buffered to pH 7.2 with 5 mM sodium phosphate salts. The vesicles were suspended in 489 mM $NaNO_3$ buffered to pH 7.2 with 5 mM sodium phosphate salts. At the end of the experiment, the vesicles were lysed to calibrate 100 % chloride efflux. Each point represents the average of 3 trials. All standard deviations are < 5 %.

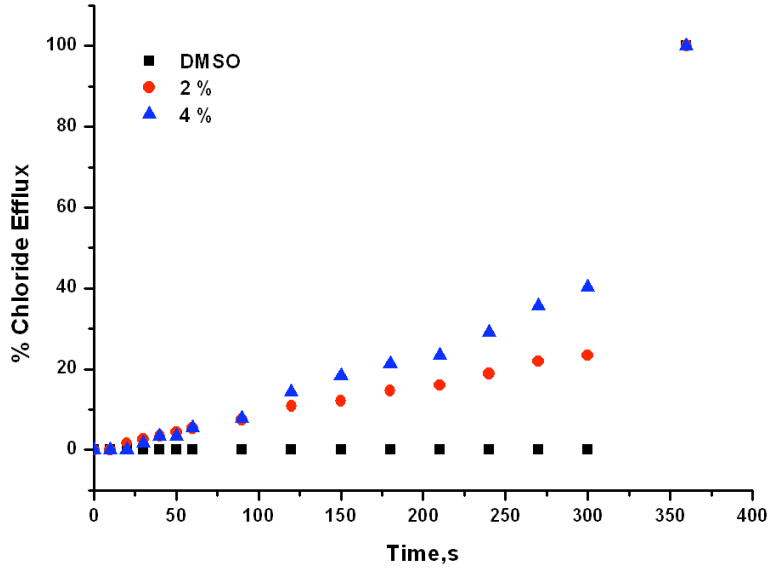

Figure A1.10 Chloride efflux promoted by various concentrations receptor **160** from unilamllar POPC vesicles containing 489 mM NaCl buffered to pH 7.2 with 5 mM sodium phosphate salts. The vesicles were suspended in 489 mM $NaNO_3$ buffered to pH 7.2 with 5 mM sodium phosphate salts. At the end of the experiment, the vesicles were lysed to calibrate 100 % chloride efflux. Each point represents the average of 3 trials. All standard deviations are < 5 %.

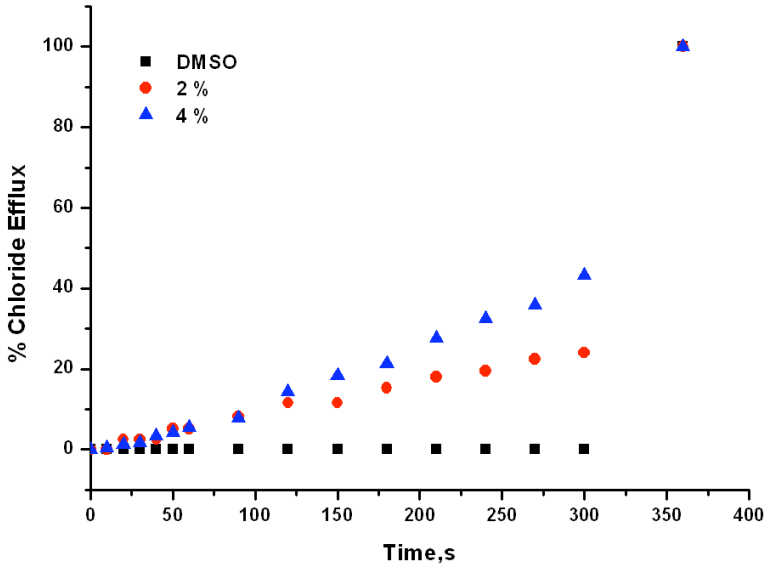

Figure A1.11 Chloride efflux promoted by various concentrations receptor **161** from unilamllar POPC vesicles containing 489 mM NaCl buffered to pH 7.2 with 5 mM sodium phosphate salts. The vesicles were suspended in 489 mM $NaNO_3$ buffered to pH 7.2 with 5 mM sodium phosphate salts. At the end of the experiment, the vesicles were lysed to calibrate 100 % chloride efflux. Each point represents the average of 3 trials. All standard deviations are < 5 %.

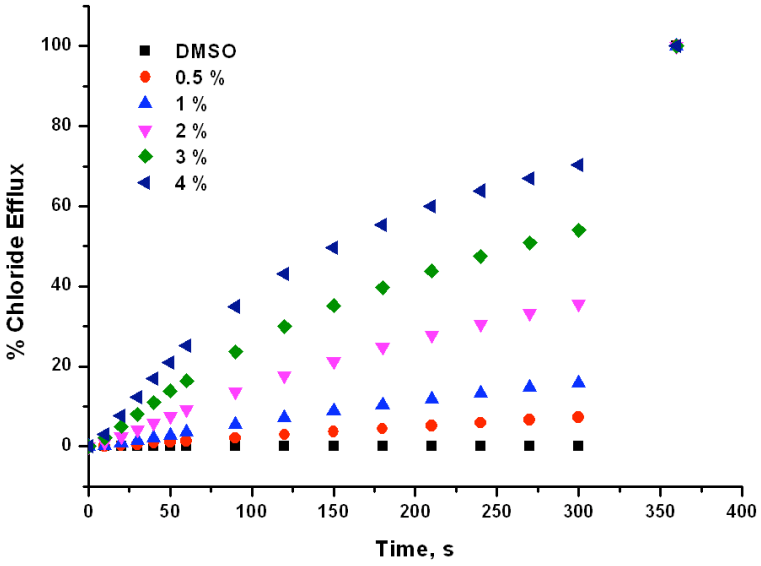

Figure A1.12 Chloride efflux promoted by various concentrations receptor **162** from unilamllar POPC vesicles containing 489 mM NaCl buffered to pH 7.2 with 5 mM sodium phosphate salts. The vesicles were suspended in 489 mM $NaNO_3$ buffered to pH 7.2 with 5 mM sodium phosphate salts. At the end of the experiment, the vesicles were lysed to calibrate 100 % chloride efflux. Each point represents the average of 3 trials. All standard deviations are < 5 %.

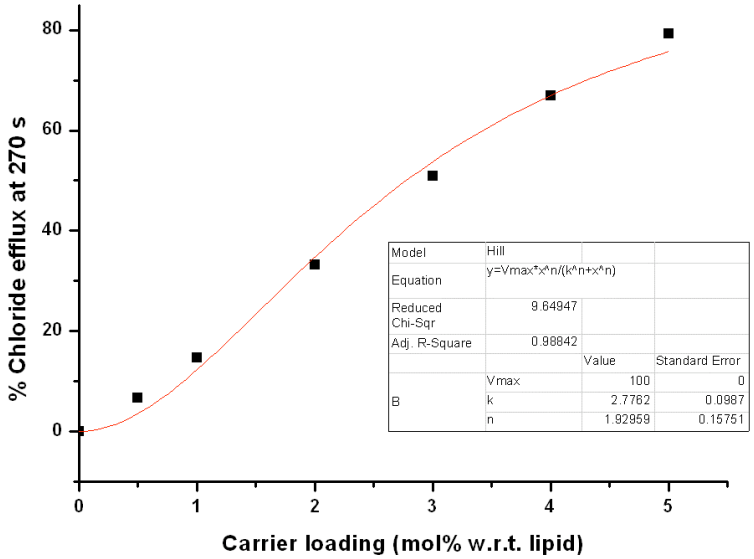

Figure A1.13 Hill plot for the Cl^-/NO_3^- antiport promoted by receptor **162**. The data was fitted to the Hill equation using Origin® 8.1.

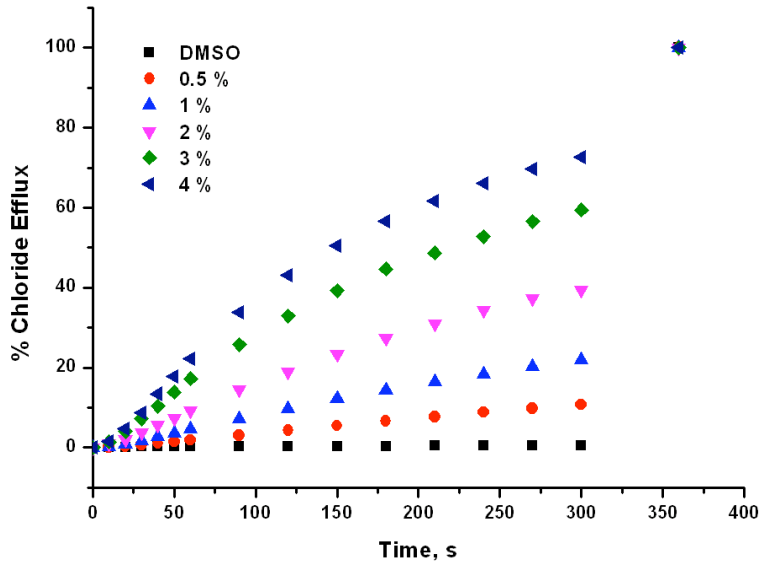

Figure A1.14 Chloride efflux promoted by various concentrations receptor **163** from unilamllar POPC vesicles containing 489 mM NaCl buffered to pH 7.2 with 5 mM sodium phosphate salts. The vesicles were suspended in 489 mM $NaNO_3$ buffered to pH 7.2 with 5 mM sodium phosphate salts. At the end of the experiment, the vesicles were lysed to calibrate 100 % chloride efflux. Each point represents the average of 3 trials. All standard deviations are < 5 %.

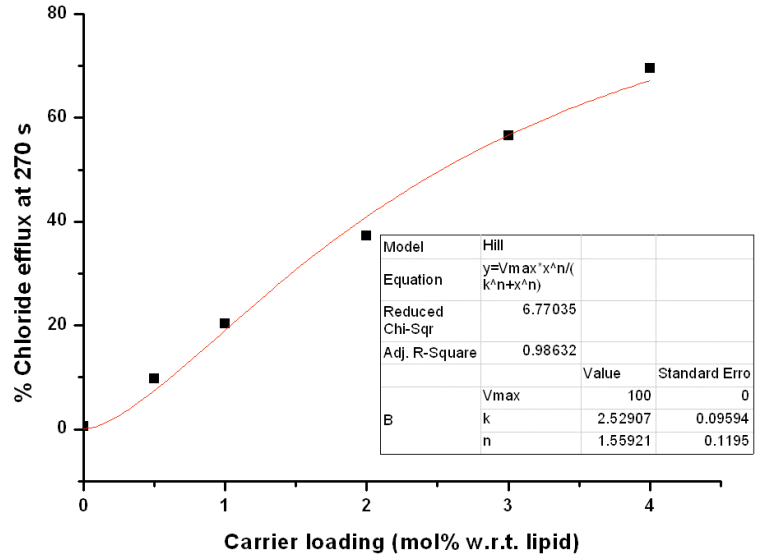

Figure A1.15 Hill plot for the Cl^-/NO_3^- antiport promoted by receptor **163**. The data was fitted to the Hill equation using Origin® 8.1.

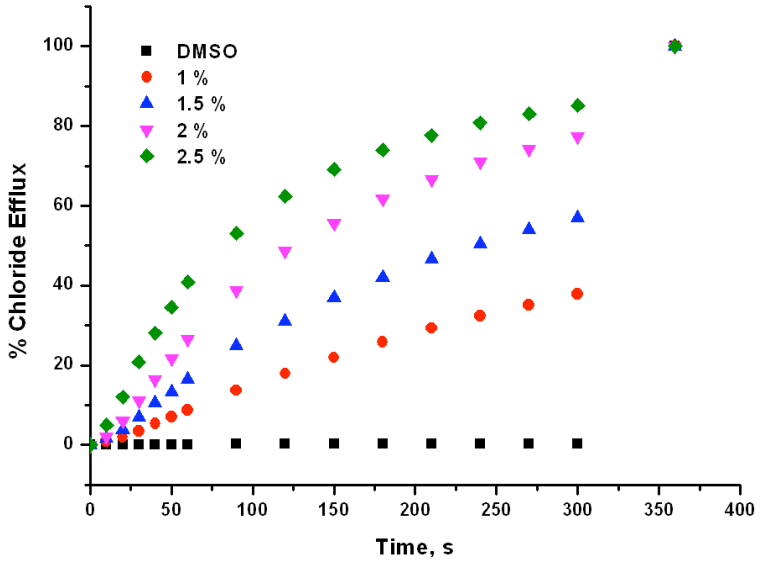

Figure A1.16 Chloride efflux promoted by various concentrations receptor **164** from unilamllar POPC vesicles containing 489 mM NaCl buffered to pH 7.2 with 5 mM sodium phosphate salts. The vesicles were suspended in 489 mM $NaNO_3$ buffered to pH 7.2 with 5 mM sodium phosphate salts. At the end of the experiment, the vesicles were lysed to calibrate 100 % chloride efflux. Each point represents the average of 3 trials. All standard deviations are < 5 %.

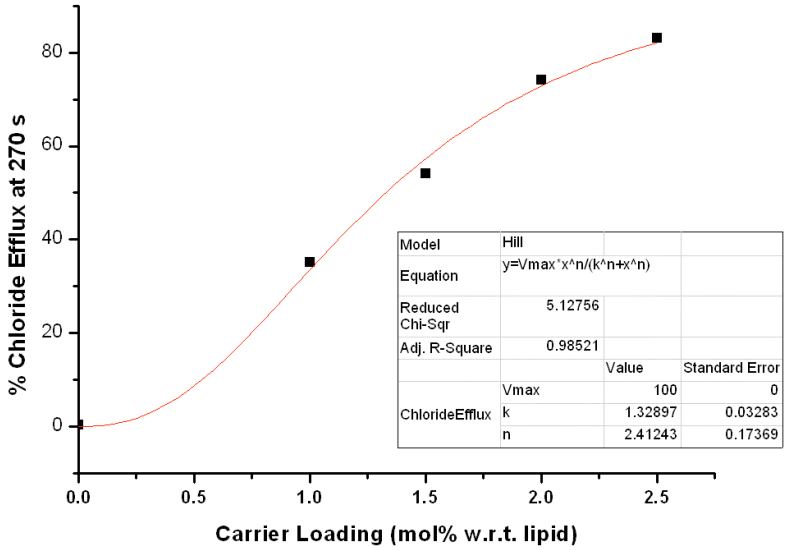

Figure A1.17 Hill plot for the Cl^-/NO_3^- antiport promoted by receptor **164**. The data was fitted to the Hill equation using Origin® 8.1.

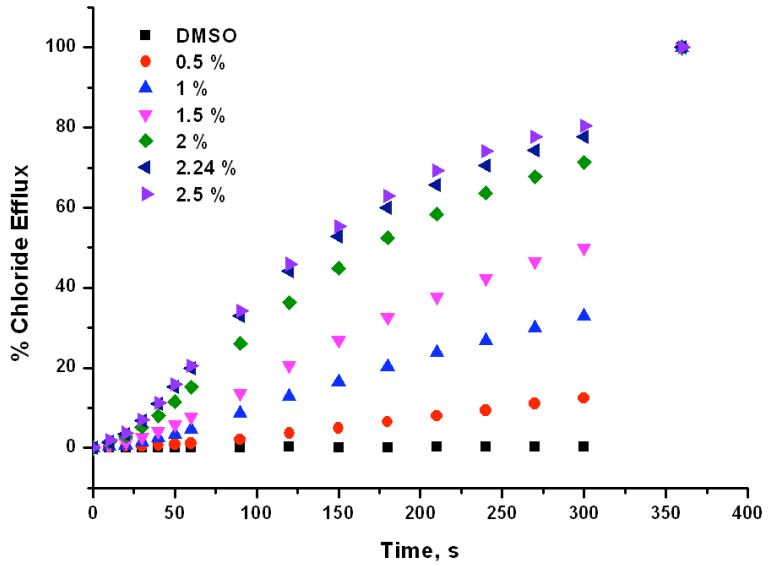

Figure A1.18 Chloride efflux promoted by various concentrations receptor **165** from unilamllar POPC vesicles containing 489 mM NaCl buffered to pH 7.2 with 5 mM sodium phosphate salts. The vesicles were suspended in 489 mM $NaNO_3$ buffered to pH 7.2 with 5 mM sodium phosphate salts. At the end of the experiment, the vesicles were lysed to calibrate 100 % chloride efflux. Each point represents the average of 3 trials. All standard deviations are < 5 %.

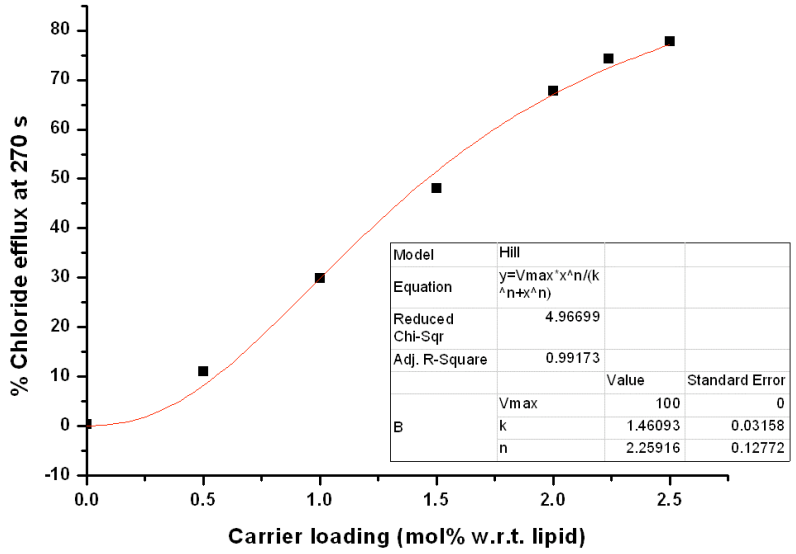

Figure A1.19 Hill plot for the Cl^-/NO_3^- antiport promoted by receptor **165**. The data was fitted to the Hill equation using Origin® 8.1.

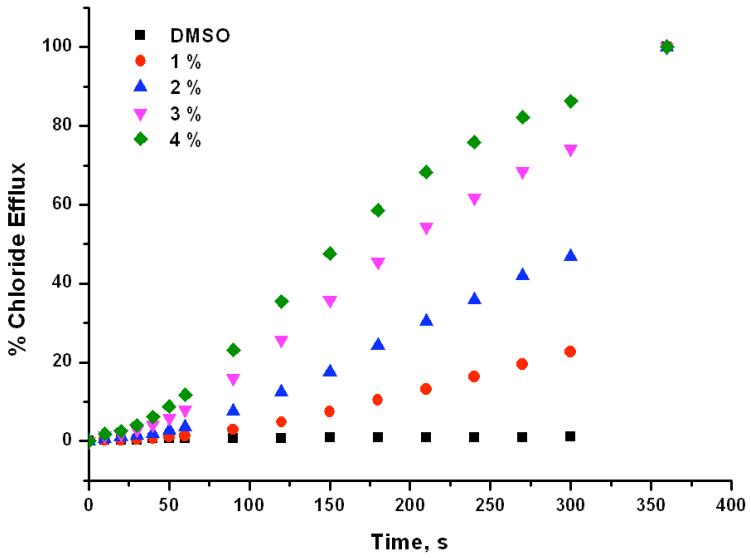

Figure A1.20 Chloride efflux promoted by various concentrations receptor **166** from unilamllar POPC vesicles containing 489 mM NaCl buffered to pH 7.2 with 5 mM sodium phosphate salts. The vesicles were suspended in 489 mM $NaNO_3$ buffered to pH 7.2 with 5 mM sodium phosphate salts. At the end of the experiment, the vesicles were lysed to calibrate 100 % chloride efflux. Each point represents the average of 3 trials. All standard deviations are < 5 %.

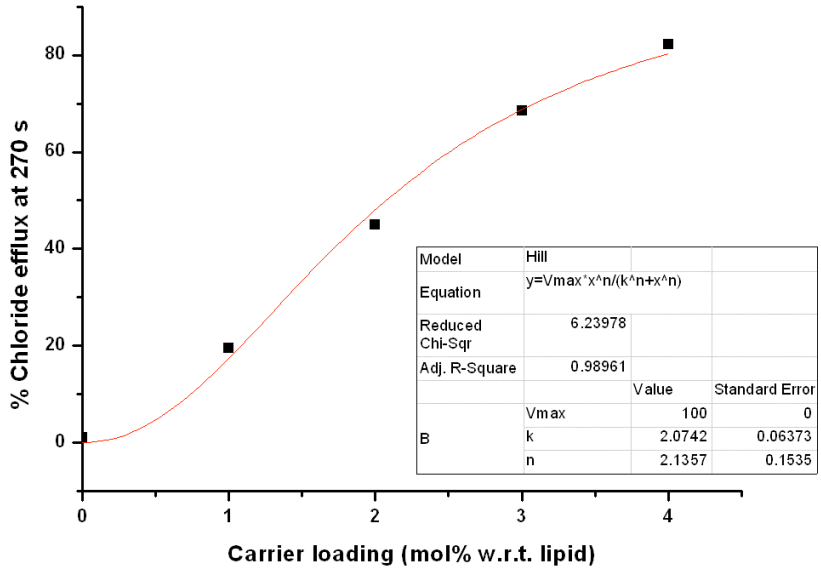

Figure A1.21 Hill plot for the Cl^-/NO_3^- antiport promoted by receptor **166**. The data was fitted to the Hill equation using Origin® 8.1.

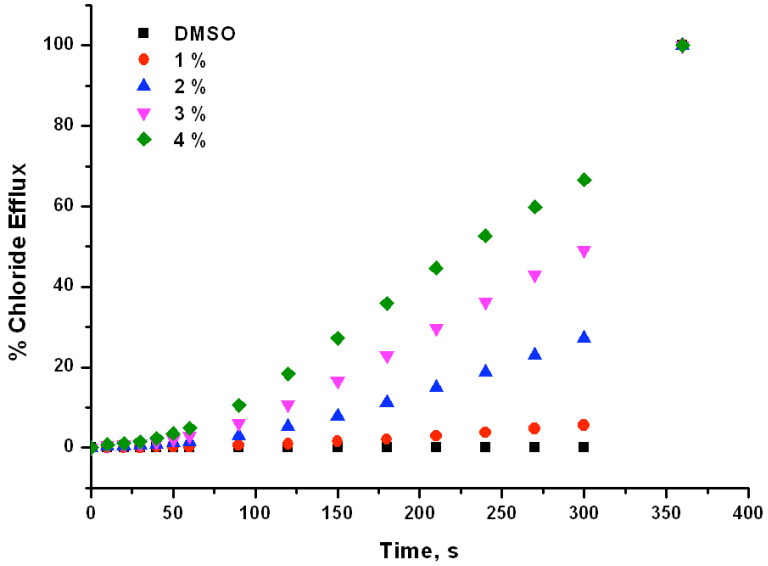

Figure A1.22 Chloride efflux promoted by various concentrations receptor **167** from unilamllar POPC vesicles containing 489 mM NaCl buffered to pH 7.2 with 5 mM sodium phosphate salts. The vesicles were suspended in 489 mM $NaNO_3$ buffered to pH 7.2 with 5 mM sodium phosphate salts. At the end of the experiment, the vesicles were lysed to calibrate 100 % chloride efflux. Each point represents the average of 3 trials. All standard deviations are < 5 %.

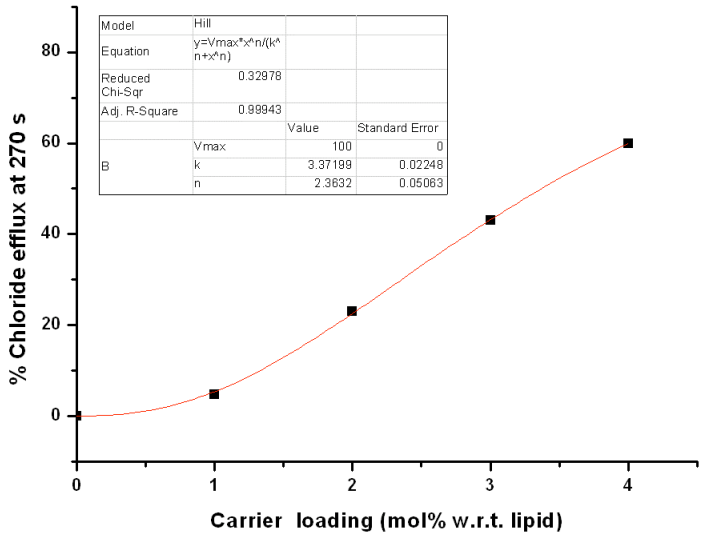

Figure A1.23 Hill plot for the Cl^-/NO_3^- antiport promoted by receptor **167**. The data was fitted to the Hill equation using Origin® 8.1.

A1.2.3 Mobility assays- cholesterol

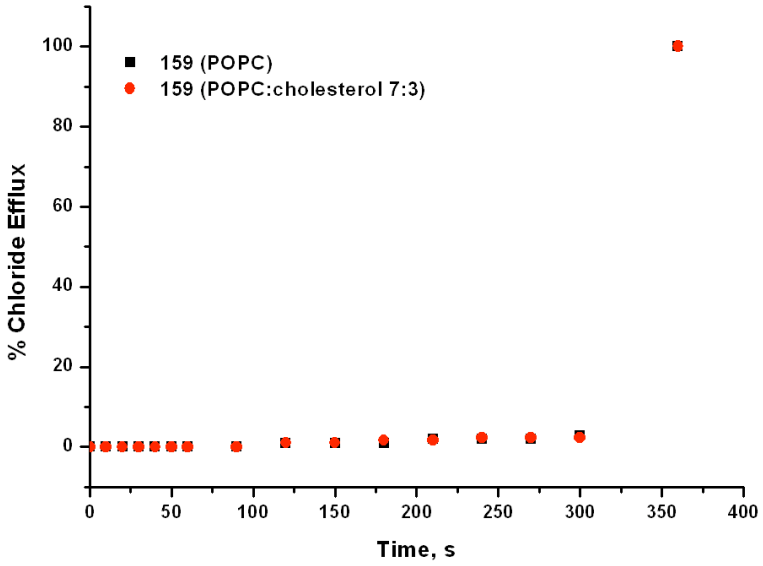

Figure A1.24 Chloride efflux promoted by receptor **159** (2 mol% w.r.t. lipid) from unilamllar vesicles composed of POPC or POPC:cholesterol (7:3) containing 489 mM NaCl buffered to pH 7.2 with 5 mM sodium phosphate salts. The vesicles were suspended in 167 mM Na_2SO_4 buffered to pH 7.2 with 5 mM sodium phosphate salts. At the end of the experiment, the vesicles were lysed to calibrate 100 % chloride efflux. Each point represents the average of 3 trials. All standard deviations are < 5 %.

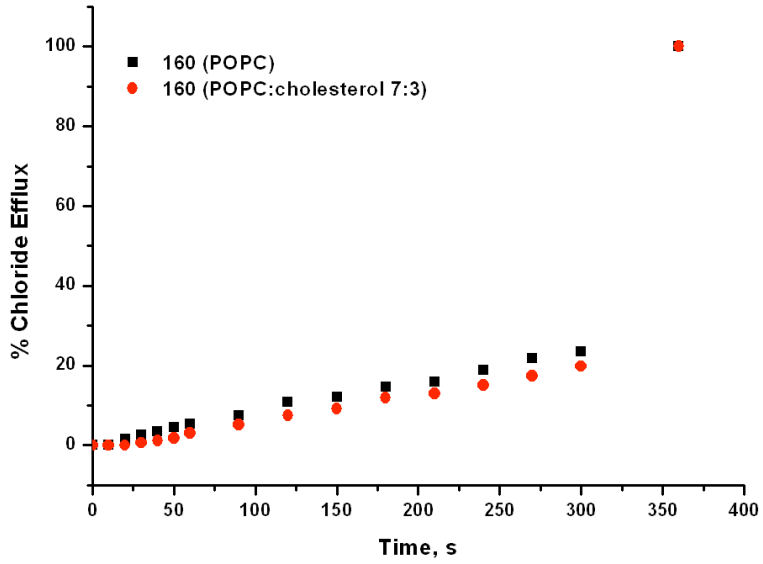

Figure A1.25 Chloride efflux promoted by receptor **160** (2 mol% w.r.t. lipid) from unilamllar vesicles composed of POPC or POPC:cholesterol (7:3) containing 489 mM NaCl buffered to pH 7.2 with 5 mM sodium phosphate salts. The vesicles were suspended in 167 mM Na_2SO_4 buffered to pH 7.2 with 5 mM sodium phosphate salts. At the end of the experiment, the vesicles were lysed to calibrate 100 % chloride efflux. Each point represents the average of 3 trials. All standard deviations are < 5 %.

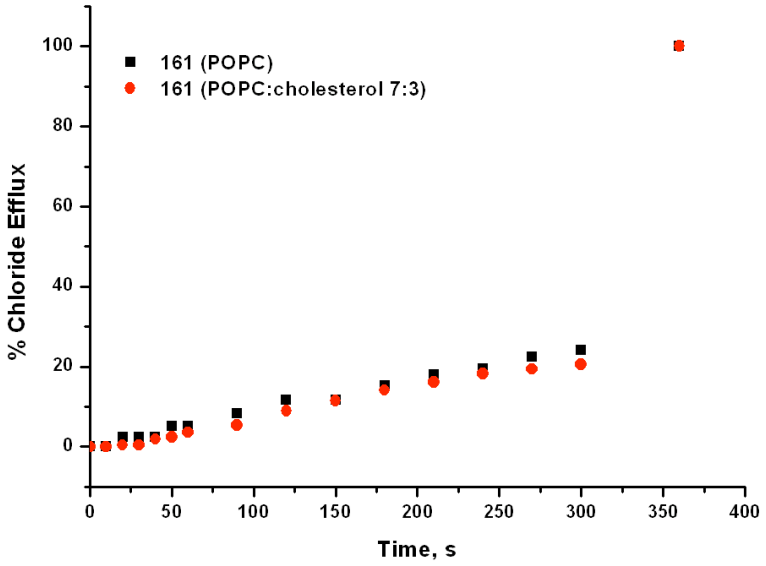

Figure A1.26 Chloride efflux promoted by receptor **161** (2 mol% w.r.t. lipid) from unilamllar vesicles composed of POPC or POPC:cholesterol (7:3) containing 489 mM NaCl buffered to pH 7.2 with 5 mM sodium phosphate salts. The vesicles were suspended in 167 mM Na_2SO_4 buffered to pH 7.2 with 5 mM sodium phosphate salts. At the end of the experiment, the vesicles were lysed to calibrate 100 % chloride efflux. Each point represents the average of 3 trials. All standard deviations are < 5 %.

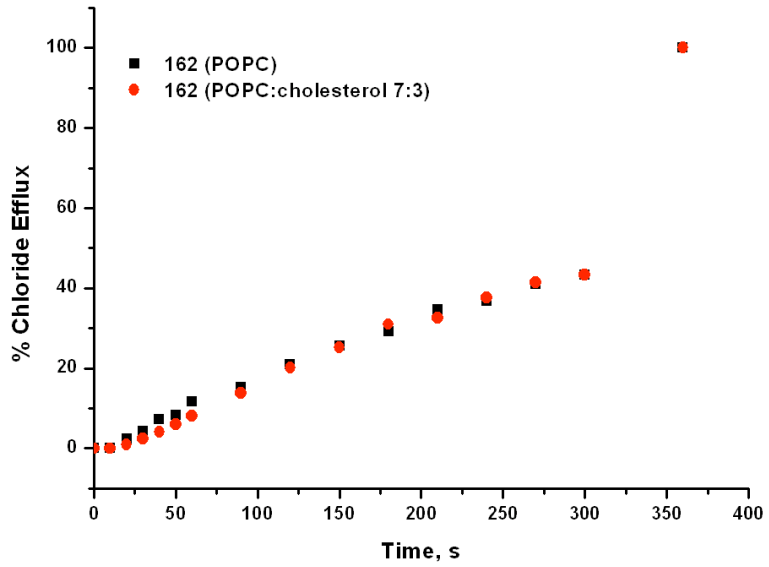

Figure A1.27 Chloride efflux promoted by receptor **162** (2 mol% w.r.t. lipid) from unilamllar vesicles composed of POPC or POPC:cholesterol (7:3) containing 489 mM NaCl buffered to pH 7.2 with 5 mM sodium phosphate salts. The vesicles were suspended in 167 mM Na_2SO_4 buffered to pH 7.2 with 5 mM sodium phosphate salts. At the end of the experiment, the vesicles were lysed to calibrate 100 % chloride efflux. Each point represents the average of 3 trials. All standard deviations are < 5 %.

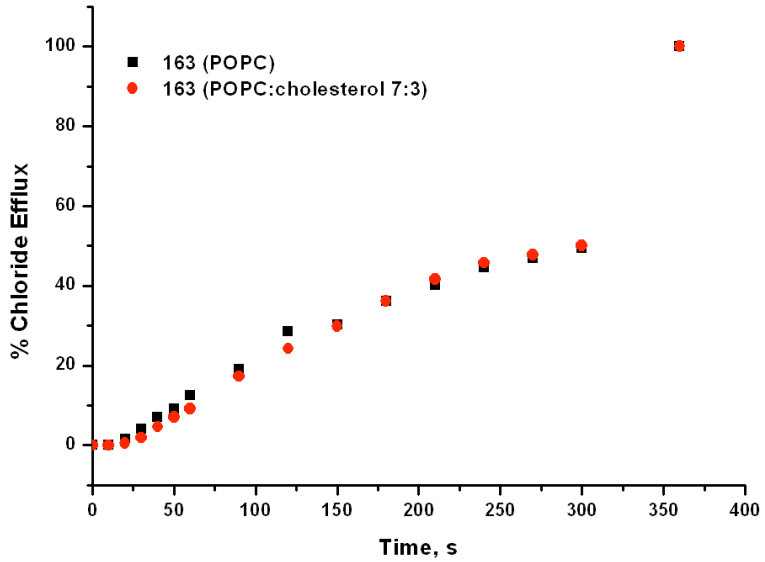

Figure A1.28 Chloride efflux promoted by receptor **163** (2 mol% w.r.t. lipid) from unilamllar vesicles composed of POPC or POPC:cholesterol (7:3) containing 489 mM NaCl buffered to pH 7.2 with 5 mM sodium phosphate salts. The vesicles were suspended in 167 mM Na_2SO_4 buffered to pH 7.2 with 5 mM sodium phosphate salts. At the end of the experiment, the vesicles were lysed to calibrate 100 % chloride efflux. Each point represents the average of 3 trials. All standard deviations are < 5 %.

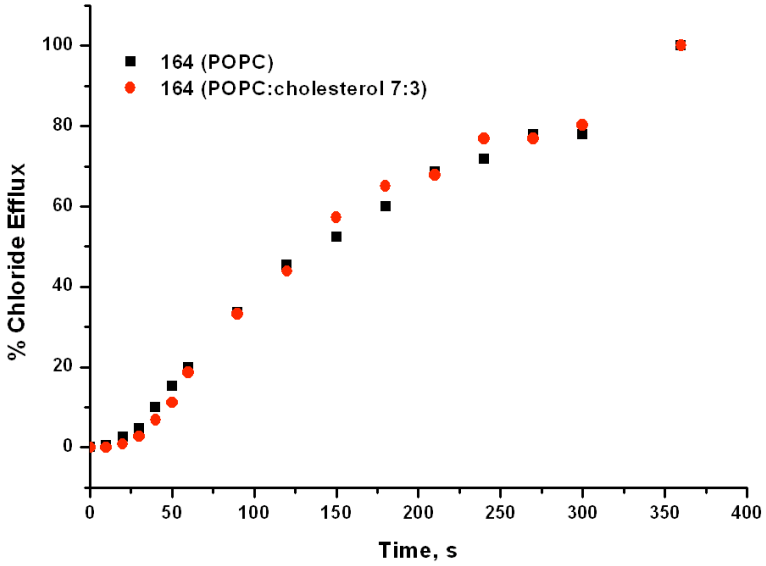

Figure A1.29 Chloride efflux promoted by receptor **164** (2 mol% w.r.t. lipid) from unilamllar vesicles composed of POPC or POPC:cholesterol (7:3) containing 489 mM NaCl buffered to pH 7.2 with 5 mM sodium phosphate salts. The vesicles were suspended in 167 mM Na_2SO_4 buffered to pH 7.2 with 5 mM sodium phosphate salts. At the end of the experiment, the vesicles were lysed to calibrate 100 % chloride efflux. Each point represents the average of 3 trials. All standard deviations are < 5 %.

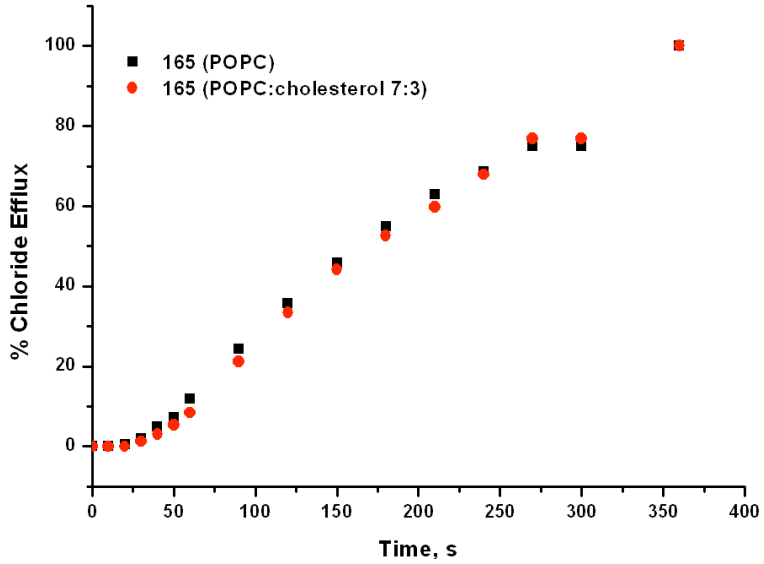

Figure A1.30 Chloride efflux promoted by receptor **165** (2 mol% w.r.t. lipid) from unilamllar vesicles composed of POPC or POPC:cholesterol (7:3) containing 489 mM NaCl buffered to pH 7.2 with 5 mM sodium phosphate salts. The vesicles were suspended in 167 mM Na_2SO_4 buffered to pH 7.2 with 5 mM sodium phosphate salts. At the end of the experiment, the vesicles were lysed to calibrate 100 % chloride efflux. Each point represents the average of 3 trials. All standard deviations are < 5 %.

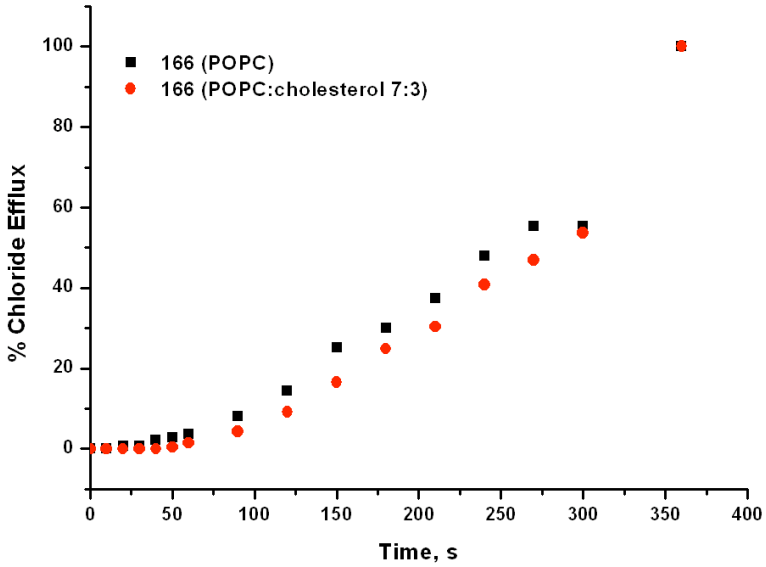

Figure A1.31 Chloride efflux promoted by receptor **166** (2 mol% w.r.t. lipid) from unilamllar vesicles composed of POPC or POPC:cholesterol (7:3) containing 489 mM NaCl buffered to pH 7.2 with 5 mM sodium phosphate salts. The vesicles were suspended in 167 mM Na_2SO_4 buffered to pH 7.2 with 5 mM sodium phosphate salts. At the end of the experiment, the vesicles were lysed to calibrate 100 % chloride efflux. Each point represents the average of 3 trials. All standard deviations are < 5 %.

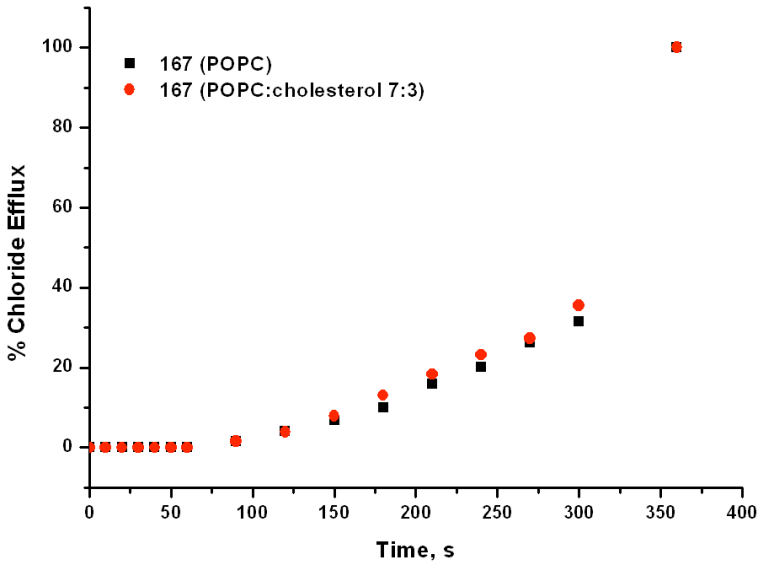

Figure A1.32 Chloride efflux promoted by receptor **167** (2 mol% w.r.t. lipid) from unilamllar vesicles composed of POPC or POPC:cholesterol (7:3) containing 489 mM NaCl buffered to pH 7.2 with 5 mM sodium phosphate salts. The vesicles were suspended in 167 mM Na_2SO_4 buffered to pH 7.2 with 5 mM sodium phosphate salts. At the end of the experiment, the vesicles were lysed to calibrate 100 % chloride efflux. Each point represents the average of 3 trials. All standard deviations are < 5 %.

A1.3 Additional transport studies from Chapter 4

A1.3.1 Mechanistic studies

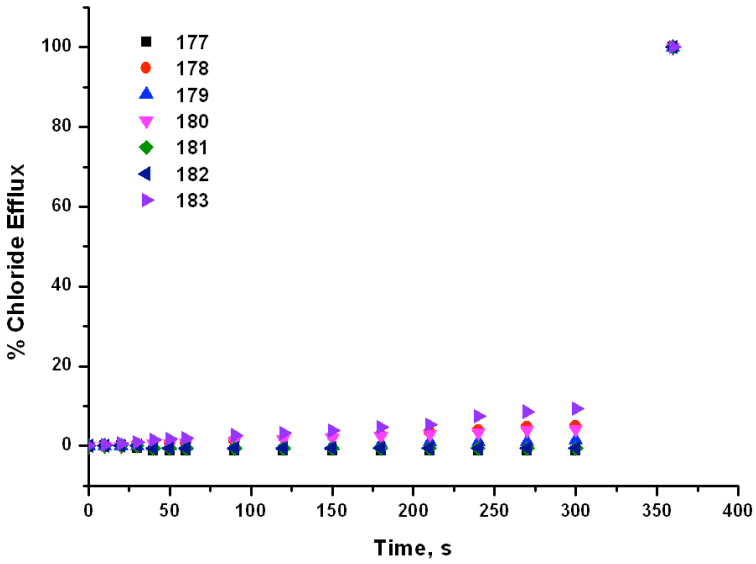

Figure A1.33 Chloride efflux promoted by receptors **177**-**183** from unilamllar POPC vesicles containing 489 mM NaCl buffered to pH 7.2 with 5 mM sodium phosphate salts. The vesicles were suspended in 167 mM Na_2SO_4 buffered to pH 7.2 with 5 mM sodium phosphate salts. At the end of the experiment, the vesicles were lysed to calibrate 100 % chloride efflux. Each point represents the average of 3 trials. All standard deviations are < 5 %.

A1.3.2 Hill analyses: Cl^-/NO_3^- antiport

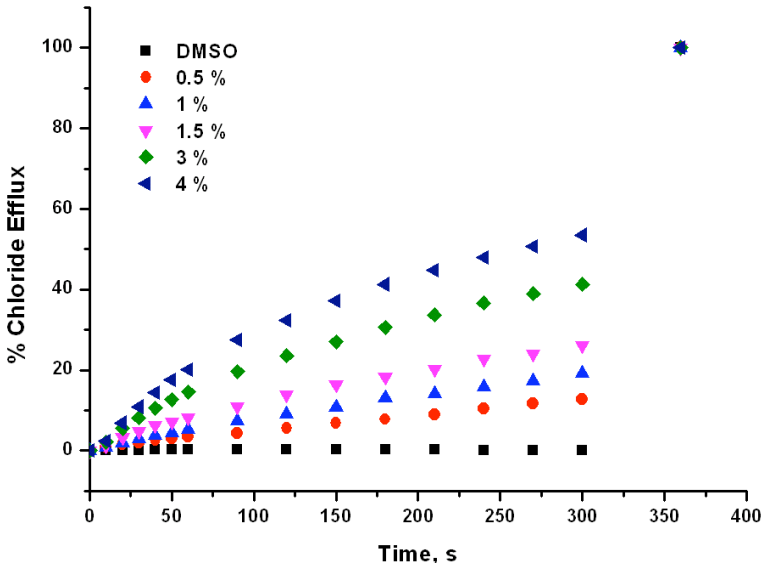

Figure A1.34 Chloride efflux promoted by various concentrations receptor **177** from unilamllar POPC vesicles containing 489 mM NaCl buffered to pH 7.2 with 5 mM sodium phosphate salts. The vesicles were suspended in 489 mM $NaNO_3$ buffered to pH 7.2 with 5 mM sodium phosphate salts. At the end of the experiment, the vesicles were lysed to calibrate 100 % chloride efflux. Each point represents the average of 3 trials. All standard deviations are < 5 %.

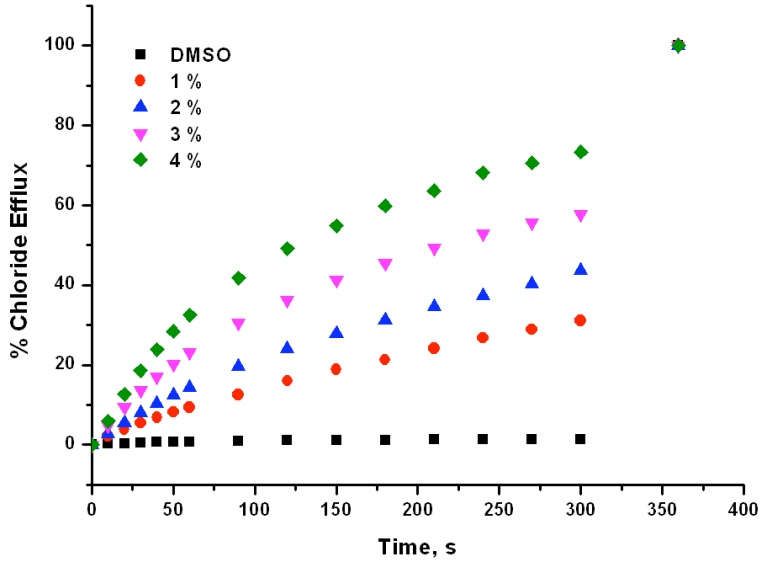

Figure A1.35 Chloride efflux promoted by various concentrations receptor **178** from unilamllar POPC vesicles containing 489 mM NaCl buffered to pH 7.2 with 5 mM sodium phosphate salts. The vesicles were suspended in 489 mM $NaNO_3$ buffered to pH 7.2 with 5 mM sodium phosphate salts. At the end of the experiment, the vesicles were lysed to calibrate 100 % chloride efflux. Each point represents the average of 3 trials. All standard deviations are < 5 %.

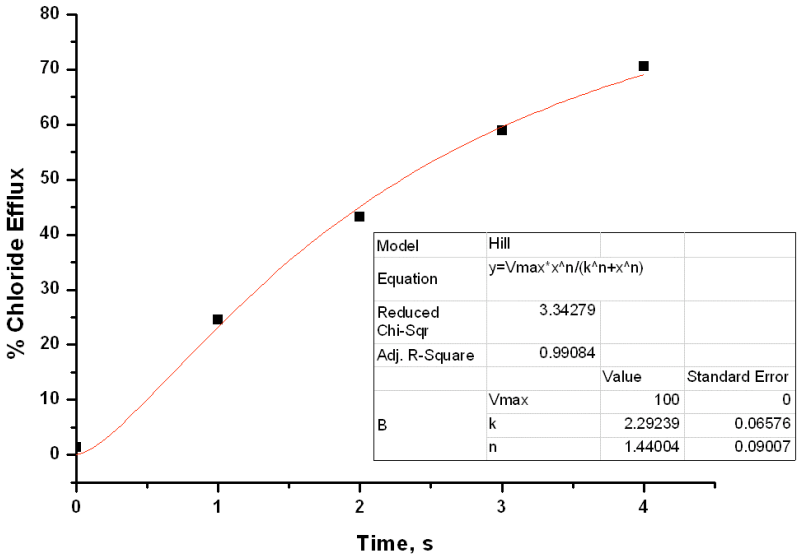

Figure A1.36 Hill plot for the Cl^-/NO_3^- antiport promoted by receptor **178**. The data was fitted to the Hill equation using Origin® 8.1.

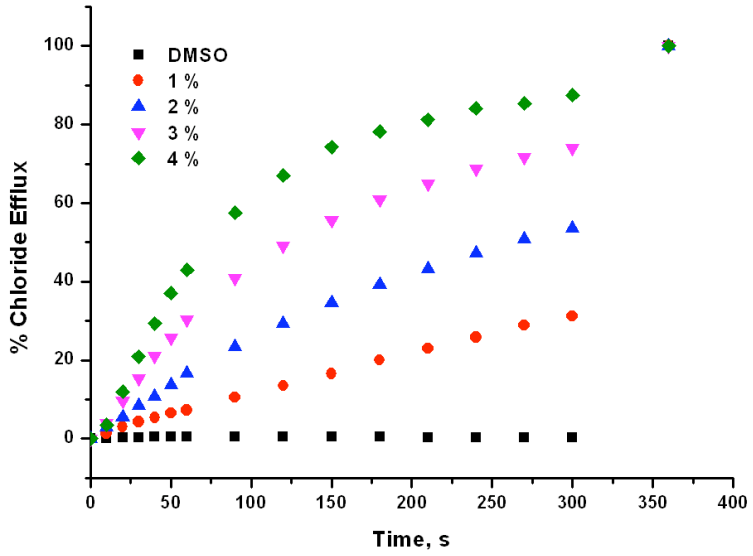

Figure A1.37 Chloride efflux promoted by various concentrations receptor **179** from unilamllar POPC vesicles containing 489 mM NaCl buffered to pH 7.2 with 5 mM sodium phosphate salts. The vesicles were suspended in 489 mM $NaNO_3$ buffered to pH 7.2 with 5 mM sodium phosphate salts. At the end of the experiment, the vesicles were lysed to calibrate 100 % chloride efflux. Each point represents the average of 3 trials. All standard deviations are < 5 %.

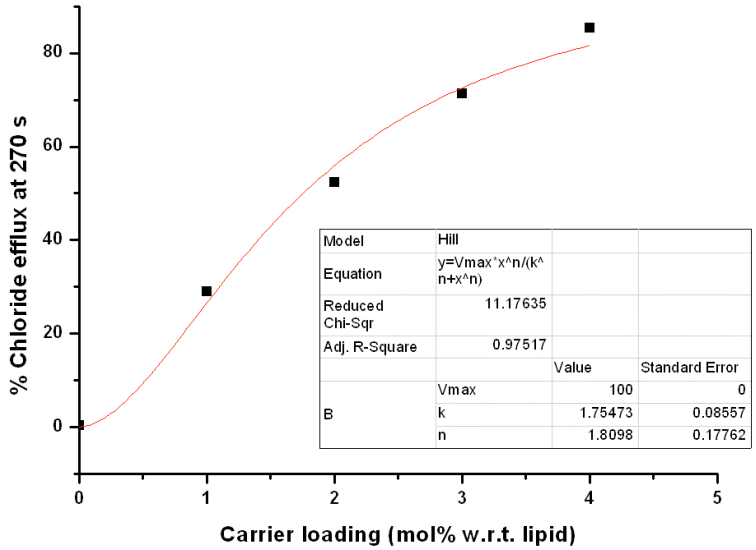

Figure A1.38 Hill plot for the Cl^-/NO_3^- antiport promoted by receptor **179**. The data was fitted to the Hill equation using Origin® 8.1.

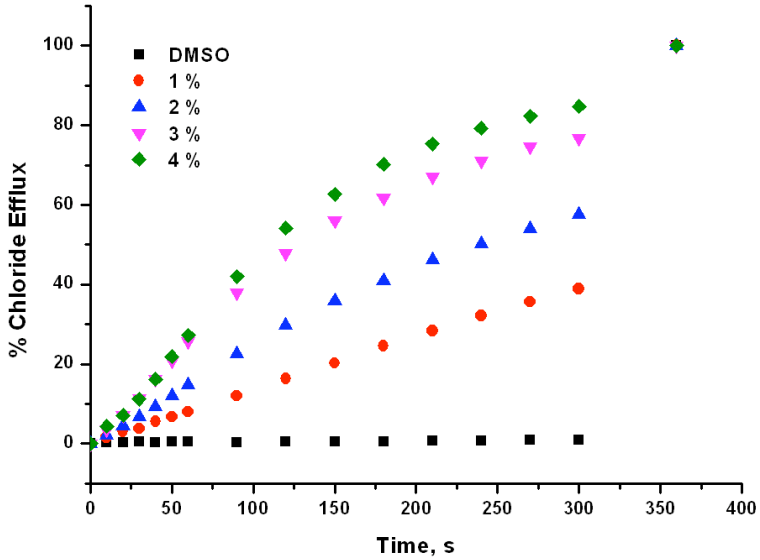

Figure A1.39 Chloride efflux promoted by various concentrations receptor **180** from unilamllar POPC vesicles containing 489 mM NaCl buffered to pH 7.2 with 5 mM sodium phosphate salts. The vesicles were suspended in 489 mM $NaNO_3$ buffered to pH 7.2 with 5 mM sodium phosphate salts. At the end of the experiment, the vesicles were lysed to calibrate 100 % chloride efflux. Each point represents the average of 3 trials. All standard deviations are < 5 %.

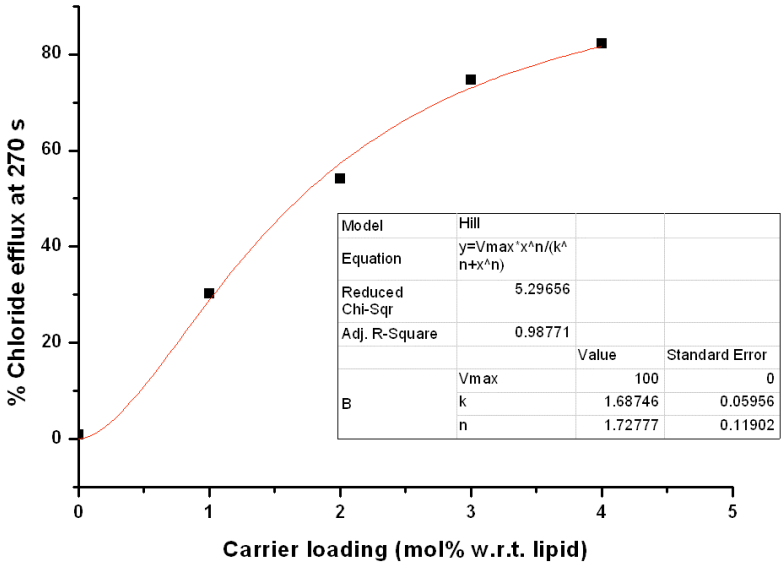

Figure A1.40 Hill plot for the Cl^-/NO_3^- antiport promoted by receptor **180**. The data was fitted to the Hill equation using Origin® 8.1.

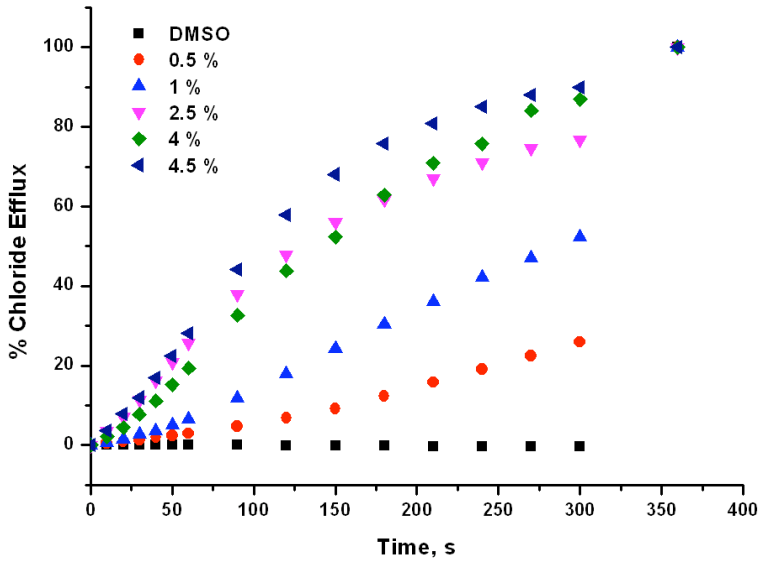

Figure A1.41 Chloride efflux promoted by various concentrations receptor **181** from unilamllar POPC vesicles containing 489 mM NaCl buffered to pH 7.2 with 5 mM sodium phosphate salts. The vesicles were suspended in 489 mM $NaNO_3$ buffered to pH 7.2 with 5 mM sodium phosphate salts. At the end of the experiment, the vesicles were lysed to calibrate 100 % chloride efflux. Each point represents the average of 3 trials. All standard deviations are < 5 %.

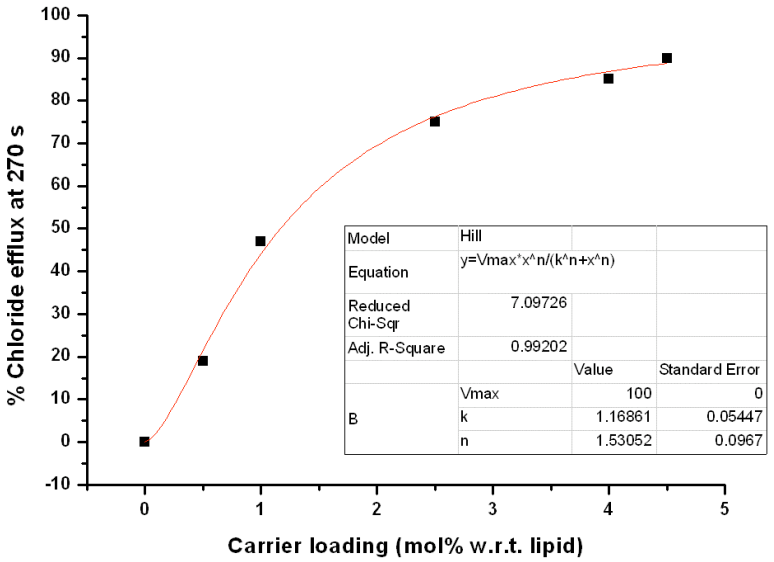

Figure A1.42 Hill plot for the Cl^-/NO_3^- antiport promoted by receptor **181**. The data was fitted to the Hill equation using Origin® 8.1.

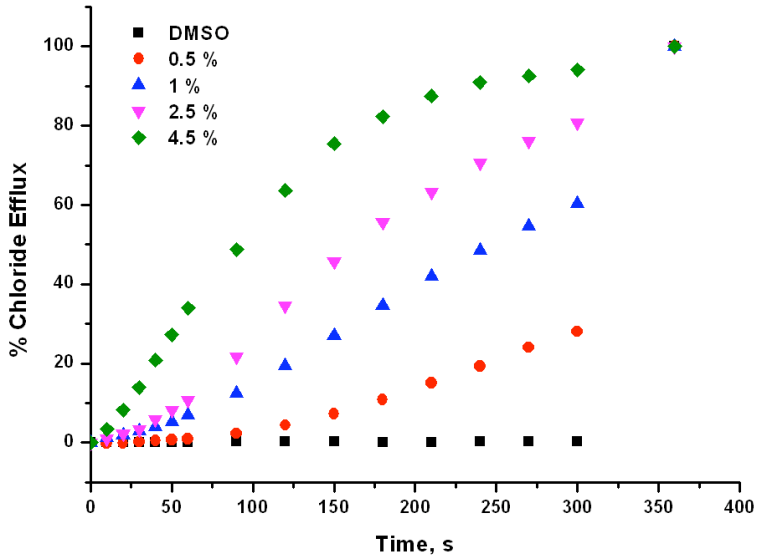

Figure A1.43 Chloride efflux promoted by various concentrations receptor **182** from unilamllar POPC vesicles containing 489 mM NaCl buffered to pH 7.2 with 5 mM sodium phosphate salts. The vesicles were suspended in 489 mM $NaNO_3$ buffered to pH 7.2 with 5 mM sodium phosphate salts. At the end of the experiment, the vesicles were lysed to calibrate 100 % chloride efflux. Each point represents the average of 3 trials. All standard deviations are < 5 %.

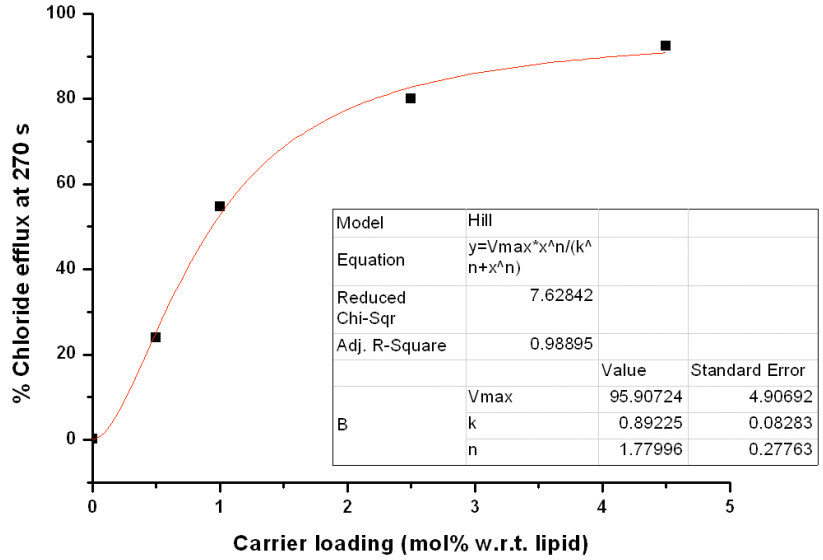

Figure A1.44 Hill plot for the Cl^-/NO_3^- antiport promoted by receptor **182**. The data was fitted to the Hill equation using Origin® 8.1.

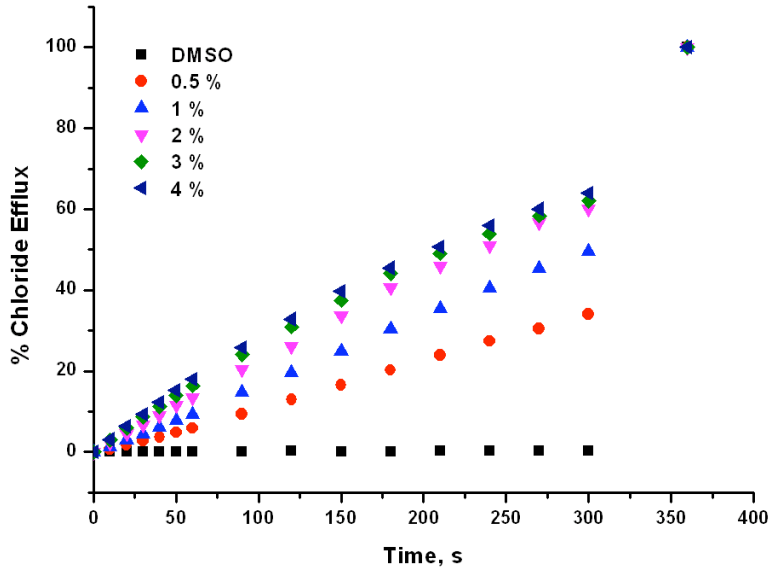

Figure A1.45 Chloride efflux promoted by various concentrations receptor **183** from unilamllar POPC vesicles containing 489 mM NaCl buffered to pH 7.2 with 5 mM sodium phosphate salts. The vesicles were suspended in 489 mM $NaNO_3$ buffered to pH 7.2 with 5 mM sodium phosphate salts. At the end of the experiment, the vesicles were lysed to calibrate 100 % chloride efflux. Each point represents the average of 3 trials. All standard deviations are < 5 %.

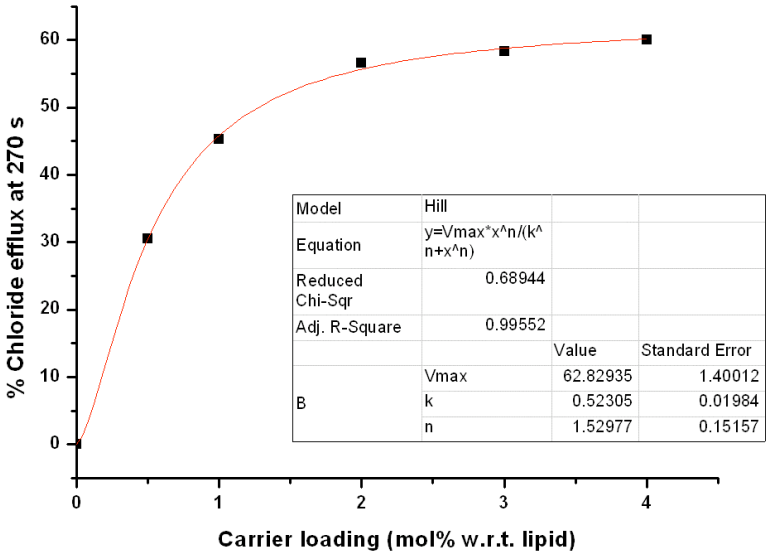

Figure A1.46 Hill plot for the Cl^-/NO_3^- antiport promoted by receptor **183**. The data was fitted to the Hill equation using Origin® 8.1.

A1.3.3 Hill analyses: Cl^-/HCO_3^- antiport

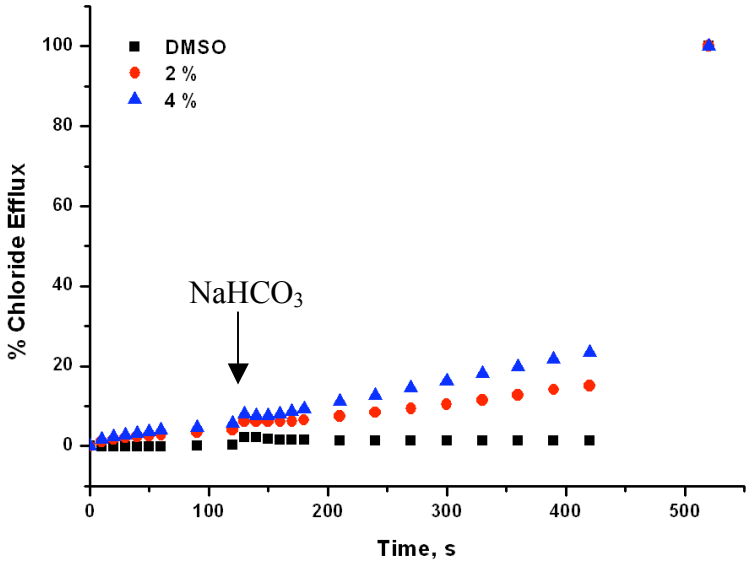

Figure A1.47 Chloride efflux promoted by various concentrations of receptor **177** from unilamllar POPC vesicles containing 489 mM NaCl buffered to pH 7.2 with 20 mM sodium phosphate salts. The vesicles were suspended in 167 mM Na_2SO_4 buffered to pH 7.2 with 20 mM sodium phosphate salts. At t = 120 s, a pulse of $NaHCO_3$ was added such that the final HCO_3^- concentration was 40 mM. At the end of the experiment, the vesicles were lysed to calibrate 100 % chloride efflux. Each point represents the average of 3 trials. All standard deviations are < 5 %.

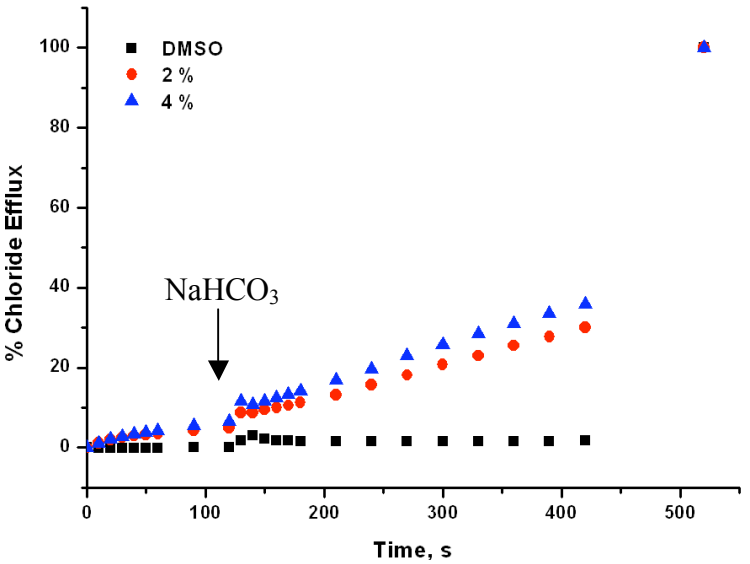

Figure A1.48 Chloride efflux promoted by various concentrations of receptor **178** from unilamllar POPC vesicles containing 489 mM NaCl buffered to pH 7.2 with 20 mM sodium phosphate salts. The vesicles were suspended in 167 mM Na_2SO_4 buffered to pH 7.2 with 20 mM sodium phosphate salts. At t = 120 s, a pulse of $NaHCO_3$ was added such that the final HCO_3^- concentration was 40 mM. At the end of the experiment, the vesicles were lysed to calibrate 100 % chloride efflux. Each point represents the average of 3 trials. All standard deviations are < 5 %.

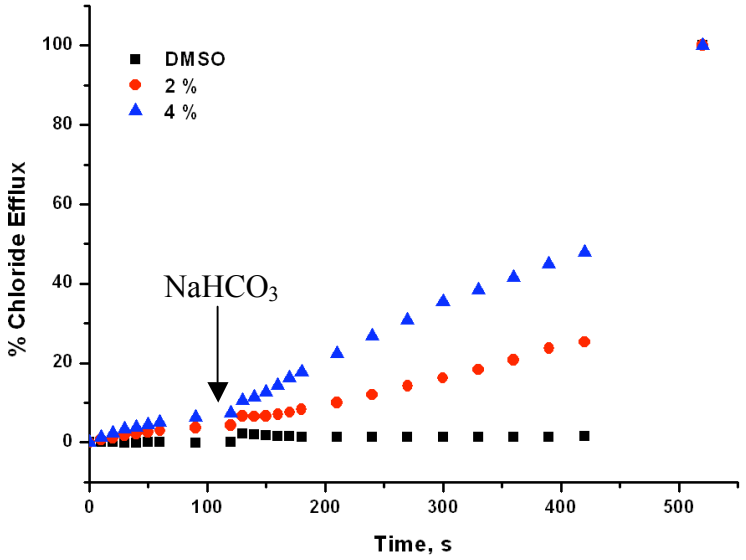

Figure A1.49 Chloride efflux promoted by various concentrations of receptor **179** from unilamllar POPC vesicles containing 489 mM NaCl buffered to pH 7.2 with 20 mM sodium phosphate salts. The vesicles were suspended in 167 mM Na_2SO_4 buffered to pH 7.2 with 20 mM sodium phosphate salts. At t = 120 s, a pulse of $NaHCO_3$ was added such that the final HCO_3^- concentration was 40 mM. At the end of the experiment, the vesicles were lysed to calibrate 100 % chloride efflux. Each point represents the average of 3 trials. All standard deviations are < 5 %.

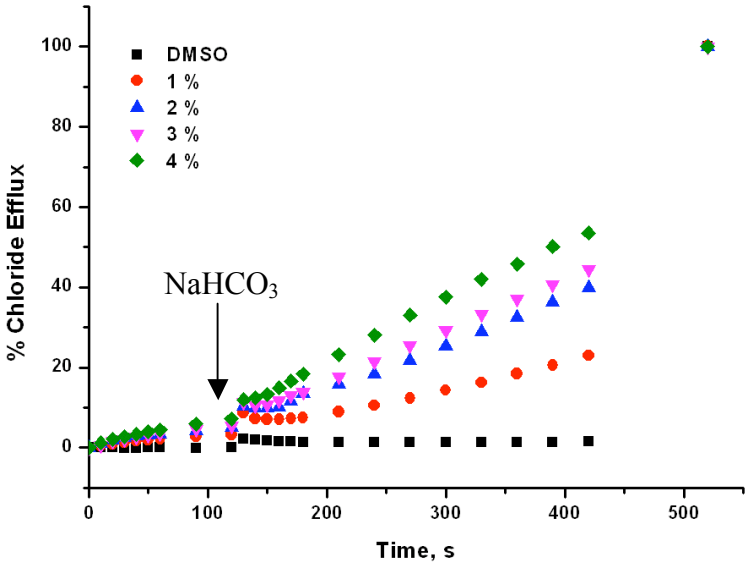

Figure A1.50 Chloride efflux promoted by various concentrations of receptor **180** from unilamllar POPC vesicles containing 489 mM NaCl buffered to pH 7.2 with 20 mM sodium phosphate salts. The vesicles were suspended in 167 mM Na_2SO_4 buffered to pH 7.2 with 20 mM sodium phosphate salts. At t = 120 s, a pulse of $NaHCO_3$ was added such that the final HCO_3^- concentration was 40 mM. At the end of the experiment, the vesicles were lysed to calibrate 100 % chloride efflux. Each point represents the average of 3 trials. All standard deviations are < 5 %.

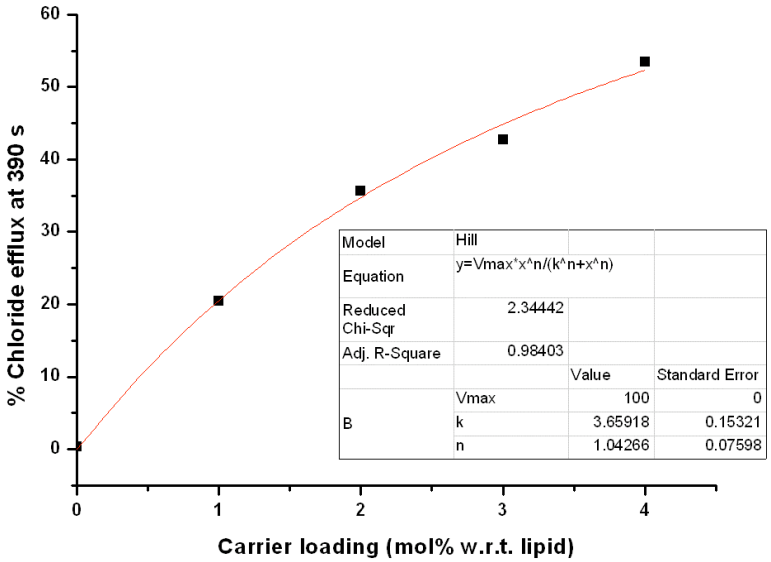

Figure A1.51 Hill plot for the Cl^-/HCO_3^- antiport promoted by receptor **180**. The data was fitted to the Hill equation using Origin® 8.1.

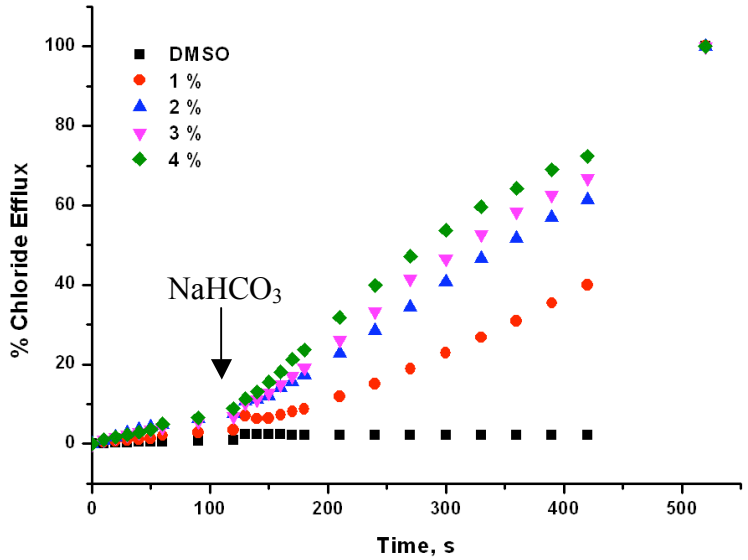

Figure A1.52 Chloride efflux promoted by various concentrations of receptor **181** from unilamllar POPC vesicles containing 489 mM NaCl buffered to pH 7.2 with 20 mM sodium phosphate salts. The vesicles were suspended in 167 mM Na_2SO_4 buffered to pH 7.2 with 20 mM sodium phosphate salts. At t = 120 s, a pulse of $NaHCO_3$ was added such that the final HCO_3^- concentration was 40 mM. At the end of the experiment, the vesicles were lysed to calibrate 100 % chloride efflux. Each point represents the average of 3 trials. All standard deviations are < 5 %.

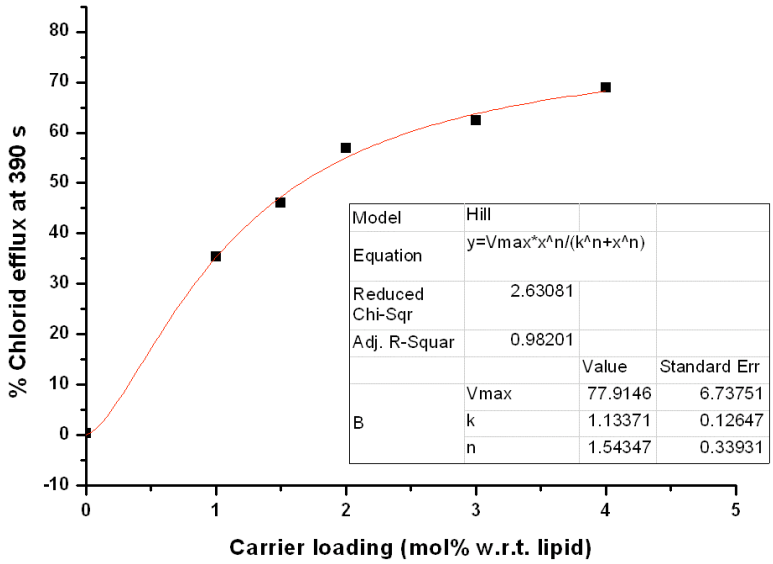

Figure A1.53 Hill plot for the Cl^-/HCO_3^- antiport promoted by receptor **181**. The data was fitted to the Hill equation using Origin® 8.1.

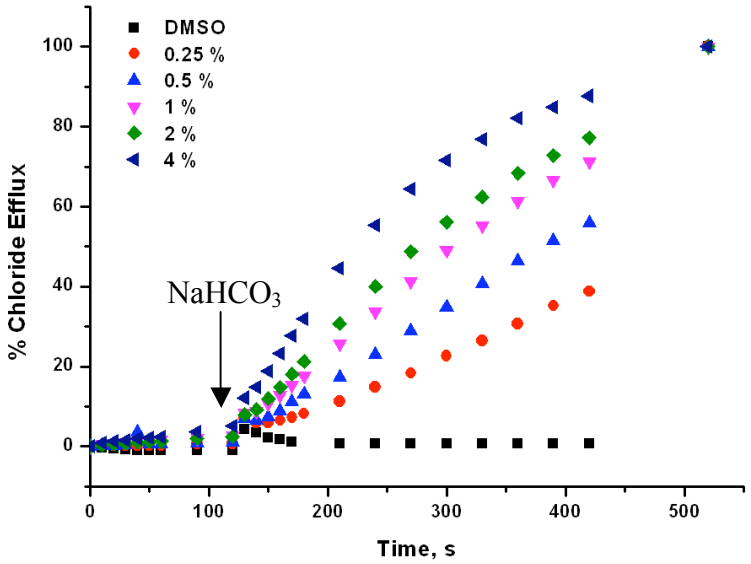

Figure A1.54 Chloride efflux promoted by various concentrations of receptor **182** from unilamllar POPC vesicles containing 489 mM NaCl buffered to pH 7.2 with 20 mM sodium phosphate salts. The vesicles were suspended in 167 mM Na_2SO_4 buffered to pH 7.2 with 20 mM sodium phosphate salts. At t = 120 s, a pulse of $NaHCO_3$ was added such that the final HCO_3^- concentration was 40 mM. At the end of the experiment, the vesicles were lysed to calibrate 100 % chloride efflux. Each point represents the average of 3 trials. All standard deviations are < 5 %.

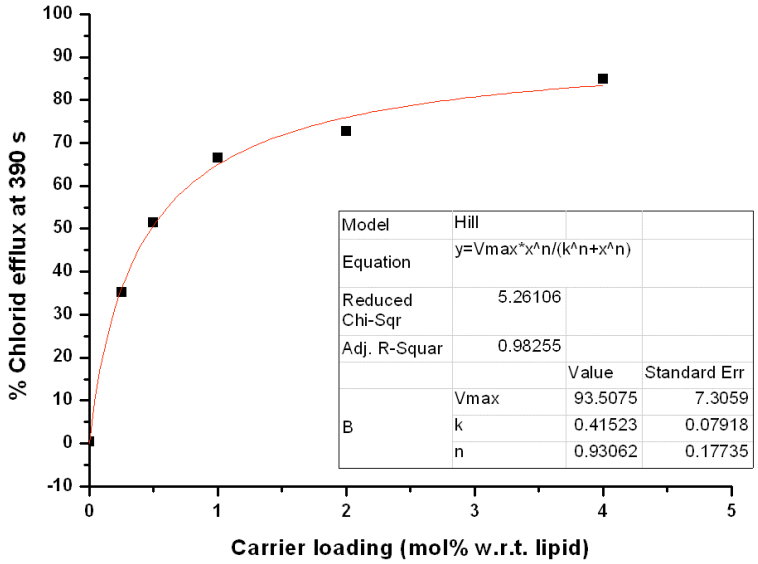

Figure A1.55 Hill plot for the Cl^-/HCO_3^- antiport promoted by receptor **182**. The data was fitted to the Hill equation using Origin® 8.1.

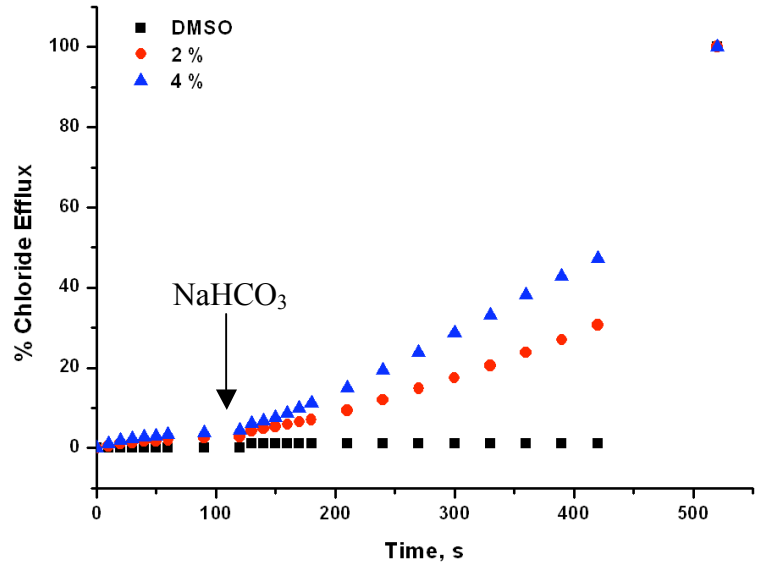

Figure A1.56 Chloride efflux promoted by various concentrations of receptor **183** from unilamllar POPC vesicles containing 489 mM NaCl buffered to pH 7.2 with 20 mM sodium phosphate salts. The vesicles were suspended in 167 mM Na_2SO_4 buffered to pH 7.2 with 20 mM sodium phosphate salts. At t = 120 s, a pulse of $NaHCO_3$ was added such that the final HCO_3^- concentration was 40 mM. At the end of the experiment, the vesicles were lysed to calibrate 100 % chloride efflux. Each point represents the average of 3 trials. All standard deviations are < 5 %.

A1.3.4 Mobility assays- cholesterol

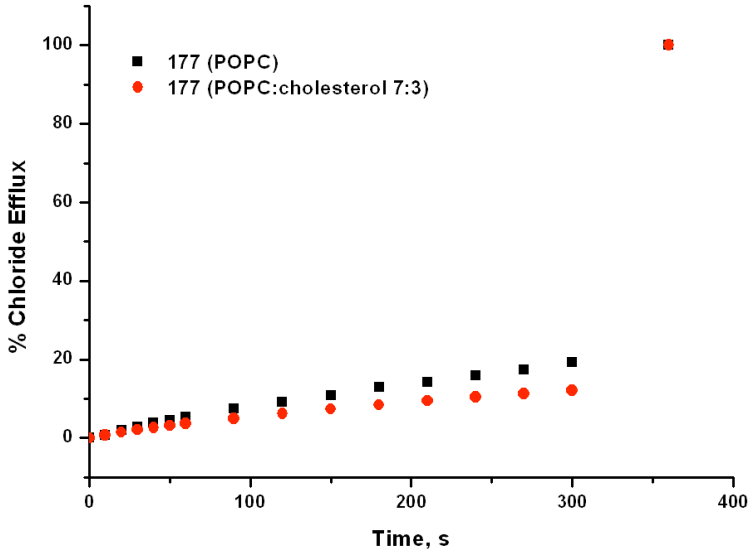

Figure A1.57 Chloride efflux promoted by receptor **177** (1 mol% w.r.t. lipid) from unilamllar vesicles composed of POPC or POPC:cholesterol (7:3) containing 489 mM NaCl buffered to pH 7.2 with 5 mM sodium phosphate salts. The vesicles were suspended in 167 mM Na_2SO_4 buffered to pH 7.2 with 5 mM sodium phosphate salts. At the end of the experiment, the vesicles were lysed to calibrate 100 % chloride efflux. Each point represents the average of 3 trials. All standard deviations are < 5 %.

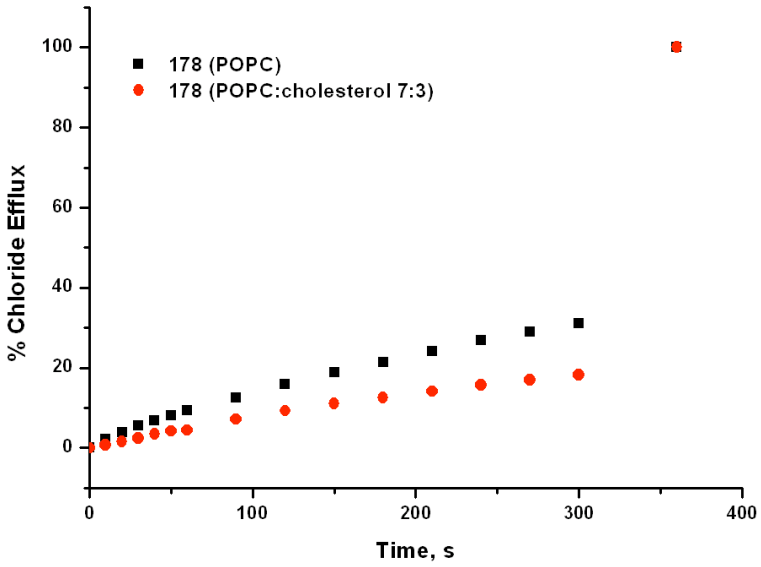

Figure A1.58 Chloride efflux promoted by receptor **178** (1 mol% w.r.t. lipid) from unilamllar vesicles composed of POPC or POPC:cholesterol (7:3) containing 489 mM NaCl buffered to pH 7.2 with 5 mM sodium phosphate salts. The vesicles were suspended in 167 mM Na_2SO_4 buffered to pH 7.2 with 5 mM sodium phosphate salts. At the end of the experiment, the vesicles were lysed to calibrate 100 % chloride efflux. Each point represents the average of 3 trials. All standard deviations are < 5 %.

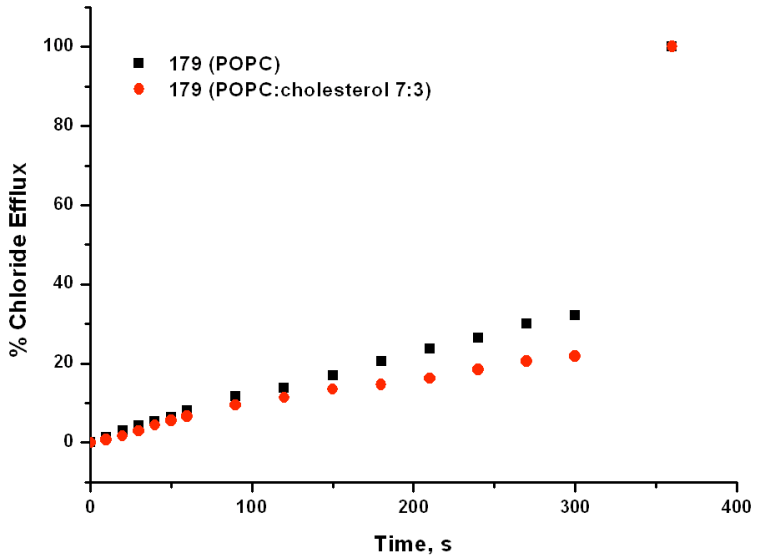

Figure A1.59 Chloride efflux promoted by receptor **179** (1 mol% w.r.t. lipid) from unilamllar vesicles composed of POPC or POPC:cholesterol (7:3) containing 489 mM NaCl buffered to pH 7.2 with 5 mM sodium phosphate salts. The vesicles were suspended in 167 mM Na_2SO_4 buffered to pH 7.2 with 5 mM sodium phosphate salts. At the end of the experiment, the vesicles were lysed to calibrate 100 % chloride efflux. Each point represents the average of 3 trials. All standard deviations are < 5 %.

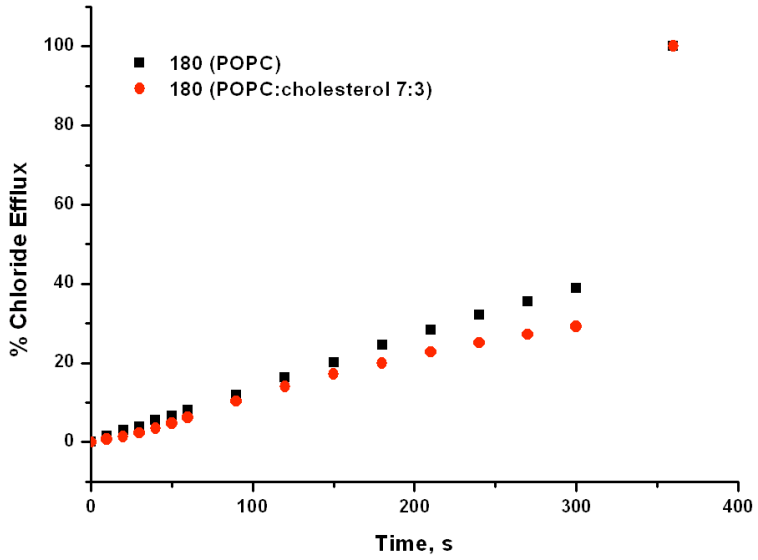

Figure A1.60 Chloride efflux promoted by receptor **180** (1 mol% w.r.t. lipid) from unilamllar vesicles composed of POPC or POPC:cholesterol (7:3) containing 489 mM NaCl buffered to pH 7.2 with 5 mM sodium phosphate salts. The vesicles were suspended in 167 mM Na_2SO_4 buffered to pH 7.2 with 5 mM sodium phosphate salts. At the end of the experiment, the vesicles were lysed to calibrate 100 % chloride efflux. Each point represents the average of 3 trials. All standard deviations are < 5 %.

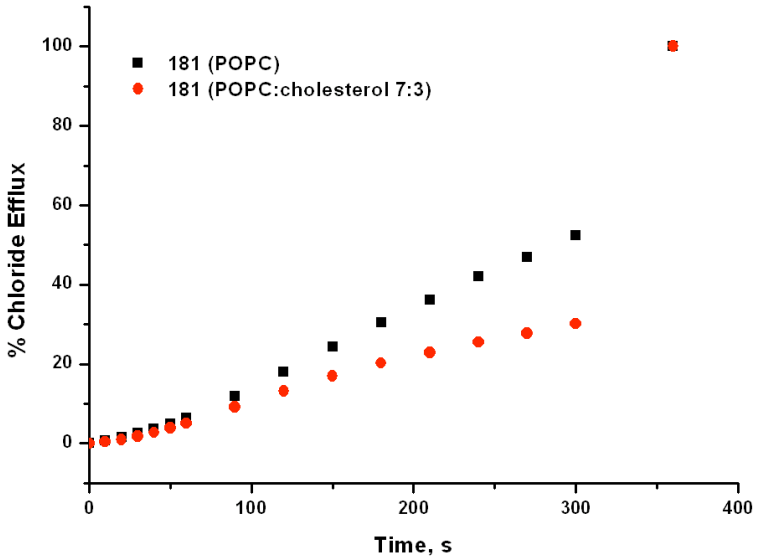

Figure A1.61 Chloride efflux promoted by receptor **181** (1 mol% w.r.t. lipid) from unilamllar vesicles composed of POPC or POPC:cholesterol (7:3) containing 489 mM NaCl buffered to pH 7.2 with 5 mM sodium phosphate salts. The vesicles were suspended in 167 mM Na_2SO_4 buffered to pH 7.2 with 5 mM sodium phosphate salts. At the end of the experiment, the vesicles were lysed to calibrate 100 % chloride efflux. Each point represents the average of 3 trials. All standard deviations are < 5 %.

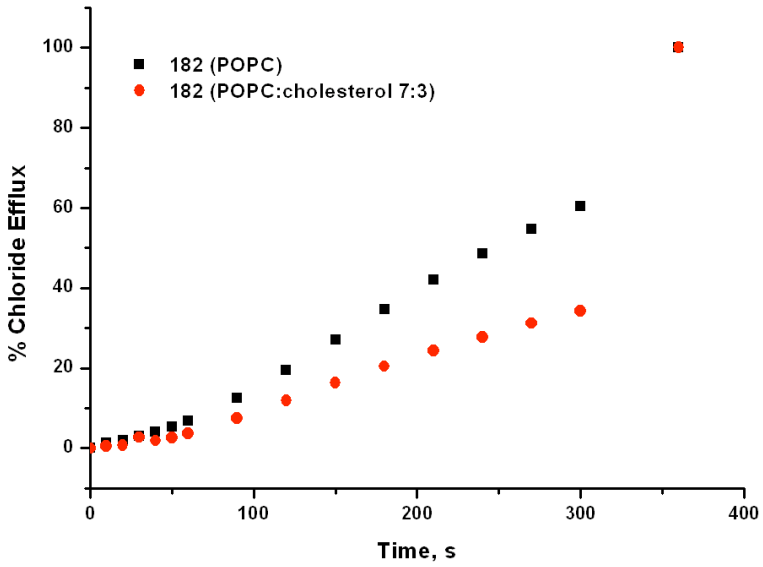

Figure A1.62 Chloride efflux promoted by receptor **182** (1 mol% w.r.t. lipid) from unilamllar vesicles composed of POPC or POPC:cholesterol (7:3) containing 489 mM NaCl buffered to pH 7.2 with 5 mM sodium phosphate salts. The vesicles were suspended in 167 mM Na_2SO_4 buffered to pH 7.2 with 5 mM sodium phosphate salts. At the end of the experiment, the vesicles were lysed to calibrate 100 % chloride efflux. Each point represents the average of 3 trials. All standard deviations are < 5 %.

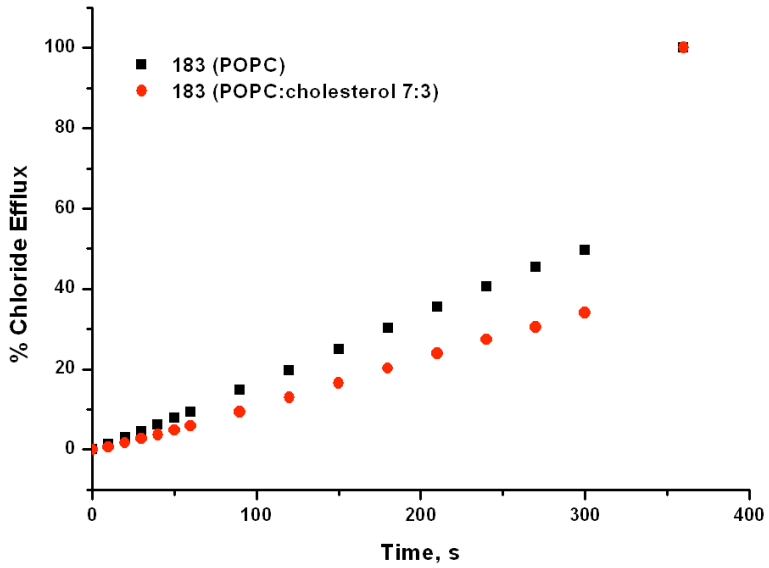

Figure A1.63 Chloride efflux promoted by receptor **183** (1 mol% w.r.t. lipid) from unilamllar vesicles composed of POPC or POPC:cholesterol (7:3) containing 489 mM NaCl buffered to pH 7.2 with 5 mM sodium phosphate salts. The vesicles were suspended in 167 mM Na_2SO_4 buffered to pH 7.2 with 5 mM sodium phosphate salts. At the end of the experiment, the vesicles were lysed to calibrate 100 % chloride efflux. Each point represents the average of 3 trials. All standard deviations are < 5 %.

A1.4 Additional transport studies from Chapter 5

A1.4.1 Mobility assay

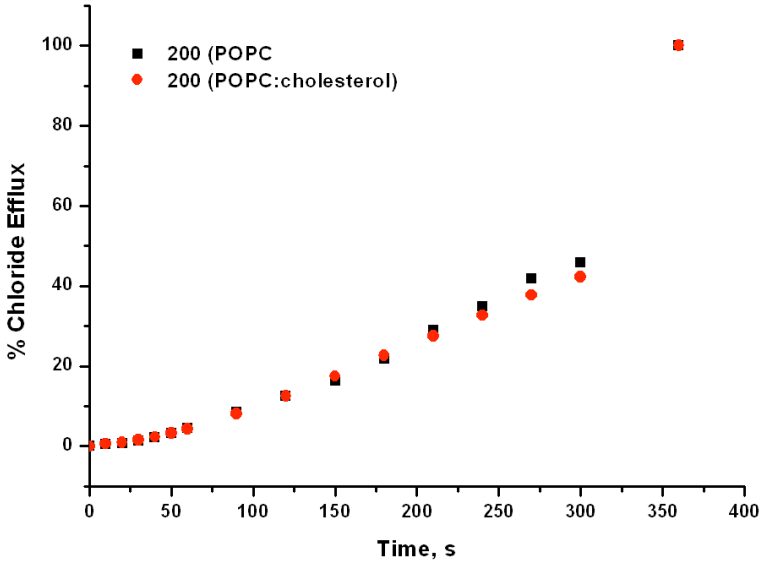

Figure A1.64 Chloride efflux promoted by receptor **200** (4 mol% w.r.t. lipid) from unilamllar vesicles composed of POPC or POPC:cholesterol (7:3) containing 489 mM NaCl buffered to pH 7.2 with 5 mM sodium phosphate salts. The vesicles were suspended in 167 mM Na_2SO_4 buffered to pH 7.2 with 5 mM sodium phosphate salts. At the end of the experiment, the vesicles were lysed to calibrate 100 % chloride efflux. Each point represents the average of 3 trials. All standard deviations are < 5 %.

A1.4.2 Hill analysis

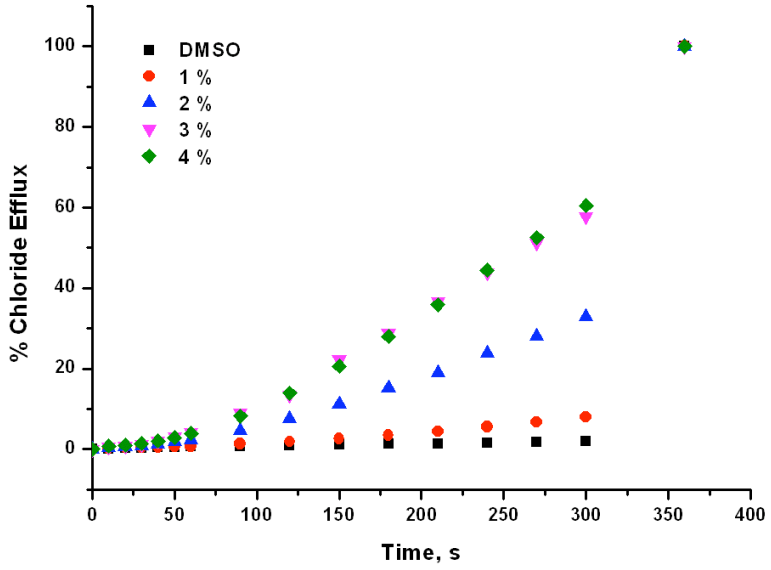

Figure A1.65 Chloride efflux promoted by various concentrations receptor **200** from unilamllar POPC vesicles containing 489 mM CsCl buffered to pH 7.2 with 5 mM sodium phosphate salts. The vesicles were suspended in 167 mM Na_2SO_4 buffered to pH 7.2 with 5 mM sodium phosphate salts. At the end of the experiment, the vesicles were lysed to calibrate 100 % chloride efflux. Each point represents the average of 3 trials. All standard deviations are < 5 %.

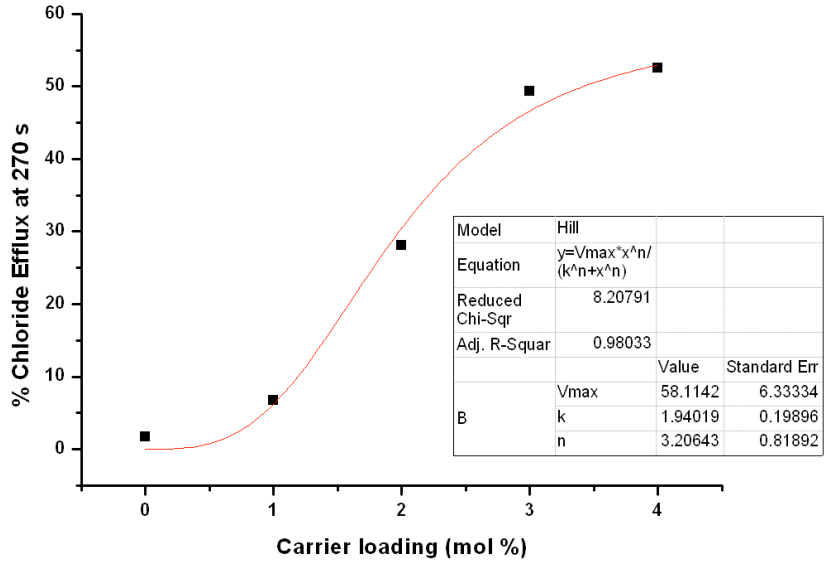

Figure A1.66 Hill plot for the Cs^+/Cl^- symport promoted by receptor **200**. The data was fitted to the Hill equation using Origin® 8.1.

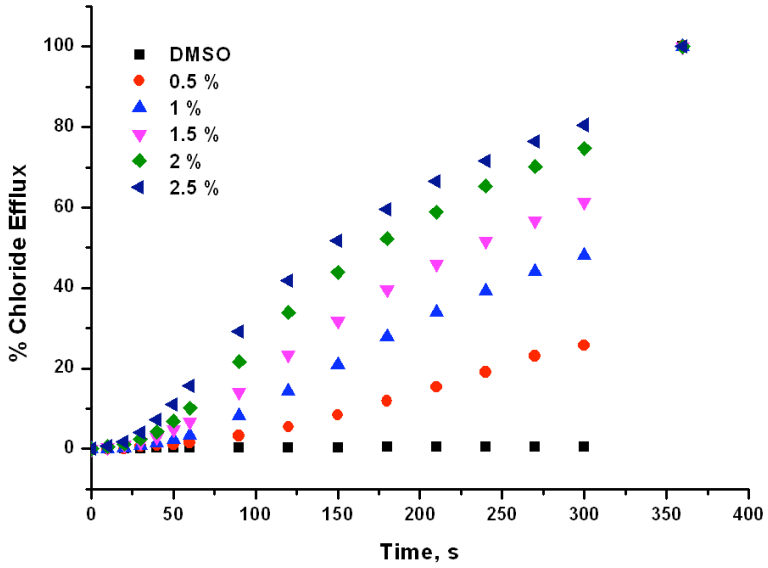

Figure A1.67 Chloride efflux promoted by various concentrations receptor **200** from unilamllar POPC vesicles containing 489 mM CsCl buffered to pH 7.2 with 5 mM sodium phosphate salts. The vesicles were suspended in 489 mM $NaNO_3$ buffered to pH 7.2 with 5 mM sodium phosphate salts. At the end of the experiment, the vesicles were lysed to calibrate 100 % chloride efflux. Each point represents the average of 3 trials. All standard deviations are < 5 %.

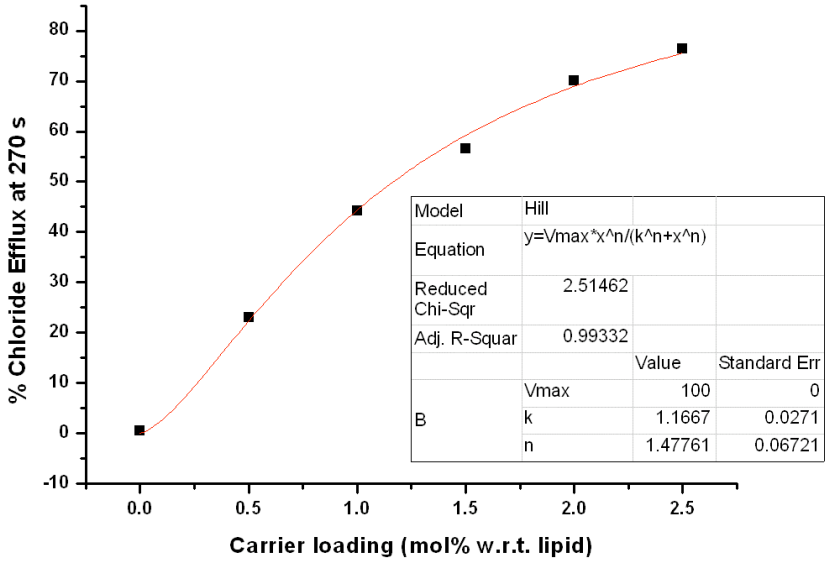

Figure A1.68 Hill plot for the chloride efflux promoted by receptor **200** from unilamellar POPC vesicles containging 489 mM CsCl buffered to pH 7.2 with 5 mM sodium phosphate salts. The vesicles were suspended in 489 mM $NaNO_3$ buffered to pH 7.2 with 5 mM sodium phosphate salts. The data was fitted to the Hill equation using Origin® 8.1.

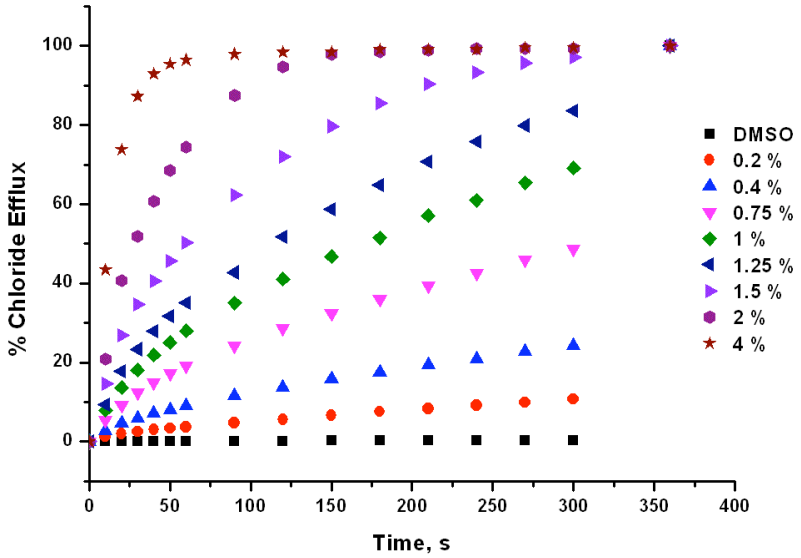

Figure A1.69 Chloride efflux promoted by various concentrations receptor **201** from unilamllar POPC vesicles containing 489 mM CsCl buffered to pH 7.2 with 5 mM sodium phosphate salts. The vesicles were suspended in 489 mM Na_2SO_4 buffered to pH 7.2 with 5 mM sodium phosphate salts. At the end of the experiment, the vesicles were lysed to calibrate 100 % chloride efflux. Each point represents the average of 3 trials. All standard deviations are < 5 %.

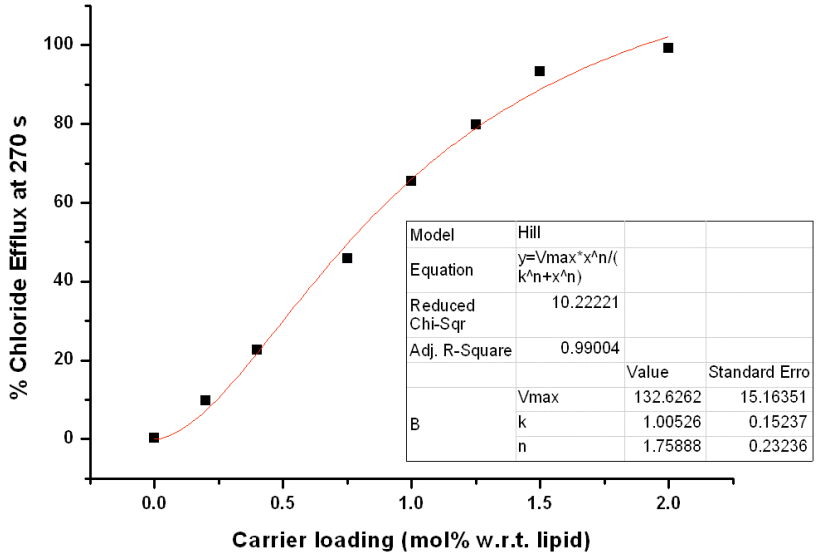

Figure A1.70 Hill plot for the Cs^+/Cl^- symport promoted by receptor **201**. The data was fitted to the Hill equation using Origin® 8.1.

A2 ^{1}H NMR titrations

Where reported, anion stability constants have been elucidated by ^{1}H NMR titrations with the anions added as the tetrabutylammonium or tetraethylammonium salts in DMSO-d_6/H_2O 0.5% at 298 K. The resulting data was fitted to a 1:1 or 1:2 binding model using WinEQNMR 2. The resulting titration profiles are reported in this section, with the relevant Job plot analyses used to ascertain the most suitable binding model. Also included are the stack plots from titrations used to investigate potential deprotonation events.

A2.1 Chapter 3

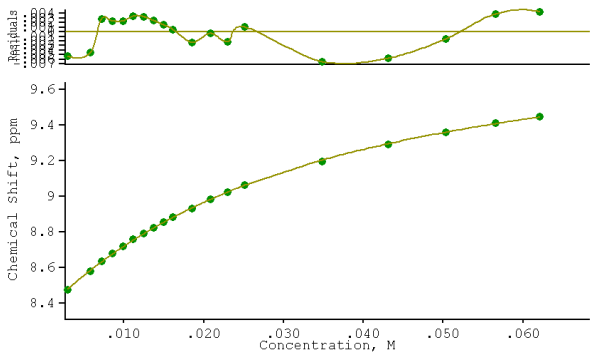

Figure A2.1 Binding curve from the ^{1}H NMR titration of receptor **159** with TBACl in DMSO-d_5/ H_2O 0.5 % following the urea NH resonance at ~8.3 ppm. The data was fitted to a 1:1 biding model using WinEQNMR 2. K_a = 37 M^{-1} (0.857).

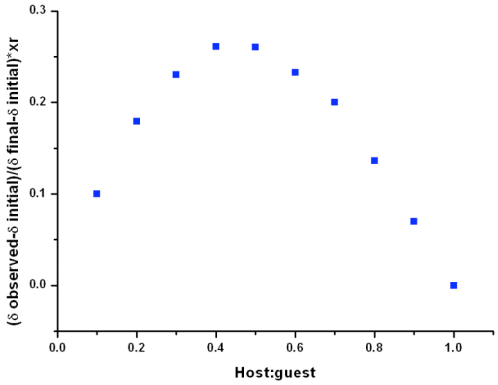

Figure A2.2 Job plot analysis for the interaction of receptor **159** with TBACl following the urea NH resonance at ~8.3 ppm.

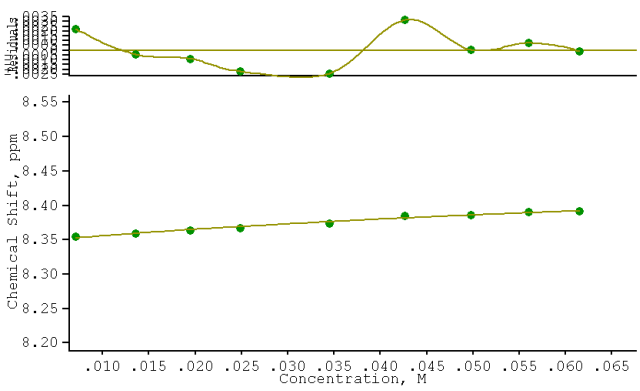

Figure A2.3 Binding curve from the ^{1}H NMR titration of receptor **159** with $TBANO_3$ in DMSO-d_5/ H_2O 0.5 % following the urea NH resonance at ~8.3 ppm. The data was fitted to a 1:1 binding model using WinEQNMR 2. $K_a < 10$ M^{-1}.

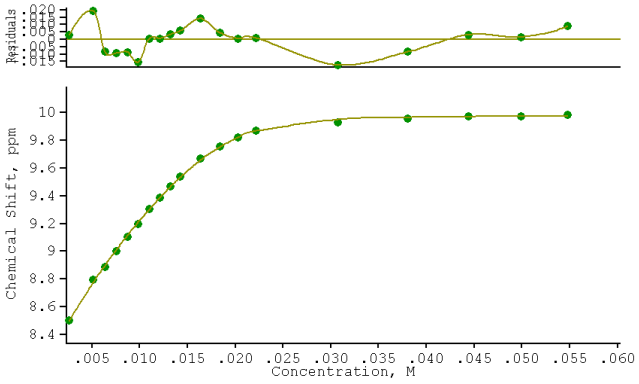

Figure A2.4 Binding curve from the ^{1}H NMR titration of receptor **159** with $TEAHCO_3$ in DMSO-d_5/ H_2O 0.5 % following the urea NH resonance at ~8.3 ppm. The data was fitted to a 1:2 binding model using WinEQNMR 2. $\beta_1 = K_1 = 802\ M^{-1}$ (105.4), $\beta_2 = 660442\ M^{-2}$ (20610).

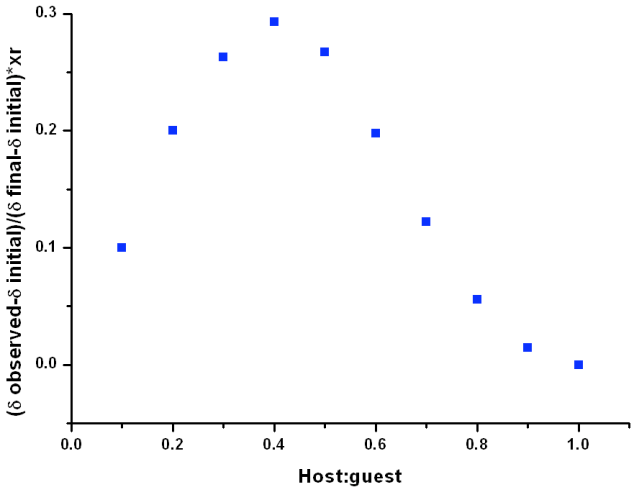

Figure A2.5 Job plot analysis for the interaction of receptor **159** with $TEAHCO_3$ following the urea NH resonance at ~8.3 ppm.

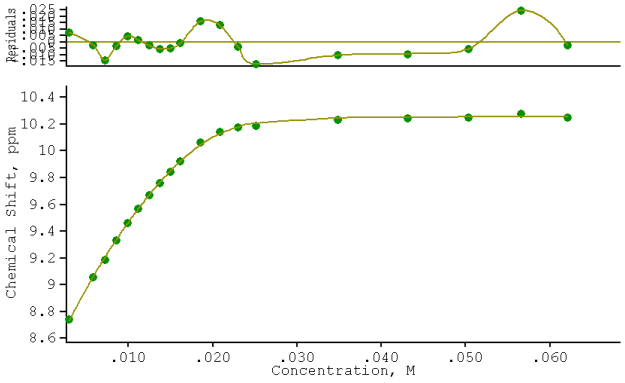

Figure A2.6 Binding curve from the ^{1}H NMR titration of receptor **159** with $TBAH_2PO_4$ in DMSO-d_5/ H_2O 0.5 % following the urea NH resonance at ~8.3 ppm. The data was fitted to a 1:2 binding model using WinEQNMR 2. $\beta_1 = K_1 = 722\ M^{-1}$ (105.2), $\beta_2 = 752348\ M^{-2}$ (31800).

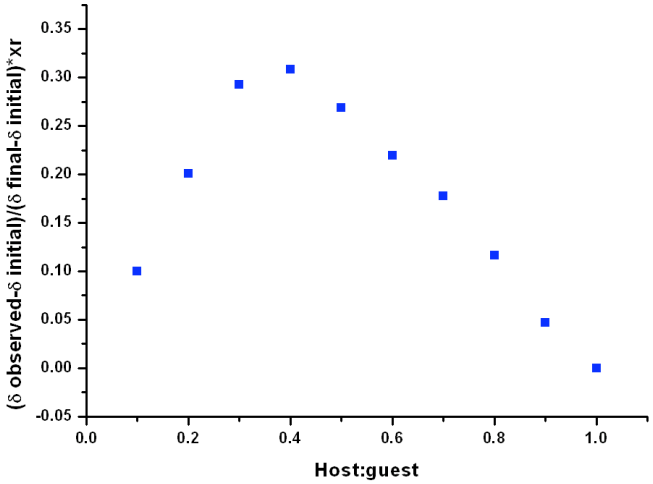

Figure A2.7 Job plot analysis for the interaction of receptor **159** with $TBAH_2PO_4$ following the urea NH resonance at ~8.3 ppm.

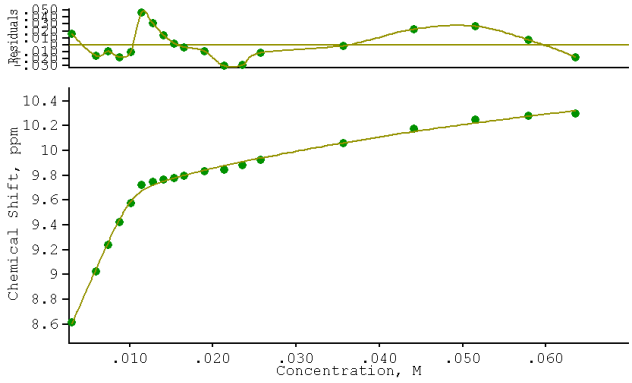

Figure A2.8 Binding curve from the ^{1}H NMR titration of receptor **159** with TBA_2SO_4 in DMSO-d_5/ H_2O 0.5 % following the urea NH resonance at ~8.3 ppm. The data was fitted to a 1:2 binding model using WinEQNMR 2. $\beta_1 = K_1 > 10^4$ M^{-1}, $\beta_2 = 178800$ M^{-2} (40880).

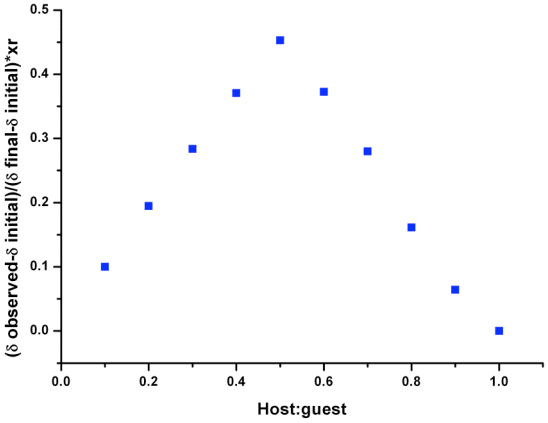

Figure A2.9 Job plot analysis for the interaction of receptor **159** with TBA_2SO_4 following the urea NH resonance at ~8.3 ppm.

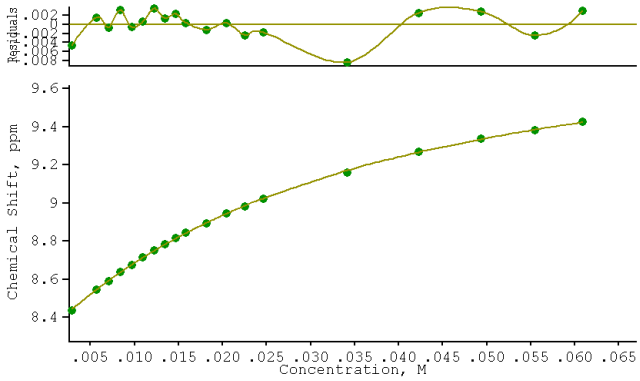

Figure A2.10 Binding curve from the ^{1}H NMR titration of receptor **160** with TBACl in DMSO-d_5/ H_2O 0.5 % following the urea NH resonance at ~8.3 ppm. The data was fitted to a 1:1 biding model using WinEQNMR 2. K_a = 35 M^{-1} (0.6944).

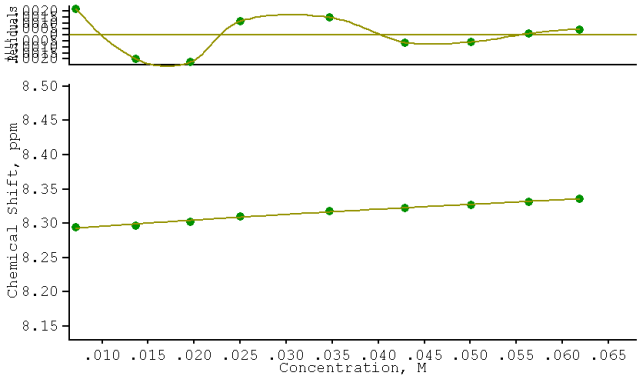

Figure A2.11 Binding curve from the ^{1}H NMR titration of receptor **160** with $TBANO_3$ in DMSO-d_5/ H_2O 0.5 % following the urea NH resonance at ~8.3 ppm. The data was fitted to a 1:1 biding model using WinEQNMR 2. K_a < 10 M^{-1}.

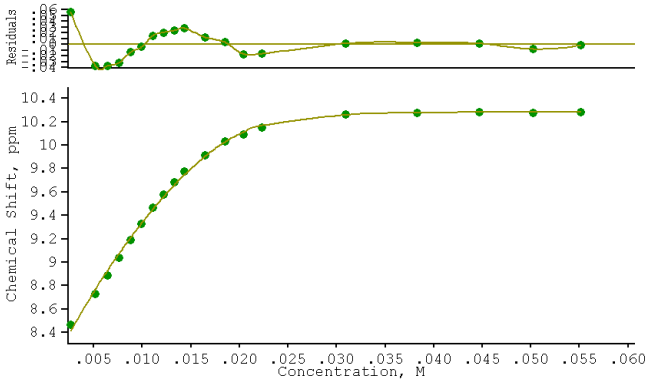

Figure A2.12 Binding curve from the ^{1}H NMR titration of receptor **160** with $TEAHCO_3$ in DMSO-d_5/ H_2O 0.5 % following the urea NH resonance at ~8.3 ppm. The data was fitted to a 1:2 binding model using WinEQNMR 2. $\beta_1 = K_1 = 1178\ M^{-1}$ (304.4), $\beta_2 = 1067700\ M^{-2}$ (45340).

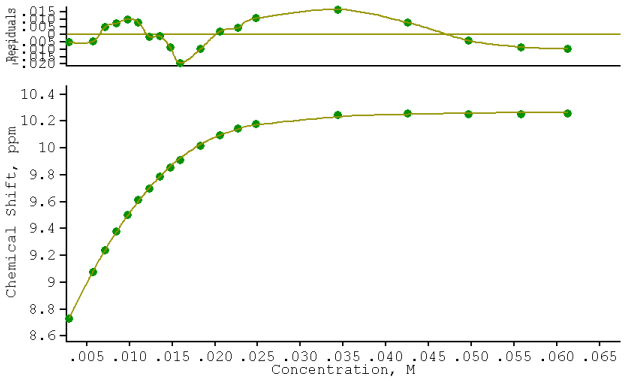

Figure A2.13 Binding curve from the ^{1}H NMR titration of receptor **160** with $TBAH_2PO_4$ in DMSO-d_5/ H_2O 0.5 % following the urea NH resonance at ~8.3 ppm. The data was fitted to a 1:2 binding model using WinEQNMR 2. $\beta_1 = K_1 = 1542\ M^{-1}$ (131.5), $\beta_2 = 702727\ M^{-2}$ (19250).

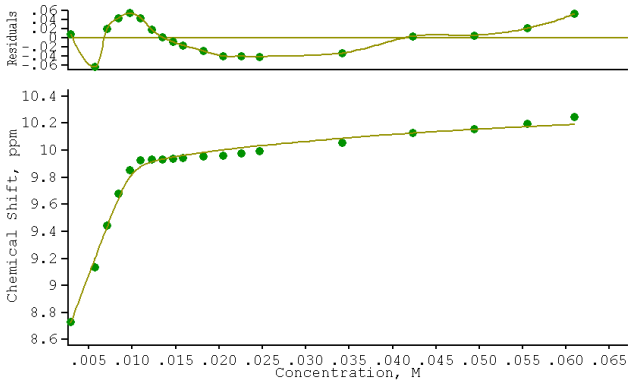

Figure A2.14 Binding curve from the ^{1}H NMR titration of receptor **160** with TBA_2SO_4 in DMSO-d_5/ H_2O 0.5 % following the urea NH resonance at ~8.3 ppm. The data was fitted to a 1:2 binding model using WinEQNMR 2. $\beta_1 = K_1 > 10^4$ M^{-1}, $\beta_2 = 567017$ M^{-2} (99590).

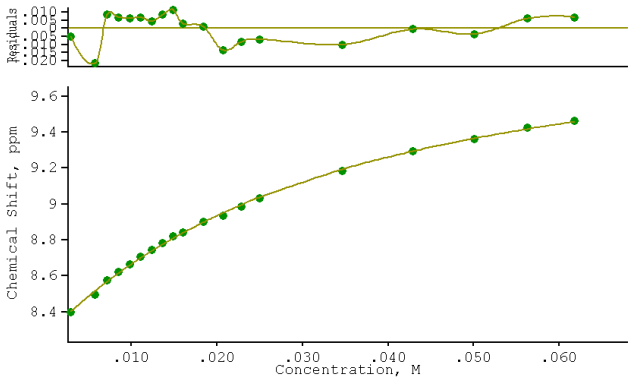

Figure A2.15 Binding curve from the ^{1}H NMR titration of receptor **161** with TBACl in DMSO-d_5/ H_2O 0.5 % following the urea NH resonance at ~8.3 ppm. The data was fitted to a 1:1 biding model using WinEQNMR 2. $K_a = 37$ M^{-1} (1.953).

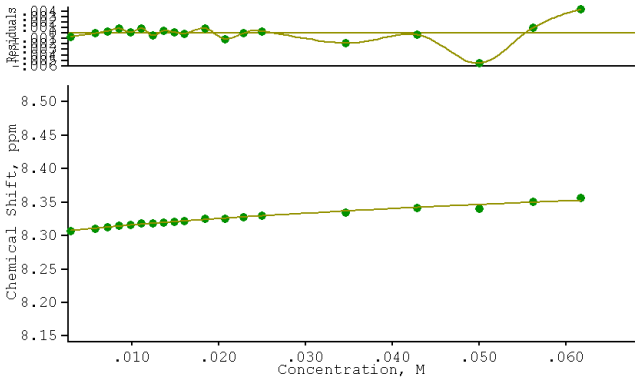

Figure A2.16 Binding curve from the ^{1}H NMR titration of receptor **161** with $TBANO_3$ in DMSO-d_5/ H_2O 0.5 % following the urea NH resonance at ~8.3 ppm. The data was fitted to a 1:1 biding model using WinEQNMR 2. $K_a < 10$ M^{-1}.

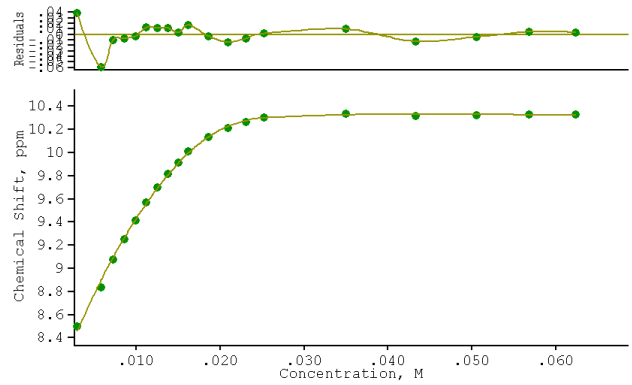

Figure A2.17 Binding curve from the ^{1}H NMR titration of receptor **161** with $TEAHCO_3$ in DMSO-d_5/ H_2O 0.5 % following the urea NH resonance at ~8.3 ppm. The data was fitted to a 1:2 binding model using WinEQNMR 2. $\beta_1 = K_1 = 8131$ M^{-1} (176.2), $\beta_2 = 862682$ M^{-2} (45590).

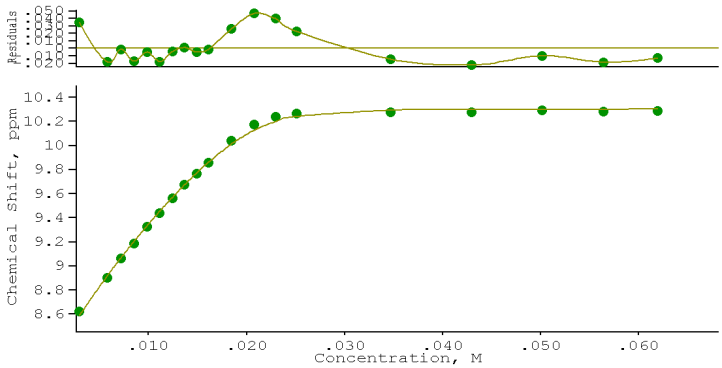

Figure A2.18 Binding curve from the ^{1}H NMR titration of receptor **161** with $TBAH_2PO_4$ in DMSO-d_5/ H_2O 0.5 % following the urea NH resonance at ~8.3 ppm. The data was fitted to a 1:2 binding model using WinEQNMR 2. $\beta_1 = K_1 = 386\ M^{-1}$ (108.2), $\beta_2 = 627030\ M^{-2}$ (80940).

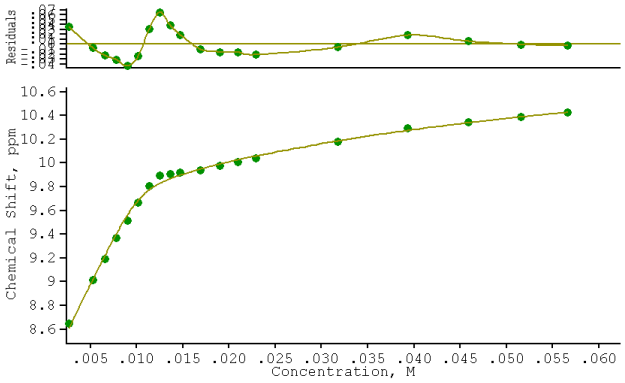

Figure A2.19 Binding curve from the ^{1}H NMR titration of receptor **161** with TBA_2SO_4 in DMSO-d_5/ H_2O 0.5 % following the urea NH resonance at ~8.3 ppm. The data was fitted to a 1:2 binding model using WinEQNMR 2. $\beta_1 = K_1 = 9768\ M^{-1}$ (1932), $\beta_2 = 192435\ M^{-2}$ (48660).

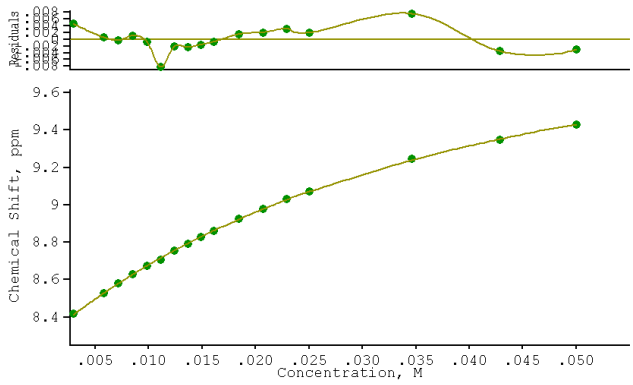

Figure A2.20 Binding curve from the ^{1}H NMR titration of receptor **162** with TBACl in DMSO-d_5/ H_2O 0.5 % following the urea NH resonance at ~8.3 ppm. The data was fitted to a 1:1 biding model using WinEQNMR 2. K_a = 32 M^{-1} (0.8869).

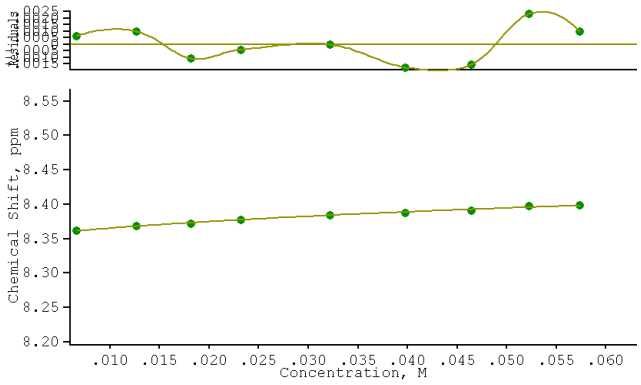

Figure A2.21 Binding curve from the ^{1}H NMR titration of receptor **162** with $TBANO_3$ in DMSO-d_5/ H_2O 0.5 % following the urea NH resonance at ~8.3 ppm. The data was fitted to a 1:1 biding model using WinEQNMR 2. K_a < 10 M^{-1}.

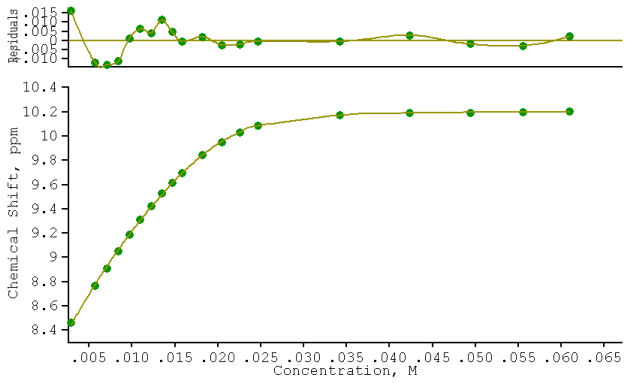

Figure A2.22 Binding curve from the ^{1}H NMR titration of receptor **162** with $TEAHCO_3$ in DMSO-d_5/ H_2O 0.5 % following the urea NH resonance at ~8.3 ppm. The data was fitted to a 1:2 binding model using WinEQNMR 2. $\beta_1 = K_1 = 584\ M^{-1}$ (61.44), $\beta_2 = 465949\ M^{-2}$ (16290).

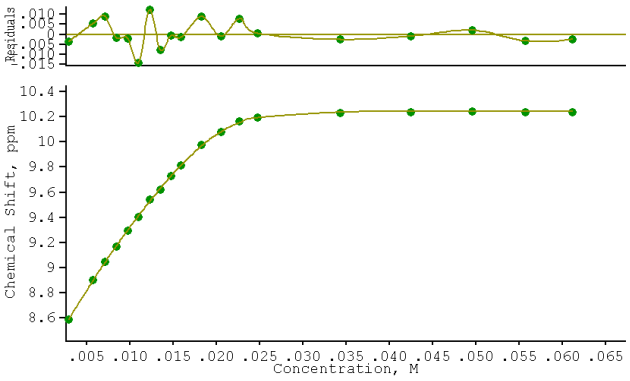

Figure A2.23 Binding curve from the ^{1}H NMR titration of receptor **162** with $TBAH_2PO_4$ in DMSO-d_5/ H_2O 0.5 % following the urea NH resonance at ~8.3 ppm. The data was fitted to a 1:2 binding model using WinEQNMR 2. $\beta_1 = K_1 = 341\ M^{-1}$ (66.77), $\beta_2 = 789322\ M^{-2}$ (17010).

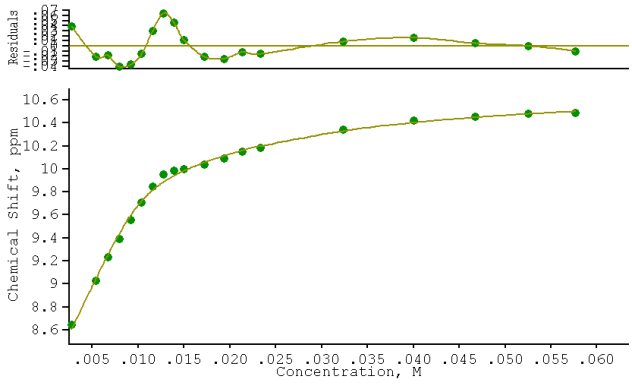

Figure A2.24 Binding curve from the ^{1}H NMR titration of receptor **162** with TBA_2SO_4 in DMSO-d_5/ H_2O 0.5 % following the urea NH resonance at ~8.3 ppm. The data was fitted to a 1:2 binding model using WinEQNMR 2. $\beta_1 = K_1 = 7170\ M^{-1}$ (1216), $\beta_2 = 512992\ M^{-2}$ (59230).

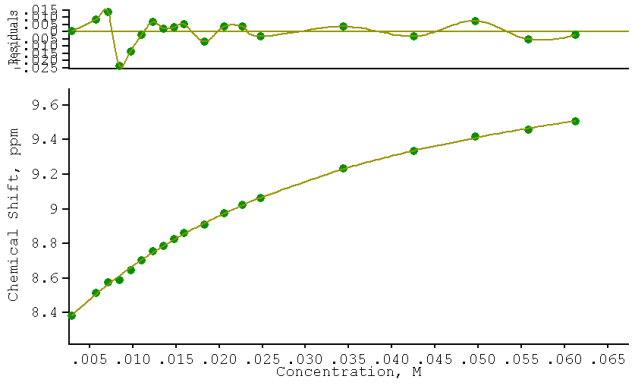

Figure A2.25 Binding curve from the ^{1}H NMR titration of receptor **163** with TBACl in DMSO-d_5/ H_2O 0.5 % following the urea NH resonance at ~8.3 ppm. The data was fitted to a 1:1 biding model using WinEQNMR 2. $K_a = 39\ M^{-1}$ (1.806).

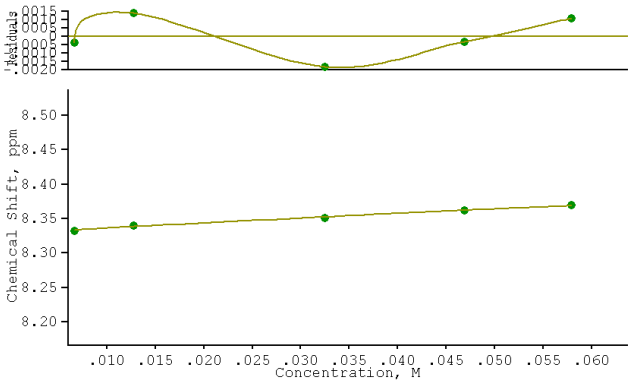

Figure A2.26 Binding curve from the ^{1}H NMR titration of receptor **163** with $TBANO_3$ in DMSO-d_5/ H_2O 0.5 % following the urea NH resonance at ~8.3 ppm. The data was fitted to a 1:1 biding model using WinEQNMR 2. $K_a < 10$ M^{-1}.

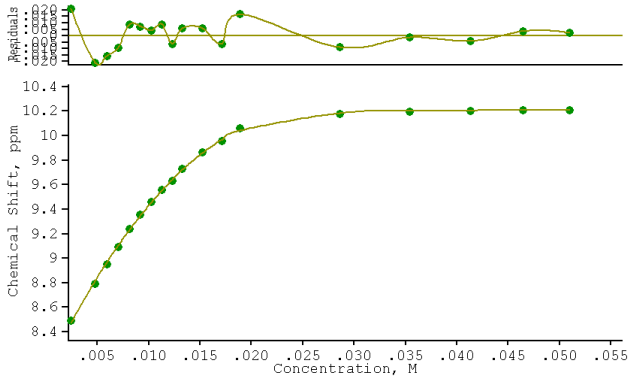

Figure A2.27 Binding curve from the ^{1}H NMR titration of receptor **163** with $TEAHCO_3$ in DMSO-d_5/ H_2O 0.5 % following the urea NH resonance at ~8.3 ppm. The data was fitted to a 1:2 binding model using WinEQNMR 2. $\beta_1 = K_1 = 1101$ M^{-1} (169), $\beta_2 = 837798$ M^{-2} (35830).

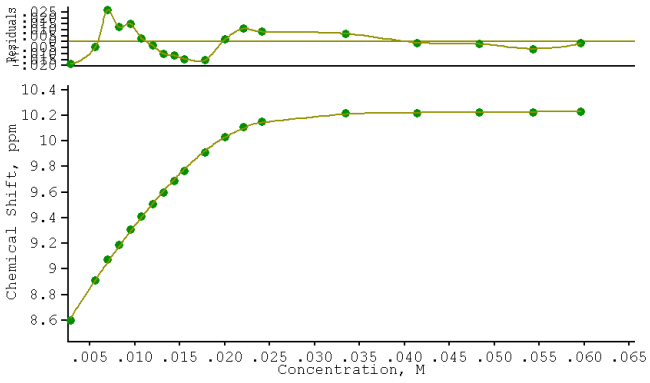

Figure A2.28 Binding curve from the ^{1}H NMR titration of receptor **163** with $TBAH_2PO_4$ in DMSO-d_5/ H_2O 0.5 % following the urea NH resonance at ~8.3 ppm. The data was fitted to a 1:2 binding model using WinEQNMR 2. $\beta_1 = K_1 = 420\ M^{-1}$ (99.67), $\beta_2 = 542492\ M^{-2}$ (27860).

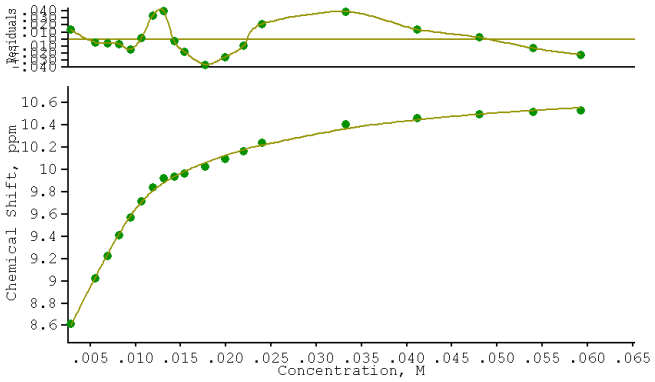

Figure A2.29 Binding curve from the ^{1}H NMR titration of receptor **163** with TBA_2SO_4 in DMSO-d_5/ H_2O 0.5 % following the urea NH resonance at ~8.3 ppm. The data was fitted to a 1:2 binding model using WinEQNMR 2. $\beta_1 = K_1 = 8560\ M^{-1}$ (1125), $\beta_2 = 623547\ M^{-2}$ (36340).

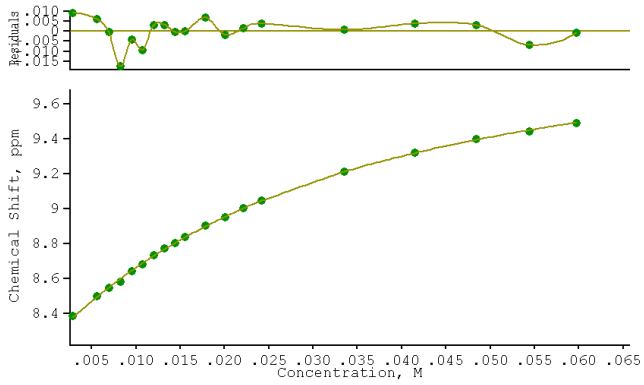

Figure A2.30 Binding curve from the ^{1}H NMR titration of receptor **164** with TBACl in DMSO-d_5/ H_2O 0.5 % following the urea NH resonance at ~8.3 ppm. The data was fitted to a 1:1 biding model using WinEQNMR 2. K_a = 38 M^{-1} (1.309).

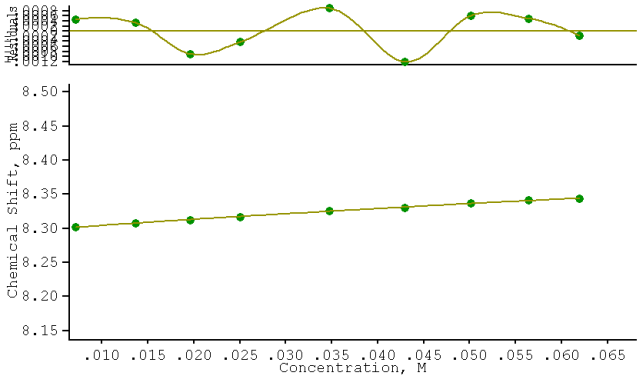

Figure A2.31 Binding curve from the ^{1}H NMR titration of receptor **164** with $TBANO_3$ in DMSO-d_5/ H_2O 0.5 % following the urea NH resonance at ~8.3 ppm. The data was fitted to a 1:1 biding model using WinEQNMR 2. K_a < 10 M^{-1}.

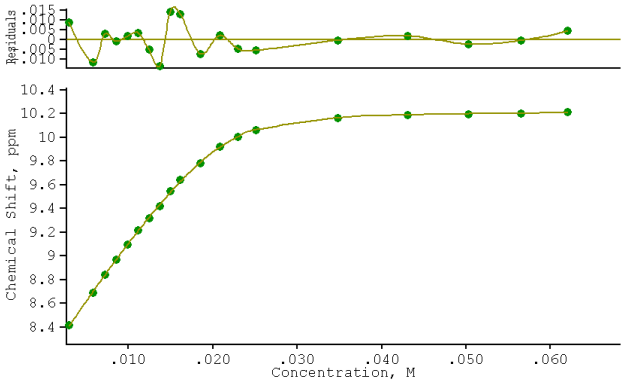

Figure A2.32 Binding curve from the ^{1}H NMR titration of receptor **164** with $TEAHCO_3$ in DMSO-d_5/ H_2O 0.5 % following the urea NH resonance at ~8.3 ppm. The data was fitted to a 1:2 binding model using WinEQNMR 2. $\beta_1 = K_1 = 560\ M^{-1}$ (60.5), $\beta_2 = 583357\ M^{-2}$ (21680).

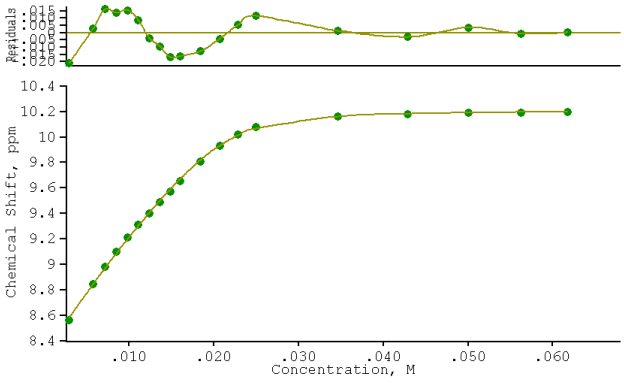

Figure A2.33 Binding curve from the ^{1}H NMR titration of receptor **164** with $TBAH_2PO_4$ in DMSO-d_5/ H_2O 0.5 % following the urea NH resonance at ~8.3 ppm. The data was fitted to a 1:2 binding model using WinEQNMR 2. $\beta_1 = K_1 = 572\ M^{-1}$ (103.6), $\beta_2 = 585002\ M^{-2}$ (32430).

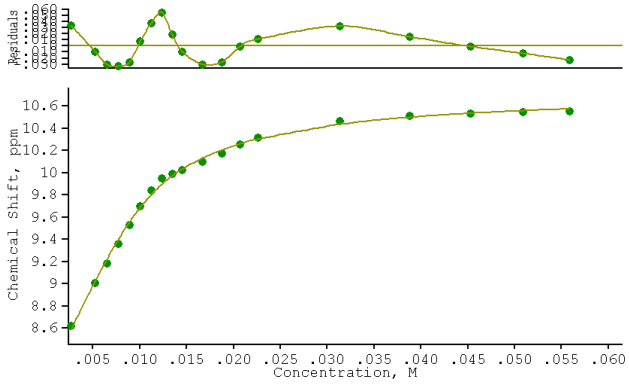

Figure A2.34 Binding curve from the ^{1}H NMR titration of receptor **164** with TBA_2SO_4 in DMSO-d_5/ H_2O 0.5 % following the urea NH resonance at ~8.3 ppm. The data was fitted to a 1:2 binding model using WinEQNMR 2. $\beta_1 = K_1 = 3280$ M^{-1} (643.9), $\beta_2 = 360871$ M^{-2} (45020).

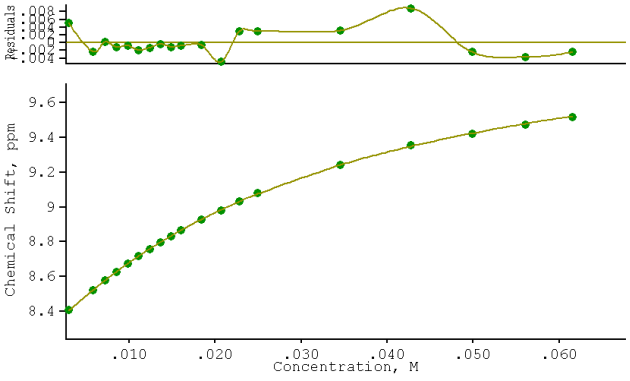

Figure A2.35 Binding curve from the ^{1}H NMR titration of receptor **165** with TBACl in DMSO-d_5/ H_2O 0.5 % following the urea NH resonance at ~8.3 ppm. The data was fitted to a 1:1 biding model using WinEQNMR 2. $K_a = 37$ M^{-1} (0.6931).

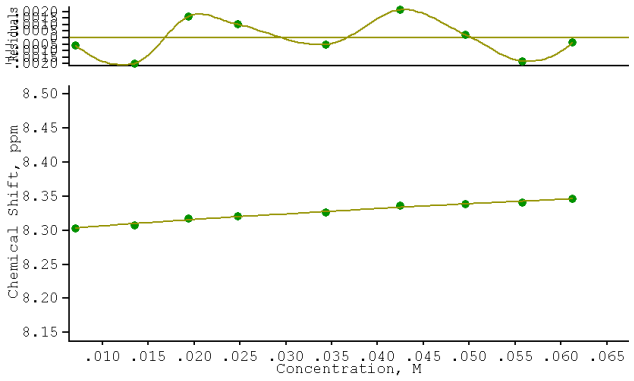

Figure A2.36 Binding curve from the ^{1}H NMR titration of receptor **165** with $TBANO_3$ in DMSO-d_5/ H_2O 0.5 % following the urea NH resonance at ~8.3 ppm. The data was fitted to a 1:1 biding model using WinEQNMR 2. $K_a < 10$ M^{-1}.

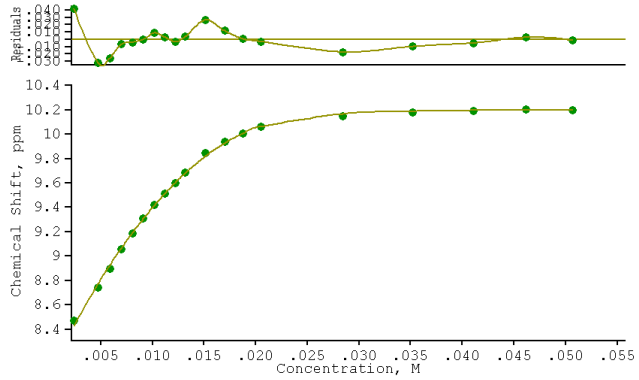

Figure A2.37 Binding curve from the ^{1}H NMR titration of receptor **165** with $TEAHCO_3$ in DMSO-d_5/ H_2O 0.5 % following the urea NH resonance at ~8.3 ppm. The data was fitted to a 1:2 binding model using WinEQNMR 2. $\beta_1 = K_1 = 1328$ M^{-1} (283.6), $\beta_2 = 870364$ M^{-2} (46370).

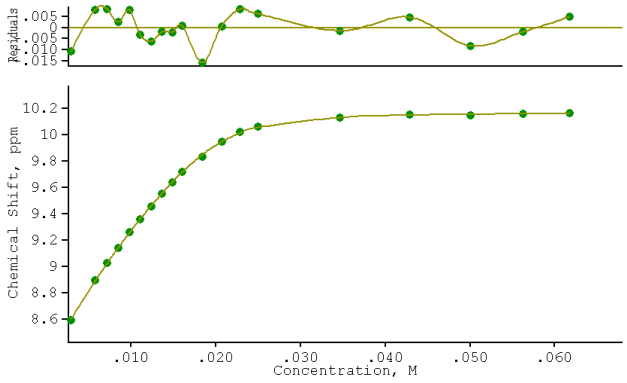

Figure A2.38 Binding curve from the ^{1}H NMR titration of receptor **165** with $TBAH_2PO_4$ in DMSO-d_5/ H_2O 0.5 % following the urea NH resonance at ~8.3 ppm. The data was fitted to a 1:2 binding model using WinEQNMR 2. $\beta_1 = K_1 = 631\ M^{-1}$ (65.27), $\beta_2 = 52739\ M^{-2}$ (14270).

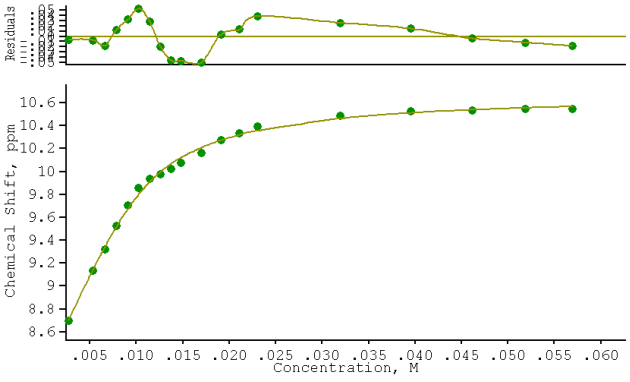

Figure A2.39 Binding curve from the ^{1}H NMR titration of receptor **165** with TBA_2SO_4 in DMSO-d_5/ H_2O 0.5 % following the urea NH resonance at ~8.3 ppm. The data was fitted to a 1:2 binding model using WinEQNMR 2. $\beta_1 = K_1 = 3320\ M^{-1}$ (651.3), $\beta_2 = 411641\ M^{-2}$ (66940).

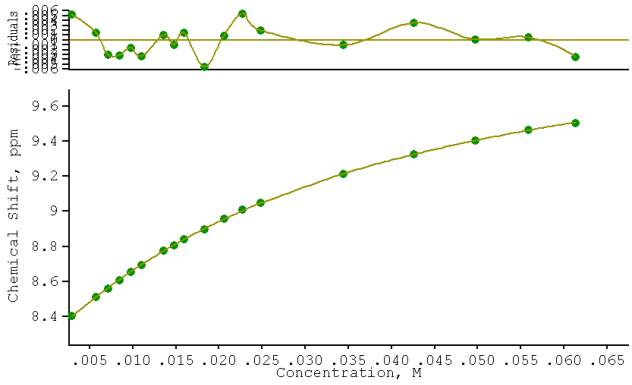

Figure A2.40 Binding curve from the ^{1}H NMR titration of receptor **166** with TBACl in DMSO-d_5/ H_2O 0.5 % following the urea NH resonance at ~8.3 ppm. The data was fitted to a 1:1 biding model using WinEQNMR 2. K_a = 32 M^{-1} (0.5787).

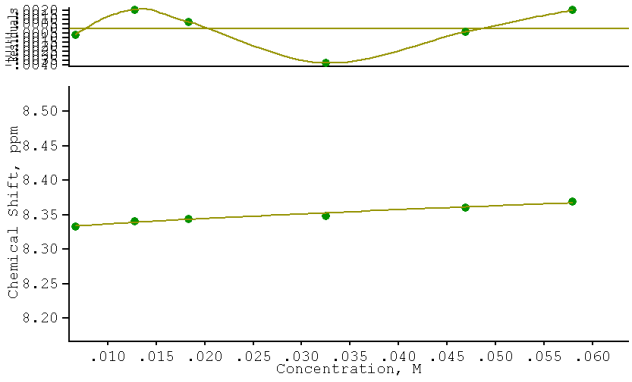

Figure A2.41 Binding curve from the ^{1}H NMR titration of receptor **166** with $TBANO_3$ in DMSO-d_5/ H_2O 0.5 % following the urea NH resonance at ~8.3 ppm. The data was fitted to a 1:1 biding model using WinEQNMR 2. K_a < 10 M^{-1}.

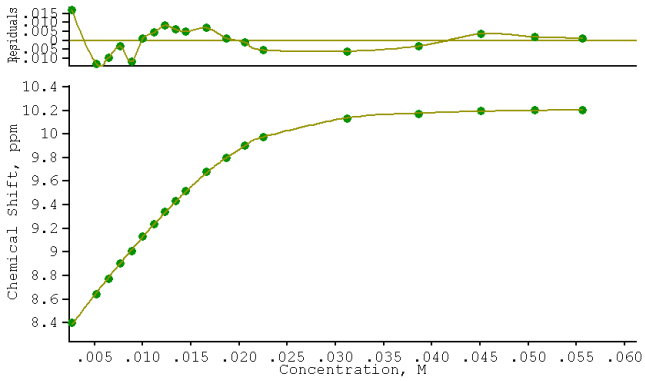

Figure A2.42 Binding curve from the ^{1}H NMR titration of receptor **166** with $TEAHCO_3$ in DMSO-d_5/ H_2O 0.5 % following the urea NH resonance at ~8.3 ppm. The data was fitted to a 1:2 binding model using WinEQNMR 2. $\beta_1 = K_1 = 290$ M^{-1} (28.62), $\beta_2 = 246354$ M^{-2} (14300).

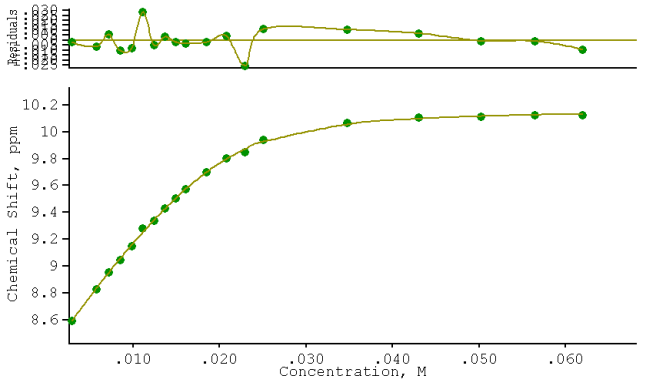

Figure A2.43 Binding curve from the ^{1}H NMR titration of receptor **166** with $TBAH_2PO_4$ in DMSO-d_5/ H_2O 0.5 % following the urea NH resonance at ~8.3 ppm. The data was fitted to a 1:2 binding model using WinEQNMR 2. $\beta_1 = K_1 = 508$ M^{-1} (118), $\beta_2 = 206422$ M^{-2} (22410).

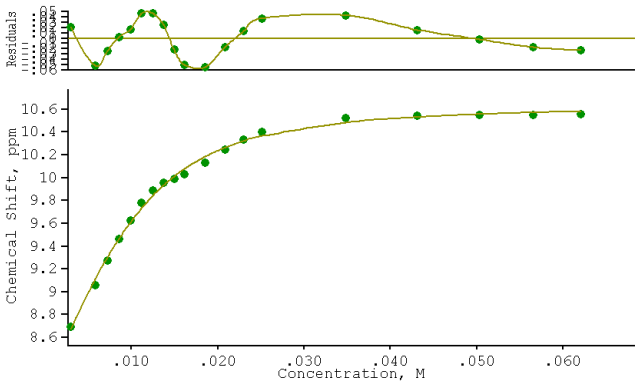

Figure A2.44 Binding curve from the ^{1}H NMR titration of receptor **166** with TBA_2SO_4 in DMSO-d_5/ H_2O 0.5 % following the urea NH resonance at ~8.3 ppm. The data was fitted to a 1:2 binding model using WinEQNMR 2. $\beta_1 = K_1 = 1267\ M^{-1}$ (345.3), $\beta_2 = 207037\ M^{-2}$ (47340).

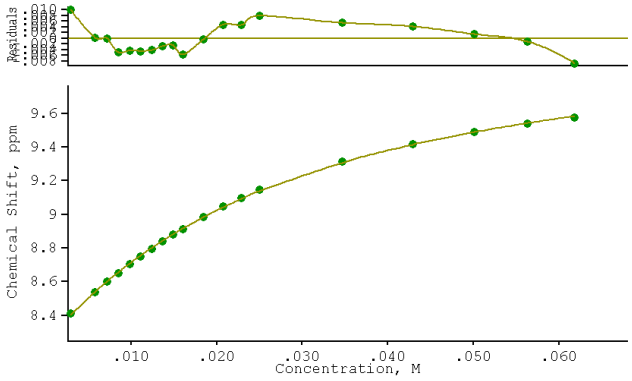

Figure A2.45 Binding curve from the ^{1}H NMR titration of receptor **167** with TBACl in DMSO-d_5/ H_2O 0.5 % following the urea NH resonance at ~8.3 ppm. The data was fitted to a 1:1 biding model using WinEQNMR 2. K_a = 44 M^{-1} (1.097).

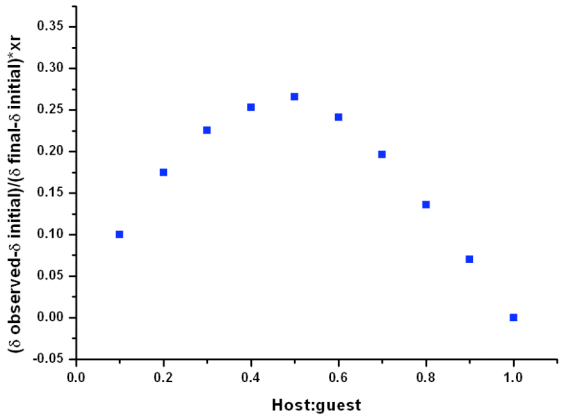

Figure A2.46 Job plot analysis for the interaction of receptor **167** with TBACl following the urea NH resonance at ~8.3 ppm.

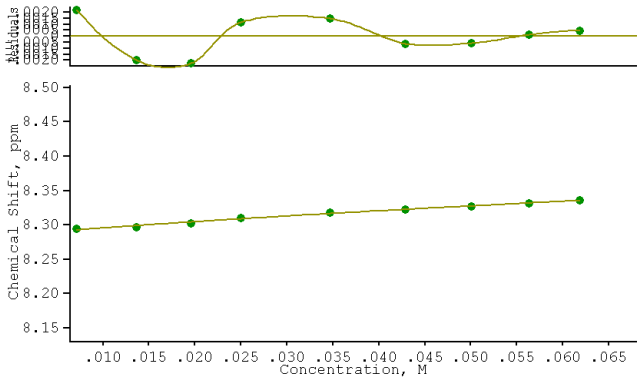

Figure A2.47 Binding curve from the ^{1}H NMR titration of receptor **167** with $TBANO_3$ in DMSO-d_5/ H_2O 0.5 % following the urea NH resonance at ~8.3 ppm. The data was fitted to a 1:1 biding model using WinEQNMR 2. $K_a < 10\ M^{-1}$.

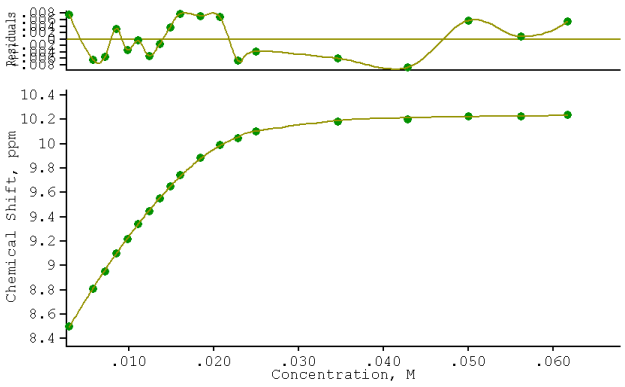

Figure A2.48 Binding curve from the ^{1}H NMR titration of receptor **167** with $TEAHCO_3$ in DMSO-d_5/ H_2O 0.5 % following the urea NH resonance at ~8.3 ppm. The data was fitted to a 1:2 binding model using WinEQNMR 2. $\beta_1 = K_1 = 1026\ M^{-1}$ (708.1), $\beta_2 = 740068\ M^{-2}$ (12680).

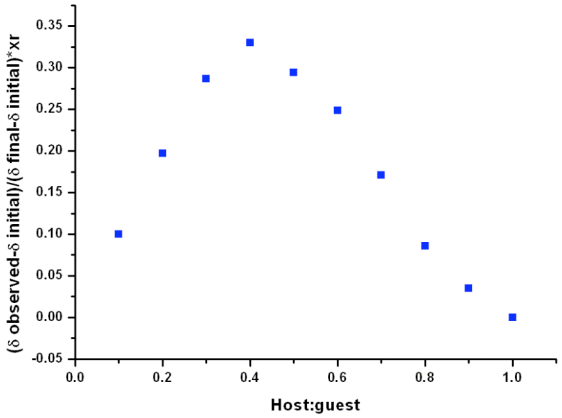

Figure A2.49 Job plot analysis for the interaction of receptor **167** with $TEAHCO_3$ following the urea NH resonance at ~8.3 ppm.

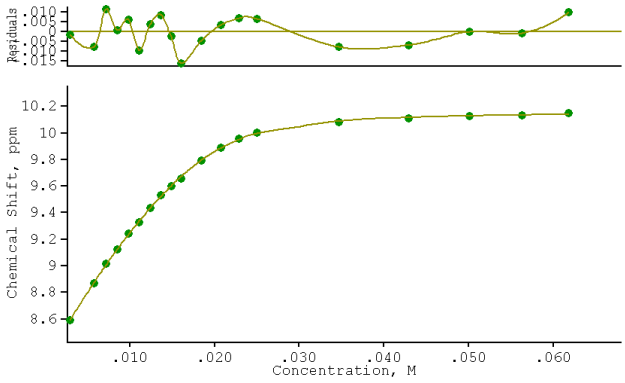

Figure A2.50 Binding curve from the ^{1}H NMR titration of receptor **167** with $TBAH_2PO_4$ in DMSO-d_5/ H_2O 0.5 % following the urea NH resonance at ~8.3 ppm. The data was fitted to a 1:2 binding model using WinEQNMR 2. $\beta_1 = K_1 = 896\ M^{-1}$ (79.49), $\beta_2 = 447317\ M^{-2}$ (21800).

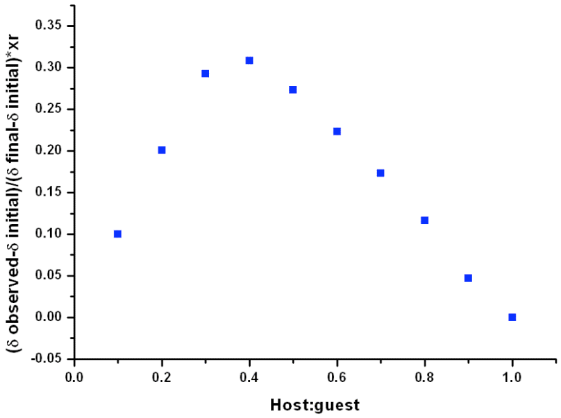

Figure A2.51 Job plot analysis for the interaction of receptor **167** with $TBAH_2PO_4$ following the urea NH resonance at ~8.3 ppm.

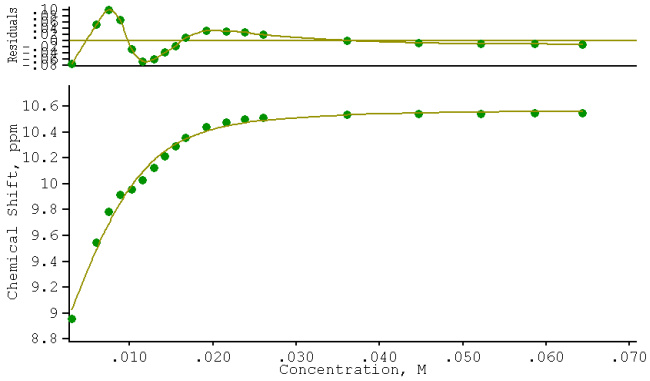

Figure A2.52 Binding curve from the ^{1}H NMR titration of receptor **167** with TBA_2SO_4 in DMSO-d_5/ H_2O 0.5 % following the urea NH resonance at ~8.3 ppm. The data was fitted to a 1:2 binding model using WinEQNMR 2. $\beta_1 = K_1 = 2296$ M^{-1} (202), $\beta_2 = 407788$ M^{-2} (82750).

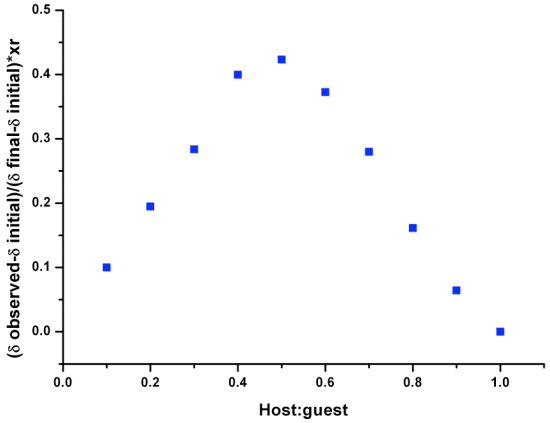

Figure A2.53 Job plot analysis for the interaction of receptor **167** with TBA_2SO_4 following the urea NH resonance at ~8.3 ppm.

A2.2 Chapter 4

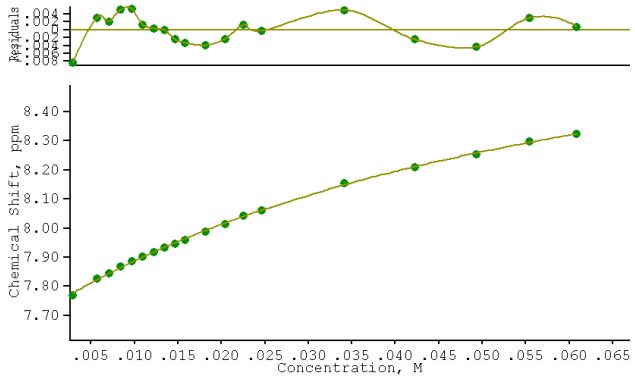

Figure A2.54 Binding curve from the ^{1}H NMR titration of receptor **177** with TBACl in DMSO-d_5/ H_2O 0.5 % following the thiourea NH resonance at ~7.7 ppm. The data was fitted to a 1:1 biding model using WinEQNMR 2. K_a = 16 M^{-1} (0.8447).

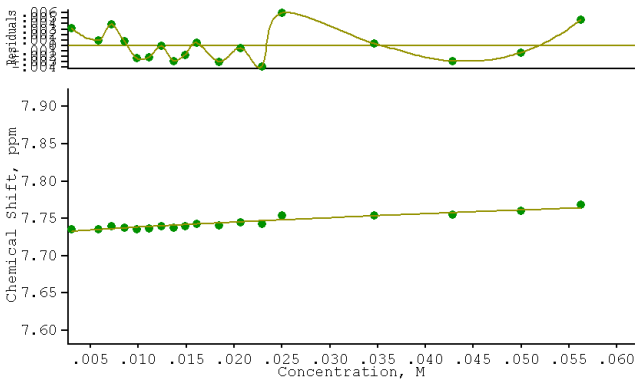

Figure A2.55 Binding curve from the ^{1}H NMR titration of receptor **177** with $TBANO_3$ in DMSO-d_5/ H_2O 0.5 % following the thiourea NH resonance at ~7.7 ppm. The data was fitted to a 1:1 biding model using WinEQNMR 2. K_a < 10 M^{-1}.

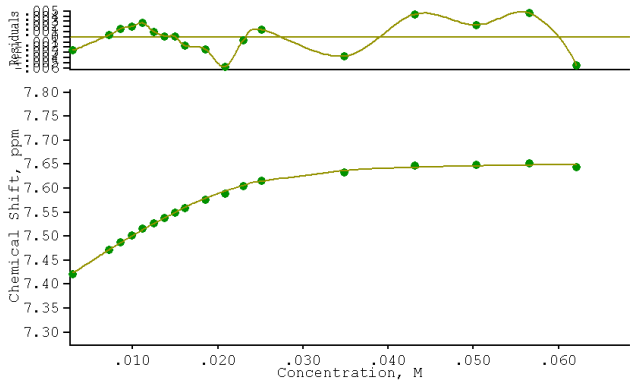

Figure A2.56 Binding curve from the ^{1}H NMR titration of receptor **177** with $TEAHCO_3$ in DMSO-d_5/ H_2O 0.5 % following the aromatic CH doublet centered at ~7.4 ppm. The data was fitted to a 1:2 binding model using WinEQNMR 2. $\beta_1 = K_1 = 384\ M^{-1}$ (104.6), $\beta_2 = 159015\ M^{-2}$ (11340).

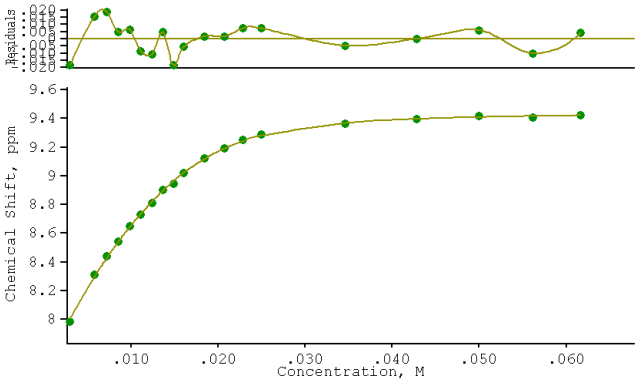

Figure A2.57 Binding curve from the ^{1}H NMR titration of receptor **177** with $TBAH_2PO_4$ in DMSO-d_5/ H_2O 0.5 % following the thiourea NH resonance at ~7.7 ppm. The data was fitted to a 1:2 binding model using WinEQNMR 2. $\beta_1 = K_1 = 718\ M^{-1}$ (53.63), $\beta_2 = 196699\ M^{-2}$ (19920).

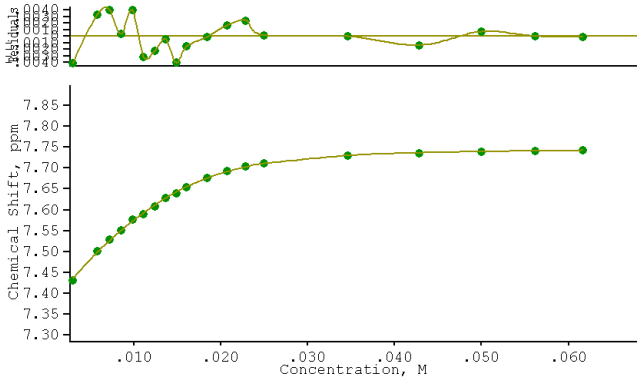

Figure A2.58 Binding curve from the ^{1}H NMR titration of receptor **177** with $TBAH_2PO_4$ in DMSO-d_5/ H_2O 0.5 % following the aromatic CH doublet centered at ~7.4 ppm. The data was fitted to a 1:2 binding model using WinEQNMR 2. $\beta_1 = K_1 = 715\ M^{-1}$ (24.31), $\beta_2 = 184464\ M^{-2}$ (61910).

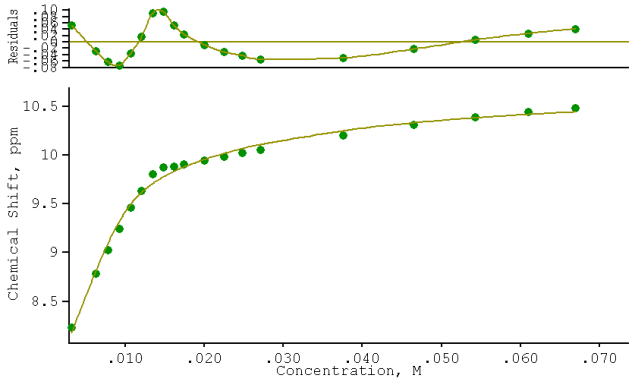

Figure A2.59 Binding curve from the ^{1}H NMR titration of receptor **177** with TBA_2SO_4 in DMSO-d_5/ H_2O 0.5 % following the thiourea NH resonance at ~7.7 ppm. The data was fitted to a 1:2 binding model using WinEQNMR 2. $\beta_1 = K_1 = 4612\ M^{-1}$ (139.7), $\beta_2 = 124601\ M^{-2}$ (76010).

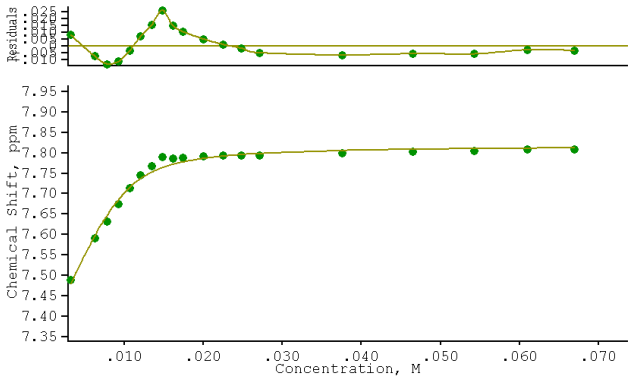

Figure A2.60 Binding curve from the ^{1}H NMR titration of receptor **177** with TBA_2SO_4 in DMSO-d_5/ H_2O 0.5 % following the aromatic CH doublet centered at ~7.4 ppm. The data was fitted to a 1:1 binding model using WinEQNMR 2. K_α = 1293 M^{-1} (87.8).

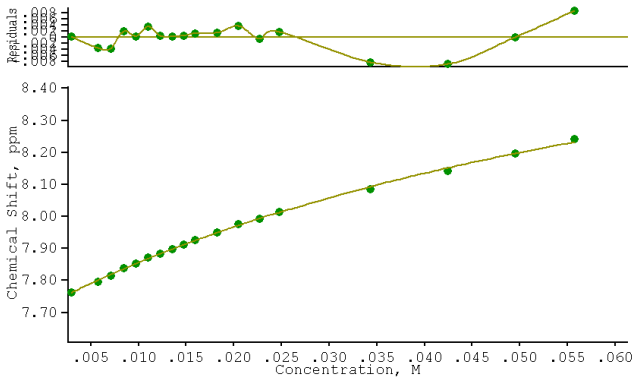

Figure A2.61 Binding curve from the ^{1}H NMR titration of receptor **178** with TBACl in DMSO-d_5/ H_2O 0.5 % following the thiourea NH resonance at ~7.7 ppm. The data was fitted to a 1:1 biding model using WinEQNMR 2. K_a = 15 M^{-1} (1.209).

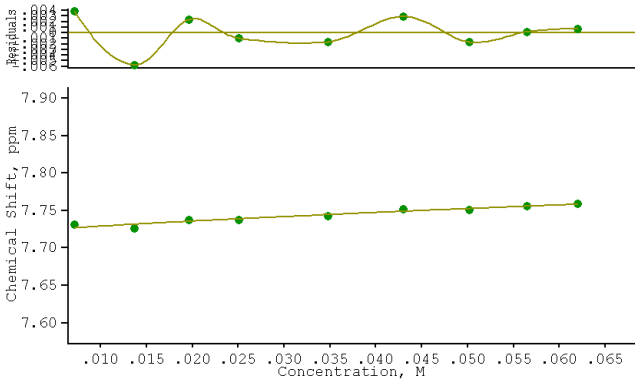

Figure A2.62 Binding curve from the ^{1}H NMR titration of receptor **178** with $TBANO_3$ in DMSO-d_5/ H_2O 0.5 % following the thiourea NH resonance at ~7.7 ppm. The data was fitted to a 1:1 biding model using WinEQNMR 2. $K_a < 10$ M^{-1}.

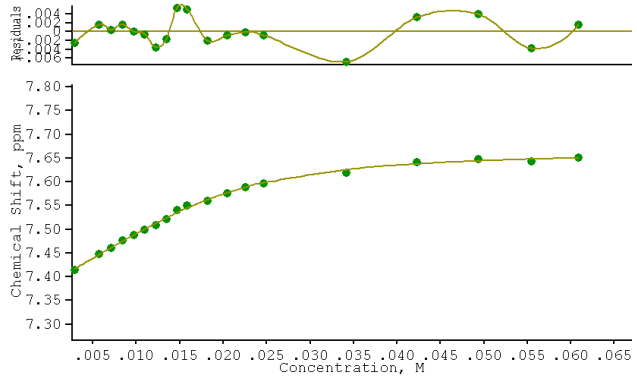

Figure A2.63 Binding curve from the ^{1}H NMR titration of receptor **178** with $TEAHCO_3$ in DMSO-d_5/ H_2O 0.5 % following the aromatic CH doublet centered at ~7.4 ppm. The data was fitted to a 1:2 binding model using WinEQNMR 2. $\beta_1 = K_1 = 1280$ M^{-1} (170.2), $\beta_2 = 232547$ M^{-2} (10900).

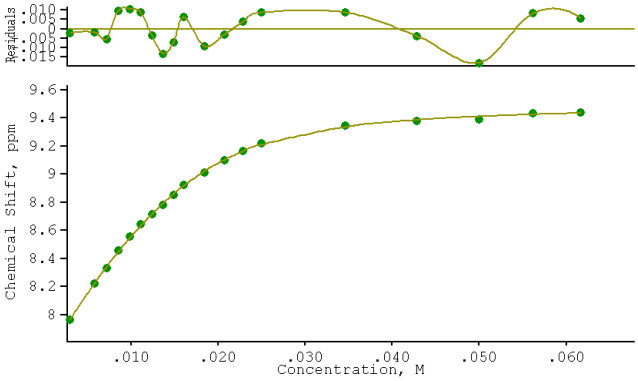

Figure A2.64 Binding curve from the ^{1}H NMR titration of receptor **178** with $TBAH_2PO_4$ in DMSO-d_5/ H_2O 0.5 % following the thiourea NH resonance at ~7.7 ppm. The data was fitted to a 1:2 binding model using WinEQNMR 2. $\beta_1 = K_1 = 806$ M^{-1} (75.17), $\beta_2 = 167388$ M^{-2} (11170).

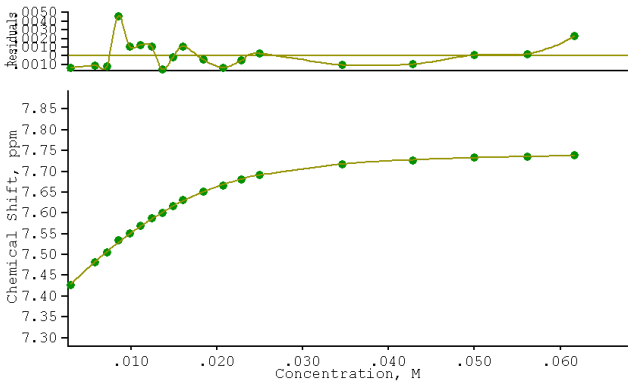

Figure A2.65 Binding curve from the ^{1}H NMR titration of receptor **178** with $TBAH_2PO_4$ in DMSO-d_5/ H_2O 0.5 % following the aromatic CH doublet centered at ~7.4 ppm. The data was fitted to a 1:2 binding model using WinEQNMR 2. $\beta_1 = K_1 = 716$ M^{-1} (37.01), $\beta_2 = 155321$ M^{-2} (25230).

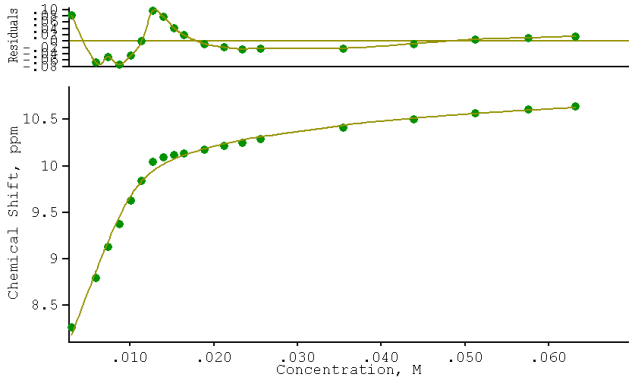

Figure A2.66 Binding curve from the ^{1}H NMR titration of receptor **178** with TBA_2SO_4 in DMSO-d_5/ H_2O 0.5 % following the thiourea NH resonance at ~7.7 ppm. The data was fitted to a 1:2 binding model using WinEQNMR 2. $\beta_1 = K_1 = 5248\ M^{-1}$ (163.8), $\beta_2 = 191265\ M^{-2}$ (97750).

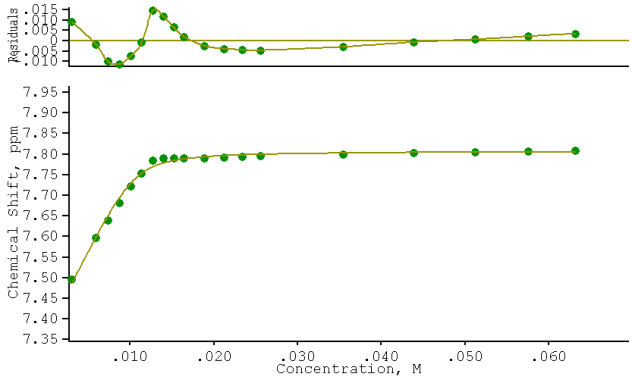

Figure A2.67 Binding curve from the ^{1}H NMR titration of receptor **178** with TBA_2SO_4 in DMSO-d_5/ H_2O 0.5 % following the aromatic CH doublet centered at ~7.4 ppm. The data was fitted to a 1:1 binding model using WinEQNMR 2. $K_\alpha = 3379\ M^{-1}$ (487.1).

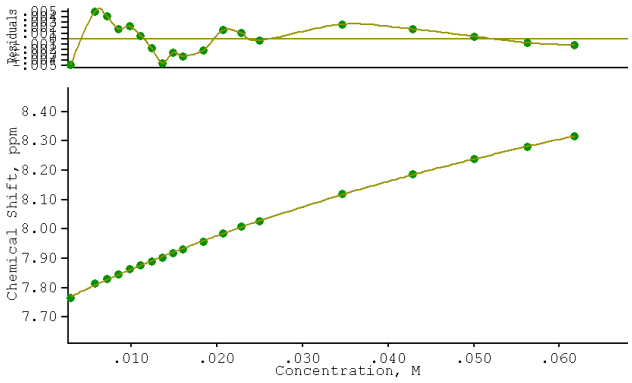

Figure A2.68 Binding curve from the ^{1}H NMR titration of receptor **179** with TBACl in DMSO-d_5/ H_2O 0.5 % following the thiourea NH resonance at ~7.7 ppm. The data was fitted to a 1:1 biding model using WinEQNMR 2. K_a = 10 M^{-1} (0.512).

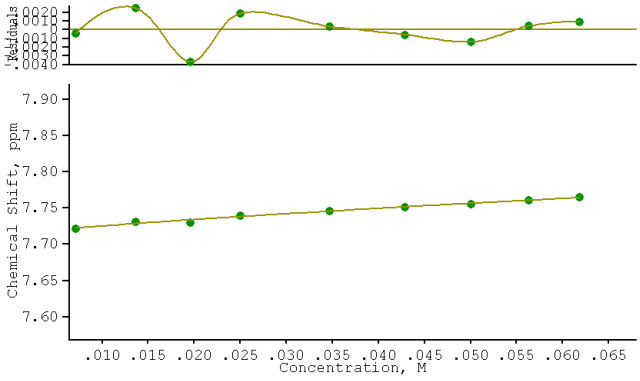

Figure A2.69 Binding curve from the ^{1}H NMR titration of receptor **179** with $TBANO_3$ in DMSO-d_5/ H_2O 0.5 % following the thiourea NH resonance at ~7.7 ppm. The data was fitted to a 1:1 biding model using WinEQNMR 2. K_a < 10 M^{-1}.

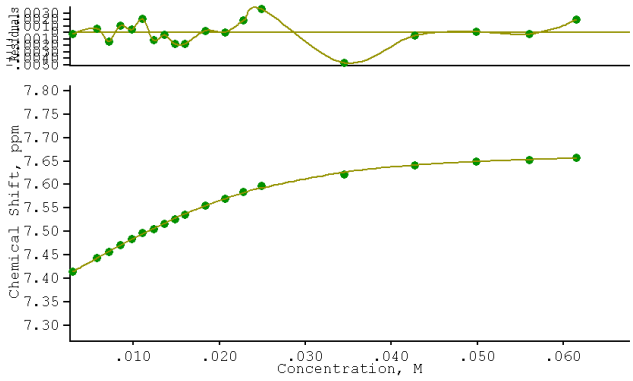

Figure A2.70 Binding curve from the ^{1}H NMR titration of receptor **179** with $TEAHCO_3$ in DMSO-d_5/ H_2O 0.5 % following the aromatic CH doublet centered at ~7.4 ppm. The data was fitted to a 1:2 binding model using WinEQNMR 2. $\beta_1 = K_1 = 114\ M^{-1}$ (20.65), $\beta_2 = 21730\ M^{-2}$ (491).

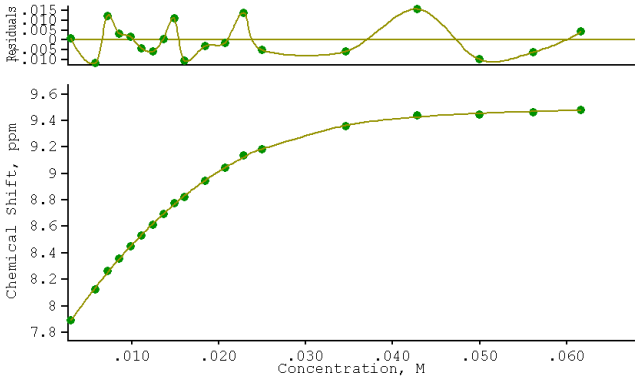

Figure A2.71 Binding curve from the ^{1}H NMR titration of receptor **179** with $TBAH_2PO_4$ in DMSO-d_5/ H_2O 0.5 % following the thiourea NH resonance at ~7.7 ppm. The data was fitted to a 1:2 binding model using WinEQNMR 2. $\beta_1 = K_1 = 157\ M^{-1}$ (64.53), $\beta_2 = 34612\ M^{-2}$ (11710).

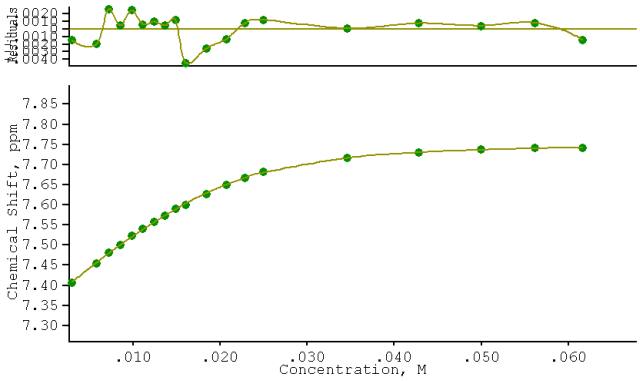

Figure A2.72 Binding curve from the ^{1}H NMR titration of receptor **179** with $TBAH_2PO_4$ in DMSO-d_5/ H_2O 0.5 % following the aromatic CH doublet centered at ~7.4 ppm. The data was fitted to a 1:2 binding model using WinEQNMR 2. $\beta_1 = K_1 = 346$ M^{-1} (37.69), $\beta_2 = 88311$ M^{-2} (521.4).

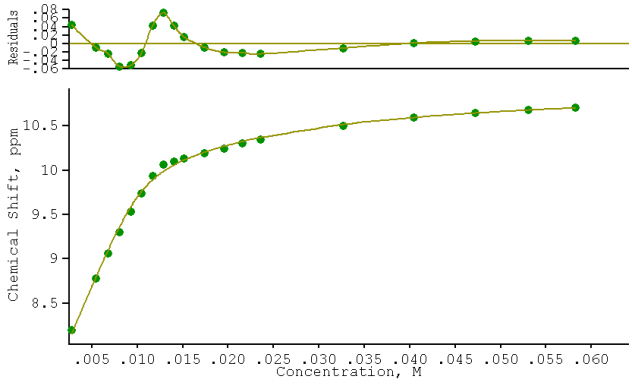

Figure A2.73 Binding curve from the ^{1}H NMR titration of receptor **179** with TBA_2SO_4 in DMSO-d_5/ H_2O 0.5 % following the thiourea NH resonance at ~7.7 ppm. The data was fitted to a 1:2 binding model using WinEQNMR 2. $\beta_1 = K_1 = 6339\ M^{-1}$ (1119), $\beta_2 = 444065\ M^{-2}$ (48400).

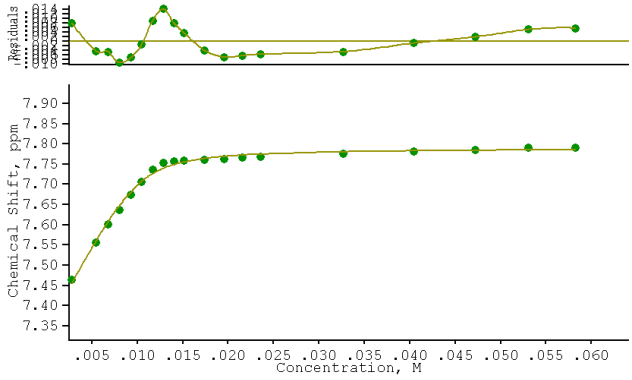

Figure A2.74 Binding curve from the ^{1}H NMR titration of receptor **179** with TBA_2SO_4 in DMSO-d_5/ H_2O 0.5 % following the aromatic CH doublet centered at ~7.4 ppm. The data was fitted to a 1:1 binding model using WinEQNMR 2. $K_\alpha = 2091\ M^{-1}$ (273.5).

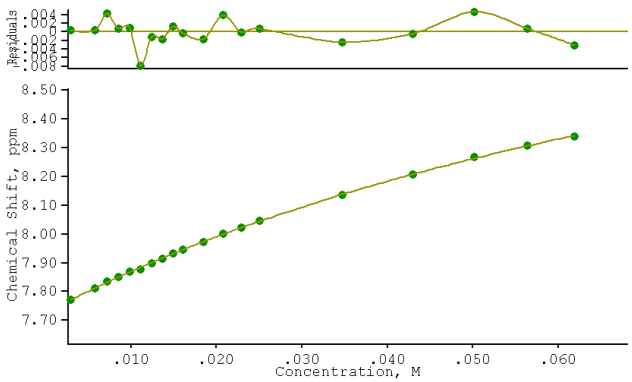

Figure A2.75 Binding curve from the ^{1}H NMR titration of receptor **180** with TBACl in DMSO-d_5/ H_2O 0.5 % following the thiourea NH resonance at ~7.7 ppm. The data was fitted to a 1:1 biding model using WinEQNMR 2. K_a = 11 M^{-1} (0.5375).

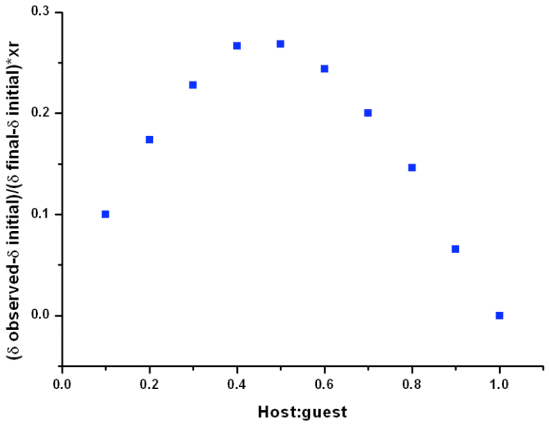

Figure A2.76 Job plot analysis for the interaction of receptor **180** with TBACl following the thiourea NH resonance at ~7.7 ppm.

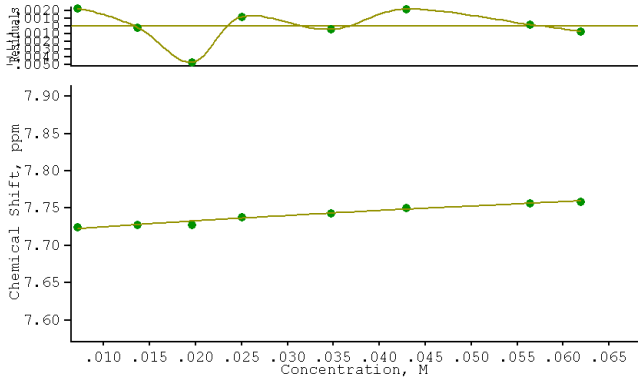

Figure A2.77 Binding curve from the ^{1}H NMR titration of receptor **180** with $TBANO_3$ in DMSO-d_5/ H_2O 0.5 % following the thiourea NH resonance at ~7.7 ppm. The data was fitted to a 1:1 biding model using WinEQNMR 2. $K_a < 10\ M^{-1}$.

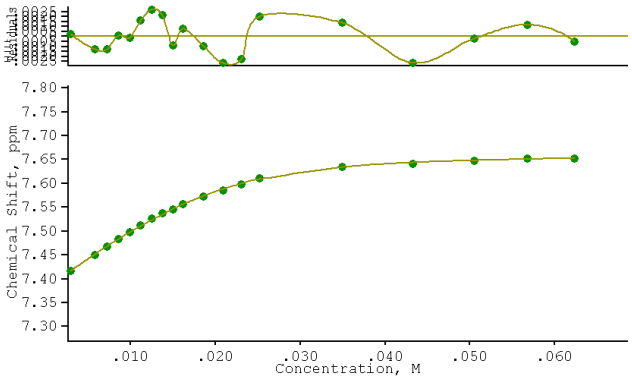

Figure A2.78 Binding curve from the ^{1}H NMR titration of receptor **180** with $TEAHCO_3$ in DMSO-d_5/ H_2O 0.5 % following the aromatic CH doublet centered at ~7.4 ppm. The data was fitted to a 1:2 binding model using WinEQNMR 2. $\beta_1 = K_1 = 264\ M^{-1}$ (4.811), $\beta_2 = 59925\ M^{-2}$ (430.2).

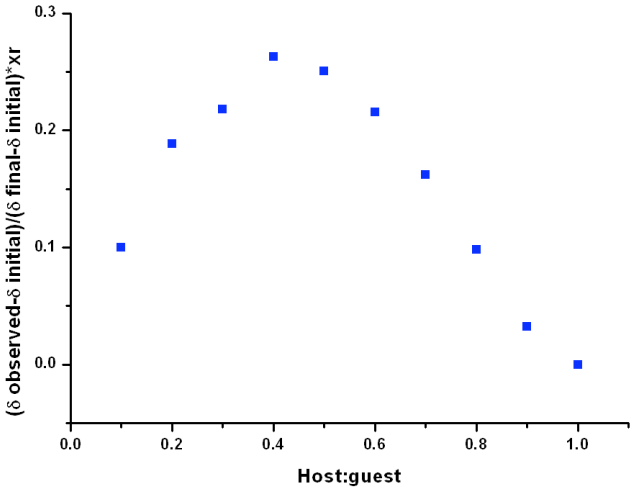

Figure A2.79 Job plot analysis for the interaction of receptor **170** with $TEAHCO_3$ following the aromatic CH resonance at ~7.4 ppm.

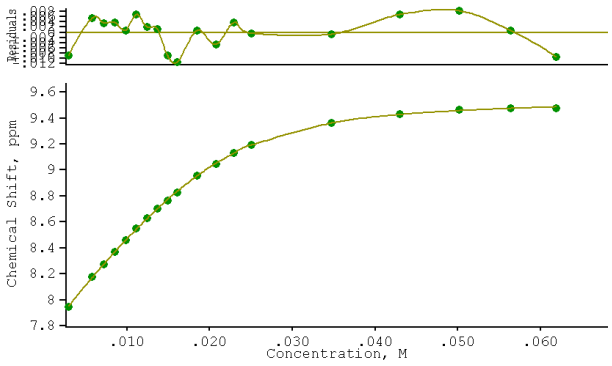

Figure A2.80 Binding curve from the ^{1}H NMR titration of receptor **180** with $TBAH_2PO_4$ in DMSO-d_5/ H_2O 0.5 % following the thiourea NH resonance at ~7.7 ppm. The data was fitted to a 1:2 binding model using WinEQNMR 2. $\beta_1 = K_1 = 343\ M^{-1}$ (23.34), $\beta_2 = 87795\ M^{-2}$ (591.9).

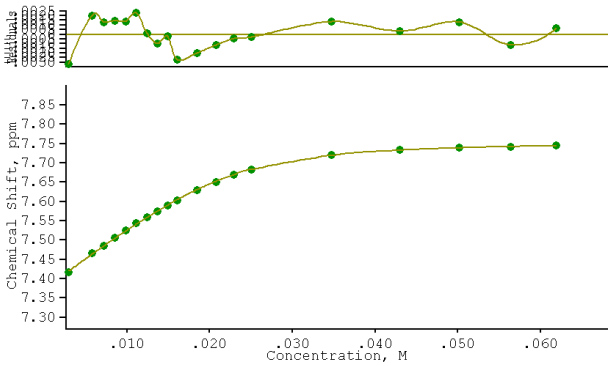

Figure A2.81 Binding curve from the ^{1}H NMR titration of receptor **180** with $TBAH_2PO_4$ in DMSO-d_5/ H_2O 0.5 % following the aromatic CH doublet centered at ~7.4 ppm. The data was fitted to a 1:2 binding model using WinEQNMR 2. $\beta_1 = K_1 = 308\ M^{-1}$ (38.7), $\beta_2 = 96231\ M^{-2}$ (3777).

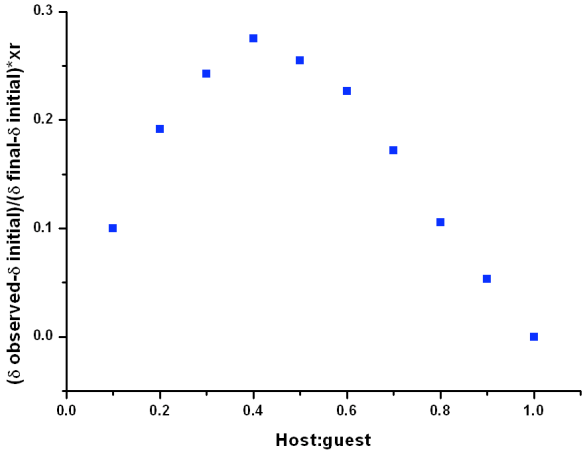

Figure A2.82 Job plot analysis for the interaction of receptor **180** with $TBAH_2PO_4$ following the thiourea NH resonance at ~7.7 ppm

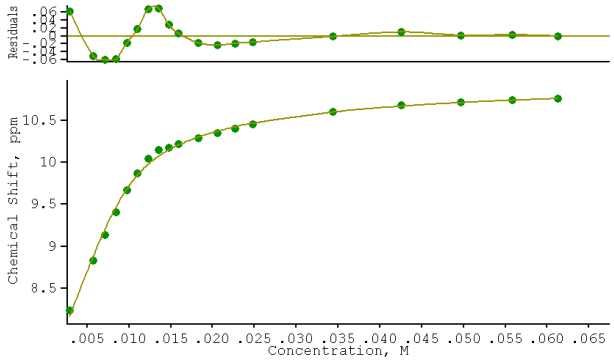

Figure A2.83 Binding curve from the ^{1}H NMR titration of receptor **180** with TBA_2SO_4 in DMSO-d_5/ H_2O 0.5 % following the thiourea NH resonance at ~7.7 ppm. The data was fitted to a 1:2 binding model using WinEQNMR 2. $\beta_1 = K_1 = 3195\ M^{-1}$ (766.9), $\beta_2 = 122175\ M^{-2}$ (73710).

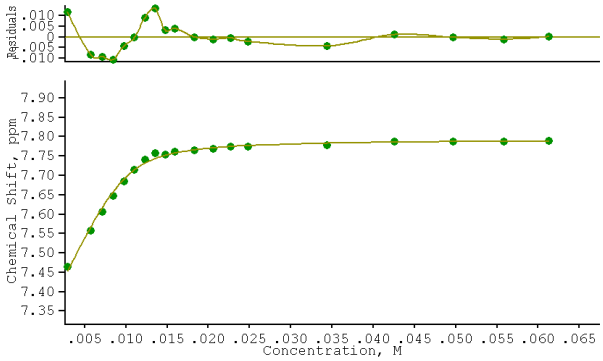

Figure A2.84 Binding curve from the ^{1}H NMR titration of receptor **180** with TBA_2SO_4 in DMSO-d_5/ H_2O 0.5 % following the aromatic CH doublet centered at ~7.4 ppm. The data was fitted to a 1:1 binding model using WinEQNMR 2. $K_\alpha = 1764\ M^{-1}$ (65.37).

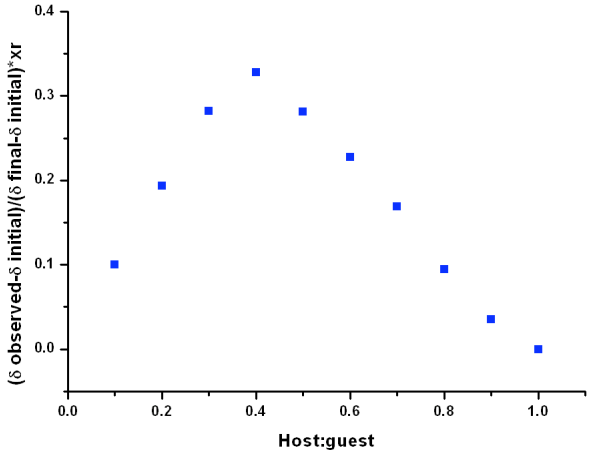

Figure A2.85 Job plot analysis for the interaction of receptor **180** with TBA_2SO_4 following the urea NH resonance at ~8.3 ppm.

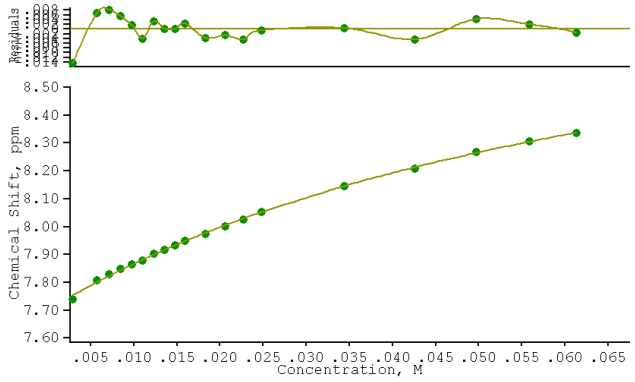

Figure A2.86 Binding curve from the ^{1}H NMR titration of receptor **181** with TBACl in DMSO-d_5/ H_2O 0.5 % following the thiourea NH resonance at ~7.7 ppm. The data was fitted to a 1:1 biding model using WinEQNMR 2. K_a = 16 M^{-1} (1.182).

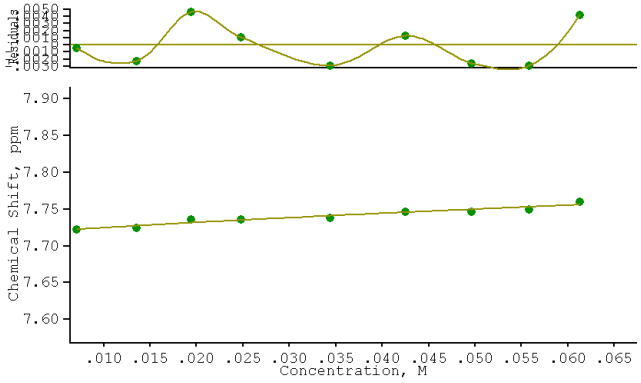

Figure A2.87 Binding curve from the ^{1}H NMR titration of receptor **181** with $TBANO_3$ in DMSO-d_5/ H_2O 0.5 % following the thiourea NH resonance at ~7.7 ppm. The data was fitted to a 1:1 biding model using WinEQNMR 2. K_a < 10 M^{-1}.

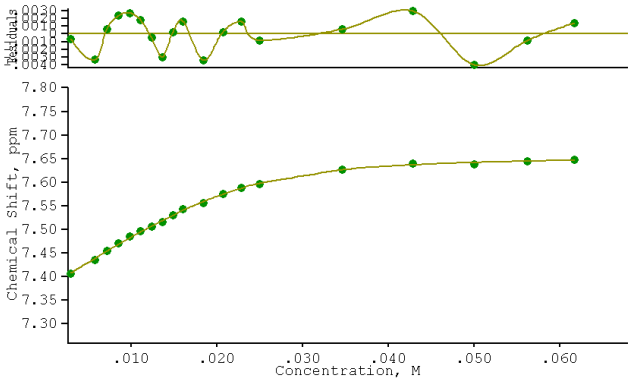

Figure A2.88 Binding curve from the ^{1}H NMR titration of receptor **181** with $TEAHCO_3$ in DMSO-d_5/ H_2O 0.5 % following the aromatic CH doublet centered at ~7.4 ppm. The data was fitted to a 1:2 binding model using WinEQNMR 2. $\beta_1 = K_1 = 189\ M^{-1}$ (45.47), $\beta_2 = 54817\ M^{-2}$ (4834).

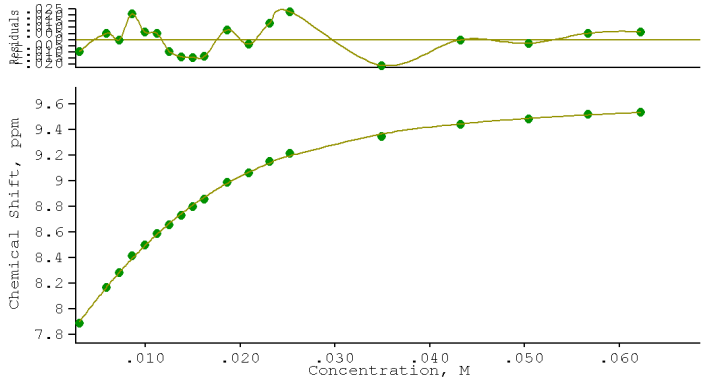

Figure A2.89 Binding curve from the ^{1}H NMR titration of receptor **181** with $TBAH_2PO_4$ in DMSO-d_5/ H_2O 0.5 % following the thiourea NH resonance at ~7.7 ppm. The data was fitted to a 1:2 binding model using WinEQNMR 2. $\beta_1 = K_1 = 458\ M^{-1}$ (44.48), $\beta_2 = 50590\ M^{-2}$ (7370).

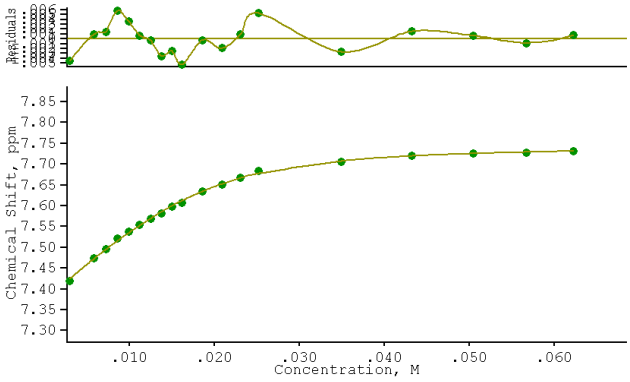

Figure A2.90 Binding curve from the ^{1}H NMR titration of receptor **181** with $TBAH_2PO_4$ in DMSO-d_5/ H_2O 0.5 % following the aromatic CH doublet centered at ~7.4 ppm. The data was fitted to a 1:2 binding model using WinEQNMR 2. $\beta_1 = K_1 = 516\ M^{-1}$ (75.21), $\beta_2 = 105518\ M^{-2}$ (7700).

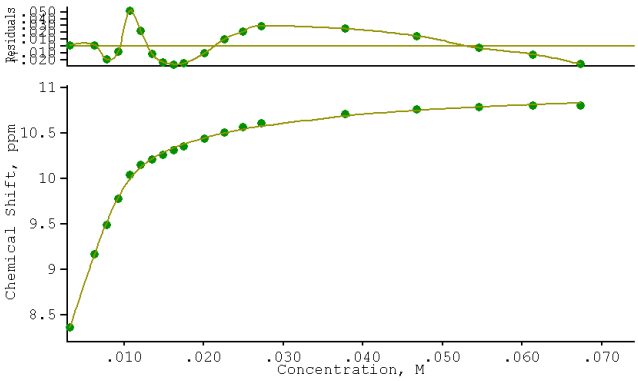

Figure A2.91 Binding curve from the ^{1}H NMR titration of receptor **181** with TBA_2SO_4 in DMSO-d_5/ H_2O 0.5 % following the thiourea NH resonance at ~7.7 ppm. The data was fitted to a 1:2 binding model using WinEQNMR 2. $\beta_1 = K_1 = 5179$ M^{-1} (208.9), $\beta_2 = 316833$ M^{-2} (34190).

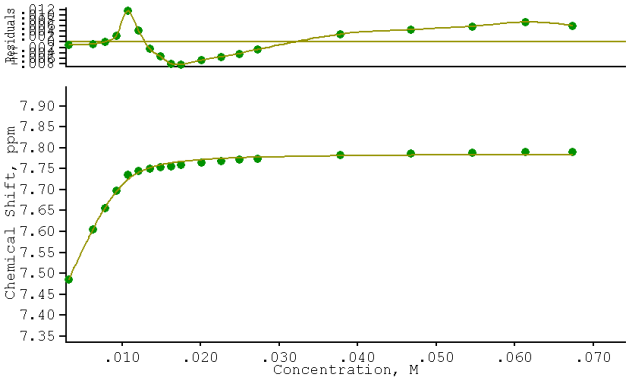

Figure A2.92 Binding curve from the ^{1}H NMR titration of receptor **181** with TBA_2SO_4 in DMSO-d_5/ H_2O 0.5 % following the aromatic CH doublet centered at ~7.4 ppm. The data was fitted to a 1:1 binding model using WinEQNMR 2. $K_\alpha = 2593$ M^{-1} (300.1).

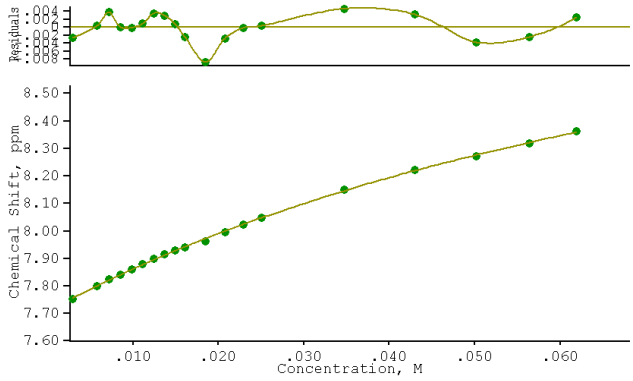

Figure A2.93 Binding curve from the ^{1}H NMR titration of receptor **182** with TBACl in DMSO-d_5/ H_2O 0.5 % following the thiourea NH resonance at ~7.7 ppm. The data was fitted to a 1:1 biding model using WinEQNMR 2. K_a = 11 M^{-1} (0.6014).

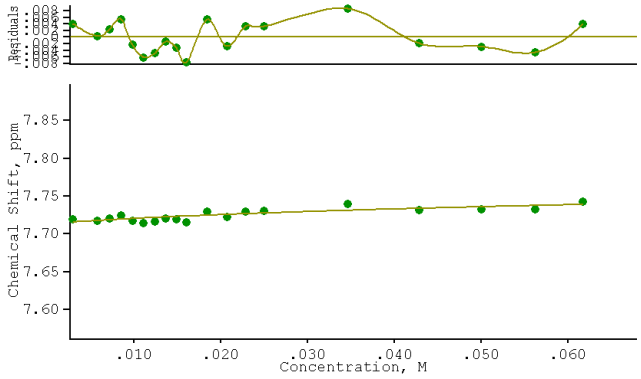

Figure A2.94 Binding curve from the ^{1}H NMR titration of receptor **182** with $TBANO_3$ in DMSO-d_5/ H_2O 0.5 % following the thiourea NH resonance at ~7.7 ppm. The data was fitted to a 1:1 biding model using WinEQNMR 2. K_a < 10 M^{-1}.

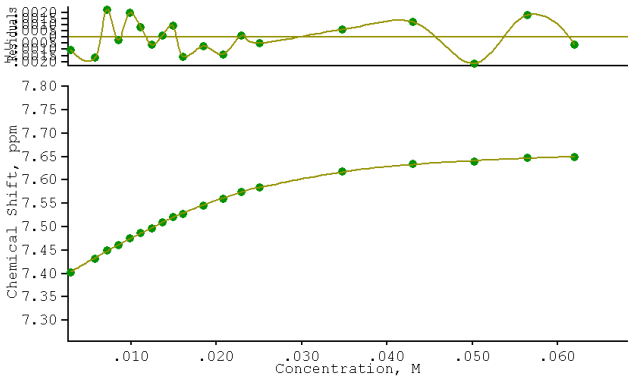

Figure A2.95 Binding curve from the ^{1}H NMR titration of receptor **182** with $TEAHCO_3$ in DMSO-d_5/ H_2O 0.5 % following the aromatic CH doublet centered at ~7.4 ppm. The data was fitted to a 1:2 binding model using WinEQNMR 2. $\beta_1 = K_1 = 247$ M^{-1} (31.26), $\beta_2 = 33963$ M^{-2} (3818).

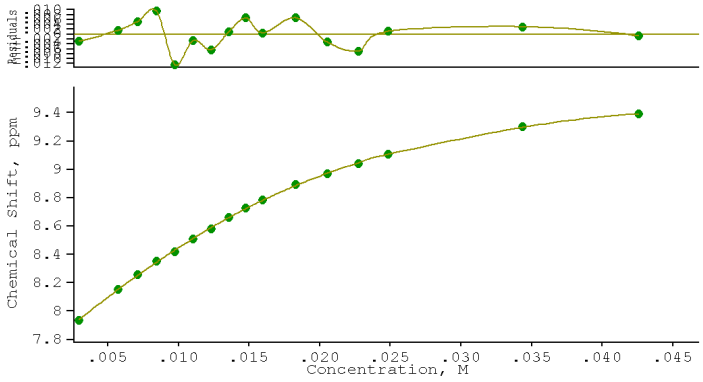

Figure A2.96 Binding curve from the ^{1}H NMR titration of receptor **182** with $TBAH_2PO_4$ in DMSO-d_5/ H_2O 0.5 % following the thiourea NH resonance at ~7.7 ppm. The data was fitted to a 1:2 binding model using WinEQNMR 2. $\beta_1 = K_1 = 676$ M^{-1} (153.5), $\beta_2 = 69062$ M^{-2} (11810).

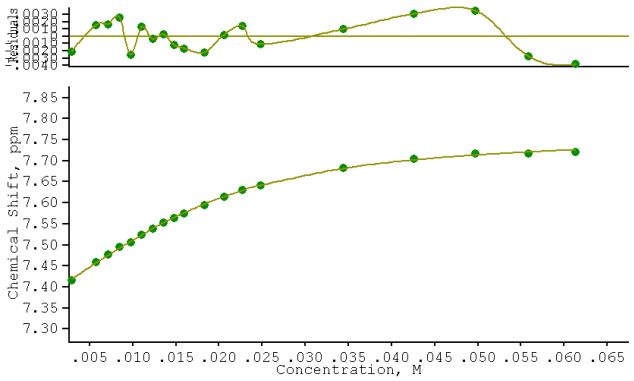

Figure A2.97 Binding curve from the ^{1}H NMR titration of receptor **182** with $TBAH_2PO_4$ in DMSO-d_5/ H_2O 0.5 % following the aromatic CH doublet centered at ~7.4 ppm. The data was fitted to a 1:2 binding model using WinEQNMR 2. $\beta_1 = K_1 = 473\ M^{-1}$ (21.05), $\beta_2 = 48132\ M^{-2}$ (2978).

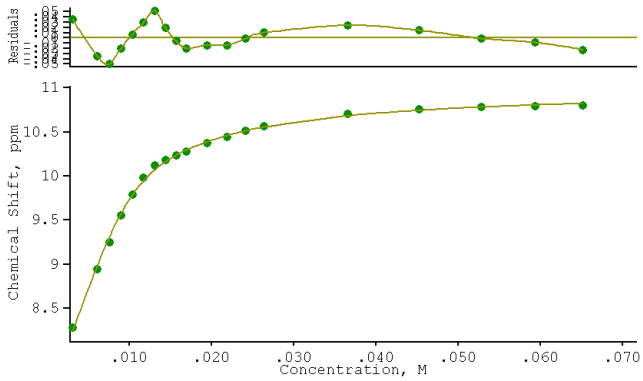

Figure A2.98 Binding curve from the ^{1}H NMR titration of receptor **182** with TBA_2SO_4 in DMSO-d_5/ H_2O 0.5 % following the thiourea NH resonance at ~7.7 ppm. The data was fitted to a 1:2 binding model using WinEQNMR 2. $\beta_1 = K_1 = 3427\ M^{-1}$ (541), $\beta_2 = 308496\ M^{-2}$ (45540).

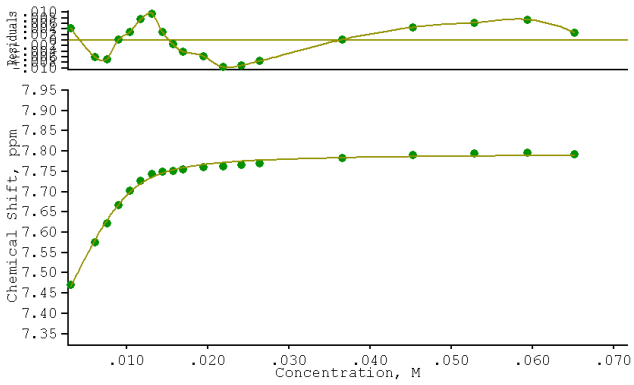

Figure A2.99 Binding curve from the ^{1}H NMR titration of receptor **182** with TBA_2SO_4 in DMSO-d_5/ H_2O 0.5 % following the aromatic CH doublet centered at ~7.4 ppm. The data was fitted to a 1:1 binding model using WinEQNMR 2. K_α = 1525 M^{-1} (161.5).

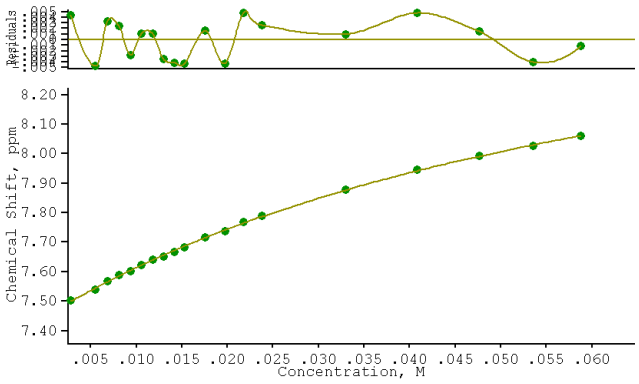

Figure A2.100 Binding curve from the ^{1}H NMR titration of receptor **183** with TBACl in DMSO-d_5/ H_2O 0.5 % following the thiourea NH resonance at ~7.4 ppm. The data was fitted to a 1:1 biding model using WinEQNMR 2. K_a = 17 M^{-1} (0.8565).

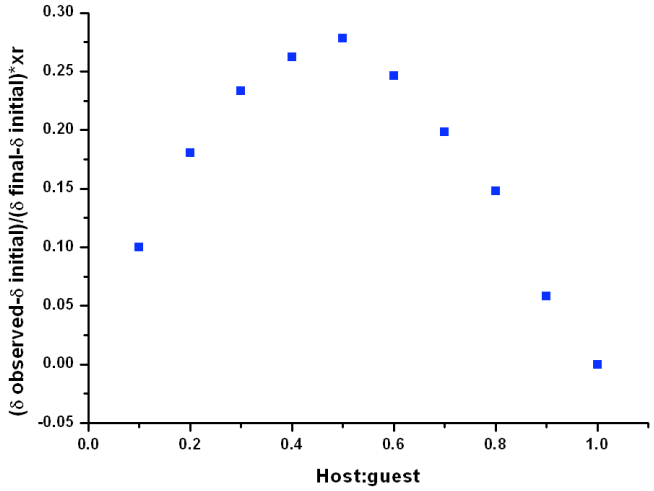

Figure A2.101 Job plot analysis for the interaction of receptor **183** with TBACl following the thiourea NH resonance at ~7.4 ppm.

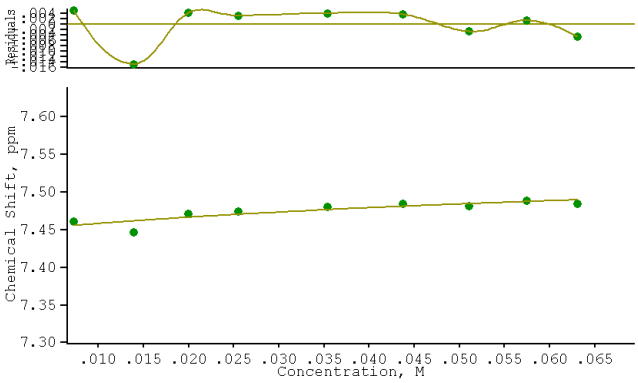

Figure A2.102 Binding curve from the ^{1}H NMR titration of receptor **183** with $TBANO_3$ in DMSO-d_5/ H_2O 0.5 % following the thiourea NH resonance at ~7.4 ppm. The data was fitted to a 1:1 biding model using WinEQNMR 2. $K_a < 10$ M^{-1}.

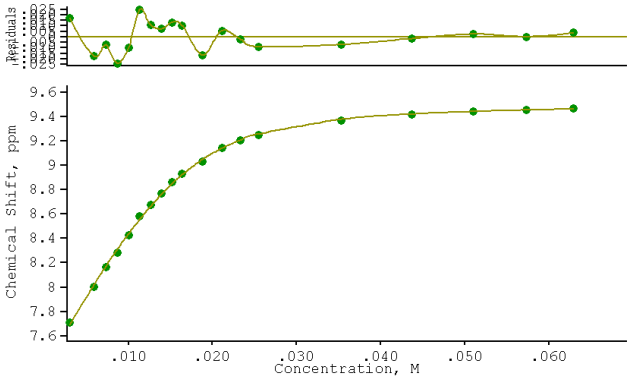

Figure A2.103 Binding curve from the ^{1}H NMR titration of receptor **183** with $TEAHCO_3$ in DMSO-d_5/ H_2O 0.5 % following the thiourea NH resonance at ~7.4 ppm. The data was fitted to a 1:2 binding model using WinEQNMR 2. $\beta_1 = K_1 = 2907\ M^{-1}$ (252.8), $\beta_2 = 982512\ M^{-2}$ (33830).

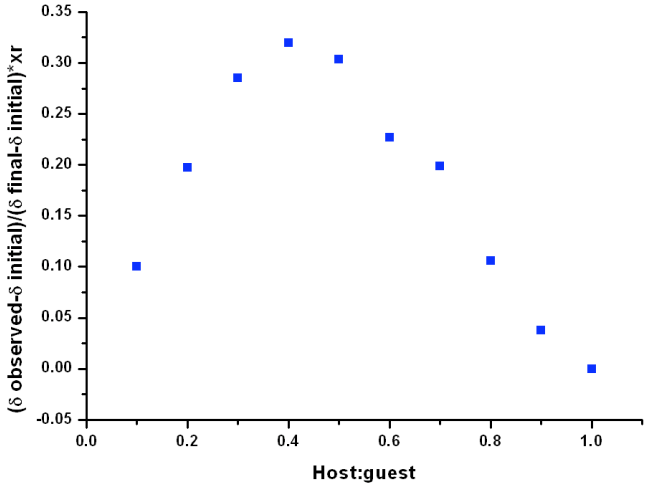

Figure A2.104 Job plot analysis for the interaction of receptor **183** with $TEAHCO_3$ following the thiourea NH resonance at ~7.4 ppm.

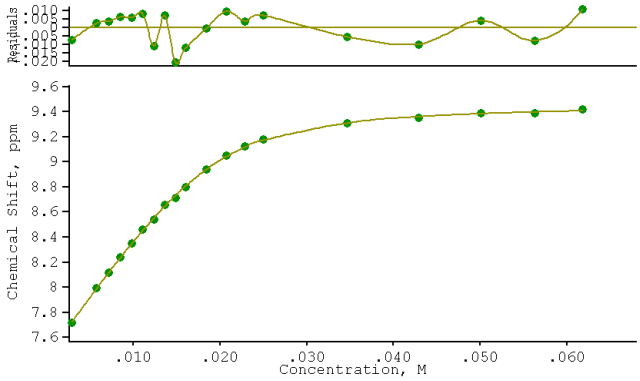

Figure A2.105 Binding curve from the ^{1}H NMR titration of receptor **183** with $TBAH_2PO_4$ in DMSO-d_5/ H_2O 0.5 % following the thiourea NH resonance at ~7.4 ppm. The data was fitted to a 1:2 binding model using WinEQNMR 2. $\beta_1 = K_1 = 2281$ M^{-1} (167.7), $\beta_2 = 785442$ M^{-2} (19430).

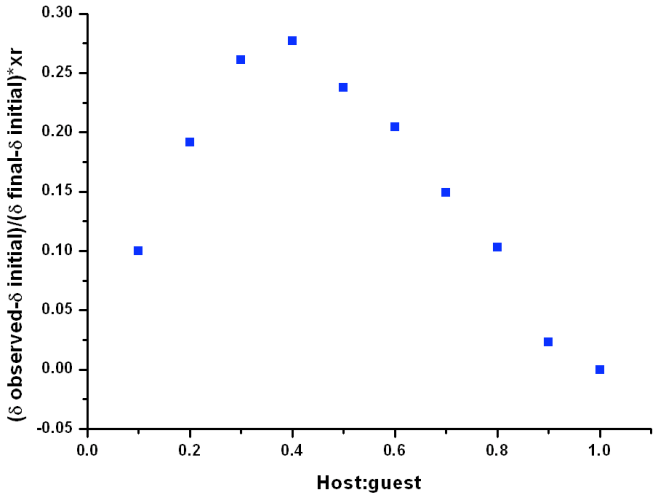

Figure A2.106 Job plot analysis for the interaction of receptor **183** with $TBAH_2PO_4$ following the thiourea NH resonance at ~7.4 ppm.

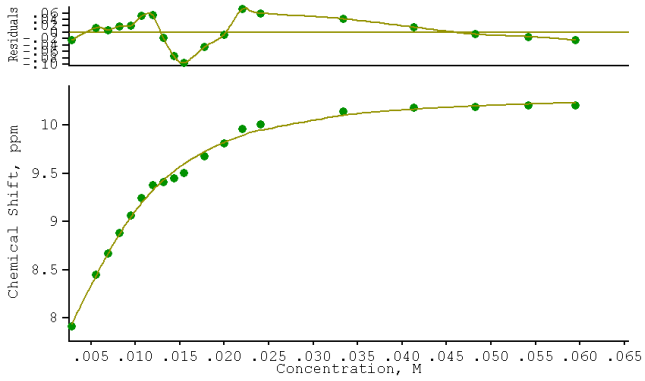

Figure A2.107 Binding curve from the ^{1}H NMR titration of receptor **183** with TBA_2SO_4 in DMSO-d_5/ H_2O 0.5 % following the thiourea NH resonance at ~7.4 ppm. The data was fitted to a 1:2 binding model using WinEQNMR 2. $\beta_1 = K_1 = 5632$ M^{-1} (392.4), $\beta_2 = 1219980$ M^{-2} (107300).

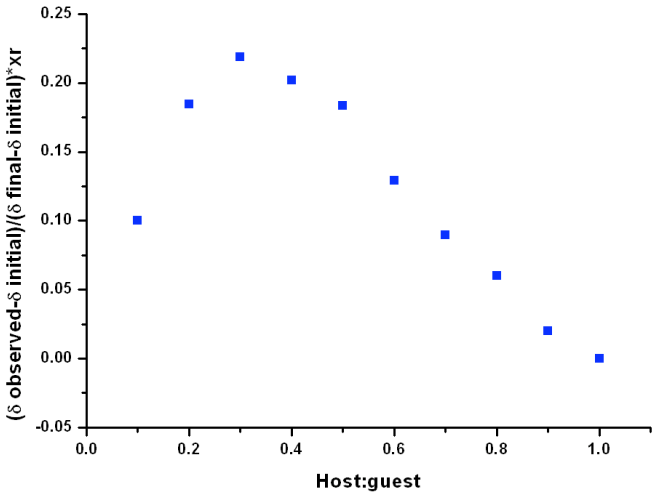

Figure A2.108 Job plot analysis for the interaction of receptor **183** with TBA_2SO_4 following the thiourea NH resonance at ~7.4 ppm.

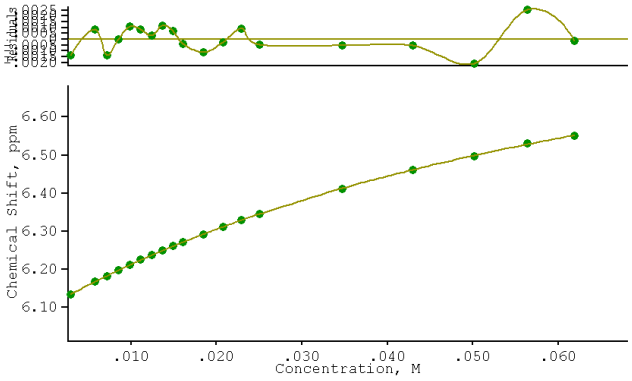

Figure A2.109 Binding curve from the ^{1}H NMR titration of receptor **184** with TBACl in DMSO-d_5/ H_2O 0.5 % following the urea NH resonance at ~6.1 ppm. The data was fitted to a 1:1 biding model using WinEQNMR 2. K_a = 14 M^{-1} (0.3389).

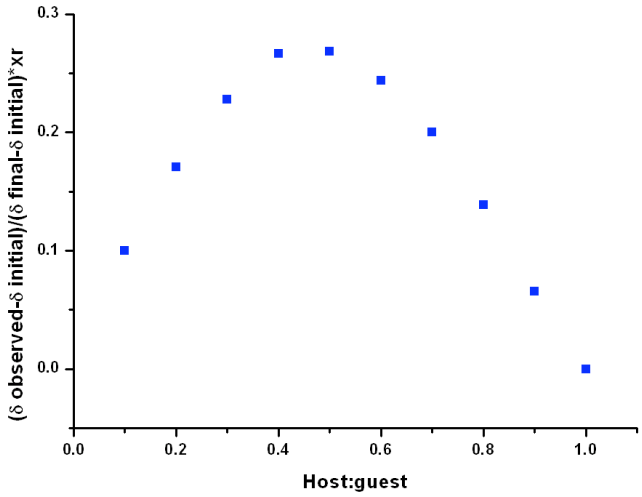

Figure A2.110 Job plot analysis for the interaction of receptor **184** with TBACl following the thiourea NH resonance at ~6.1 ppm.

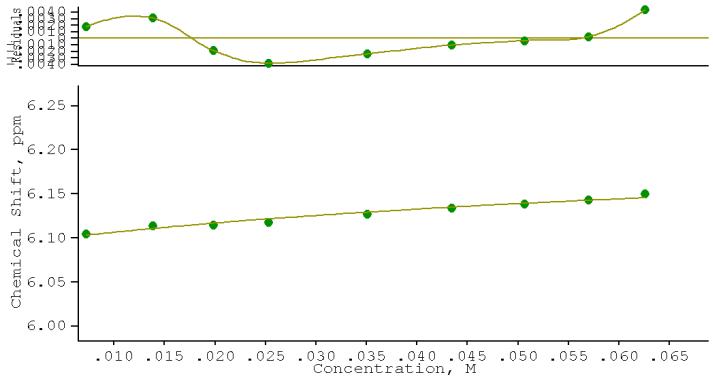

Figure A2.111 Binding curve from the ^{1}H NMR titration of receptor **184** with $TBANO_3$ in DMSO-d_5/ H_2O 0.5 % following the urea NH resonance at ~6.1 ppm. The data was fitted to a 1:1 biding model using WinEQNMR 2. $K_a < 10\ M^{-1}$.

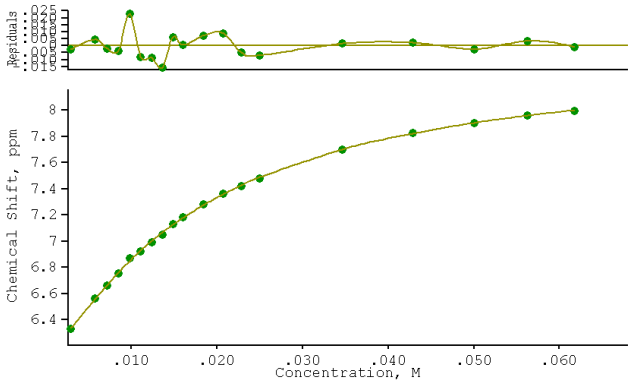

Figure A2.112 Binding curve from the ^{1}H NMR titration of receptor **184** with $TEAHCO_3$ in DMSO-d_5/ H_2O 0.5 % following the urea NH resonance at ~6.1 ppm. The data was fitted to a 1:2 binding model using WinEQNMR 2. $\beta_1 = K_1 = 3882\ M^{-1}$ (345.7), $\beta_2 = 215025\ M^{-2}$ (18020).

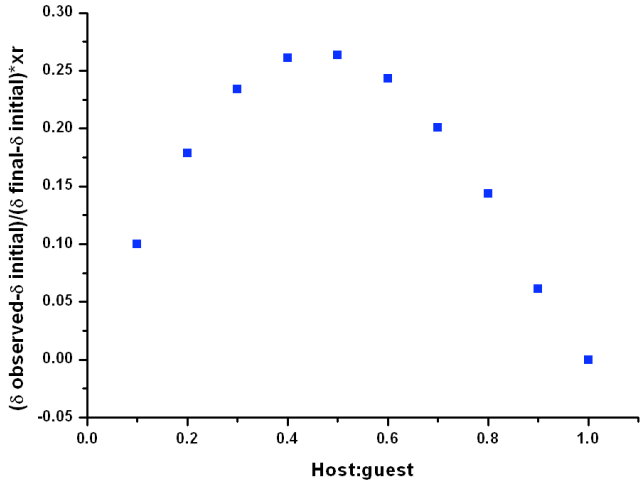

Figure A2.113 Job plot analysis for the interaction of receptor **184** with $TEAHCO_3$ following the thiourea NH resonance at ~6.1 ppm.

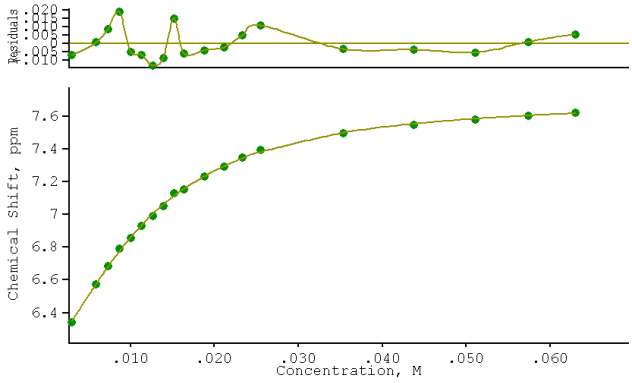

Figure A2.114 Binding curve from the ^{1}H NMR titration of receptor **184** with $TBAH_2PO_4$ in DMSO-d_5/ H_2O 0.5 % following the thiourea NH resonance at ~7.4 ppm. The data was fitted to a 1:2 binding model using WinEQNMR 2. $\beta_1 = K_1 = 3584\ M^{-1}$ (239.7), $\beta_2 = 483236\ M^{-2}$ (13770).

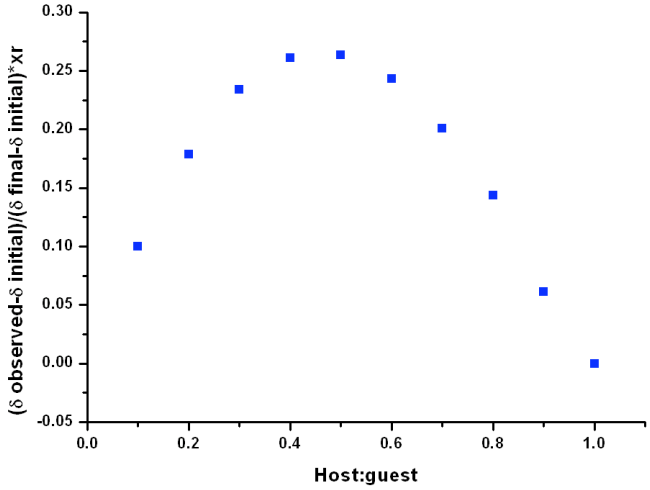

Figure A2.115 Job plot analysis for the interaction of receptor **184** with $TBAH_2PO_4$ following the thiourea NH resonance at ~6.1 ppm.

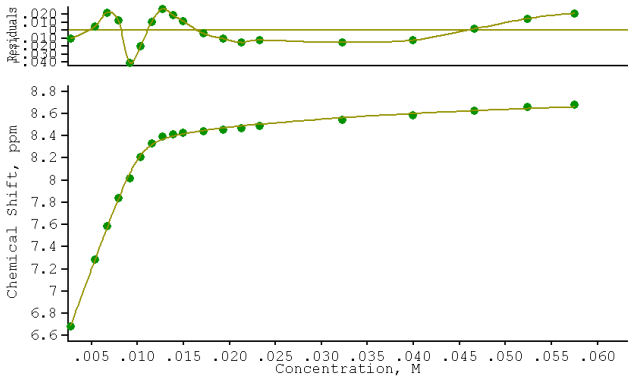

Figure A2.116 Binding curve from the ^{1}H NMR titration of receptor **184** with TBA_2SO_4 in DMSO-d_5/ H_2O 0.5 % following the thiourea NH resonance at ~7.4 ppm. The data was fitted to a 1:2 binding model using WinEQNMR 2. $\beta_1 = K_1 > 10^4$ M^{-1}, $\beta_2 = 419700$ M^{-2} (44060).

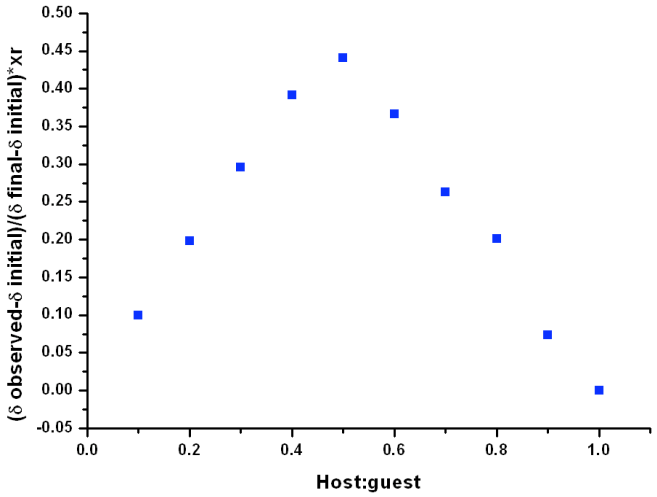

Figure A2.117 Job plot analysis for the interaction of receptor **184** with TBA_2SO_4 following the thiourea NH resonance at ~6.1 ppm.

A2.3 Stack plots

A2.3.1 Chapter 3

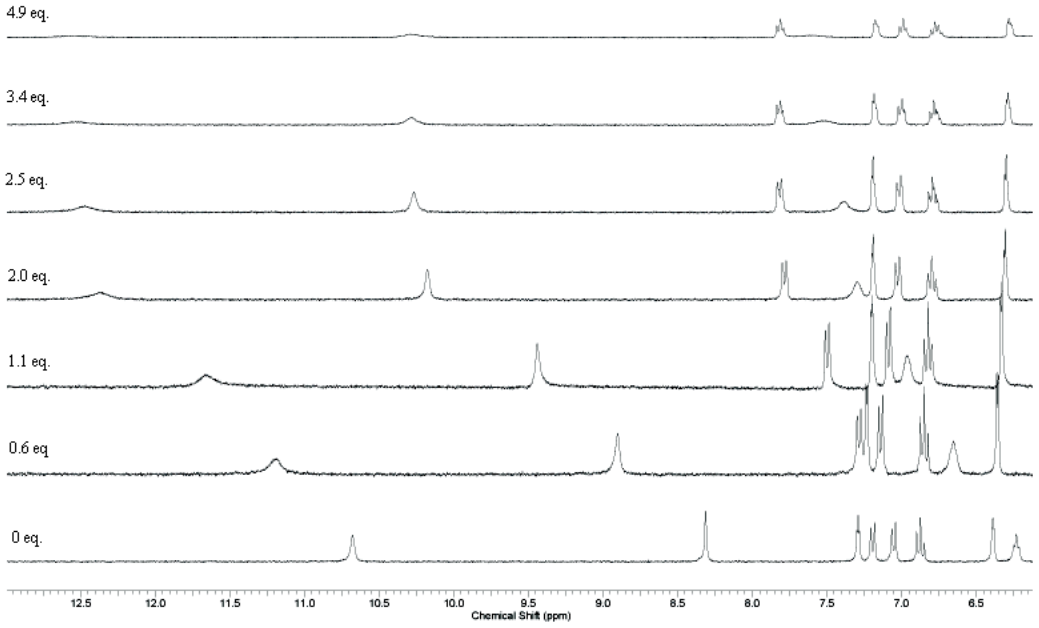

Figure A2.118 Stack plot showing the titration of receptor **161** with $TBAH_2PO_4$ in DMSO-d_6/H_2O 0.5 %.

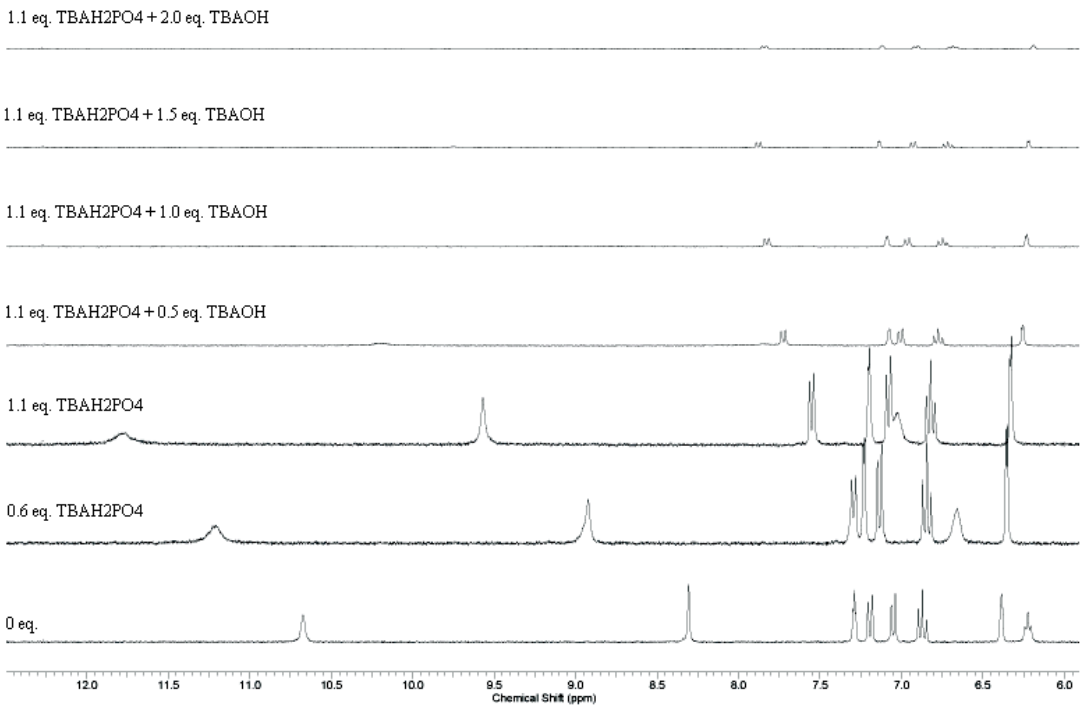

Figure A2.119 Stack plot showing the titration of receptor **161** with up to 1.1 eq. $TBAH_2PO_4$ in DMSO-d_6/H_2O 0.5 % followed by the addition of TBAOH (1 M in MeOH).

A2.3.2 Stack plots from Chapter 4

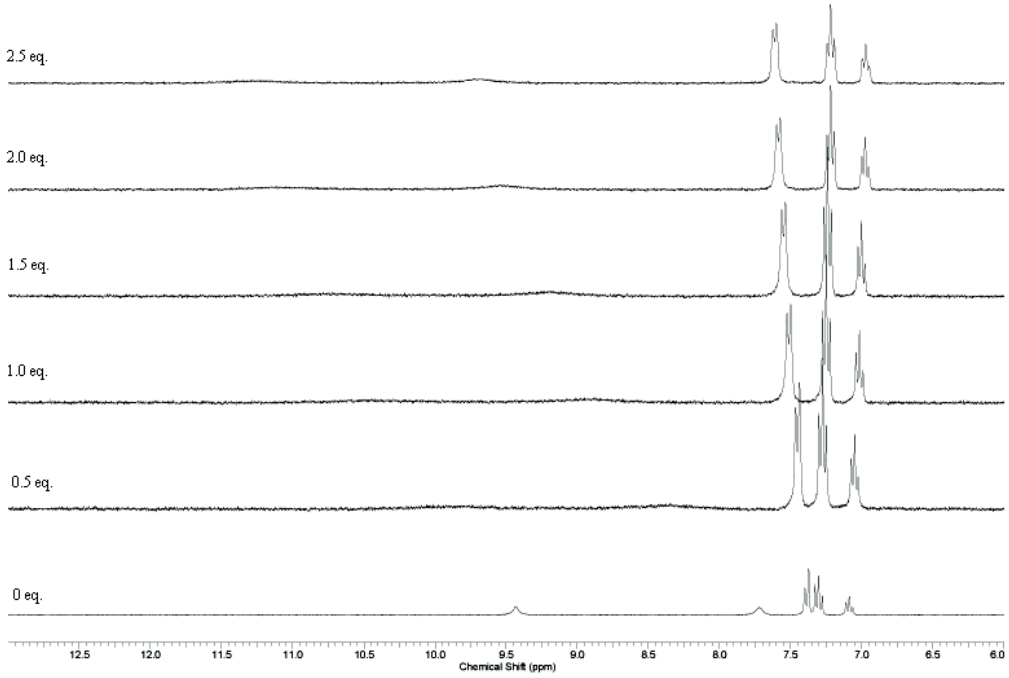

Figure A2.120 Stack plot showing the titration of receptor **180** with $TEAHCO_3$ in DMSO-d_6/ H_2O 0.5 %.

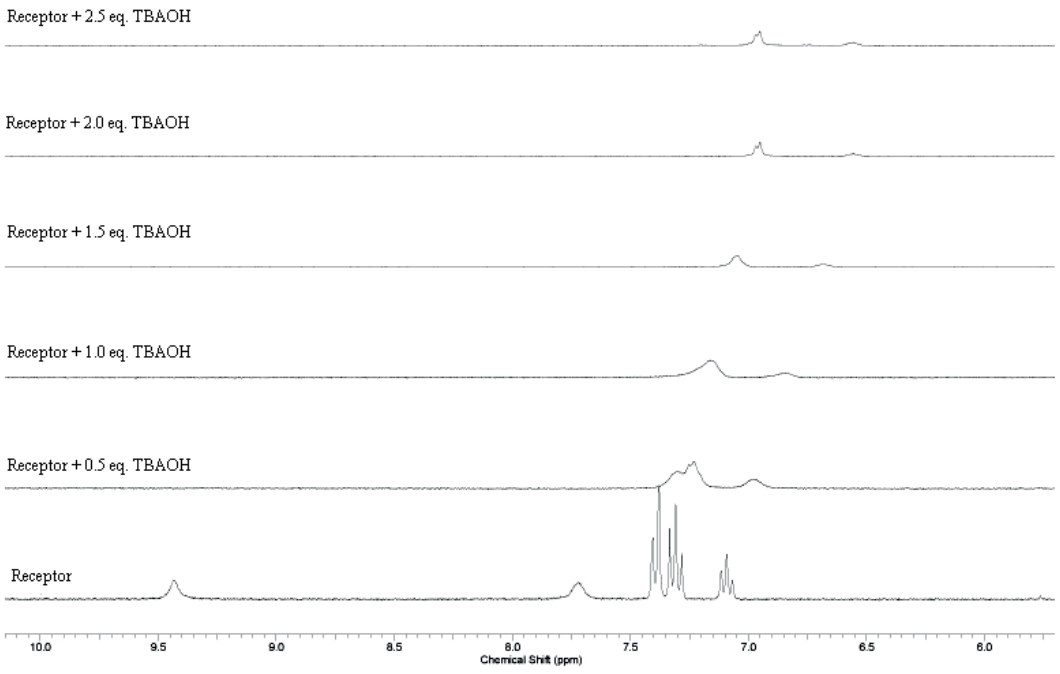

Figure A2.121 Stack plot showing the titration of receptor **180** with TBAOH (1 M in MeOH) in DMSO-d_6/H_2O 0.5 %.

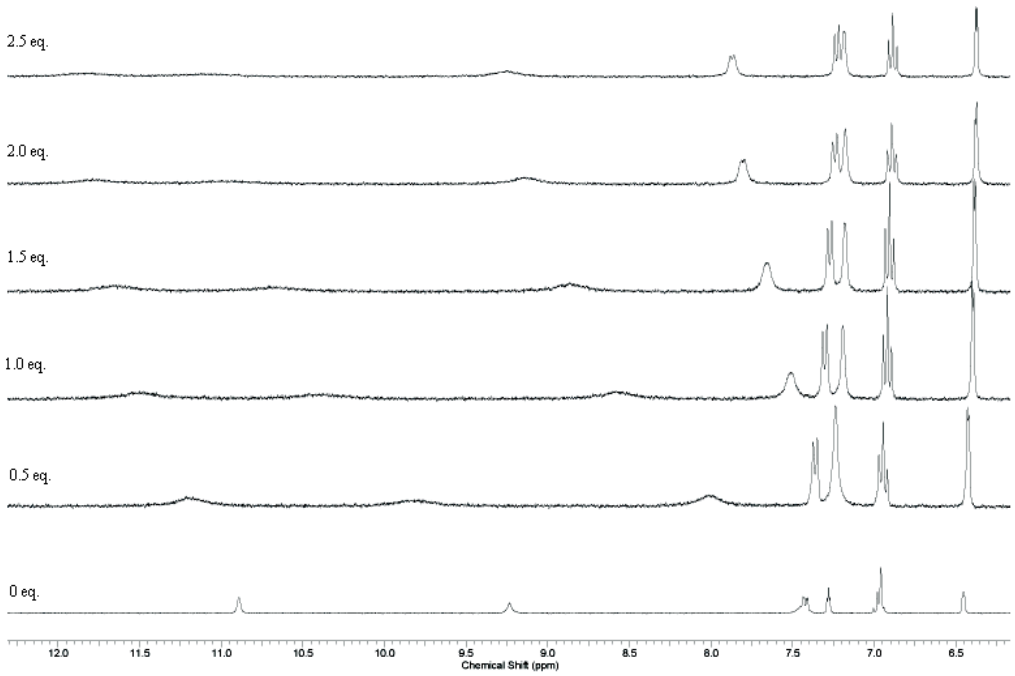

Figure A2.122 Stack plot showing the titration of receptor **183** with $TEAHCO_3$ in DMSO-d_6/H_2O 0.5 %.

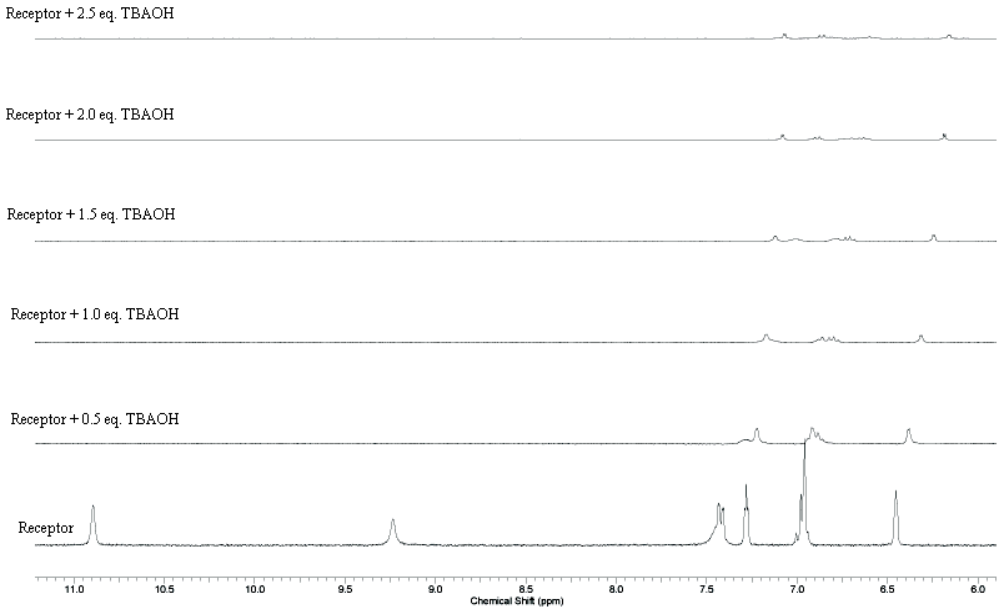

Figure A2.123 Stack plot showing the titration of receptor **183** with TBAOH (1 M in MeOH) in DMSO-d_6/H_2O 0.5 %.

A3 X-ray Crystal Structure Data

The crystal structures presented in **Chapters 2** and **3** were solved by the EPSRC National Crystallography Service (Dr M. E. Light). The refinement of the structures and the fractional coordinates are reported for the sake of completeness and so that the structure may be regenerated from the text of this thesis if necessary.

A3.1 Chapter 2

A3.1.1 Receptor 127

Table A3.1 Crystal data and structure refinement details.

Identification code	**2010sot0813** (indole thiourea)
Empirical formula	$C_{14}H_{19}N_3S$
Formula weight	261.38
Temperature	120(2) K
Wavelength	0.71073 Å
Crystal system	Tetragonal
Space group	$I4_1/a$
Unit cell dimensions	a = 29.2158(5) Å
	c = 7.5897(2) Å
Volume	6478.3(2) Å^3
Z	16
Density (calculated)	1.072 Mg / m^3
Absorption coefficient	0.189 mm^{-1}
F(000)	2240
Crystal	Needle; Colourless
Crystal size	0.23 × 0.03 × 0.03 mm^3
θ range for data collection	3.10 – 25.02°
Index ranges	$-23 \le h \le 24$, $0 \le k \le 34$, $0 \le l \le 9$
Reflections collected	2849
Independent reflections	2849 [R_{int} = 0.0000]
Completeness to θ = 25.02°	99.9 %
Absorption correction	Semi–empirical from equivalents
Max. and min. transmission	0.9944 and 0.9579
Refinement method	Full-matrix least-squares on F^2
Data / restraints / parameters	2849 / 0 / 165
Goodness-of-fit on F^2	1.059
Final R indices [$F^2 > 2\sigma(F^2)$]	$R1$ = 0.0815, $wR2$ = 0.1815
R indices (all data)	$R1$ = 0.1060, $wR2$ = 0.1930
Largest diff. peak and hole	0.592 and –0.314 e Å^{-3}

Diffractometer: *Nonius KappaCCD* area detector (ϕ scans and ω scans to fill *asymmetric unit*). **Cell determination:** DirAx (Duisenberg, A.J.M.(1992). J. Appl. Cryst. 25, 92-96.) **Data collection:** Collect (Collect: Data collection software, R. Hooft, Nonius B.V., 1998). **Data reduction and cell refinement**: *Denzo* (Z. Otwinowski & W. Minor, *Methods in Enzymology* (1997) Vol. **276**: *Macromolecular Crystallography*, part A, pp. 307–326; C. W. Carter, Jr. & R. M. Sweet, Eds., Academic Press). **Absorption correction**: Sheldrick, G. M. SADABS - Bruker Nonius area detector scaling and absorption correction - V2.10 **Structure solution**: *SHELXS97* (G. M. Sheldrick, Acta Cryst. (1990) A**46** 467–473). **Structure refinement**: *SHELXL97* (G. M. Sheldrick (1997), University of Göttingen, Germany). **Graphics:** Cameron - A Molecular Graphics Package. (D. M. Watkin, L. Pearce and C. K. Prout, Chemical Crystallography Laboratory, University of Oxford, 1993).

Special details: All hydrogens were identified in the difference map and subsequently placed in idealised positions and refined using a riding model. An unidentified (probably Et2O) disordered solvent is present in channels running along the c direction. This was treated using the Squeeze algorithm (SQUEEZE - Sluis, P. v.d. & Spek, A. L. (1990) Acta Cryst. A46, 194-201.). This has left a void of 252.00 A**3.

Table A3.2 Atomic coordinates [$\times 10^4$], equivalent isotropic displacement parameters [$Å^2 \times 10^3$] and site occupancy factors. U_{eq} is defined as one third of the trace of the orthogonalized U^{ij} tensor.

Atom	*x*	*y*	*z*	U_{eq}	*S.o.f.*
S1	7285(1)	7879(1)	98(1)	38(1)	1
N1	8523(1)	7021(1)	–2097(3)	27(1)	1
N2	8051(1)	7465(1)	1019(3)	27(1)	1
N3	8116(1)	7984(1)	–1240(4)	36(1)	1
C1	8712(1)	7127(1)	–482(4)	23(1)	1
C2	8854(1)	6829(1)	–3136(4)	29(1)	1
C3	9256(1)	6805(1)	–2251(4)	26(1)	1
C4	9179(1)	6991(1)	–520(4)	23(1)	1
C5	9444(1)	7036(1)	1007(4)	24(1)	1
C6	9243(1)	7217(1)	2496(4)	26(1)	1
C7	8789(1)	7366(1)	2485(4)	24(1)	1
C8	8520(1)	7327(1)	1003(4)	22(1)	1
C9	7854(1)	7771(1)	–73(4)	30(1)	1
C10	7947(1)	8301(1)	–2599(5)	49(1)	1
C11	8329(1)	8561(2)	–3369(6)	55(1)	1
C12	8194(1)	8862(1)	–4936(5)	49(1)	1
C13	8107(2)	8601(2)	–6615(7)	72(1)	1
C14	8576(2)	9207(2)	–5203(7)	67(1)	1

A3.2 Chapter 3

A3.2.1 Receptor 161 ($TBAH_2PO_4$ complex)

Table A3.3 Crystal data and structure refinement details.

Identification code	**2011sot0537**(CHC6 TBAH2PO4)
Empirical formula	$C_{56}H_{104}N_8O_{10}P_2$ $C_{24}H_{28}N_6O_2$, 2($C_{16}H_{36}N$), 2(H_2PO_4)
Formula weight	1111.41
Temperature	120(2) K
Wavelength	0.71073 Å
Crystal system	Monoclinic
Space group	*C*2/*c*
Unit cell dimensions	a = 19.3998(17) Å b = 20.670(2) Å β = 112.026(4)° c = 16.7096(11) Å
Volume	6211.3(9) $Å^3$
Z	4
Density (calculated)	1.188 Mg / m^3
Absorption coefficient	0.129 mm^{-1}
F(000)	2424
Crystal	Block; Colourless
Crystal size	0.25 × 0.20 × 0.20 mm^3
θ range for data collection	3.00 – 25.03°
Index ranges	$-23 \le h \le 23$, $-24 \le k \le 24$, $-19 \le l \le 19$
Reflections collected	27258
Independent reflections	5477 [R_{int} = 0.1733]
Completeness to θ = 25.03°	99.8 %
Absorption correction	Semi–empirical from equivalents
Max. and min. transmission	0.9746 and 0.9683
Refinement method	Full-matrix least-squares on F^2
Data / restraints / parameters	5477 / 0 / 350
Goodness-of-fit on F^2	1.040
Final *R* indices [$F^2 > 2\sigma(F^2)$]	*R1* = 0.0760, *wR2* = 0.1636
R indices (all data)	*R1* = 0.1719, *wR2* = 0.2048
Largest diff. peak and hole	0.428 and –0.319 e $Å^{-3}$

Diffractometer: *Nonius KappaCCD* area detector (ϕ scans and ω scans to fill *asymmetric unit*). **Cell determination:** DirAx (Duisenberg, A.J.M.(1992). J. Appl. Cryst. 25, 92-96.) **Data collection:** Collect (Collect: Data collection software, R. Hooft, Nonius B.V., 1998). **Data reduction and cell refinement**: *Denzo* (Z. Otwinowski & W. Minor, *Methods in Enzymology* (1997) Vol. **276**: *Macromolecular Crystallography*, part A, pp. 307–326; C. W. Carter, Jr. & R. M. Sweet, Eds., Academic Press). **Absorption correction**: Sheldrick, G. M. SADABS - Bruker Nonius area detector scaling and absorption correction - V2.10 **Structure solution**: *SHELXS97* (G. M. Sheldrick, Acta Cryst. (1990) A**46** 467–473). **Structure refinement**: *SHELXL97* (G. M. Sheldrick (1997), University of Göttingen, Germany). **Graphics:** Cameron - A Molecular Graphics Package. (D. M. Watkin, L. Pearce and C. K. Prout, Chemical Crystallography Laboratory, University of Oxford, 1993).

Special details: All hydrogen atoms were identified in the difference map, the torsion angle of CH_3 and O-H groups was allowed to refine. Due to symmetry constraints the occupancies of H2B and H3A were fixed at 0.5

Table A3.4 Atomic coordinates [$\times 10^4$], equivalent isotropic displacement parameters [$Å^2 \times 10^3$] and site occupancy factors. U_{eq} is defined as one third of the trace of the orthogonalized U^{ij} tensor.

Atom	*x*	*y*	*z*	U_{eq}	*S.o.f.*
O1	2000(2)	2694(2)	1492(2)	57(1)	1
N1	3279(2)	3260(2)	2430(2)	53(1)	1
N2	1774(2)	3788(2)	1235(2)	44(1)	1
N3	873(2)	3109(2)	1317(2)	46(1)	1
C1	4020(3)	3257(3)	2969(4)	73(2)	1
C2	4352(3)	3815(3)	2899(3)	67(2)	1
C3	3830(3)	4199(3)	2280(3)	50(1)	1
C4	3813(3)	4813(3)	1923(3)	58(1)	1
C5	3174(3)	5064(3)	1328(3)	56(1)	1
C6	2493(2)	4712(2)	1077(3)	38(1)	1
C7	2497(3)	4091(3)	1435(3)	48(1)	1
C8	3138(3)	3835(3)	1994(3)	52(1)	1
C9	1587(3)	3171(3)	1366(3)	43(1)	1
C10	579(3)	2511(2)	1502(3)	48(1)	1
C11	783(3)	2405(2)	2466(3)	50(1)	1
C12	425(3)	1809(3)	2681(3)	62(2)	1
P1	–60(1)	4758(1)	3728(1)	39(1)	1
O2	–228(2)	5329(2)	3099(2)	49(1)	1
O3	31(2)	4136(1)	3277(2)	49(1)	1
O4	–654(2)	4685(2)	4100(2)	51(1)	1
O5	710(2)	4878(2)	4482(2)	48(1)	1
N4	2315(2)	4198(2)	8390(2)	37(1)	1
C13	2227(3)	4911(2)	8127(3)	41(1)	1
C14	2312(3)	5380(2)	8855(3)	39(1)	1
C15	2204(3)	6063(2)	8542(3)	63(2)	1
C16	2371(3)	6563(2)	9249(3)	66(2)	1
C17	2320(2)	3801(2)	7622(3)	41(1)	1
C18	1595(2)	3726(2)	6872(3)	45(1)	1
C19	1703(3)	3310(3)	6180(3)	59(2)	1
C20	1007(3)	3205(3)	5403(3)	63(2)	1
C21	1660(2)	4011(2)	8638(3)	39(1)	1
C22	1646(2)	3310(2)	8903(3)	39(1)	1
C23	908(2)	3144(2)	8962(3)	46(1)	1
C24	887(3)	2452(2)	9254(3)	51(1)	1
C25	3039(2)	4075(2)	9145(3)	41(1)	1
C26	3750(2)	4270(2)	9018(3)	44(1)	1
C27	4422(3)	4086(2)	9802(3)	55(1)	1
C28	5155(3)	4186(3)	9677(4)	66(2)	1

Table A3.5. Hydrogen bonds [Å and °].

D–H···*A*	*d*(*D*–H)	*d*(H···*A*)	*d*(*D*···*A*)	∠(*D*H*A*)
N1–H1···O1	0.88	1.96	2.659(5)	135.2
N2–H2···O4^{i}	0.88	1.91	2.749(5)	158.2
N3–H3···O3^{i}	0.88	2.26	2.989(5)	140.1
N3–H3···O4^{i}	0.88	2.61	3.324(5)	139.3
O2–H2B···O2^{i}	0.84	1.67	2.475(6)	159.3
O3–H3A···O3^{i}	0.84	1.76	2.553(5)	157.3
O5–H5A···O4^{ii}	0.84	1.75	2.577(4)	169.1

Symmetry transformations used to generate equivalent atoms:
(i) –x,y,–z+1/2 (ii) –x,–y+1,–z+1

A3.2.2 Receptor 159 (Potassium oxalate/ 18-crown-6 complex)

Table A3.6 Crystal data and structure refinement details.

Identification code	**2011sot0006** (C4CX18-C-6)
Empirical formula	$C_{48}H_{72}K_2N_6O_{18}$
	$2(C_{12}H_{24}O_6)$, $C_{22}H_{24}N_6O_2$, $2K^+$, $C_2O_4^{2-}$
Formula weight	1099.32
Temperature	120(2) K
Wavelength	0.68890 Å
Crystal system	Monoclinic
Space group	*P*21/*n*
Unit cell dimensions	a = 22.76(3) Å
	b = 7.558(9) Å β = 97.626(19)°
	c = 31.61(5) Å
Volume	5389(13) Å^3
Z	4
Density (calculated)	1.355 Mg / m^3
Absorption coefficient	0.252 mm^{-1}
F(000)	2336
Crystal	Platelet; Brown
Crystal size	0.05 × 0.03 × 0.01 mm^3
θ range for data collection	2.85 – 24.30°
Index ranges	$-27 \le h \le 25$, $-6 \le k \le 8$, $-37 \le l \le 20$
Reflections collected	13658
Independent reflections	8840 [R_{int} = 0.2070]
Completeness to θ = 24.30°	92.0 %
Absorption correction	Semi–empirical from equivalents
Max. and min. transmission	1.000 and 0.277
Refinement method	Full-matrix least-squares on F^2
Data / restraints / parameters	8840 / 288 / 667
Goodness-of-fit on F^2	0.981
Final *R* indices [$F^2 > 2\sigma(F^2)$]	*R1* = 0.1183, *wR2* = 0.2544
R indices (all data)	*R1* = 0.3426, *wR2* = 0.4094
Largest diff. peak and hole	0.368 and –0.404 e Å^{-3}

Diffractometer: *Nonius KappaCCD* area detector (ϕ scans and ω scans to fill *asymmetric unit*). **Cell determination:** DirAx (Duisenberg, A.J.M.(1992). J. Appl. Cryst. 25, 92-96.) **Data collection:** Collect (Collect: Data collection software, R. Hooft, Nonius B.V., 1998). **Data reduction and cell refinement**: *Denzo* (Z. Otwinowski & W. Minor, *Methods in Enzymology* (1997) Vol. **276**: *Macromolecular Crystallography*, part A, pp. 307–326; C. W. Carter, Jr. & R. M. Sweet, Eds., Academic Press). **Absorption correction**: Sheldrick, G. M. SADABS - Bruker Nonius area detector scaling and absorption correction - V2.10 **Structure solution**: *SHELXS97* (G. M. Sheldrick, Acta Cryst. (1990) A**46** 467–473). **Structure refinement**: *SHELXL97* (G. M. Sheldrick (1997), University of Göttingen, Germany). **Graphics:** Cameron - A Molecular Graphics Package. (D. M. Watkin, L. Pearce and C. K. Prout, Chemical Crystallography Laboratory, University of Oxford, 1993).

Special details: All hydrogen atoms were placed in idealised positions and refined using a riding model.

Table A3.7 Atomic coordinates [× 10^4], equivalent isotropic displacement parameters [Å^2 × 10^3] and site occupancy factors. U_{eq} is defined as one third of the trace of the orthogonalized U^{ij} tensor.

Atom	*x*	*y*	*z*	U_{eq}	*S.o.f.*
N1	−593(5)	6136(14)	7339(3)	58(3)	1
N2	276(4)	5402(13)	6723(3)	49(3)	1
N3	295(5)	5052(14)	6014(4)	64(3)	1
N4	1838(5)	7825(15)	5057(3)	61(3)	1
N5	2622(5)	7024(14)	4738(3)	58(3)	1
N6	2890(5)	6591(14)	3865(3)	59(3)	1
C1	−809(7)	6430(19)	7719(5)	71(4)	1
C2	−381(7)	6300(20)	8045(5)	81(5)	1
C3	159(6)	5885(17)	7888(4)	56(4)	1
C4	747(6)	5635(16)	8059(5)	62(4)	1
C5	1173(6)	5280(18)	7811(4)	60(4)	1
C6	1027(5)	5159(15)	7364(4)	49(3)	1
C7	453(6)	5439(15)	7170(4)	48(3)	1
C8	8(5)	5858(17)	7429(4)	50(3)	1
C9	611(7)	5002(16)	6412(4)	48(3)	1
C10	572(6)	4464(19)	5646(4)	64(4)	1
C11	787(6)	5963(18)	5394(4)	65(4)	1
C12	1279(6)	7043(17)	5651(4)	58(4)	1
C13	1532(6)	8504(19)	5407(4)	60(4)	1
C14	2421(6)	7473(17)	5100(4)	51(3)	1
C15	3211(6)	6675(16)	4665(4)	46(3)	1
C16	3697(5)	6536(18)	4958(5)	65(4)	1
C17	4272(6)	6262(18)	4855(5)	61(4)	1
C18	4322(7)	6055(18)	4435(5)	73(4)	1
C19	3854(6)	6173(17)	4117(4)	53(3)	1
C20	3763(7)	6052(19)	3640(5)	69(4)	1
C21	3178(7)	6311(19)	3519(4)	71(4)	1
C22	3281(5)	6539(18)	4239(4)	58(4)	1
K1	−1350(1)	9483(4)	6369(1)	68(1)	1
O1	1139(4)	4651(12)	6480(3)	63(3)	1
O2	2733(4)	7487(12)	5456(3)	61(2)	1
O3	−1322(5)	10328(13)	7255(3)	72(3)	1
O4	−2410(5)	9489(13)	6731(3)	76(3)	1
O5	−2321(5)	7863(13)	5923(3)	78(3)	1
O6	−1325(4)	8697(12)	5498(3)	67(3)	1
O7	−256(4)	9397(11)	6047(3)	60(2)	1
O8	−334(4)	10958(12)	6841(3)	70(3)	1
C23	−1872(8)	10900(20)	7332(5)	86(5)	1
C24	−2332(8)	9540(20)	7187(5)	92(6)	1

C25	−2795(8)	8200(20)	6549(5)	84(5)	1
C26	−2887(6)	8210(20)	6061(5)	72(4)	1
C27	−2364(6)	7880(19)	5467(4)	68(4)	1
C28	−1772(7)	7450(20)	5338(5)	80(5)	1
C29	−737(7)	8250(20)	5413(5)	73(4)	1
C30	−343(7)	9650(20)	5600(4)	75(4)	1
C31	154(6)	10670(20)	6244(5)	71(4)	1
C32	208(7)	10460(20)	6712(5)	75(4)	1
C33	−320(7)	11000(20)	7303(5)	76(4)	1
C34	−887(8)	11510(20)	7405(4)	78(5)	1
K2	3256(1)	8536(4)	6203(1)	62(1)	1
O9	2558(5)	11621(17)	6126(4)	98(4)	1
O10	2408(5)	9230(20)	6786(3)	94(4)	1
O11	3097(6)	6178(15)	6860(3)	86(3)	1
O12	4198(5)	6362(15)	6551(4)	92(4)	1
O13	4351(5)	8591(17)	5881(3)	89(3)	1
O14	3644(7)	11640(16)	5785(4)	107(4)	1
C35	2247(10)	12010(30)	6468(7)	117(7)	1
C36	1947(8)	10460(30)	6611(6)	99(6)	1
C37	2156(9)	7750(30)	6886(7)	118(7)	1
C38	2653(9)	6620(30)	7131(6)	105(6)	1
C39	3595(10)	5480(20)	7074(7)	112(7)	1
C40	4042(9)	4970(30)	6772(7)	111(7)	1
C41	4598(9)	6000(30)	6260(7)	114(7)	1
C42	4831(8)	7660(30)	6125(7)	112(7)	1
C43	4536(8)	10210(30)	5703(7)	117(7)	1
C44	4013(11)	11130(30)	5486(6)	124(8)	1
C45	3127(11)	12440(30)	5584(6)	114(7)	1
C46	2761(9)	13080(20)	5884(7)	100(6)	1
O15	−1728(5)	4354(15)	6657(3)	87(3)	1
O16	−968(4)	6031(13)	6487(3)	65(3)	1
O17	−889(4)	3907(13)	5793(3)	68(3)	1
O18	−1728(4)	2542(13)	5930(3)	75(3)	1
C47	−1350(7)	4760(20)	6420(5)	66(4)	1
C48	−1299(7)	3660(20)	6008(5)	63(4)	1

Table A3.8. Hydrogen bonds [Å and °].

D–H···*A*	*d*(*D*–H)	*d*(H···*A*)	*d*(*D*···*A*)	∠(*D*H*A*)
N1–H901···O16	0.88	1.88	2.717(14)	159.2
N2–H902···O16	0.88	2.00	2.871(14)	172.9
N3–H903···O17	0.88	2.20	2.828(15)	128.1
N4–H904···O18^{v}	0.88	2.37	3.108(15)	141.2
N4–H904···O17^{v}	0.88	2.63	3.471(14)	159.4
N5–H905···O18^{v}	0.88	1.90	2.750(14)	162.6
N6–H906···O18^{v}	0.88	2.05	2.882(15)	157.2
N6–H906···O15^{v}	0.88	2.39	3.012(15)	127.9

Symmetry transformations used to generate equivalent atoms:
(i) –x+1/2,y–1/2,–z+3/2 (ii) x,y+1,z (iii) –x+1/2,y+1/2,–z+3/2
(iv) x,y–1,z (v) –x,–y+1,–z+1